Year : 2023

Development of gene edating-based therapeutic strategies for Huntington's disease

Duarte Fábio

Duarte Fábio, 2023, Development of gene edating-based therapeutic strategies for Huntington's disease

Originally published at : Thesis, University of Lausanne

Posted at the University of Lausanne Open Archive http://serval.unil.ch
Document URN : urn:nbn:ch:serval-BIB_44B87ACA7F977

UNIL | Université de Lausanne
Faculté de biologie et de médecine

Département de Neurosciences Cliniques

Development of gene editing-based therapeutic strategies for Huntington's disease

Thèse de doctorat en Neurosciences

présentée à la

Faculté de biologie et de médecine
de l'Université de Lausanne

par

Fábio DUARTE

Neurobiologist diplômé de l'Université de Coimbra, Portugal

Jury

Prof. David Gatfield, Président
Prof. Nicole Déglon, Directrice de thèse
Prof. Luís Pereira de Almeida, Expert
Prof. Johan Jakobsson, Expert

Thèse n° 370

Lausanne
(2023)

Programme doctoral interuniversitaire en Neurosciences des Universités de Lausanne et Genève

LEMANIC NEURO SCIENCE DOCTORAL SCHOOL

UNIL | Université de Lausanne

UNIVERSITÉ DE GENÈVE

UNIL | Université de Lausanne
Faculté de biologie et de médecine

Département de Neurosciences Cliniques

Development of gene editing-based therapeutic strategies for Huntington's disease

Thèse de doctorat en Neurosciences

présentée à la

Faculté de biologie et de médecine
de l'Université de Lausanne

par

Fábio DUARTE

Neurobiologist diplômé de l'Université de Coimbra, Portugal

Jury

Prof. David Gatfield, Président
Prof. Nicole Déglon, Directrice de thèse
Prof. Luís Pereira de Almeida, Expert
Prof. Johan Jakobsson, Expert

Thèse n° 370

Lausanne
(2023)

Programme doctoral interuniversitaire en Neurosciences des Universités de Lausanne et Genève

LEMANIC NEURO SCIENCE DOCTORAL SCHOOL

UNIL | Université de Lausanne

UNIVERSITÉ DE GENÈVE

UNIL | Université de Lausanne

UNIVERSITÉ DE GENÈVE

Programme doctoral interuniversitaire en Neurosciences des Universités de Lausanne et Genève

Imprimatur

Vu le rapport présenté par le jury d'examen, composé de

Président·e	Monsieur	Prof.	David	**Gatfield**
Directeur·trice de thèse	Madame	Prof.	Nicole	**Déglon**
Expert·e·s	Monsieur	Prof.	Luís	**Pereira de Almeida**
	Monsieur	Prof.	Johan	**Jakobsson**

le Conseil de Faculté autorise l'impression de la thèse de

Monsieur Fábio Duarte

Neurobiologiste diplômé de l'Université de Coimbra, Portugal

intitulée

Development of gene editing-based therapeutic strategies for Huntington's disease

Lausanne, le 12 mai 2023

pour Le Doyen
de la Faculté de Biologie et de Médecine

Prof. David Gatfield

ACKNOWLEDGEMENTS

It is a pleasure to acknowledge those who made this thesis possible. I would like to thank:

My supervisor and mentor Prof. Nicole Déglon for giving me the possibility to conduct this project and for making available all the necessary resources. Thank you for sharing your scientific knowledge and expertise. I am deeply grateful for all your professional guidance and support through these last four years. I will take with me the pleasant and countless brainstorming discussions.

The experts Prof. Luís Pereira de Almeida and Prof. Johan Jakobsson for having kindly accepted to review and evaluate my thesis project.

Prof. Liliane Tanenbaum for the promotion of scientific discussions and for exchanging your expertise. Thank you also for providing the coffee that kept me awake during the writing of this thesis.

Maria Rey for teaching me about cell culture, molecular biology, and viral production. Thank you for your advisement on most all laboratory procedures and techniques. I mention “most” because the animal facility is a forbidden place for you. On this topic, I deeply thank Melanie Sipion, who (very) patiently taught me *in vivo* surgery and animated the animal facility with her humor and DJ skills.

Dr. Gabriel Vachey for his preliminary work related to this project. Thank you for sharing your knowledge on cell culture and molecular biology and for all your nerd jokes. On this regard, I also thank Dr. Mergim Ramosaj and Margareta Rybarikova for your help in conducting and analyzing some of the experiments.

The students Elisa Montorfani, Nylsa Chammartin and Nicol Ghisleri that I co-supervised in these last four years for your contribution to the project.

Sibilla, Valentine, Lukas, Julien, and Pierre for all the enjoyable moments we spent together, including the ones we do not remember.

Marcelo for all the moments since my arrival in Lausanne. I am grateful that our paths have crossed, and I could have not asked for a better buddy. Thank you for all the late-night discussions and for showing me that I am not the most suborn person in the world.

My family for the unconditional support and advisement during these last four years. A special thank you to my parents and brother for all the motivational and encouraging words at the most difficult moments. I would have never been capable to achieve this goal without you.

Finally, a very special thanks to Sara Regio for all your kind support and patience in these last months during the finalization of the project. Thank you for not stopping believing in me, and for keeping me mentally sane even though at the expense of your sanity sometimes. You definitely played a critical part during this period, and I could not imagine finishing this project without you.

ABSTRACT

Huntington's disease (HD) is a fatal neurodegenerative disorder caused by a toxic gain-of-function CAG expansion in the first exon of the huntingtin (*HTT*) gene. Striatal neurodegeneration is the main hallmark in HD, but cortical neurons are also affected at early stages of the disease. Currently, there are no treatments stopping or slowing disease progression. The monogenic nature of HD makes CRISPR/Cas9-mediated *HTT* inactivation a promising therapeutic strategy. To facilitate the development of CNS gene therapies and maximize therapeutic efficacy for HD, we first developed 2D and 3D imaging workflows to evaluate the therapeutic potential of a novel strategy for HD by assessing transduction efficiency in multiple brain regions. We combine the retrograde transport properties of the AAV2.retro with the broad striatal diffusion of the AAV2/rh.10 to simultaneously inactivate the *HTT* gene in both striatal (SPNs) and cortical projection neurons (CPNs). Because constitutive SpCas9 expression increases the likelihood for the occurrence of off-target events and immunogenic responses, we used a transient AAV-based KamiCas9 system. Our analysis predicted that 54% of striatal cells and 7% of cortical cells had been transduced in highly targeted brain regions. Remarkably, in those regions, *HTT* gene inactivation reached 54.5% and 9.6%, respectively. These results validate the maximized therapeutic strategy and demonstrate the power of these quantitative workflows to predict the potential of gene therapy strategies for neurological disorders. Nevertheless, it is still unclear to which extent the loss of the wild-type *HTT* (*wtHTT*) normal functions may impact on disease progression. One of the current allele-specific therapeutic strategies for HD consists of the excision of the first exon of mutant *HTT* allele (*mHTT*) by inducing simultaneous double-strand breaks at upstream and downstream positions of the *mHTT* exon 1. However, its efficiency has never been assessed. Given the ultimate goal for clinical application, it is critical to accurately determine its efficiency to anticipate therapeutic potential. Therefore, here we developed digital PCR-based assays to accurately quantify the frequency of *HTT* exon 1 deletion events. Consistently with previous studies, we observed that deletion events are frequent *in vitro*, but extremely rare *in vivo*. Our results do not support the application of dual sgRNA-based deletion strategies for the *in vivo* treatment of HD or other CNS disorders. In addition, we highlight that the current methodologies to evaluate deletion events greatly overestimate their frequency. Overall, we encourage the scientific community to adopt more quantitative methods when analyzing complex gene editing events to avoid misleading conclusions concerning the applicability of such therapeutic strategies *in vivo*.

RÉSUMÉ

La maladie de Huntington (MH) est une maladie neurodégénérative mortelle causée par une expansion CAG toxique à gain de fonction dans le premier exon du gène de la huntingtine (*HTT*). Cette maladie se caractérise principalement par la dégénérescence des neurones striataux, mais les neurones corticaux sont également touchés dans les premiers stades de la maladie. Actuellement, il n'existe aucun traitement capable d'arrêter ou de ralentir la progression de la maladie. La nature monogénique de la MH fait de l'inactivation *HTT* médiée par CRISPR/Cas9 une stratégie thérapeutique prometteuse. Pour faciliter le développement de thérapies géniques pour des maladies qui affectent le SNC et maximiser son efficacité thérapeutique pour la MH, nous avons développé des flux de travails basés sur de l'imagerie 2D et 3D. Cette méthodologie permet d'évaluer le potentiel thérapeutique d'une nouvelle stratégie pour la MH en évaluant l'efficacité de la transduction dans plusieurs régions du cerveau. Nous avons combiné les propriétés de transport rétrograde de l'AAV2.retro avec la large diffusion striatale de l'AAV2/rh.10 pour inactiver simultanément le gène *HTT* dans les neurones de projection striataux (NPSs) et corticaux (NPCs). Nous avons utilisé un système AAV-KamiCas9 transitoire car l'expression constitutive de SpCas9 augmente la possibilité d'événements hors cible et de réactions immunogènes. Les prédictions, selon notre analyse, sont que 54% des cellules striatales et 7% des cellules corticales ont été transduites dans des régions cérébrales hautement ciblées. De façon remarquable, dans ces régions, l'inactivation du gène *HTT* a atteint 54,5% et 9,6%, respectivement. Ces résultats valident la stratégie thérapeutique maximisée et démontrent la puissance de ces flux de travail pour prédire quantitativement le potentiel des stratégies de thérapie génique pour les maladies neurologiques. Néanmoins, on ne sait toujours pas dans quelle mesure la perte des fonctions normales de la *HTT* de type sauvage (*wtHTT*) peut avoir un impact sur la progression de la maladie. L'une des stratégies thérapeutiques actuelles, spécifique à l'allèle, pour la MH consiste à exciser le premier exon de l'allèle *HTT* mutant (*mHTT*) en induisant des cassures double brin simultanées en amont et en aval de l'exon 1 de la *mHTT*. Cependant, son efficacité n'a jamais été évaluée. Compte tenu de l'objectif ultime d'une application clinique, une détermination précise de l'efficacité est essentielle pour anticiper le potentiel thérapeutique. Par conséquent, nous avons développé ici des tests basés sur la PCR digitale pour quantifier avec précision la fréquence des événements de délétion de l'exon 1 du *HTT*. Conformément aux études précédentes, nous avons observé que les événements de délétion sont fréquents *in vitro*, mais extrêmement rares *in vivo*. Nos résultats ne soutiennent pas l'application de stratégies de délétion à base de double sgRNA pour le traitement *in vivo* de la MH ou d'autres maladies affectantle SNC. Par ailleurs, les méthodologies d'évaluation actuelles surestiment largement la fréquence d'événements de délétion. Dans l'ensemble, la communauté scientifique devrait adopter des méthodes plus quantitatives lors de l'analyse des événements complexes d'édition de gènes afin d'éviter des conclusions trompeuses concernant l'applicabilité de telles stratégies thérapeutiques *in vivo*.

ABBREVIATIONS

53BP1 - p53-binding protein 1
aa – Amino acid
AADC – Aromatic L-amino acid decarboxylase deficiency
AAV – Adeno-associated virus
ABBA – Aligning big brains and atlases
ACA – Anterior cingulate area
AHD – Adult-onset Huntington's Disease
AI – Agranular insular area
ARA – Allen Reference Atlas
ASO – Antisense oligonucleotide
ATXN – Ataxin
BAC - Bacterial artificial chromosome
BBB – Blood-brain barrier
BDNF - Brain-derived neurotrophic factor
BPNLS – Bipartite nuclear localization signal
CamKII - Ca^{2+}/calmodulin-dependent protein kinase II
cAMP - Cyclic AMP
CAP - CAG age product
CCFv3 – Allen mouse brain common coordinate framework version 3
cDNA – Complementary DNA
CNS – Central nervous system
CPNs – Cortical projection neurons
CREB - cAMP response element-binding protein
CRISPR - Clustered regularly interspaced short palindromic repeats
crRNA - CRISPR RNA
CRY2 - Photoreceptor protein cryptochrome 2
CSF - Cerebrospinal fluid
DARPP32 – Dopamine- and cAMP-regulated phosphoprotein, 32 kDa
DCL - Diagnostic confidence level
Drp1 - Dynamin-related protein 1
dsAAV – Double-stranded AAV
DSB – Double strand break
dsDNA – Double-stranded DNA
dSPNs - Striatal projection neurons of the direct pathway
ESCs - Embryonic stem cells
FAN1 - Fanconi anemia FANC1/FANCD2-associated nuclease 1
FRP – Frontal pole
GeM-HD - Genetic modifiers of Huntington's disease
GFP – Green fluorescence protein
GLT-1 – Glutamate uptake receptor 1
GPCR52 - G-protein coupled receptor 52
GU – Gustatory area
GWAS - Genome-wide association study
HD – Huntington's Disease
HD-ISS – Huntington's disease integrating stagging system
HD-NPCs – Huntington patient-derived neural progenitor cells
HDR – Homology-directed repair
HEAT – Huntingtin, elongation factor 3, protein phosphatase 2A and yeast kinase TOR1
HEK293T – Human embryonic kidney 293T cells

hGPCs - Human glial progenitor cells
HITI – Homology-independent targeted integration
HIV - Human immunodeficiency virus
HMEJ – Homology-mediated end joining
HSR - Heat stress response
HTT – Huntingtin
IL-2 - Interleukin 2
IL-6 - Interleukin 6
IL1β - Interleukin 1 beta
ILA – Infralimbic area
IN – Integrase
Indels – Insertions and deletions
iPSCs - Induced pluripotent stem cells
IRES - Internal ribosome entry site
iSPNs - Striatal projection neurons of the indirect pathway
IT – Intratelencephalic neurons
ITR – Inverted terminal repeats
IV – Intravenous
JHD – Juvenile-onset Huntington's Disease
Kb – Kilobase
KDa – Kilodaltons
KI – Knock-in
KO – Knock-out
LC3 - Microtubule-associated protein 1A/1B light chain 3
LCA10 – Leber congenital amaurosis type 10
LGALS3 - Galectin-3
LIG1 – Ligase 1
LSFM – Light sheet fluorescence microscopy
LTR – Long terminal repeats
LV – Lentivirus
Mb – Megabase
mHTT – Mutant huntingtin
MIRACL – Multimodal image registration and connectivity analysis
miRNA – microRNA
MMEJ – Microhomology-mediated end joining
MOp – Primary motor area
MOs – Secondary motor area
MOTA – Map objects to atlas
MPS – Mucopolysaccharidosis
MRI - Magnetic resonance imaging
MSH3 - MutS homolog 3
NES – Nuclear export signal
NeuN - Neuronal nuclear protein
NfL - Neurofilament light chain
NLS – Nuclear localization signal
NMD – Nonsense-mediated RNA decay
NMDA - N-methyl-D-aspartate
nt – Nucleotide
ORB – Orbital area
PAM – Protospacer adjacent motif
PAS – PAM-altering SNP
PBS – Primer binding site

PCBP2 – poly(rC)-binding protein 2
PDE10 - Phosphodiesterase 10
PET - Positron emission tomography
PIC - Preintegration complex
PKA - Protein kinase A
PL – Prelimbic area
PolyQ – Polyglutamine
PPIB – Peptidylprolyl isomerase B
PRD – Proline-rich domain
PSD95 - Postsynaptic density 95 protein
PT - Pyramidal tract neurons
PTM - Post-translational modifications
PV – Parvalbumin
RAN - Repeat-associated non-AUG
RFLP – Restriction Fragment Length Polymorphisms
RISC - RNA-induced silencing complex
RNAi – RNA interference
RRE – Rev response element
RSP – Restrosplenial area
RT – Reverse transcriptase
RT-qPCR – Reverse-transcriptase polymerase chain reaction
SATI - Single homology arm donor-mediated intron targeting integration
SCA – Spinocerebellar ataxia
scRNA-seq – Single-cell RNA sequencing
sgRNA – Single guide RNA
shRNA – Short hairpin RNA
SIN – Self-inactivating LVs
siRNA – Small interfering RNA
SMA - Spinal muscular atrophy
SMN - Survival of motor neuron
SNPs - Single nucleotide polymorphisms
SPNs - Striatal projection neurons
SS – Somatosensory area
ssAAV – Single-stranded AAV
ssDNA – Single-stranded DNA
SSRIs - Selective serotonin re-uptake inhibitors
ssRNA – Single-stranded RNA
SST – Somatostatin
TAR – Trans-activation response element
TIDE – Tracking of indels by decomposition
TIM23 - Translocase of mitochondrial inner membrane 23
TNFα - Tumor necrosis factor alpha
TNT - Tunneling nanotube
tracrRNA - Trans-activating CRISPR RNA
TWAS - Transcription-wide association study
UHDRS-SDMT – Symbol digit modality test of Huntington’s disease rating scale
UHDRS-TFC - Total functional capacity of Huntington’s disease rating scale
UHDRS-TMS – Total motor score of Huntington’s disease rating scale
UPS - Ubiquitin-proteasome system
UTR – Untranslated region
VIP – Vasoactive intestinal peptide
VSV-G – Vesicular stomatitis virus glycoprotein

wtHTT – Wild-type huntingtin
YAC – Yeast artificial chromosome
ZF – Zinc finger
ZFN – Zinc finger nuclease

TABLE OF CONTENTS

LIST OF FIGURES

Supplementary Figures

LIST OF TABLES

Supplementary Tables

CHAPTER 1

Introduction

1. Introduction

1.1. Historical context of Huntington's disease

1.1.1. Discovery of HD

Huntington's disease (HD) (OMIM: 143100) is a fatal hereditary neurological disease involving the progressive decline of motor and cognitive functions as well as psychiatric disturbances. Although HD is well characterized nowadays, its discovery had been quite a journey. One of the primary features of HD is chorea, which is defined by abnormal involuntary movements as a result of brief and irregular muscle contractions (Vale & Cardoso, 2015). One of the first references of choreic behaviors dates back to the Middle Ages, when Greeks described chorea as a "dancing mania" (Cubo, 2016; Vale & Cardoso, 2015). Since then, many have tried to better categorize choreic movements and link them to specific causes and/or diseases. Paracelsus (1493-1541) was the first attempting to classify chorea into chorea lasciva (caused by sexual desire), chorea imaginativa (caused by imagination) and chorea naturalis (caused by a physical pathology). Although the interest in choreic symptoms had begun in ancient ages, it was only in the 19th century that chorea started being considered as a cause of neurological pathologies. Among the several physicians that have reporter HD-like symptoms, Dr Charles Oscar Waters communicated in 1842 a hereditary neurological disease which he named "magrums", involving motor and cognitive degeneration (Waters, 1842). Two decades later, the Norwegian Johan Lund provided the first description of hereditary chorea, later known as HD (Cubo, 2016). Although Lund had described it previously, the disease was named after the report of George Huntington on adult-onset hereditary chorea in 1871. In his report, Huntington highlighted the autosomal-dominant pattern of inheritance and comprehensively described the progressive exacerbation of choreic symptoms associated with dementia and behavioral alterations (Huntington, 1872). Importantly, he defined that chorea comprises a large spectrum throughout life span and that it can be related to different causes (HD or others). The next important landmark in HD discovery took place in 1955, when Américo Negrette reported a community in Maracaibo, Venezuela with a bizarre number of patients with Huntington's chorea (Okun & Thommi, 2004). The extremely high prevalence of HD patients in this community (1 in every 10 people) allowed the exhaustive characterization of the disease clinical manifestations and later, of its genetic profile. At this time, several foundations were created to better study the disease as HD was starting to have an impact in both American and European societies (Cubo, 2016).

1.1.2. Huntingtin (*HTT*) is the responsible gene in HD

Given the autosomal-dominant inheritance of the disease, efforts started taking place to identify the causative gene of the disease. The identification of restriction fragment-length polymorphisms (RFLPs) in 1978 (Kan & Dozy, 1978) made possible the genetic mapping of genes in the human chromosomes. In 1979, James Gusella and Nancy Wexler started organizing expeditions to Venezuela to collect blood samples from the community in Maracaibo (Bates et al., 2015; Cubo, 2016) and mapped the HD-causative gene to the short arm of the chromosome 4 (Gusella et al., 1983). However, the identification of the HD gene was still challenging at the time due to the lack of technology required for gene isolation. Nonetheless, in the subsequent years, researchers used genetic polymorphisms and linkage disequilibrium analysis to narrow the location of the gene to a 2 megabase (Mb) region in chromosome 4 (Bates et al., 1991; MacDonald et al., 1991; Snell et al., 1989). In 1991, Buckler and colleagues developed a strategy to identify genes based on exon amplification (Buckler et al., 1991). The establishment of this technology permitted the identification and isolation of the HD causative huntingtin (*HTT*) gene (previously named *IT15* gene, OMIM: 613004) (MacDonald et al., 1993), which contained a polymorphic CAG-triplet repeat that was expanded in HD patients. Quickly, worldwide genetic screenings were carried out to compare the genotype to the phenotype of the disease (Andrew et al., 1993; Duyao et al., 1993; Snell et al., 1993). It was established that *HTT* alleles with 40 or more CAG repeats invariably cause the disease whereas *HTT* alleles with CAG trinucleotides spanning between 36 and 39 repeats increase the risk to develop HD (McNeil et al., 1997).

1.2 Epidemiology, symptomology, and diagnosis of Huntington's disease

1.2.1. Epidemiology of HD

Huntington's disease is a rare neurogenerative disorder distributed across the globe with great geographical variability (Figure 1.1). Higher prevalence is observed in Europe and North America. In 2012, Pringsheim and colleagues performed a meta-analysis of data collected between 1985 and 2010 regarding the prevalence and incidence of HD (Pringsheim et al., 2012). In this systematic review, the worldwide HD prevalence was 2.71 cases per 100'000 persons and the incidence 0.38 cases per 100'000 persons-year. However, HD prevalence and incidence are varying over the years due to factors such as accessibility to health care, genetic testing, migration, and/or identification of new HD regional clusters (Medina et al., 2022). Epidemiological data generated using updated clinical diagnostic protocols alongside with the accessibility to confirmatory genetic testing is likely to be more accurate. For this reason, Medina and colleagues recently updated the previous meta-analysis study using data from to 2011 to 2022 (Medina et

al., 2022). Overall, merged data from 1985 to 2022 revealed that both worldwide prevalence and incidence of HD were higher than previously estimated, counting for a prevalence of 3.92 cases per 100'000 persons and an incidence of 0.47 cases per 100'000 persons-year. The higher estimates may also be related to the increased accessibility to genetic testing and to advances in the treatment of medical comorbidities, expanding the life span of HD patients. Regarding the epidemiological analysis per continent, it confirmed that HD is more widespread in Europe (6.37 per 100'000 persons) and North America (8.87 per 100'000 persons).

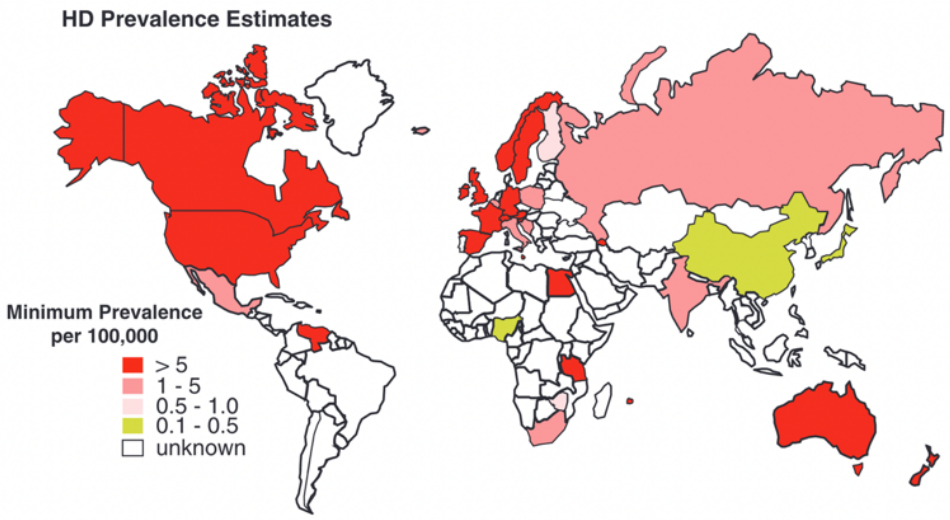

Figure 1.1: Worldwide distribution of HD. (Warby et al., 2011)

1.2.2. Symptomology of HD

Huntington's disease is characterized by a triad of symptoms involving motor deterioration, cognitive impairment, and neuropsychiatric disturbances (Bates et al., 2015; Ross et al., 2014). The disease can be divided into two branches depending on the onset age of the clinical manifestations. The most common form of HD is the adult-onset form (AHD), with clinical manifestations typically arising between the ages of 35 and 50, and death occurring within the next 15 to 20 years (Figure 1.2). In contrast, the disease is defined as juvenile-onset (JHD) when the HD symptoms appear before the age of 21 years-old, which only corresponds to approximately 5% of all HD patients (Bakels et al., 2022; Fusilli et al., 2018).

The motor disability in AHD usually starts with the execution of involuntary movements previously described as chorea (known as hyperkinetic phase) (Figure 1.2). As diseases progresses, HD patients start displaying hyperkinetic symptoms characterized by difficulties in the controlling voluntary actions due to the loss of coordination, slowness of movements (bradykinesia) and gait disturbance. At the later stages of the disease, parkinsonism features, dystonia and rigidity strongly impair the control of voluntary movements. Concerning cognitive impairments, AHD is characterized by deterioration of memory and learning capabilities and it

affects mental flexibility, attention, and the ability to make judgements and/or decisions. Patients also often present emotional disturbances such as irritability, swing moods and apathy. While irritability is sometimes observed at initial stages of the disease, social impairment and distancing occurs at more later stages and worsens as the diseases progresses. In addition, depression is highly common among patients and there is an increased prevalence of suicidal thoughts compared to the general population (Hubers et al., 2013).

In JHD patients, motor onset is often defined by bradykinesia and rigidity whereas chorea is rarely observed at initial stages. Cognitive dysfunction is associated to developmental delay in areas such as speech and language which highly affect their social skills. While obsessive-compulsive disturbances are not a frequent behavior in AHD, more than 50% of the adolescent-onset JHD patients display this psychiatric symptom (Langbehn et al., 2020). Interestingly, a notable difference between the two forms of the disease is the higher risk of epileptic seizures in JHD patients (30-35%) (Cloud et al., 2012). Despite the most frequent clinical features are related to the nervous system, HD patients can also experience metabolic and immune disturbances, weight loss, testicular atrophy, cardiac failure, and osteoporosis (Gómez-Jaramillo et al., 2022; van der Burg et al., 2009).

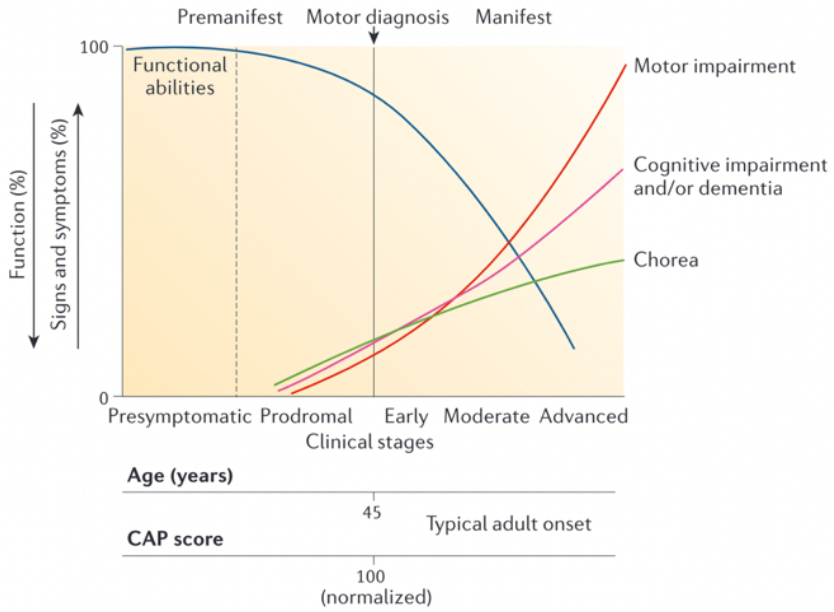

Figure 1.2: Natural clinical history of HD. (Bates et al., 2015)

1.2.3. Diagnosis of HD

The diagnosis of HD is based on clinical criteria, family history, and genetic screening for the presence of the expanded CAG repeat in the *HTT* gene (Bates et al., 2015; Stoker et al., 2022). HD is generally diagnosed at the onset of the motor deficits (Bakels et al., 2022; Bates et al., 2015; McAllister et al., 2021; Ross et al., 2014). The total motor score of the unified Huntington's disease rating scale (UHDRS-TMS) (Kieburtz, 1996) is the ranking system more often used to

assess motor disturbances in HD despite other alternative motor scales have been suggested (Mestre et al., 2018). To determine the certainty that motor symptoms are due to HD, physicians can attribute a diagnostic confidence level (DCL) (Liu et al., 2015). Confidence levels ranges from 0 to 4 and a DCL4 means that motor symptoms were attributed to HD with a physician's confidence level of 99%. Given the autosomal dominant heritage pattern of the disease, familiar background is an excellent indicator to predict disease's the development of the disease. For individuals with a HD familiar history, the appearance of motor symptoms such as chorea, impaired ocular motility, rapid alternating movements and loss of motor coordination is usually enough to validate the diagnosis (Ross & Shoulson, 2009). In other cases, magnetic resonance imaging (MRI) to verify striatal atrophy can also be used to complement the diagnosis before genetic confirmatory testing.

Genetic testing can be either predictive or confirmatory depending on the clinical status. Predictive testing occurs when potential non-symptomatic carriers (due to the familiar history) are tested for the presence of the mutation while confirmatory tests are used to validate diagnosis when clinical manifestations are suggestive of HD. Predictive testing not only assesses the presence of the mutation but can also be used to estimate the onset age of motor symptoms (Penney et al., 1997; Tabrizi et al., 2013; Warner et al., 2022). The age of motor onset seems to be inversely correlated to the number of CAG repeats and the CAG age product (CAP) score has been used to predict the age of disease onset (Zhang et al., 2011) (Figure 1.3). Because predictive testing has a major impact on individual's life, the International Huntington Association established guidelines for genetic predictive testing of HD (International Huntington Association, 1994) right after the identification of the genetic cause, recommending the use of predictive testing only from the age of majority.

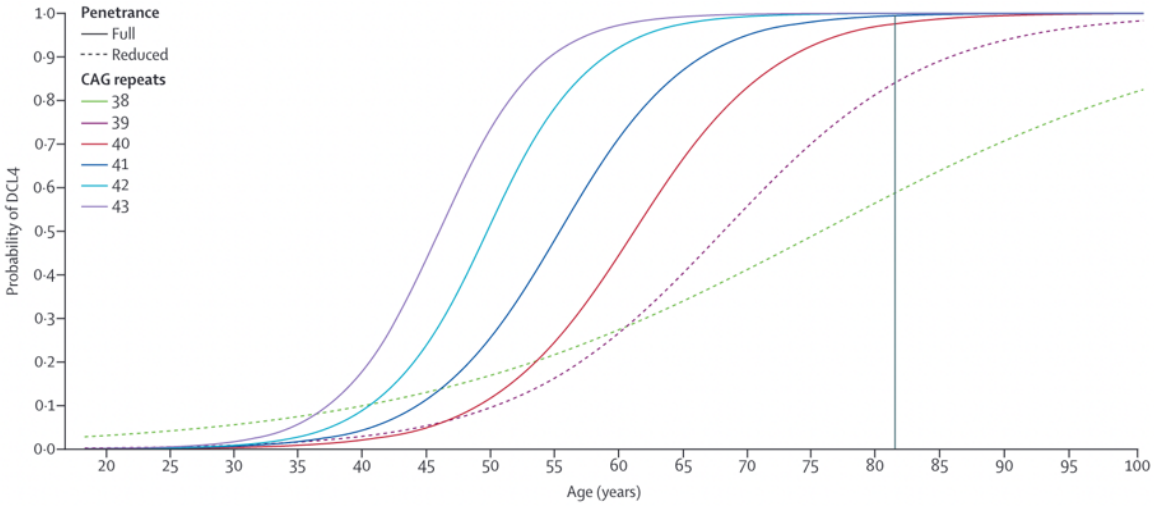

Figure 1.3: DCL4 probability by age and number of CAG repeats. Vertical line represents the worldwide life expectancy. (Tabrizi et al., 2022a)

1.3 Progression and management of Huntington's disease

1.3.1. Progression and biomarkers of HD

The identification of individuals carrying the HD mutation prior to diagnosis (by familiar history and genetic predictive testing) has been crucial to improve our understanding about how the disease evolves. Longitudinal studies with HD participants such as the COHORT (NCT00313495) (Dorsey & Group COHORT Investigators, 2012), PHAROS (NCT00052143) (Group PHAROS Investigators, 2006), PREDICT-HD (NCT00051324) (Aylward et al., 2011; Epping et al., 2016; Paulsen et al., 2014), TRACK-HD (Tabrizi et al., 2011, 2012, 2013) and REGISTRY (NCT01590589) (McAllister et al., 2021) have shown that pathological changes in HD start many years before the onset of motor symptoms.

For example, the TRACK-HD trial collected data on motor and cognitive performances over 36 months in control individuals, early-stage HD patients and premanifest individuals who were predicted to develop symptoms in more (preHD-A) or less than 10 years (preHD-B) (Tabrizi et al., 2013). Cognitive deterioration (speeded tapping, symbol digit modality - SDMT, and stroop word reading tests) and motor impairment (UHDRS-TMS) in premanifest individuals were more accentuated in those who were predicted to develop the disease in less than 10 years (preHD-B). This is consistent with the hypothesis that disease progresses faster in individuals closer to predicted disease onset. Psychiatric evaluation also demonstrated that apathy worsens in the premanifest period (Tabrizi et al., 2013). A recent report from the REGISTRY trial indicated that prevalence of psychiatric symptoms is more associated to advanced stages of the disease although depression and, less often, irritability can precede motor symptoms by many years (McAllister et al., 2021). Similarly, Epping and colleagues evaluated a battery of HD psychiatric symptoms over ten years in premanifest patients from the PREDICT-HD and observed that psychiatric disturbances are present in premanifest stages of the disease more often than previously thought (Epping et al., 2016). Interestingly, they noticed that symptom rating scores were higher when companions of the premanifest individuals were interrogated. This suggests that affected individuals may be less aware of psychiatric alterations occurring during the premanifest phase and advocates the incorporation of third-party inquiries to better assess HD psychiatric symptoms.

Regarding neuropathology, striatal volumes are markedly reduced compared to age-matched normal volumes (45-70% loss) at the time of clinical motor diagnosis (Kinnunen et al., 2021). Volumetric MRI data from the TRACK-HD and PREDICT-HD trials indicated that striatal atrophy occurs at least 15 years prior to the motor symptoms onset (Aylward et al., 2011, 2013; Tabrizi et al., 2012, 2013) (Figure 1.4). This data further demonstrated that caudate and putamen volumes can be used to predict future clinical diagnosis in presymptomatic patients. In young HD carriers, reduced striatal volume could be detected as early as 24 years before expected symptom onset (Scahill et al., 2020). In contrast, even though there is cortical volume loss before the onset

of motor symptoms, it becomes more widespread after the clinical diagnosis (Kinnunen et al., 2021). Loss of cortical grey-matter volume is more apparent in occipital, motor, dorsomedial prefrontal, and parietal cortices (Rosas et al., 2008).

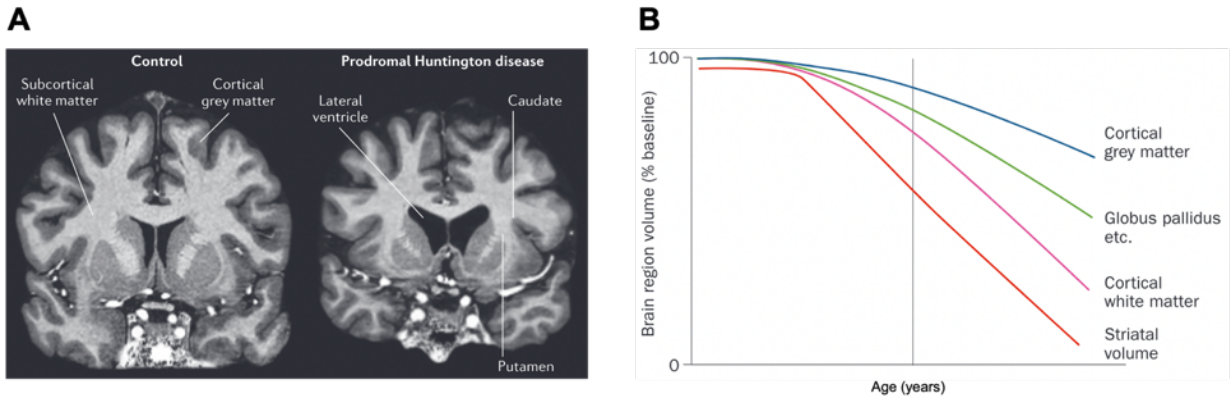

Figure 1.4: Striatum and cortex show signs of atrophy before diagnosis at motor onset. (A) Comparison between of brains of control (left) and prodromal HD (right) subjects by MRI. (Bates et al., 2015). **(B)** Hypothetical evolution of the degeneration of several brain regions with the progression of the disease. The vertical line represents the age of motor onset. (Ross et al., 2014)

These observations were confirmed in a recent study investigating the rates of brain degeneration over 10 years around the time of HD diagnosis in participants from the TRACK-HD and TrackOn-HD cohorts (Johnson et al., 2021) (Figure 1.5). At the time of diagnosis, the caudate and putamen show the largest atrophy levels compared to the age-matched controls, but extensive cortical atrophy is already detected across all lobes (Figure 1.5-A). Over the 10 years period studied, the striatum also showed the fastest degeneration rate with cortical atrophy being more pronounced in posterior regions at the occipital and parietal cortices (Figure 1.5-B). Interestingly, atrophy of the occipital lobe was highly correlated to the CAG repeat length, suggesting a particular vulnerability of this region for degeneration when patients carry higher numbers of CAG repeats. By incorporating motor (UHDRS-TMS) and cognitive (SDMT) tests in the longitudinal analysis framework, the authors identified that several regions such as the entorhinal area, cingulate, parahippocampal gyrus, caudate, calcarine cortex, supplementary motor cortex, temporal pole, and frontal gyrus contributed to worsening motor functions (Figure 1.5-C). In contrast, the worsening of the cognitive performances was more associated in patients who, in addition to putamen atrophy, also showed greater atrophy in the cingulate, orbital gyrus, occipital gyrus, lingual gyrus, and entorhinal area (Figure 1.5-D). This longitudinal data is important to predict behavioral changes in HD patients and to adjust and/or modify potential therapies.

Additionally, Novak and colleagues showed that the overall basal ganglia-cortical structural connectivity was altered in early HD patients (Novak et al., 2015). McColgan and colleagues used diffusion tractography and graph theoretical analysis to show that the connectivity of specific cortical hubs (superior frontal, superior parietal, precuneus and insula) is

already affected in premanifest individuals (McColgan et al., 2015). Other imaging technique that has been used to study HD progression is the positron emission tomography (PET) imaging. Ciarmiello and colleagues showed that glucose metabolism is affected in presymptomatic HD subjects and worsens with disease progression using PET imaging combined with the F^{18}-FDG ligand to measure glucose uptake (Ciarmiello et al., 2012). Also, the use of radioligands to measure reduced levels of striatal phosphodiesterase 10 (PDE10) (Fazio et al., 2020), or increased levels of mutant huntingtin (mHTT) aggregates have shown promising results as potential biomarkers of HD progression (Bertoglio et al., 2022).

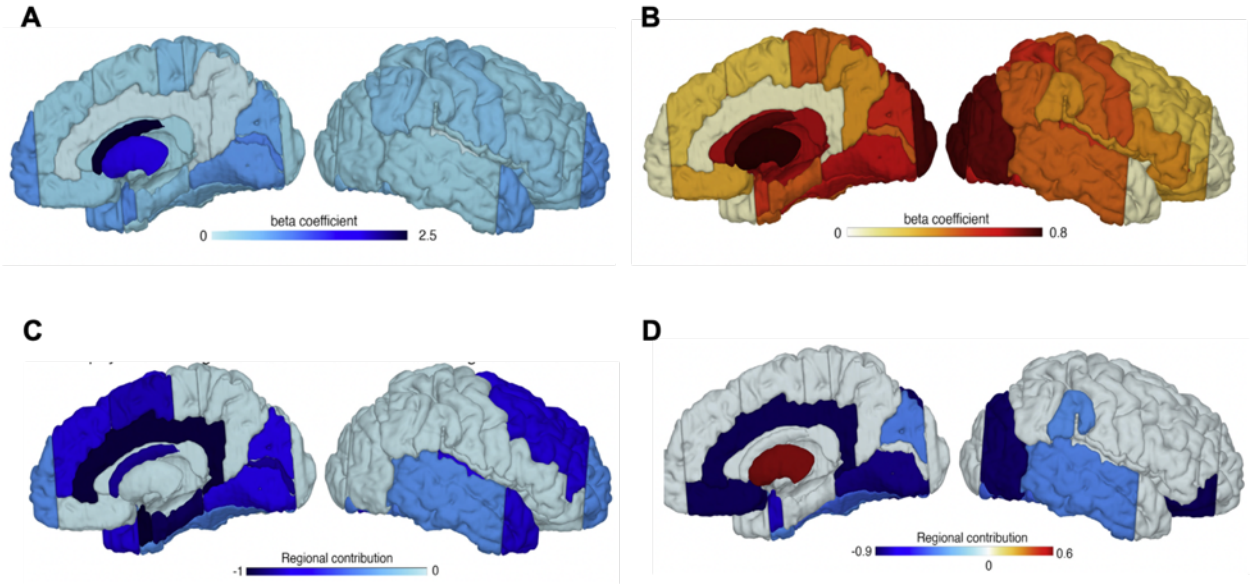

Figure 1.5: Illustration of brain volume changes in HD measured by MRI. (A) Significant brain atrophy differences between HD and age-matched control subjects at the time of motor diagnosis. **(B)** Significant rates of brain atrophy of HD subjects over age-matched control subjects during a decade around the time of HD motor onset. Brain-behavioral model predicting which brain regions significantly contribute to worsening in **(C)** motor (UHDRS-TMS) and **(D)** cognitive (SDMT) performances over a decade around the time of HD motor onset. (Johnson et al., 2021)

The measurement of neurodegeneration-related protein levels in the cerebrospinal fluid (CSF) and plasma has been used to assess both disease progression and engagement of drugs aiming at reducing the mHTT protein. Byrne and colleagues reported that increased concentrations of toxic mHTT and neurofilament light chain (NfL), an axonal protein indicative of neuronal injury, are among the earliest detectable changes in HD (Byrne et al., 2018). While CSF mHTT levels accurately distinguished controls from HD mutation carriers, NfL concentrations in the CSF and plasma were able to further segregate premanifest from manifest HD subjects (Figure 1.6). In a subsequent follow-up study, the same group demonstrated that the baseline values of these analytes are better predictors than their annualized rates of change (Rodrigues et al., 2020). In addition, plasma, and CSF levels of NfL showed overall higher correlation with several clinical and imaging measures then CSF mHTT after adjustment for age and CAG repeat length. The authors concluded that NfL levels in these biofluids should be favorable as a

prognostic biomarker for HD while mHTT might be a valuable pharmacodynamic marker for huntingtin-lowering trials in the CNS. The lower prognostic importance of mHTT in HD progression can be explained by the limitation of the current assays to measure the low concentrations of mHTT in the CSF of presymptomatic subjects. Several groups have developed more sensitive assays to measure total HTT and mHTT levels (Baldo et al., 2018; Fodale et al., 2017; Landles et al., 2021; Southwell et al., 2015). More recently, Fodale and colleagues demonstrated that they were able to measure both mHTT and non-expanded wild-type HTT (wtHTT) separately in the CSF of HD patients using an ultrasensitive bead-based, single molecule counting immunoassay platform (Fodale et al., 2022). However, a major current limitation of this technology is that it does not provide an absolute quantification of mHTT levels, and therefore concentrations cannot be compared among HD subjects.

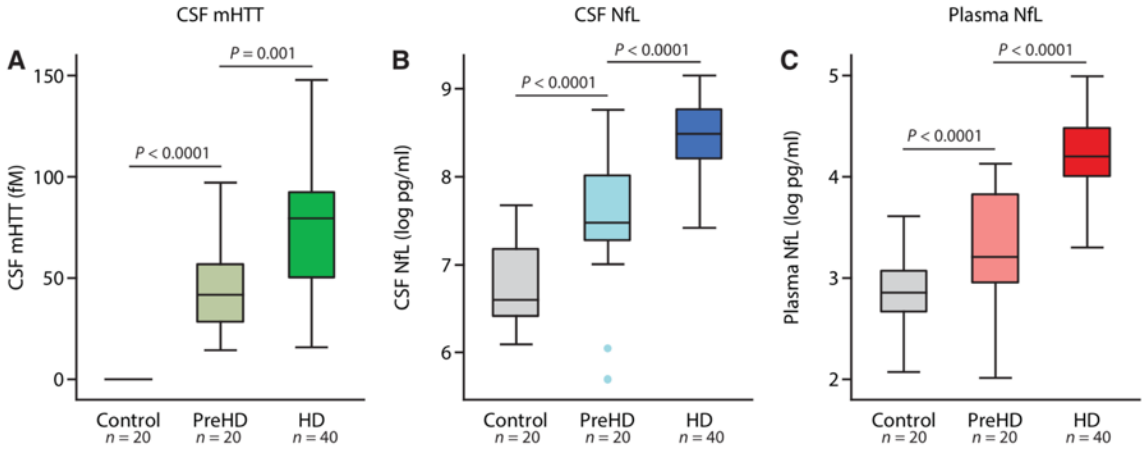

Figure 1.6: Comparison of several fluid biomarkers across disease stages. (Byrne et al., 2018)

These continuing efforts for the search of reliable biomarkers of disease progression is important to classify HD patients into different stages of the disease. It is also essential for the development of alternative therapeutic strategies as it will improve inclusion criteria in clinical trials and enhance the analysis of trial outcomes. In addition, early and precise biomarkers will provide more accurate prognosis of disease progression, granting additional time for planning disease management.

1.3.2. HD Integrating Stagging System (HD-ISS)

Since HD diagnosis is still based on the onset of motor symptoms efforts have been taken to better characterize the initial stages of the pathology. In 2019, HD progression was categorized into 3 phases based on clinical criteria: presymptomatic HD, prodromal HD, and manifest HD (Ross et al., 2019). The presymptomatic phase was defined by no cognitive changes and a DCL of 0 or 1 regarding motor signs. The prodromal phase was defined by a motor diagnostic confidence of 2 or 3 and the presence of minor neurocognitive changes while the manifest phase

corresponded to the formal motor diagnosis of HD with a DCL4. However, this classification was based uniquely on clinical data and did not consider biomarkers. Recently, the Huntington's Disease Regulatory Science Consortium has proposed the HD Integrating Stagging System (HD-ISS) (Figure 1.7) to classify individuals with 40 or more CAG repeats based on the underlying neurodegeneration, detectable symptoms and acquired functional changes (Tabrizi et al., 2022a). Carriers who are negative for all biomarkers and do not exhibit any symptoms or functional changes are classified in stage 0. The stage 1 includes individuals showing significant striatal atrophy measured by caudate and putamen volumetric MRI. The stage 2 comprises individuals with detectable motor or cognitive symptoms assessed by the UHDRS-TMS and the SDMT, respectively. Disease reaches the stage 3 when HD patients start having difficulties in performing daily activities. The total functional capacity (TFC) score of the UHDRS is then used to further subdivide stage 3 HD patients into mild, moderate, or severe phases depending on their level of dependence to execute routine activities.

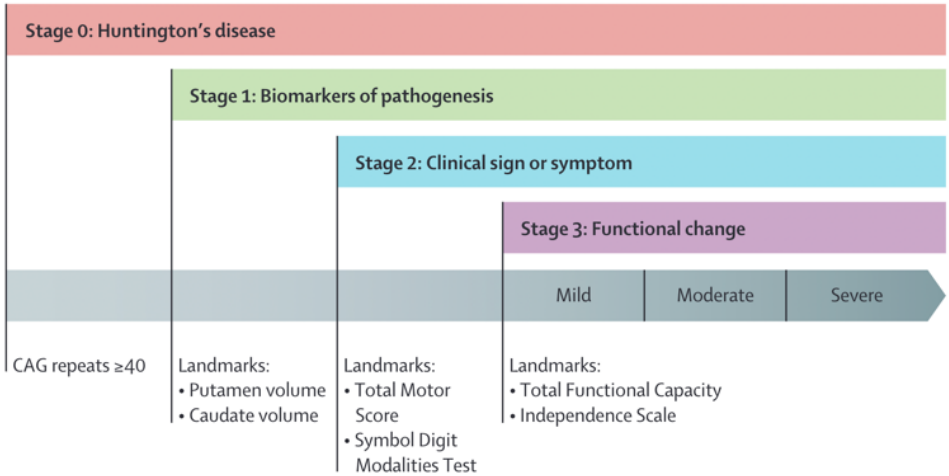

Figure 1.7: Cumulative stagging framework and landmarks of the Huntington's disease Integrated Staging System (HD-ISS). (Tabrizi et al., 2022a)

1.3.3. Disease management in HD

Currently there is no available therapies to stop the progression of the disease and all the available treatments focus on the control of the symptoms along with physiotherapy and psychological support. There are recommendations for the treatment of HD (Bachoud-Lévi et al., 2019), but effectiveness of the medications is based on few evidence. The choice of the medication considers the symptomatic profile of each HD patient and is dependent on the experience of the clinician (Stoker et al., 2022). The only drug approved for the treatment of chorea in HD is tetrabenazine. Tetrabenazine has been shown to treat chorea effectively, but it has the potential to exacerbate neuropsychiatric manifestations such as sedation and depression (Marshall, 2006). Therefore, the use of anti-psychotic drugs is usually preferred in patients exhibiting strong neuropsychiatric symptoms (Stoker et al., 2022). Among them, the olanzapine

is often the first-line agent but others antipsychotic drugs or even drug combination have also been used to treat both chorea and neuropsychiatric symptoms. Regarding anxiety and depression, the use of selective serotonin re-uptake inhibitors (SSRIs) such as citalopram and sertraline usually yield good results. Modafinil or mirtazapine can be usefull to restore sleep cycle when patients suffer from sleep disturbances.

A large set of anti-psychotic, anti-depressives and mood-stabilizing medications have been used to manage the multiplicity of HD symptoms but most of these treatments have shown no proven efficacy (Bachoud-Lévi et al., 2019). Additionally, symptoms are likely to become refractory after long periods of medication. It is then also important to consider non-pharmacological support for HD patients such as physiotherapy, psychotherapy, and occupational therapy. Increasing level of activity has suggested to be beneficial to maintain fitness, motor function, and gait during disease progression (Quinn et al., 2020; Thompson et al., 2013; Trovato et al., 2022). Finally, access to care packages and palliative treatments are able to relieve suffering with the aim to provide the best possible quality of life for patients in terminal stage of the disease.

Although there is still no cure for HD, we keep improving our understanding regarding the pathobiological mechanisms of the disease and multiple clinical trials aiming at modifying the disease progression are currently ongoing.

1.4 HTT protein

1.4.1. HTT protein structure

Since the identification of *HTT* gene (MacDonald et al., 1993), researchers have studied the characteristics and functions of the HTT protein. Huntingtin is a 348 kilodaltons (kDa) conserved protein of 3144 amino acids (aa) containing a polymorphic polyglutamine (polyQ) tract (Saudou & Humbert, 2016). The variable number of glutamines in this tract depends on the number of CAG repeats present on the *HTT* gene. In the normal population, the wtHTT polyQ tract is composed of 9 to 35 glutamines whereas individuals with more than 39 glutamines utterly experience HD symptoms at some point in life (mHTT). Guo and colleagues demonstrated by cryo-electron microscopy that wtHTT mainly adopts an α-helical structure (Guo et al., 2018). Most studies have focused on the characterization of the wtHTT N-terminal region as it contains the HD-causing expandable polyQ stretch. The wtHTT N-terminal comprises a highly conserved 17 aa sequence followed by the polymorphic polyQ tract and a variable proline-rich domain (PRD) (Figure 1.8). The first 17 aa are target for several post-translational modifications (PTMs) and they structurally form an amphipatic α-helix with functions related to subcellular localization (Atwal et al., 2007). While the polyQ tract can adopt several conformations, the PRD forms a less flexible proline-proline helix (Kim et al., 2009). Besides these three highly characterized structures, HTT

protein also contains huntingtin, elongation factor 3 (EF3), protein phosphatase 2A (PP2A), and the yeast kinase TOR1 (HEAT) repeats clusters, nuclear localization (NLS) and export (NES) signals. HEAT repeats are repetitive arrays of short amphiphilic α-helices involved in inter- and intra-molecular interactions (Déglon, 2017). In addition, several wtHTT variants and/or conformations have been reporter as a result of alternative splicing during transcription (Hughes et al., 2014; Ruzo et al., 2015), translation regulation (Xu et al., 2017) and/or from PTMs.

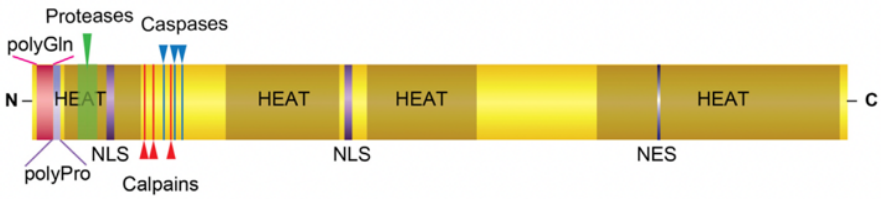

Figure 1.8: Schematic representation of the human HTT protein sequence. (Déglon, 2017)

1.4.2. wtHTT protein function and regulation

Huntingtin is expressed ubiquitously in many tissues, but higher levels are observed in the nervous system and testis (Marques Sousa & Humbert, 2013). It is mainly a cytoplasmatic protein, but it can also be found in the nuclear compartment. In the cytoplasm, wtHTT is usually found in association with organelles such as mitochondria, golgi apparatus, endoplasmic reticulum, and synaptic vesicles (Gil & Rego, 2008). Wild-type HTT is involved in several cellular processes including cellular dynamics, metabolism, proteostasis and gene expression (Saudou & Humbert, 2016). It is also highly regulated by PTMs, which regulate its intracellular localization, stability, and function (Koyuncu et al., 2017; Lontay et al., 2020; Saudou & Humbert, 2016; Tabrizi et al., 2020). These modifications include the attachment of chemical groups (e.g., phosphorylation, acetylation, palmitoylation, ubiquitylation, SUMOylating and glycosylation) and/or proteolytic cleavage by caspases and calpains (Figure 1.8). For instance, the simultaneous cleavage of wtHTT at the positions 552 and 586 generates a small fragment involved in the autophagosome formation (Martin et al., 2015) and the phosphorylation of serine residue at the position 421 controls the transport direction of vesicles in neurons (Colin et al., 2008). The high level of regulation and the great number of identified HTT interactors suggest that wtHTT mainly serves as molecular scaffolding, regulating the formations of protein complexes to coordinate cellular processes (Harjes & Wanker, 2003; Kennedy et al., 2022). In 2012, Shirasaki and colleagues identified 747 candidate proteins that are potentially complexed with wtHTT (Shirasaki et al., 2012). Recently, a plataform was generated to facilitate the visualization and exploration of the more than 3400 potential HTT interactors described in the HINT database (Kennedy et al., 2022).

One of the most described functions of wtHTT comprises the regulation of cellular processes through its interaction with microtubules and other cytoskeletal structures (Taran et al., 2020). For instance, wtHTT is implicated in the anterograde and retrograde transport of several

organelles and membrane vesicles in both axons and dendrites (Colin et al., 2008; Gauthier et al., 2004). In neuronal primary cilia, wtHTT plays a role in neurodevelopment and neuronal plasticity as it regulates the transport of essential molecules to the ciliogenesis (Haremaki et al., 2015; Keryer et al., 2011). During cell division, it regulates the orientation of the spindle (Elias et al., 2014; Godin et al., 2010). At the synapse level, wtHTT interacts with the postsynaptic density 95 (PSD95) protein to regulate the anchoring of receptors in the postsynaptic membrane such as N-methyl-D-aspartate (NMDA) and kainate receptors (Sun et al., 2001). It has also been shown to regulate endocytosis by interacting with proteins involved in the clathrin-mediated endocytosis (Engqvist-Goldstein et al., 2001; Waelter et al., 2001a). In addition, wtHTT regulates gene transcription and it has been found to bind to multiple transcription factors (Saudou & Humbert, 2016). Among them, wtHTT can interact with p53 and indirectly mediate death cellular programs such as apoptosis (Steffan et al., 2000). Other functions involve cellular homeostasis since wtHTT is involved in the autophagosome formation (Martin et al., 2015).

In summary, wtHTT scaffolding structure promotes the interaction with multiple proteins. The highly interactive profile of wtHTT translates implies the implication of wtHTT in several cellular mechanism, some of which are impaired or decreased by the presence of mHTT in HD. Therefore, additional knowledge on wtHTT function and regulation may help the characterization of pathological mechanisms in HD as well as determine safety of therapeutic approaches aiming at the reduction of mHTT in a non-selective manner.

1.5 Mutant HTT protein (mHTT) and pathogenic mechanisms in HD

1.5.1. HD is driven by mHTT toxic properties

It has been postulated that HD pathology simultaneously results from a toxic mHTT gain-of-function and from a partial loss-of-function of the wtHTT. There is several evidence supporting that HD is mainly driven by toxic properties of mHTT rather than just loss of wtHTT function: (i) HD presents an autosomal dominant inheritance pattern; (ii) there are no clear phenotypic differences between homozygous and heterozygous HD patients (MacDonald & Gusella, 1996; Myers et al., 1989; Wexler et al., 1987), (iii) individual with only one functional *HTT* allele (due to the inactivation of the other allele by a translocation) has no symptoms of HD (Ambrose et al., 1994) and (iv) the expression of mHTT is sufficient to induce HD-like phenotypic features in animal models (Farshim & Bates, 2018; Howland et al., 2020). However, whether a direct (in homozygous patients) or indirect partial loss-of-function of the *wtHTT* allele (via mHTT) is also implicated in the HD pathology is still not fully understood.

Among the different HTT variants, N-terminal mHTT fragments have been shown to play a major role in HD pathobiology (Yang et al., 2020a). Such highly toxic N-terminal fragments (containing the extended polyQ) are generated by proteolysis of the mHTT protein (Landles et al.,

2010) or by alternative splicing (Neueder et al., 2017; Sathasivam et al., 2013). While wild-type and mutant forms of HTT are target for proteases, the aberrant splicing seems to be CAG length-dependent and it is only observed in mutant transcripts (Sathasivam et al., 2013). The abundance of N-terminal mHTT fragments is well correlated with the disease progression and have been found both in HD models and in post-mortem HD brain samples (Neueder et al., 2017). They tend to aggregate and form nuclear and cytoplasmatic inclusions, which are one of the main histological features of HD. Aggregation starts with the nucleation of mHTT oligomers which potentially evolve into fibrils. These forms induce conformational changes of other proteins and recruit them into aggregation complexes, generating insoluble HTT inclusions (Boatz et al., 2020). Despite the ubiquitous expression of HTT and preferential striatal neurodegeneration in HD, these mHTT inclusions are most abundant in the cortical layers II/III, V and VI, which correspond to the same layers that are most vulnerable in HD (DiFiglia et al., 1997; Hedreen et al., 1991; Sotrel et al., 1991). Juvenile HD brains show a higher number of intranuclear inclusions, whereas brains of AHD subjects have mostly extranuclear inclusions (Becher et al., 1998; DiFiglia et al., 1997; Gutekunst et al., 1999; Maat-Schieman et al., 1999). This could influence the phenotypic differences between the two disease forms as intranuclear and cytoplasmatic inclusions exhibit distinct biochemical compositions and interactomes (Riguet et al., 2021). More recently, Hickman and colleagues evaluated the density and subcellular localization of HTT inclusions in post-mortem brain samples of HD individuals (Hickman et al., 2022). They found that the density of HTT inclusions correlates with CAG repeat length and gradually increases from caudal to rostral cortices. In addition, caudal cortices had predominantly intranuclear HTT inclusions, while more extranuclear inclusions were seen in the more frontal cortices. Although these recent studies have provided insights regarding distribution and composition of HTT aggregates, the role of the HTT inclusions on the disease evolution remains controversial. The formation of mHTT inclusions has been associated to neuronal death (Becher et al., 1998; Davies et al., 1997; DiFiglia et al., 1997; Ordway et al., 1997). However, it has been demonstrated that soluble forms of mHTT oligomers are more toxic than insoluble mHTT aggregates (Bates et al., 2015; Tabrizi et al., 2020). In line with the higher toxicity induced by soluble mHTT, it has been hypothesized that the formation of HTT inclusions protects neurons from mHTT toxicity by sequestering levels of potentially toxic soluble oligomeric species of mHTT (Arrasate et al., 2004; Lajoie & Snapp, 2010; Taylor et al., 2003). How these toxic soluble forms are generated and whether mHTT monomers can self-template into toxic oligomer species is still not known. Gropp and colleagues demonstrated that the expression of a toxic mHTT exon 1 fragment fused to the photoreceptor protein cryptochrome 2 (CRY2) (PolyQ-Opto) generated toxic mHTT oligomers and mHTT inclusions in control yeast, but not in prion-free (*PIN*$^-$) yeast (Gropp et al., 2022) (Figure 1.9). The formation of mHTT oligomers induced a heat stress response (HSR) in control yeast whereas the light-mediated formation of mHTT inclusions in *PIN*$^-$ yeast even decreased HSR. These observations suggest that insoluble mHTT inclusions are not the primary toxic species and that mHTT monomers may

require cross-seeding by pre-existing cellular prions to form toxic mHTT oligomers. Finally, mHTT can be released in the extracellular space and up taken by other cells (Pecho-Vrieseling et al., 2014), or be transmitted to neighboring cells via tunneling nanotube (TNT)-like membranous protrusions (Ramírez-Jarquín et al., 2022). Whether mHTT propagates in a prion-like manner is still unclear (Donnelly et al., 2022).

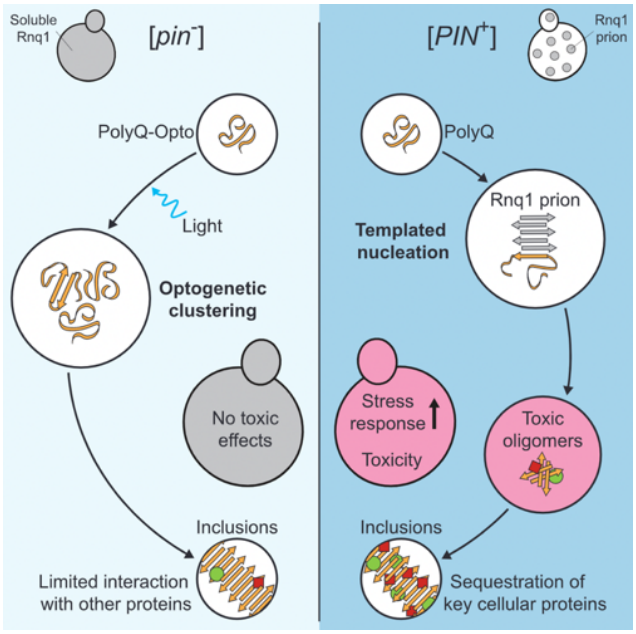

Figure 1.9: Hypothetical model for the generation of mHTT toxic species. The generation of soluble toxic mHTT oligomers and mHTT inclusions involves the templating by pre-existing cellular prions. (Gropp et al., 2022)

Canonical translation initiation requires the presence of the 5' cap and 3' polyA elements in the mRNA as well as an AUG start codon (Figure 1.10). However, RNA elements such as internal ribosome entry site (IRES) and nucleotide repeats can bypass some of these requirements and initiate translation. Repeat-associated non-AUG (RAN) translation efficiency is critically dependent on the repeat length, which typically ranges from hundreds to thousands of repeats (Cleary et al., 2018). Nevertheless, it has been discovered that CAG expansions in the *HTT* gene can generate toxic RAN proteins (Bañez-Coronel et al., 2015). This non-canonical translation can occur in all three reading frames in both CAG sense and CUG anti-sense transcripts (Chung et al., 2011), generating RAN proteins containing multiple alanines (polyAla), serines (polySer), cysteines (polyCys) and leucines (polyLeu). Bañez-Coronel and colleagues demonstrated that HD-RAN proteins show abundant positive staining in regions of the brain most affected by HD, including the striatum and, in JHD cases, also the cerebellum (Bañez-Coronel et al., 2015). Interestingly, RAN proteins foci were more predominant in the striatum and in white matter of the prefrontal cortex than mHTT inclusions. Furthermore, they showed the presence of RAN polyAla and polySer in the striatum of N171-82Q HD transgenic mice of 5 months-old of age. These results suggest that RAN proteins may modulate neuropathology in HD since they

are present in the most vulnerable regions to neurodegeneration. In addition, higher accumulation of polyAla and aggregation of polySer RAN proteins was observed *in vitro* when longer repeats were expressed, which can be related to the increasingly CAG length worsening effect on the HD phenotype (Bañez-Coronel et al., 2015). In addition, Gu and colleagues detected RAN polySer in the striatum and cortex of a bacterial artificial chromosome (BAC) transgenic mouse model of HD expressing full-length human *mHTT* with 120 uninterrupted CAG repeats (BAC-CAG) (Gu et al., 2022). They demonstrated that polySer proteins progressively accumulate from the age of 12-months-old, when multiple HD-related pathogenic phenotypes are already evident. The toxicity RAN proteins was further studied by Rudich and collaborators, who demonstrated that only polyLeu caused both neuropathological changes and functional defects in a CAG-derived RAN *Caenorhabditis elegans* model (Rudich et al., 2020). Recently, Das and colleagues observed that RAN-coding RNA accumulate in nuclear foci and when exported to the cytoplasm they associate with RNAs generating cytoplasmatic RNA-RAN protein agglomerates (Das et al., 2023). They suggest that these agglomerates disrupt the nucleocytoplasmic transport by sequestering multiple RNA-binding proteins. A study comparing knock-in (KI) HD mice expressing N-terminal mHTT expansion (140Q) or only HTT-CAG-mediated RAN proteins (due to the loss of the ATG start codon) did not find any RAN-mediated toxicity at 7 months of age (Yang et al., 2020b). The authors concluded that when mHTT is expressed at physiological endogenous levels in KI mice, eventual production of RAN proteins has minimal or no contribution to the HD pathogenesis. However, as observed in the BAC-CAG (Gu et al., 2022), aggregation of RAN proteins may be only detectable at later stages of the disease.

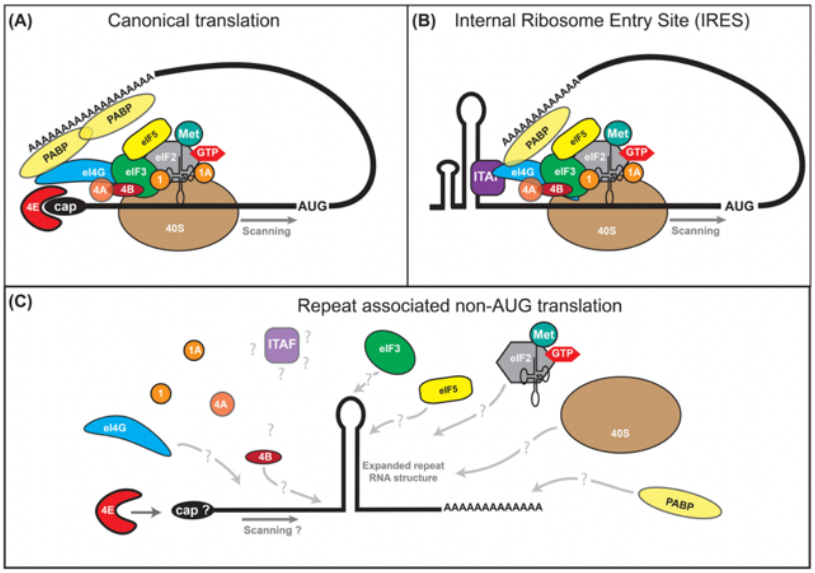

Figure 1.10: Translation initiation mechanisms. (A) The canonical translation initiation involves the binding of the 5' mRNA cap and mRNA polyA tail followed by scanning of the mRNA 5'UTR in a 5' to 3' direction. **(B)** The internal ribosome entry site (IRES) initiation occurs in a 5' cap-independent manner from multiple viral and cellular RNA sequences**. (C)** The repeat-associated non-ATG (RAN) translation initiation is a repeat-length–dependent process that allows for initiation at non canonical codons either within or adjacent to the expanded repeat tract. It is still unclear whether RAN translation is dependent on 5' cap and/or scanning mechanisms. (Cleary et al., 2018)

In summary, while toxic oligomeric forms of mHTT seem to be the main drivers of mHTT-induced toxicity, its toxicity may be influenced by other cellular existing proteins/factors or by its propagation mechanisms throughout the brain. In addition, there has been proposed that polyQ-independent toxicity driven by RAN proteins and/or RNA species transcribed from the *mHTT* allele may also contribute for the disease phenotype. Finally, as discussed previously, the loss of wtHTT function may also modulate or promote pathogenic mechanisms.

1.5.2. Pathogenic molecular mechanisms in HD

1.5.2.1. Disruption of protein homeostasis

Protein homeostasis depends on multiple protein clearance mechanisms such as the ubiquitin-proteasome system (UPS) and autophagy (Koyuncu et al., 2017). They are essential to regulate protein composition required to a particular cell type and/or status. Lin and colleagues observed that the proteasome system is impaired in mHTT-expressing striatal cells derived from HD mice (Lin et al., 2013). They showed that the dysregulation of the cyclic AMP (cAMP) - protein kinase A (PKA) pathway is induced by a mHTT-dependent alteration of the proteosome activity. The presence of ubiquitin and proteosome subunits in mHTT inclusions suggests that mHTT aggregates may sequester components of the UPS (Díaz-Hernández et al., 2003; Schipper-Krom et al., 2014). Soluble mHTT has been postulated to affect UPS activity by blocking its access to other ubiquitinated substrates (Ortega & Lucas, 2014) but it seems that the impairment of this clearance mechanism most likely results from the overall disrupted protein folding homeostasis (Hipp et al., 2012). This is consistent with the decrease of basal levels of chaperones during HD progression (Labbadia & Morimoto, 2013). In addition, N-terminal mHTT fragments were shown to be fully degraded by the UPS itself (Juenemann et al., 2013; Michalik & Van Broeckhoven, 2004), so its impairment further prompts the accumulation of these toxic fragments. In agreement with this, the pharmacological inhibition of the UPS has been shown to increase aggregation of mHTT (Waelter et al., 2001b).

Whereas UPS is specialized in the clearance of damaged proteins, autophagy-lysosomal system degrades protein complexes and damaged organelles. Huntingtin interacts with the autophagy cargo receptor p62 and mediates selective macro autophagy (Rui et al., 2015). In HD models and patient cells, the p62-mediated cargo recognition disruption leads to the formation of empty autophagosomes (Martinez-Vicente et al., 2010). Importantly, these features were observed in both neuronal and non-neuronal cells. The impact of the dysregulation of autophagy in HD pathology is further supported by the improved phenotype in HD models when the autophagy-lysosomal system is enhanced (Ravikumar et al., 2004).

1.5.2.2. Mitochondrial dysfunction

Mitochondria represent the major bioenergetic cellular core and their integrity is critical for preserving cell function and viability. In HD-derived cells, the reduction of adenosine 5′-triphosphate (ATP) production is inversely correlated with the polyQ length (Seong et al., 2005). Song and colleagues also observed a low energetic production at the synaptic level in HD models and high levels of mitochondrial fragmentation (Song et al., 2011). These observations in HD rat neurons and patient's fibroblasts preceded any sign of mHTT aggregation, suggesting that these alterations are induced by soluble forms of mHTT. They suggested that higher numbers of fragmented mitochondria could be due to the mHTT-dependent overactivation of the dynamin-related protein 1 (Drp1). However, high levels of fragmented mitochondria can also be explained by the decrease levels of macro autophagy. In post-mortem brain tissues from HD patients, Kim and colleagues observed a grade-dependent reduction in the number of mitochondria in striatal neurons (Kim et al., 2010). They estimated that advanced HD-patients had loss up to 66% of the mitochondria when matched to aged controls. Mitochondrial size and morphogenesis were also affected with the disease progression, with decreased mitochondrial fusion and enhanced mitochondrial fission. In addition, the activity of mitochondrial enzymes and, in particular, the mitochondrial complex II has been found to be reduced in HD models (Benchoua et al., 2006; Damiano et al., 2013) and in the striatum of HD patients (Browne et al., 1997; Gu et al., 1996). Others have reported defects in mitochondrial transport and polarization, with mitochondria depolarizing at lower calcium levels (Orr et al., 2008; Panov et al., 2002), or defects in the transcription of mitochondrial genes (Johri et al., 2013). The mutant HTT is directly implicated in mitochondrial dysfunction (Yablonska et al., 2019). Yablonska and colleagues described that mHTT presents higher affinity than wtHTT to interact with the translocase of mitochondrial inner membrane 23 (TIM23) complex and suggested that this stronger interaction inhibits the import of mitochondrial proteins, altering the mitochondrial proteome and function.

1.5.2.3. Disruption of the nuclear import/export

The nuclear trafficking is mediated by the nuclear pore complexes. Defective nuclear trafficking is present in multiple models and HD-derived brain tissues and reconstitution of the nuclear transport ameliorated neuropathology in HD models. (Grima et al., 2017). A critical mechanism regulating the flow of molecules between the nucleus and cytoplasm is the Ran gradient generated by RanGAP1 (Cavazza & Vernos, 2016). Similar to the mitochondrial TIM23 complex, mHTT was found to have higher affinity to RanGAP1 than wtHTT (Hosp et al., 2015), promoting the alteration of the Ran gradient between cytoplasm and nucleus. In addition, RanGAP1 and other nuclear pore proteins such as the nucleoporins NUP62 and NUP88 are increasingly sequestered to the mHTT aggregates as disease progresses (Grima et al., 2017).

1.5.2.4. Transcriptional dysregulation

Huntingtin translocates between the cytoplasm and nucleus, and it binds to multiple transcription factors, regulating their activity. Transcriptional alterations in HD have been shown to occur at early phases of the disease. Microarray analysis of cultured striatal-derived cells expressing N-terminal mHTT fragments revealed alteration in the expression of genes involved in cell signaling, lipid metabolism, vesicle trafficking and transcription (Sipione et al., 2002). These alterations occurred very quickly after mHTT expression, even before the formation of mHTT aggregates. Later, Hodges and colleagues also detected alterations in the transcriptome of homogenates from early symptomatic HD brains (Hodges et al., 2006). Interestingly, they noticed that alterations in the transcriptome profile of whole brain homogenates were significantly different from the ones observed in the neurons captured by laser microdissection (Hodges et al., 2006). This suggested that glial cells are a major contributor to the alteration of gene expression profile in HD brains. More recently, we used laser microdissection and chromatin immunoprecipitation sequencing (CHIP-seq) to individual analyze the epigenetic and transcriptomic alterations in neurons, astrocytes, and microglia both in HD animal models and in HD post-mortem brain tissues (Merienne et al., 2019). We detected a general trend for gene downregulation in striatal neurons and gene upregulation in glial cells. In addition, altered gene expression profiles were also different between distinct neuronal cells in the striatum. These results indicate that mHTT induces cell-type specific transcriptomic changes and also highlight the important role of non-neuronal cells in HD pathobiology.

1.5.3. Pathogenic cellular mechanisms in HD

1.5.3.1. Cortico-striatal dysfunction and vulnerability

HD is pathologically characterized by initial selective neurodegeneration of the striatum and cortex while other regions such as thalamus and hippocampus are affected at later stages of the disease (Johnson et al., 2021; Waldvogel et al., 2014). Neurodegeneration in HD involves a long process where neuronal dysfunction features the early symptoms of the disease before cell death takes place. The most striking brain morphological changes of HD are the striatal atrophy accompanied with ventricle enlargement (Bates et al., 2015; Tabrizi et al., 2020). GABAergic striatal projection neurons (SPNs) represent 95% of the striatal neuronal population. They are divided into striatonigral SPNs (which project to the internal globus pallidus and substantia pars reticulata and express dopamine D1 receptors) and striatopallidal SPNs (which project to the external globus pallidus and express dopamine D2 receptors) (Parent & Hazrati, 1995). The D1-positive striatonigral SPNs are part of the direct pathway (dSPNs) of the basal ganglia circuitry and play important roles on the movement initiation whereas D2-positive striatopallidal SPNs incorporate the indirect pathway (iSPNs) and inhibit movement. While iSPNs are preferentially lost in presymptomatic and early symptomatic HD mouse models, dSPNs can be unaffected until

later stages of the disease (Albin et al., 1992; Menalled et al., 2000; Sapp et al., 1995). This time-dependent preferential loss of different SPNs populations correlates with the disease phenotype as the initial functional loss of iSPNs can lead to deficits in controlling voluntary movements (e.g., chorea). The subsequential neurodegeneration of SPNs of the direct pathway also fits symptomology progression as HD patients show difficulties to stimulate voluntary movements at later stages of the disease (e.g., rigidity).

The striatum is a major processing center for excitatory, glutamatergic inputs from the cortex, which is also affected in HD (Blumenstock & Dudanova, 2020; Bunner & Rebec, 2016; McColgan et al., 2020) (Figure 1.11). Although cortical atrophy is more heterogeneous between HD patients, it can be detected even before the motor onset (Aylward et al., 2013; Johnson et al., 2021). At later stages, the loss of pyramidal neurons is evident in many cortical regions and can be reduced up to 30% as measured in post-mortem brain tissues from HD patients (Bunner & Rebec, 2016). Cortical projecting neurons (CPNs) can be divided into Intratelencephalic (IT) and pyramidal tract (PT) neurons (Harris & Shepherd, 2015). While IT neurons project to the ipsilateral striatum and contralateral striatum and cortex, the PT neurons send terminations to subcortical regions and to the spinal cord. The PT neurons are usually located at deeper cortical layers and the IT neurons can be found on the layers 2, 3, 5, and 6 of the cortex, which are the main affected cortical layers affected in HD (Cowan & Raymond, 2006; McColgan et al., 2020) (Figure 1.11). The observation that patients display deficient cortico-striatal connectivity and white matter volume loss suggests that IT neurons are affected at early stages of the disease. The simultaneous degeneration of both SPNs and CPNs suggests that HD patients present dysfunctional cortico-striatal connectivity. Abnormal activity of cortical circuits has been reported in multiple HD mouse models (Blumenstock & Dudanova, 2020). Overall, these studies have found exacerbated neuronal firing in the striatum and cortex.

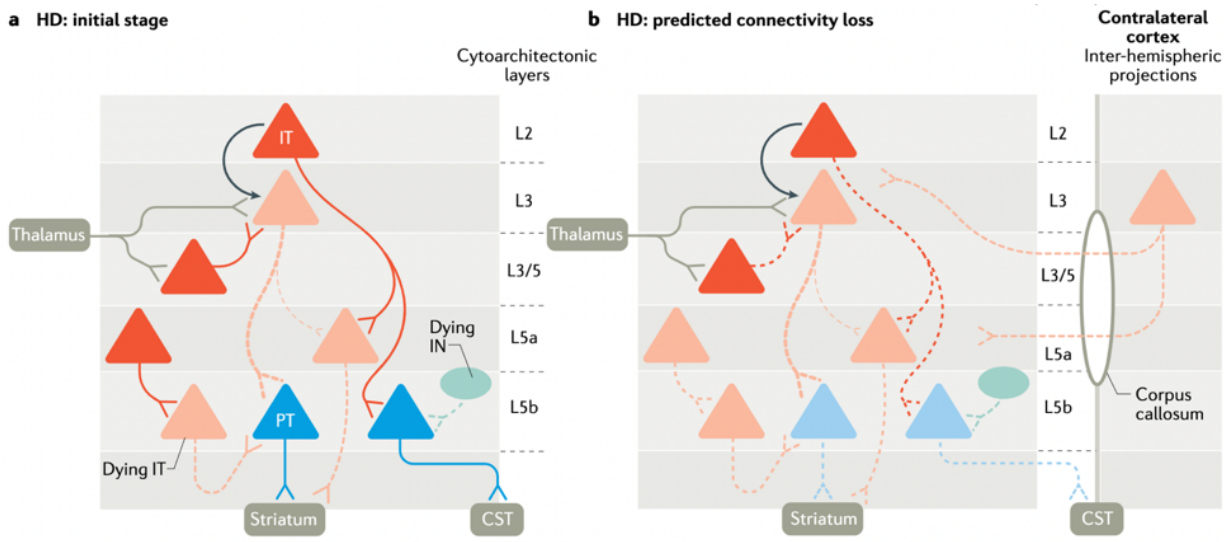

Figure 1.11: Layer-specific and cell-specific connectivity loss in HD patients. (McColgan et al., 2020)

Several hypotheses have been raised to explain the selective striatal and cortical neurodegeneration in HD. One of the hypotheses postulates that cortical glutamate-dependent excitotoxicity is the main driver of SPNs and CPNs neurodegeneration (Zuccato et al., 2010) (Figure 1.12). It is supported by the exacerbated cortical and striatal neuronal firing observed in multiple models. The overstimulation of glutamatergic receptors induces intracellular calcium release, mitochondrial damage, activation of pro-apoptotic signals and altered neuronal firing patterns (Lee et al., 2013). Overstimulation can be induced by increased responsiveness of NMDA receptors. While synaptic NMDA receptors have been shown be protective against mHTT toxicity, extra-synaptic NMDA receptors are able to prompt apoptosis by impairing the cAMP response element-binding protein (CREB) signaling (Okamoto et al., 2009; Papadia & Hardingham, 2007). The expression of mHTT *in vitro* promotes the phosphorylation of the NR2B subunit of NMDA receptors subunit, making them more susceptible to activation (Song et al., 2003). In addition to overstimulation, augmented levels of synaptic glutamate can also result from deficits in the glutamate uptake (Liévens et al., 2001).

Another hypothesis explaining striatal degeneration in HD is related to deficits in brain-derived neurotrophic factor (BDNF) signaling (Gauthier et al., 2004; Morigaki & Goto, 2017). BDNF is a neurotrophin involved in growth and maintenance of neurons and synapses and most of the striatal BDNF is produced in the cortex and delivered in the striatum by the CPNs (Zuccato & Cattaneo, 2015). Deficits in both BDNF production and transport have been shown in post-mortem tissues from HD patients and models of HD (Zuccato & Cattaneo, 2015). The cortico-striatal degeneration due to the deficiency of BDNF is also supported by studies testing the neuropathology when of reducing the expression of BDNF. The ablation of BDNF expression in the developing cortex reduces SPNs soma size, decreases complexity of dendritic arborization (Rauskolb et al., 2010) and induces striatal gene expression profiles more similar to the ones observed in HD (Strand et al., 2007).

1.5.3.2. The role of astrocytes in HD

Astrocytes are key regulatory cells in the CNS as they control ion concentration on the extracellular space, regulate neurotransmitter levels at the synaptic clefts and supply nutrients to neurons (Wilton & Stevens, 2020). During development, they are involved in synaptogenesis and synaptic elimination. Regarding astrocytic alterations in HD, astrocytes present different morphology and abnormalities in their electrical properties (Wilton & Stevens, 2020). Astrocytic activation (or astrogliosis) is observed in HD post-mortem tissues and increases with the progression of the disease (Faideau et al., 2010). In addition, astrocytic neurotoxic reactive states are enriched in post-mortem tissues from HD individuals at later stages of the disease (Diaz-Castro et al., 2019; Liddelow et al., 2017). In HD models, Tong and colleagues demonstrated that astrocytes in R6/2 and zQ175 HD mouse models display decreased function Kir4.1 potassium channel, promoting higher levels of extracellular potassium and leading to higher excitability of

SPNs(Tong et al., 2014) (Figure 1.12). Importantly, they showed that decreased protein levels of Kir4.1 are observed in astrocytes containing mHTT aggregates. The rescue Kir4.1 protein levels in astrocytes not only restored astrocyte-specific abnormalities but also corrected electrophysiological properties of SPNs in a non-cell autonomous way (Tong et al., 2014). Others have demonstrated that dysregulation of calcium signaling in astrocytes also plays a key role in regulating SPNs activity (Yu et al., 2018). They showed that calcium signaling in striatal astrocytes is modulated by GABA neurotransmission and its reduction alters SPNs firing, inducing exacerbated self-grooming behavior in wild-type mice. The self-grooming phenotype could be rescued in both altered wild-type mouse and R6/2 HD model by blocking astrocytic GABA-dependent modulation. In addition to abnormalities in astrocytic cell signaling, the inability of astrocytes to uptake extracellular glutamate has also been implicated in HD (Figure 1.12). It has been shown that levels of glutamate uptake receptor 1 (GLT-1) are decreased in mouse models and HD post-mortem tissue (Faideau et al., 2010; Wilton & Stevens, 2020). Evidence suggests that GLT-1 deficiency in HD is a consequence of the abnormal calcium signaling (Jiang et al., 2016; Liévens et al., 2001) and its rescue also ameliorates HD-like symptoms (Jiang et al., 2016). Using FRET-based proximity assay, Octeau and colleagues demonstrated that astrocytes processes are decreased in the cortico-striatal synapses but increased in the thalamic-striatal connections in the brain of R6/2 HD mice (Octeau et al., 2018). They suggested that the reduced astrocytic support of cortico-striatal connections could be one of the explanations for their selective degeneration in HD. Studies focusing on the HD-driven role of astrocytes have revealed that these glial cells are key for HD pathology. Bradford and colleagues demonstrated that the astrocytic expression of full-length mHTT with 160 CAG repeats is sufficient to induce some of the HD behavioral phenotypes (Bradford et al., 2009). Similarly, the lentiviral-mediated expression of mHTT in striatal astrocytes recapitulated progressive HD phenotype and induced lower expression of both glutamate transporters, GLAST and GLT-1, and of glutamate uptake (Faideau et al., 2010). Benraiss and colleagues demonstrated the importance of astrocytes and glial cells in general by generating human glial HD chimeras (Benraiss et al., 2016). The engraftment of human glial progenitor cells (hGPCs) expressing mHTT in wild-type mice resulted in abnormal neuronal physiology and deficits in motor performance whereas wild-type hGPCs grafted in R6/2 HD mice delayed HD pathology. The lowering of mHTT expression in R6/2 mice reduced HD astrocyte molecular signatures (Diaz-Castro et al., 2019) and the ablation of astrocytic mHTT expression slowed the motor decline and ameliorated depressive-like behaviors in the BACHD mouse model (Wood et al., 2019). It also normalized SPNs activity and rescue striatal volume compared to the mice expressing mHTT in both neurons and astrocytes.

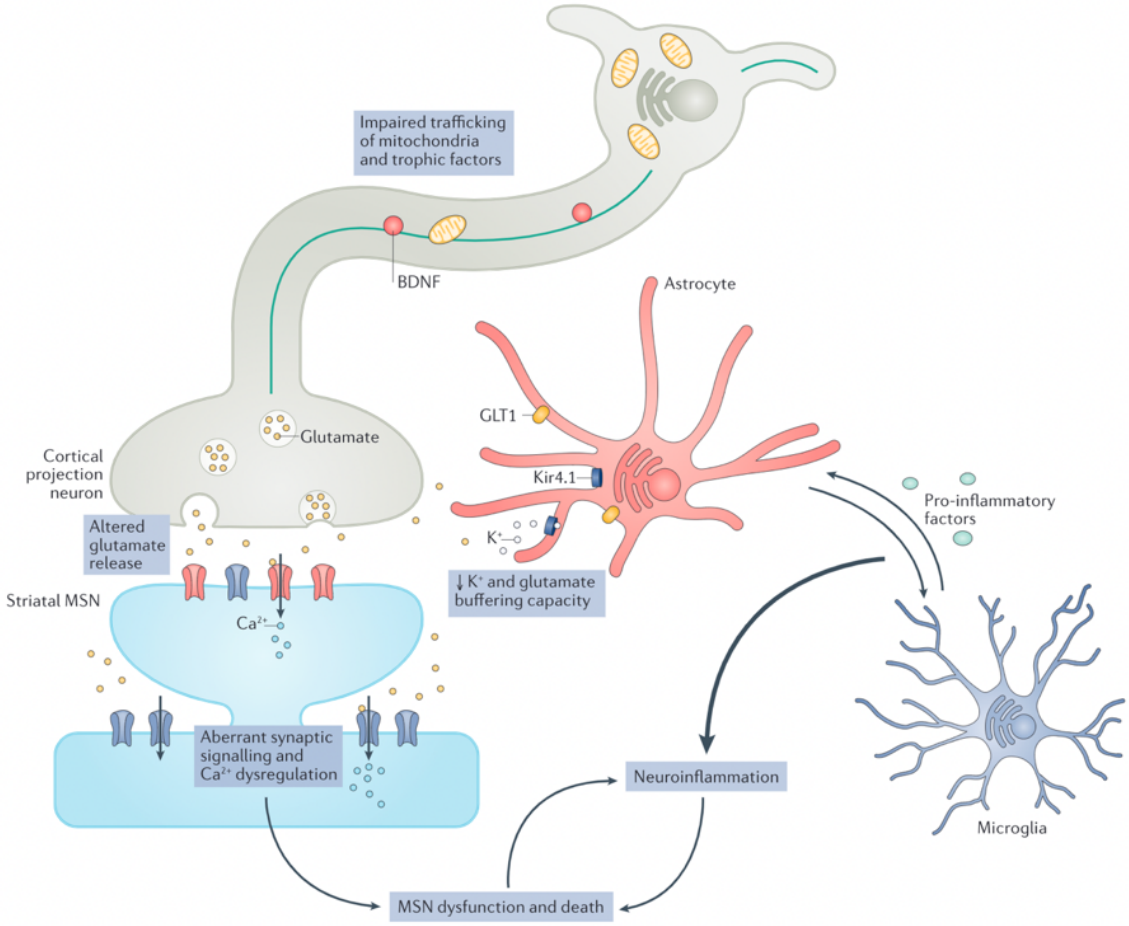

Figure 1.12: Illustration of some cellular pathogenic mechanisms in HD. (Caron et al., 2018)

1.5.3.3. The role of microglia in HD

Microglia are the resident macrophages of the CNS and play an important role in neurogenesis regulation and development of neuronal circuitries (Wilton & Stevens, 2020). Contrarily to neurons, microglial cell numbers do not seem to decrease with the disease progression but instead they present different morphology and activation states (Diaz-Castro et al., 2019). Microglial cells in HD present deficits in motility and upregulation of pro-inflammatory cytokines (Figure 1.12). Although striatal levels of cytokines such as the tumor necrosis factor alpha (TNFα), interleukin 6 (IL-6), interleukin 2 (IL-2) and interleukin 1 beta (IL1β) are elevated in several HD mouse models, Pido-Lopez and colleagues demonstrated that dendritic cells could also be a source of such high cytokine levels (Pido-Lopez et al., 2018). Nevertheless, Crotti and collaborators showed that microglial expression of mHTT induces cell-autonomous transcriptional activation of several inflammatory response genes and promote non-cell autonomous toxic effects on neurons (Crotti et al., 2014). The upregulation of pro-inflammatory cytokines was associated with the overexpression of galectin-3 (LGALS3) in microglial cells (Chen et al., 2015; Jeon et al., 2010). Siew and colleagues showed that levels of LGALS3 correlate with disease progression in both plasma and brain samples from HD patients and R6/2 HD mouse model (Siew et al., 2019). The lowering of LGALS3 in the striatum of R6/2 mice prevented decline of motor performance,

extended lifespan and prevented striatal loss of dopamine- and cAMP-regulated phosphoprotein, 32 kDa (DARPP32)-positive neurons. Although neuroinflammation induced by pro-inflammatory cytokines certainly play a role in HD neurodegeneration, careful should be taken as they also have been found to be beneficial for nerve repair (Wilton & Stevens, 2020).

In summary, cellular dysfunction caused by the HTT mutation in HD results from the dysregulation of multiple vital cellular processes that leads to toxicity over time and promotes neurodegeneration in a cell autonomous and non-cell autonomous manner. Importantly, not only neuronal cells but also glial cells play an important role in neurodegeneration in HD. The cortical glutamate excitotoxicity and the loss of trophic support in the striatum are the current two main hypothesis to explain the selective degeneration of cortico-striatal circuitry in HD. However, the primary causes promoting neurodegeneration in these specific brain regions in HD are unclear.

1.6 Genetic characterization of Huntington's disease

1.6.1. *HTT* gene and expression

The human *HTT* gene contains 67 exons spanning 180 kilobases and it is located at the short arm of chromosome 4 (4p16.3) (Ambrose et al., 1994). The *HTT* promoter has high GC content and lacks TATA and CCAAT regulatory elements (Thomson & Leavitt, 2018). Proximal *HTT* promoter and 5' untranslated region (UTR) sequences are highly conserved between humans and mice and include multiple putative regulatory regions, such as p53, Sp1 and HDBP1/2 binding sites (Coles et al., 1998; Feng et al., 2005; Lin et al., 1995; Tanaka et al., 2004), but their involvement in the regulation of *HTT* transcription is still not fully understood (Thomson & Leavitt, 2018). The transcriptional start site of *HTT* gene has been defined at multiple positions ranging -145 and -129 nucleotides (nt) upstream to the translational start site (Lee et al., 2002; Lin et al., 1995). There is mainly three physiological *HTT* transcripts due to alternative polyadenylation at the 3' UTR (Romo et al., 2017). *HTT* transcripts are expressed in a wide range of tissues, but the longest transcript of 13711 kilobases (kb) seems to be enriched in the brain (Lin et al., 1993). Romo and colleagues showed that the abundance of these 3'UTR *HTT* transcript isoforms is altered in HD (Romo et al., 2017). Other isoforms have also been reported due to exon skipping or retention of intronic regions during splicing (Hughes et al., 2014; Ruzo et al., 2015). To date, the most relevant isoforms in the context of the disease are two small transcripts containing the exon 1 and a partial sequence of the first intron, named *HTT1*α (Neueder et al., 2017; Sathasivam et al., 2013). Interestingly, Neueder and collaborators found that the abundance of these short transcripts increases in proportion to the presence of longer CAG repeats (Neueder et al., 2017). They are generated by an incomplete splicing of the *HTT* transcript and their translation results in the production of the highly pathogenic exon 1 HTT

truncated protein. In addition, *HTT1α* transcripts are also prone to be retained into nuclear transcript clusters, which can then recruit transcription factors and alter the normal transcription profile (Fienko et al., 2022).

1.6.2. Polymorphisms and haplotypes

The presence of single nucleotide polymorphisms (SNPs) in high pairwise linkage disequilibrium with the HD mutation implies that the mutation originates from common ancestors but not from a single founder (Chao et al., 2017; Fang et al., 2023; Kay et al., 2015, 2019; Warby et al., 2009, 2011). In addition, the association of specific SNPs with the CAG expansion suggests that limited recombination occurs around the *HTT* gene sequence. These observations introduced the concept of HD haplotypes, which identify HD mutations (or HD chromosomes) with shared ancestry. Hayden and collaborators have further organized haplotypes into haplogroups and showed that most of the HD chromosomes in subjects from Europe, America, South Asia, Middle East as well as in mixed South Africans belong to the haplogroup A (Kay et al., 2015, 2019). More specifically, they identified the A1 and A2 *HTT* haplotypes has the most common haplotypes of HD chromosomes. While the A1 haplotype is defined by three intragenic and two extragenic SNPs (rs72239206, rs149109767 and rs362307), the A2 haplotype is defined by five intragenic SNPs (rs2798235, rs363080, rs363107, rs362313 and rs2530595). Interestingly, in populations where HD is less prevalent such as East Asians and black South Africans, the mutation is not associated to these haplotypes (Kay et al., 2019). This evidence supports their hypothesis that HD mutations occur preferentially on specific haplotypes likely due to specific cis-acting elements that could influence the instability of the CAG tract (Warby et al., 2011). Also, they observed that control chromosomes were preferentially associated to the haplogroup C in most populations but not in populations from Latin America (Kay et al., 2019). These results have been confirmed by Jong-Min Lee in collaboration with James Gusella, who also performed haplotype stratification in HD for the European population (Chao et al., 2017). Although they defined haplotypes based on different sets of SNPs, they identified that hap.01 and hap.02 (corresponding to A1 and A2 Hayden's haplotypes, respectively) were the most common in HD chromosomes and that hap.08, hap.14 and hap.16 (corresponding to Hayden's haplogroup C) were enriched in the control chromosomes (Figure 1.13).

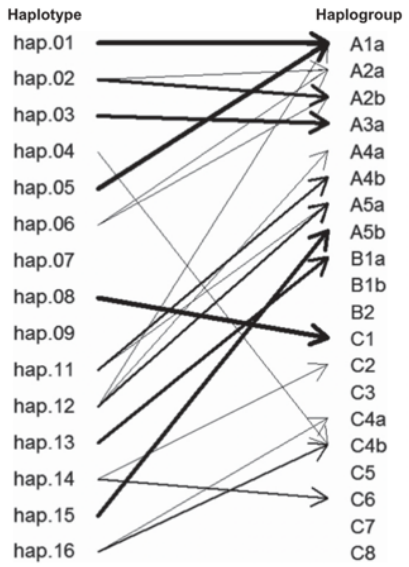

Figure 1.13: Correspondences of haplotypes (Lee and Gusella's group) and haplogroups (Hayden's group). (Chao et al., 2017)

1.6.3. CAG repeat and other genetic modifiers in HD

HD is the most frequent disorder caused by an abnormally expanded polyQ tracts in the coding protein (CAG repeats in DNA) (Lieberman et al., 2019). In the *HTT* gene, this polymorphic CAG repeat coding for the toxic expanded polyglutamine tract is followed by a less variable proline-encoding CCG repeat sequence. At the DNA level, CAG repeats adopt heteroduplex secondary structures that are sensed as damaged DNA and prone to misrepair during transcription(Lee & McMurray, 2014). These features make CAG repeats unstable and prone for expansion. The expansion event seems to be linked to a particular predisposition to instability during spermatogenesis (Goldberg et al., 1993; Kremer et al., 1995). Semaka and colleagues noticed that CAG tract displays increased instability when there are more than 33 repeats, which evolves in a nonlinear relationship with the length of CAG repeats (Semaka et al., 2013).

Although a number higher than 39 CAG repeats invariably determines the appearance of HD symptoms, the length of CAG only explains 60% of the individual variation of the age of motor symptom onset (Andrew et al., 1993; Djoussé et al., 2003; Duyao et al., 1993). More than 95% of the mutated *HTT* alleles in HD contain an uninterrupted CAG repeat expansion followed by CAACAG. Because the trinucleotide CAA also encodes for glutamine, the majority of mutated *HTT* alleles encode for two more extra glutamines than the number of uninterrupted CAG repeats. A study by the Genetic Modifiers of Huntington's Disease (GeM-HD) Consortium found that age of onset is anticipated in HD individuals carrying mutated *HTT* with pure CAG repeats and delayed in individuals carrying the CAACAG duplication (Lee et al., 2019). Based on this evidence, they assumed that the number of uninterrupted CAG repeats and not the polyQ length drives the timing of HD onset. The genome-wide association study (GWAS) on more than 9000 HD subjects in this report pointed for several genes involved in DNA maintenance and transcriptional regulation that

may play a contribution on the timing of disease onset. Among the identified genes involved in DNA repair, the MutS Homolog 3 (*MSH3*) and Fanconi anemia FANC1/FANCD2-associated nuclease 1 (*FAN1*) also achieved significance in the transcription-wide association study (TWAS). The reduced expression of *MSH3* and increased expression of *FAN1* genes were associated to later disease onset. While *MSH3* gene had already been identified as a potential disease modifier in the TRACK-HD trial (Moss et al., 2017), FAN1 was later shown to influence HD progression by stabilizing the CAG expansion (Goold et al., 2019). In addition, the GWAS also identify three modifiers at the DNA Ligase 1 (*LIG1*) locus. One of the modifications have been shown to increase LIG1 expression and promote CAG repeat instability (Castel et al., 2009) and other translates into a deleterious missense mutation and associates with a later onset. The identification of DNA repair genes as modifiers of HD and the inherent instability of the CAG tract suggests that HD pathology depends on the somatic expansion of the CAG repeat. This assumption is further supported by the existence of increased CAG repeat lengths in post-mortem tissues of HD patients (Pinto et al., 2020; Swami et al., 2009). In addition, CAG expansion occurs more frequently in neurons than glia and is more pronounced in the striatum and several cortical areas, both of which are heavily affected in HD. Currently, there is a clinical study ongoing (SHIELD HD - NCT04406636) to evaluate CAG somatic expansion in multiple biofluids and to assess whether it can be used to characterize HD progression. In addition, the modulation of DNA repair pathways to prevent CAG expansion are emerging as therapeutic strategies for HD. Two lead target candidates that are being preclinically tested are the FAN1 and MSH3 (Iyer & Pluciennik, 2021; Porro et al., 2021).

In summary, HD neuropathology is currently hypothesized to involve two distinct phases: (1) an initial stage where CAG tract reaches a critical threshold length prone for somatic expansion and, (2) a second phase where the expanded CAG repeats somehow trigger the neuropathologic effects. Concerning the CAG repeat-mediated toxicity, the production of toxic oligomeric forms of mHTT has been the main hypothesis for the last decades but emerging evidence suggests that the contribution of expanded CAG repeats to HD phenotype may be beyond the encoding the polyQ peptides, including toxicity mediated by the RNAs containing the CUG expansion (Chung et al., 2011; Nalavade et al., 2013) and RAN proteins (Bañez-Coronel et al., 2015). Also, the greater instability of CAG repeats in the striatum and cortical regions may explain the selective neurodegeneration observed in HD (Pinto et al., 2020; Swami et al., 2009).

1.7 Modeling Huntington's disease pathology

Despite the monogenic nature of HD, the molecular and cellular mechanisms implicated in the disease phenotype are quite complex. Such a variety of mechanisms (e.g., *m*HTT toxicity at DNA, RNA or protein level, cell-autonomous and non-autonomous pathological mechanisms, and selective brain degeneration) are difficult to be simultaneously recapitulated in a single HD model. Furthermore, another challenge in modeling HD is that the pathology develops over decades. Therefore, HD models should recapitulate the maximum of disease hallmarks in a shorter time period.

1.7.1. *In vitro* modeling of HD

A multiplicity of different HD models has been used to recapitulate HD *in vitro*. Most of them rely on the (1) transduction of non-HD immortalized cell lines with the pathogenic N-terminal HTT fragments or (2) culture of cells from HD patients and *in vivo* HD models. Although non-HD cell lines are useful as proof-of-concept for many studies, these models usually poorly recapitulate the physiological mHTT expression levels. In addition, transgene delivery to non-HD cells does not allow the study of the mutation on its normal chromatin environment but rather focus on the high transgene expression levels. Furthermore, the lack of relevant neuronal or glial signatures in these cell lines further discourages their use for functional analysis. The establishment of induced pluripotent stem cells (iPSCs) allowed the opportunity to study disease mechanisms in cells derived from patients (Takahashi et al., 2007; Yu et al., 2007). Unlike non-HD cell models, HD-iPSCs retain the natural genome structure of the patient and can be differentiated into specific neuronal or glial populations to study the disease in different cellular contexts (Kaye et al., 2022). Patient-derived iPSCs have been successfully differentiated into many cell types, including neural progenitor cells (HD-NPCs) (Kedaigle et al., 2020; Lim et al., 2017), striatal GABAergic neurons (Nekrasov et al., 2016; Zhang et al., 2010), and astrocytes (Garcia et al., 2019). The use differentiated or undifferentiated HD-iPSCs have been able to recapitulate some of the phenotypes observed in HD such as gene expression changes, reduced bioenergetics, dysregulated calcium, and glutamate signaling, abnormal electrophysiological properties, aberrant BDNF trafficking, oxidative stress, and impairment of proteasome activity and autophagy flux (Kaye et al., 2022) (Figure 1.14). In addition to patient-derived iPSCs, brain cells from *in vivo* HD models have also been cultured *in vitro* to study HD. While molecular signatures of primary neuronal cultures are usually well preserved *in vitro*, they cannot be maintained indefinitely. Some of these *in vivo* HD models are described below.

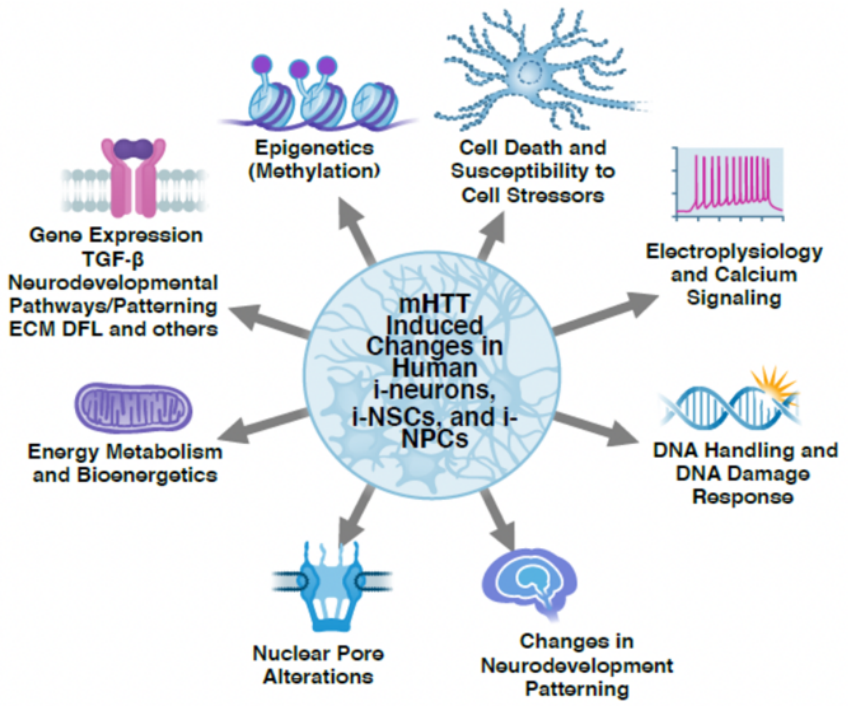

Figure 1.14: Illustration of some of the phenotypes identified in HD-iPSCs. (Kaye et al., 2022)

1.7.2. *In vivo* modeling of HD

Since the discovery of the *HTT* gene, that we have applied genetic engineering to generate *in vivo* HD models, including non-mammalian (e.g., yeast, nematodes, fruit flies and zebra fish) (Chongtham et al., 2018) and mammalian organisms (mouse, rat, sheep, pig, and non-human primates) (Farshim & Bates, 2018; Howland et al., 2020; Kosior & Leavitt, 2018).

1.7.2.1. Genetic mouse models of HD

Rodents are the most commonly used animals for modeling HD. Genetic HD rodent models can be divided into different subgroups: (1) N-terminal mHTT fragment HD models, (2) full-length mHTT HD models, (3) fully humanized HD models and (4) KI models. Huntington's disease models expressing N-terminal mHTT fragments were the first genetic models generated and can be further subdivide into viral-based and transgenic rodent models. Recombinant viral vectors such as lentivirus (LV) and adeno-associated virus (AAV) expressing N-terminal mHTT fragments have been used to induce HD pathology in rodents (De Almeida et al., 2002; Gabery et al., 2012; Jang et al., 2018). Although these viral-based models induce acute HD neuropathological features, the expression of N-terminal mHTT fragments is restricted to the injected sites. Concerning transgenic HD models expressing N-terminal mHTT fragments, the most commonly used include the R6/1 and R6/2 (Mangiarini et al., 1996), and N171-82Q (Schilling et al., 1999) lines. In terms of research, these transgenic animals have advantage of displaying earlier disease onset and more rapid disease progression compared to mice expressing the full-length mHTT. The R6 mouse models were generated by random genomic insertion of a fragment containing the

mHTT exon 1 and were the first proof that *mHTT* exon 1 alone was sufficient to induce HD phenotype in mice (Mangiarini et al., 1996). In the original models, R6/1 carried 115 uninterrupted CAG repeats, whereas R6/2 transgene contained 150 consecutive CAG repeats. In addition, the authors estimated that the mutant *HTT* transcripts in R6/1 and R6/2 were expressed at approximately 31% and 75% of the level of the wild-type mouse *HTT* gene, respectively. The lower mHTT expression and inferior number of CAG repeats in the R6/1 mice are also correlated with a slower progressive phenotype compared to the R6/2 mice (Mangiarini et al., 1996). Therefore, the R6/2 model has been the most used due to the early onset HD phenotypes and rapid disease progression. Typical HD phenotypes in these models include behavioral deficits (e.g., decreased motor and learning-related performances) and neuropathological abnormalities (e.g., intranuclear mHTT inclusions and neuroinflammation). These models have been bred in different strain backgrounds over the years and currently there are multiple variants of the R6/2 model with different CAG repeat lengths as a result of the gametic instability of the CAG expansion (Farshim & Bates, 2018). Similarly, N171-82Q mice express a slightly longer N-terminal mHTT fragment (171 aa) carrying 82 CAG repeats under the regulation of a mouse prion promoter (Schilling et al., 1999). These mice display abnormal phenotype comparable to the R6/1 and R6/2 and have a life expectancy of approximately 6 months (Harper et al., 2005).

Full-length transgenic HD models have been generated through the use of yeast (YAC) or bacterial artificial chromosomes (BAC). In contrast to N-terminal fragment models, phenotype of full-length HD models evolves much more steadily over the life course and show normal survival (Farshim & Bates, 2018). The more widely used full-length models are the YAC128 (Slow et al., 2003) and BACHD (Gray et al., 2008). The YAC128 HD mice carry four copies of *mHTT* full-length gene containing 125 CAG repeats interrupted by CAA motifs at multiple locations in the chromosome 3. The BACHD mice carry five copies of the *mHTT* gene containing an exon 1 flanked by loxP sites with 97 mixed CAG-CAA repeats and their genomic location is not known. They display similar slowly progressive behavior deficits (e.g., motor coordination and depression) and brain volume loss, particularly in the striatum and forebrain (Pouladi et al., 2012). Contrarily to the R6 line, CAG repeats in these models are less prone for germline and somatic instability due to the interruption of the CAG repeat with CAA trinucleotides. In addition, both YAC18 and BACHD models do not strongly exhibit other typical HD features such as robust striatal and cortical mHTT inclusions, and experience significant weight gain (Pouladi et al., 2010, 2012). Recently, two groups generated improved BAC transgenic models (BAC226Q and BAC-CAG) recapitulating neuropathological aspects of the disease (Gu et al., 2022; Shenoy et al., 2022). In particular, the BAC-CAG transgenic model expresses the full-length human mHTT with 120 uninterrupted CAG repeats (Gu et al., 2022). The authors demonstrated that this model containing consecutive CAG repeats exhibits additional HD features lacking in the YAC128 and BACHD models such as minimal body weight gain, somatic CAG repeat instability significantly

correlated with behavioral deficits, progressive striatal accumulation of mHTT inclusions, and striatal astrocytosis and microgliosis.

A key advantage of models containing the full-length *mHTT* gene is the preservation of *mHTT*-associated SNPs within and flanking the gene. Therefore, they are pivotal for the preclinical testing of allele-specific strategies using SNPs to distinguish *mHTT* from *wtHTT* alleles. However, allele-specific strategies must be performed in animal models presenting haplotypes identical to the patients. Southwell and colleagues generated two fully humanized HD models (HU97/18 and HU128/21) for testing allele-specific strategies by crossbreeding full-length mouse models on a background strain lacking the mouse homolog *HTT* gene (Southwell et al., 2013, 2017). The fully humanized HU97/18 model (haplotypes A/C) was generated from the BAC97 and YAC18 full-length models it is more suitable to test strategies eligible for patients mainly from Europe, America, South Asia, and Middle East (Southwell et al., 2013). In contrast, the model HU128/21 (haplotypes C/A) resulted from the intercross breeding of YAC128 and BAC21 models and can be used to test strategies targeting SNPs in heterozygosity mainly in East Asians (Southwell et al., 2017).

Despite the intense use of all of these transgenic models, transgene integration sites and potential effects of transgene-mediated activation/inactivation of host genomic regions have been poorly investigated. In 2012, Chiang and colleagues characterized the transgene integration site of several HD animal lines (Chiang et al., 2012). For instance, the R6 transgene suffered complex rearragements (deletions, duplications, inversions, and excision events) during transgene integration in both R6/1 and R6/2 lines (Figure 1.15). Later, the same group demonstrated that integration in R6/2 mice also resulted in a deletion of 5.5 kb of host genome (Jacobsen et al., 2017). Furthermore, this genomic deletion in R6/2 mice promotes the cortical expression of an unknown fragment that is differentially expressed in the brain of these mice. These findings support the characterization of transgene insertion in animal models to validate observed phenotypes and improve the choice of models for the testing of therapeutic strategies.

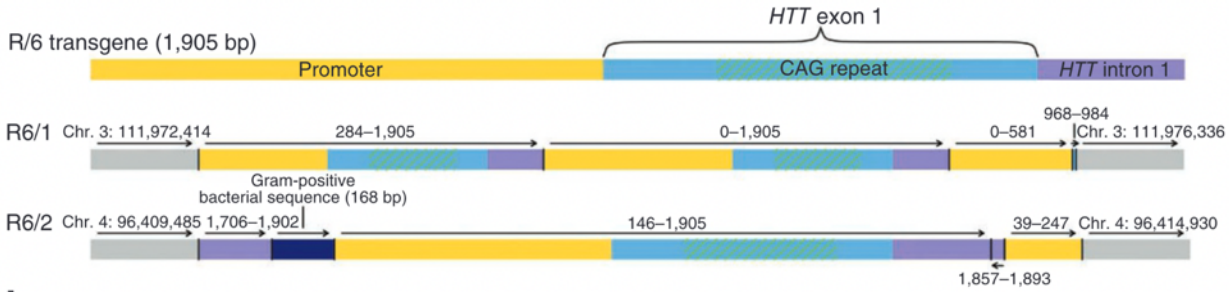

Figure 1.15: Complex rearrangements in transgenic integration sites of R6/1 and R6/2 HD mouse models. (Chiang et al., 2012)

In comparison to transgenic models, KI models also express the full-length mHTT but in the context of the mouse wtHTT (Farshim & Bates, 2018; Kosior & Leavitt, 2018). Knock-in HD mouse models have been generated using two approaches: (1) replacement of the short CAG tract of the mouse *HTT* exon 1 by an expanded CAG repeat, and (2) replacement of the entire mouse *HTT* exon 1 by the human *mHTT* exon 1. The first approach generates a mouse *HTT* gene containing an expanded CAG repeat whereas the second approach creates a chimeric gene comprising the mouse *HTT* with the human *mHTT* exon 1. Overall, KI animals represent a more precise genetic model of HD since they involve the site-specific insertion of a gene fragment. Another difference between KI and transgenic models is the presence of defined number of copies of the *mHTT* gene in KI mice – one copy (heterozygous) or two copies (homozygous) - recapitulating more the physiological conditions observed in HD patients. Multiple KI HD mice have been generated with multiple CAG lengths (Farshim & Bates, 2018). Most of the KI models carry higher number of uninterrupted CAG repeats and exhibit stronger phenotypic and neuropathological features compared to transgenic full-length mouse models (Farshim & Bates, 2018; Gu et al., 2022).

The observation that both BAC-CAG and KI models present stronger HD phenotypic differences compared to BACHD and YAC128 agrees with the hypothesis that the number of uninterrupted CAG repeats, and not the number of polyglutamines, is the main driver of HD pathogenesis (Figure 1.16). Increased somatic CAG instability in these models promotes CAG expansion through lifetime, which may trigger additional pathogenic mechanisms such as RAN translation and RNA toxicity, speeding disease progression (Swami et al., 2009).

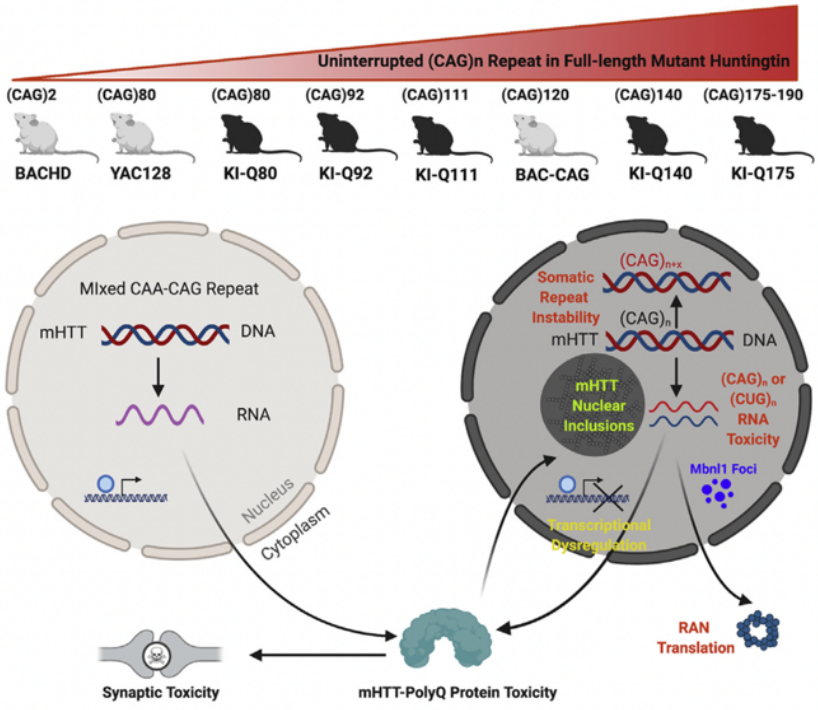

Figure 1.16: Illustration showing the most used transgenic and KI mouse models expressing the full-length *mHTT* ordered by their uninterrupted CAG repeat length and the involved pathogenic mechanism. (Gu et al., 2022)

1.7.2.2. Large genetic animal models of HD

Mouse HD models are very useful to improve our understanding on HD pathological mechanisms and to test multiple therapeutic compounds. However, extending translational research to large animals with larger brains better models CNS drug distribution and predicts efficacy in humans. Large genetic HD animal models include minipigs, sheep and non-human primates. Two genetic minipig models are available. The first generated genetic HD minipig model, named TgHD (N548), carries one copy of a transgene encoding the N-terminal part of the human mHTT (N548-124Q) under the control of the human promoter in the first porcine chromosome (1q24-q25) (Baxa et al., 2013). Similar to the BACHD mouse model, the transgenic Tg(N548) minipig carries a mixed CAG-CAA expansion and there is no evidence of somatic CAG expansion (Howland et al., 2020). This transgenic minipig model was used to preclinically test the intracranial administration of an AAV expressing a microRNA targeting the *mHTT* transcript as an HD therapeutic approach, which is currently being clinically assessed in humans (Evers et al., 2018). The other available minipig model is a KI model, named KI-HD-85Q, where the CAG repeats of the endogenous porcine *HTT* gene were expanded to 82 CAG pure repeats followed by a CAACAGCAG sequence (Howland et al., 2020). Regarding modeling in sheep, the transgenic sheep named OVT73 is the only available ovine HD model, and it carries the full coding sequence of the *mHTT* cDNA flanked upstream by the human *HTT* promoter and downstream by a polyadenylation signal (Jacobsen et al., 2010). The CAG expansion in the *mHTT* exon 1 consist of 69 consecutive CAG repeats ending with the CAACAGCAACAG sequence. To date, the transgenic OVT73 sheep is the only large model allowing the test of molecular therapies targeting any region of the human *mHTT* coding sequence (Mondo et al., 2018; Pfister et al., 2018). Finally, transgenic non-human primates have been generated (Chan et al., 2015; Yang et al., 2008), but their use for preclinical application is limited given the low number of initial founders and the difficulty to maintain macaque lines (Howland et al., 2020).

In summary, multiple *in vitro* and *in vivo* models are currently available to model HD and evaluate the efficacy of therapeutic compounds, but none of them fully recapitulates the pathology seen in patients. Therefore, the choice of the model to test a particular hypothesis and/or treatment should consider the advantages and disadvantages of each model. Animal models differ in multiple genetic features such as transgene composition and transgene site integration, number of transgene copies, number of consecutive CAG repeats and presence/absence of heterozygous SNPs. In addition, animal models also display distinct molecular and behavioral HD hallmarks, which can influence readout measurements. All these parameters should be considered to choose the model that best fits to test hypotheses/treatments.

1.8 Disease-modifying therapies lowering mHTT for Huntington's disease

To date, there are still no treatments stopping or slowing disease progression. Several approaches have been proposed by targeting pathophysiological mechanisms such as inflammation, cortical glutamate excitotoxicity, autophagy, and oxidative stress (Figure 1.17). However, none have shown significant improvements in modifying the overall disease progression and numerous clinical trials have failed in showing any therapeutic benefits. Since HD displays complex pathophysiology, the targeting of a single pathogenic mechanism may not be the optimal approach to induce general clinical benefit. Most evidence suggest that HD is driven by the gain-of-function toxic CAG expansion. While compensatory treatment based on the overexpression of wtHTT is likely to fail in preventing the disease progression (Van Raamsdonk et al., 2006), strategies tackling the CAG expansion and/or their subsequent products hold great therapeutic potential as they may prevent downstream toxic effects at both molecular and cellular levels. These so called mHTT-lowering strategies targeting the primary toxic features in HD have been proposed at different biological levels by (1) promoting mHTT protein clearance, (2) degrading or altering *mHTT* RNA transcripts and (3) modifying *mHTT* DNA sequence. In addition, a most recently considered therapeutic approach aims the stabilization of the CAG repeat throughout patient's life by (4) modulating DNA repair mechanisms, preventing CAG somatic expansion and further mHTT production.

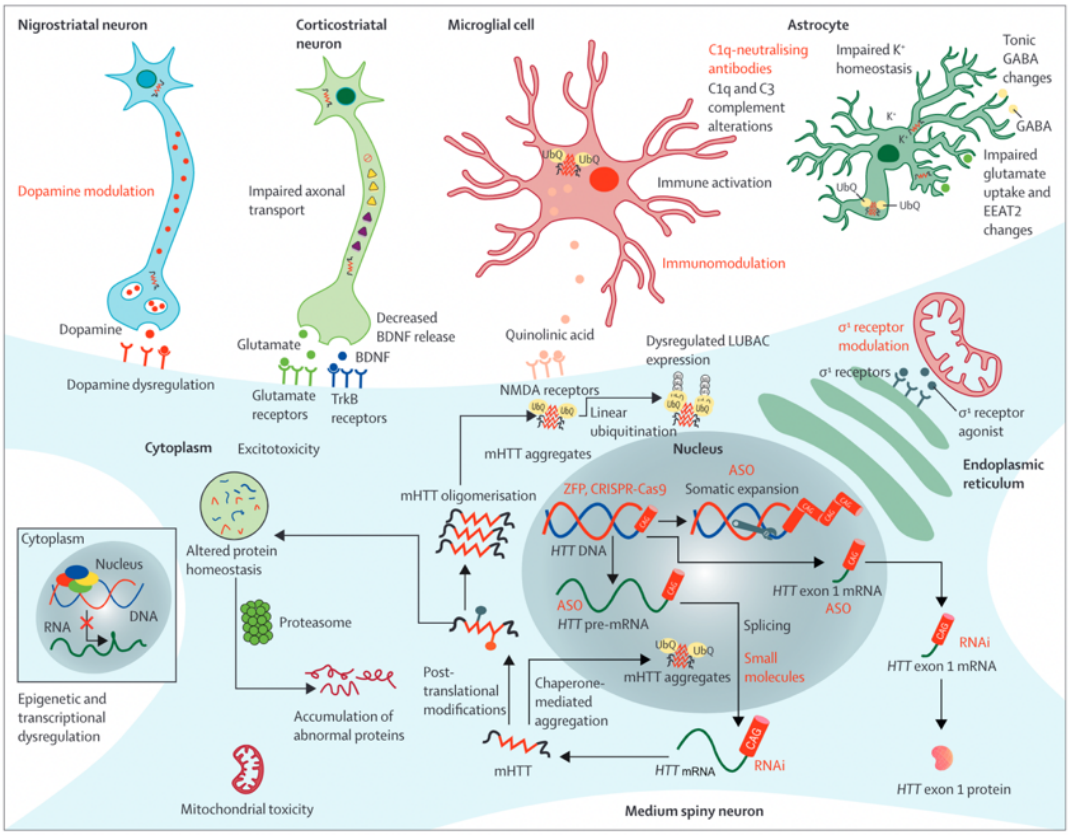

Figure 1.17: Possible therapeutic targets for HD. (Tabrizi et al., 2022b)

1.8.1. Allele-specific or non-allele-specific mHTT-lowering strategies?

Wild-type HTT is involved in multiple cellular functions, and it has been proposed that the mutation in HD also results in the wtHTT loss-of-function, which may contribute to the HD phenotype (chapter 1.4.2). Therefore, an important aspect to consider when lowering mHTT products is whether one could target both HTT forms (wtHTT and mHTT) or whether mHTT should be specifically targeted to avoid deleterious effects related to further loss of wtHTT activity.

Wild-type HTT is essential for the embryonic development since the complete deletion of the mouse homolog *HTT* gene results in embryo death between embryonic days 8.5 (E8.5) and 10.5 (E10.5) (Duyao et al., 1995; Nasir et al., 1995; Zeitlin et al., 1995). Two groups showed that chimeric embryos generated by injecting null-*HTT* embryonic stem cells (ESCs) into wild-type host blastocysts were rescued from embryonic lethality (Dragatsis et al., 1998; Reiner et al., 2001). In contrast, lethality was not rescued when wild-type ESCs were injected into null-*HTT* host blastocysts (Dragatsis et al., 1998). These results suggest that wtHTT plays a critical role in the extraembryonic tissues, likely by supporting mechanisms involved in the nutrition of embryos. Histological analysis of brains from adult rescued chimeras showed no major alterations regarding morphology, cytoarchitecture and neuronal abundance compared to controls, and indicated that null-*HTT* cells could survive until adulthood (Reiner et al., 2001). However, the distribution of null-*HTT* cells was heterogeneous among brain regions, especially in the striatum, where less than 15% of the cells were *HTT*-null. The abnormal colonization of *HTT*-null cells in the adult brain suggested that wtHTT may be involved in the proliferation and survival of neurons in some brain regions during early neurodevelopment. The critical role of wtHTT during development was further confirmed by subsequent studies knocking-out wtHTT at different developmental time points in different brain regions (Barnat et al., 2017; Dragatsis et al., 2018; McKinstry et al., 2014). Overall, the ablation of wtHTT resulted in abnormal cortical neurogenesis, deficient neuronal migration, reduced neuronal survival and behavioral abnormalities. However, all these studies evaluating the role of wtHTT at early life stages were based on its complete depletion. Partial reduction of wtHTT could translate into reduced toxic effects or induce no deleterious phenotype. This hypothesis was supported by the existence of a healthy individual carrying only one functional *wtHTT* allele (Ambrose et al., 1994). The partial decrease of wtHTT expression in development was first evaluated by Auerbach and colleagues (Auerbach et al., 2001). They observed phenotypic abnormalities in adult compound heterozygous mice expressing around 15% of wtHTT endogenous levels (Auerbach et al., 2001). Furthermore, Arteaga-Bracho and collaborators later demonstrated that these phenotypic abnormalities in adult mice were not rescued by expressing wtHTT at 50% of the endogenous levels from the post-natal day 21 (Arteaga-Bracho et al., 2016). Using a different approach, Tong and coworkers demonstrated that the knockdown of wtHTT expression by 50-75% during development also induces deficiencies in neuronal survival, proliferation, and migration (Tong et al., 2011). Overall, the extent and/or threshold level to which wtHTT can be safely reduce in the developing brain without inducing

deleterious effects is not determined. Nevertheless, evidence indicate that wtHTT plays critical roles at early life stages and suggest that more than 50% reduction of wtHTT expression in the developing brain is deleterious.

Regarding the role of wtHTT in the adult life, three studies have used conditional HTT knockout (KO) mice to evaluate the effects of wtHTT loss at different adult life stages of mice. Wang and colleagues used conditional HTT KO mice expressing a tamoxifen-activated CreER recombinase under control of the CMV immediate enhancer/β-actin (CAG-CreER; $HTT^{flox/flox}$) or Nestin (Nestin-CreER; $HTT^{flox/flox}$) promoters for ubiquitous and neuronal Cre expression upon tamoxifen injection, respectively (Wang et al., 2016). The global HTT KO at 2, 4 and 8 months of age resulted in 95%, 30% and 5% mortality, respectively. Most of the youngest treated animals died due to acute pancreatitis and the oldest treated animals survived for long term with no major differences in motor performance, body weight and peripheral markers. In contrast, while neuronal HTT KO at 2 months resulted in 18% mortality, it did not affect survival, body weight, rotarod performance, gripping ability, nor brain volume and morphology of mice treated at 4 and 8 months-old of age (Wang et al., 2016). Similarly, Dietrich and colleagues used hemizygous conditional HTT KO mice expressing the tamoxifen-induced CreER under the ubiquitous CAG promoter (CAG-CreER; $HTT^{flox/-}$) (Dietrich et al., 2017). In contrast to Wang and collaborators, they found that the tamoxifen treatment at any age (3, 6 or 9 months) resulted in gait abnormalities, tremors, decreased locomotor activity, and reduced survival compared to not treated animals. The stronger deleterious effects in this study may be due to an increased predisposition for toxicity of HTT depletion in CAG-CreER; $HTT^{flox/-}$ mice, which theoretically express less 50% of wtHTT compared to CAG-CreER; $HTT^{flox/flox}$ mice. However, these authors also observed the same time dependent deleterious effect of the treatment on the survival. In addition, they did not observe any major brain morphological changes other than reduced brain volume, thalamic calcifications and increases gliosis at older ages. In particular, striatum and cortex of treated mice did not present any significant alterations (Dietrich et al., 2017). In the last study, Pla and colleagues investigated the consequences of depleting wtHTT specifically in cortical and hippocampal mature neurons by using a conditional HTT KO mice expressing the tamoxifen-induced CreER under the Ca2+/calmodulin-dependent protein kinase-II (CamKII) promoter (CamKII-CreER; $HTT^{flox/flox}$) (Pla et al., 2013). They reported reduced maturation and survival of newborn neurons in the dentate gyrus and impaired BDNF signaling.

In paralel to these KO studies, we and others demonstrated that the knockdown of both mouse wtHTT and human mHTT expression up to 75% in the striatum of an acute lentiviral-based HD rat model and two transgenic HD mouse models (N171-82Q and BACHD) improved pathological aspects of the disease. Although these studies showed promising preclinical safety and efficacy of non-allele specific HTT silencing, wtHTT lowering also resulted in the alteration of expression of genes involved in several cellular mechanisms such as vesicular trafficking and endoplasmic reticulum (Boudreau et al., 2009a; Drouet et al., 2009). Finally, two studies in non-

human primates showed that a reduction in striatal HTT protein levels by approximately 45% induces no alterations in motor performance, motor memory or neuronal loss for at least 6 months (Grondin et al., 2012; McBride et al., 2011).

Overall, these studies indicate that ubiquitous wtHTT is essential at early life stages, but it may play a less critical function in older mice and, in particular, in the adult brain. While knockout of wtHTT in the adult brain raised contradictory results, the knockdown studies suggest that the reduction of the normal levels of wtHTT by 40 to 60% may be well tolerated. However, these results should be carefully analyzed. The contradictory results of Wang et al. (Wang et al., 2016) and Dietrich et al. (Dietrich et al., 2017) suggest that lower expression levels of wtHTT may increase vulnerability for toxicity after wtHTT depletion in the adult brain. Importantly, HTT knockdown studies were performed in animals carrying two functional copies of *wtHTT* (plus the *mHTT* transgene(s) in the rodent models). This means that preclinical safety studies of non-allele specific HTT knockdown were not performed in the real genetic settings of HD: one copy of *wtHTT* and other copy of *mHTT*. The testing of the safety of lowering both wtHTT and mHTT in the HD genetic settings would require the non-allele specific lowering in heterozygous KI carrying one copy of human *wtHTT* and other copy of *mHTT*.

While the allele specific targeting of *mHTT* may be critical to reduce potential deleterious effects concerning wtHTT reduction, it may also be critical to correctly target all mHTT toxic species to achieve therapeutic benefit. As above mentioned, *mHTT* mRNA can experience incomplete splicing, generating the short transcript *HTT1*α*,* which is then translated into the highly toxic exon 1 mHTT truncated form (Neueder et al., 2017; Sathasivam et al., 2013). Also, the *mHTT* transcripts (sense and/or antisense) can form toxic nuclear clusters (Chung et al., 2011; Fienko et al., 2022) and be translated in a non-canonical way into toxic RAN products (Bañez-Coronel et al., 2015). Therefore, the targeting of all proposed toxic forms of mHTT (RNA and peptides) should be consider to improve the likelihood of therapeutic benefit. In addition, the timing and the physically targeted brain structures for mHTT-lowering may equally be key relevant aspects to achieve therapeutic efficacy. HD pathophysiology is characterized by initial neuronal dysfunction followed by striatal atrophy. Subsequently, at later stages of the disease, atrophy of cortical, thalamic, and hypothalamic areas starts also to be imminent. The time-dependent therapeutic decrease of mHTT in the whole brain or at specific brain structures should also influence the clinical outcomes of experimental treatments.

1.8.2. Targeting mHTT protein

No clinical trials have tested drugs aiming the clearance and/or aggregation of mHTT, but there have been large efforts to screen compounds reducing HTT protein level. For example, Li and colleagues identified several compounds simultaneously interacting with the expanded polyQ stretch and microtubule-associated protein 1A/1B light chain 3 (LC3) promoting the autophagy-mediated degradation of proteins with expanded polyQ tracts (Li et al., 2019). They showed that

multiple compounds specifically decreased mHTT levels in several *in vitro* and *in vivo* HD models. In particular, they showed that the systemic delivery of the compounds 1005 and AN2 significantly improved performances of heterozygous HdhQ7/140 mice on rotarod, balance beam and gripping force tests. More recently, Long and colleagues also identified a small molecule with good blood-brain barrier (BBB) permeability, named J3, that promotes autophagy-mediated degradation of soluble and insoluble mHTT without affecting wtHTT levels *in vitro* (Long et al., 2022). However, when tested *in vivo*, J3 lowered both wtHTT and mHTT levels in the striatum of HdhQ140. Nonetheless, treated mice demonstrated increased striatal DARPP32 levels and slightly improved motor functions. Others have focused on inhibiting the G-protein coupled receptor 52 (GPCR52) to enhance mHTT degradation. The GPCR52 co-localizes with striataldopamine D2 receptors (Komatsu et al., 2014) and its activity has been shown to prevent proteasomal-mediated mHTT degradation by translocating mHTT to the endoplasmic reticulum (Yao et al., 2015). Recently, Wang and colleagues reported a BBB-penetrating GPCR52 antagonist, named Comp-43, which significantly lowered soluble and aggregated mHTT levels in the striatum of HdhQ140 mice (Wang et al., 2021). Comp-43 also decreased striatal inflammation, promoted neuronal survival, and improved motor phenotype in this HD model. Furthermore, the treatment of wild-type mice with Comp-43 showed no major alteration on wtHTT expression, suggesting that effect of GPCR52 inhibition may be mHTT-specific.

1.8.3. Targeting *mHTT* RNA

Mutant HTT lowering strategies by targeting the *mHTT* RNA rely on the alteration of *mHTT* transcript's structure, half-life and/or translation. These approaches are the most developed with several compounds being currently clinically tested and are based on different mechanisms such as (1) RNA interference (RNAi), (2) antisense oligonucleotides (ASOs) and (3) splicing modulation. More recently, two other studies started exploring RNA editing to reduce expression of *mHTT* (Morelli et al., 2022; Powell et al., 2022).

1.8.3.1. RNA interference

RNA interference is an intrinsic and evolutionary conserved mechanism that confers resistance to pathogenic nucleic acids and regulates the expression of protein-coding genes (Ha & Kim, 2014). It involves the expression and processing of small non-coding RNA named microRNAs that are complementary to targeted mRNAs. Once processed by Drosha and Dicer, microRNA is loaded into the RNA-induced silencing complex (RISC) which then recognizes the targeted mRNA and induces its destruction via cleavage by the RNase Argonaute. Adaptation of RNAi for gene knockdown approaches include the use of artificial microRNAs (miRNAs), small interfering RNAs (siRNAs), or short-hairpin RNAs (shRNAs) (Ha & Kim, 2014). While siRNA are dsRNA molecules of 21-23 nt with 2 nt overhangs able to be readily loaded into RISC, the shRNAs

contain stem-loops similar to pre-microRNA hairpins and require Dicer processing before loading into RISC. Although shRNAs potently induce gene silencing, artificial miRNAs are expressed at lower levels and display better safety profiles (Boudreau et al., 2009a; 2009b).

Viral vectors such as AAV or LV have been widely used to deliver RNAi components into the brain *in vivo* or cells *in vitro*. Harper and colleagues were the first to use RNAi to silence the *mHTT* expression *in vivo* by using the AAV2/1 (AAV of serotype 1) to deliver a shRNA targeting the exon 2 of the *mHTT* transcript in the striatum of N171-82Q HD transgenic mice (Harper et al., 2005). The intrastriatal injection of AAV2/1-shRNA resulted in the reduction of *mHTT* mRNA levels in 51-55% and significantly improved motor performance in stride length and rotarod tests compared to matched controls. Quickly, other studies demonstrated an efficient knockdown of *mHTT* RNA, which leads to histopathological and behavioral improvements (DiFiglia et al., 2007; Rodriguez-Lebron et al., 2005; Wang et al., 2005). In all these studies, the transgenic human *mHTT* was silenced, but the mouse *wtHTT* expression remained intact. In 2009, we and others investigated whether beneficial effects of mHTT silencing were also valid in a non-allele specific HTT approach by simultaneously reducing the mouse wtHTT expression. We injected lentiviral vectors expressing a shRNA targeting both wild-type and mutant *HTT* transcripts in an acute lentiviral-based HD rat model (Drouet et al., 2009). The striatal expression of shRNA prevented the loss of DARPP32 and neuronal nuclear protein (NeuN) markers suggesting striatal neuroprotection, and significantly reduced the number of HTT inclusions. Importantly, the selective inactivation of mouse *wtHTT* allele alone did not had any impact on GABAergic neuronal survival neither on the number of HTT inclusions. Similarly, Boudreau and colleagues showed that the striatal injection of AAV2/1 expressing a universal artificial miRNA (mi2.4) decreased the human *mHTT* and the mouse *wtHTT* transcript levels by approximately 75%. In addition, they showed that the treatment improved survival and completely rescue the performance of HD mice in the rotarod test (Boudreau et al., 2009a). Because artificial miRNAs were shown to induce less toxicity than shRNAs in the mammalian brain (McBride et al., 2008), subsequent studies focused mainly on miRNAs. Further evidence of the therapeutic benefits of anti-HTT miRNAs injected in the striatum were collected in fully humanized HU128/21 HD mice (Miniarikova et al., 2016), in a lentiviral-based rat HD model (Miniarikova et al., 2017) and in transgenic Tg(N548) HD minipigs (Evers et al., 2018). In this last study, the intrastriatal AAV2/5-mediated delivery of anti-*HTT* miRNA (AAV5-miHTT) in minipigs reduced *mHTT* mRNA and protein levels in widespread brain regions after 6 months, including putamen, caudate nucleus, thalamus, and cortex (Evers et al., 2018). In addition, the authors did not observe any major signs of microgliosis neither alteration in the GABAergic neuronal marker DARPP32 in the striatum of the treated animals. More recently, Vallès and colleagues have confirmed these results in HD transgenic minipigs by reporting widespread and sustained reduction (up to 1 year after injection) of *mHTT* of more than 75% in the injected areas, and about 30 to 50% in distal regions (Valles et al., 2021).

These results support the launching of the still ongoing UniQure AMT-130 human trial (NCT04120493) that targets total *HTT*. This study aims the evaluation of safety and efficacy of AAV5-miHTT in early-stage HD patients. Following promising preliminary results, UniQure has expanded this study in 2021 to a phase Ib/II open-label trial (NCT05243017) and include European HD centers to keep assessing the safety and efficacy of the treatment. In addition, Voyager Therapeutics started an AAV1-delivered anti-*HTT* miRNA clinical trial (VY-HTT01), which has been put on hold. They intend to resume the program using a novel, proprietary AAV capsid that may enable intravenous administration.

Currently, the viral delivery of genetic compounds into the brain is the most efficient method of delivery and allows a sustained stable expression for decades. RNA interference has the advantage of being compatible with viral delivery and therefore therapeutic benefit is theoretically possible with a one-time treatment administration. The UniQure AMT-130 is the one of the most promising clinical trials being currently tested in humans. This miRNA-based drug aims at the exon 1 of the *HTT* transcript and therefore targets both full-length and incomplete splicing forms of *mHTT* mRNA for degradation. However, anti-sense *mHTT* transcripts and/or subsequent RAN peptides are still potential toxic sources that eventually escape AMT-130 treatment. In addition, AMT-130 is a non-allele specific anti-*HTT* miRNA and, therefore, the consequences of reducing wtHTT in HD brain patients still remains unknown.

1.8.3.2. Antisense oligonucleotides

Antisense oligonucleotides are synthetic single-stranded DNA (ssDNA) sequences consisting of 8-50 nt that bind to complementary target RNA in the nucleus and can modulate gene expression through distinct potential mechanisms (Schoch & Miller, 2017). These mechanisms can be categorized in (1) RNase-mediated degradation, (2) mRNA modification, or (3) microRNA inhibition (Figure 1.18). ASO properties, such as solubility, binding, potency, and stability, are defined by modifications on the backbone and sugar rings. For example, while the replacement of the phosphate backbone by phosphorothioate linkages protects ASOs from nuclease degradation, it strongly activates immune responses. Moreover, these immune responses can be attenuated by sugar modifications, but fully modified sugar moieties prevent RNase H enzyme and promote non-degrading ASO mechanisms (Figure 1.18).

Most of the ASOs used for silencing *HTT* act through target mRNA degradation and therefore, they usually adopt a “gapmer” design to enable target degradation, consisting in modified sugar bases separated by a central region of unmodified nucleotides (Schoch & Miller, 2017). Because synthetic ASOs are not compatible with viral vector-mediated delivery and they are unable to cross the BBB, their administration into the CNS is usually performed via CSF by intrathecal or intracerebroventricular injections. Kordasiewicz and colleagues showed that the transient unilateral intracerebroventricular infusion of non-allele specific ASOs targeting the exon 36 of human *mHTT* in YAC128 and BACHD mouse models significantly decreased the *mHTT*

transcripts across multiple brain regions, including striatum, cortex, thalamus, and midbrain up to nine weeks after treatment termination (Kordasiewicz et al., 2012). ASO infusion in YAC128 after disease initiation (2 months-old) was able to ameliorate motor phenotype up to three months after treatment termination. In addition, they observed sustained effect of improved motor and behavioral performances in the rotarod and open-field tests from 8 weeks up to 6 months after ASO infusion in BACHD. Meanwhile, Southwell and colleagues continued their efforts to develop *mHTT* allele specific ASOs (Southwell et al., 2014). In this report, they identified four potent *mHTT* allele-specific ASOs by targeting heterozygous HD-associated SNPs in the humanized mouse model of HU97/18.

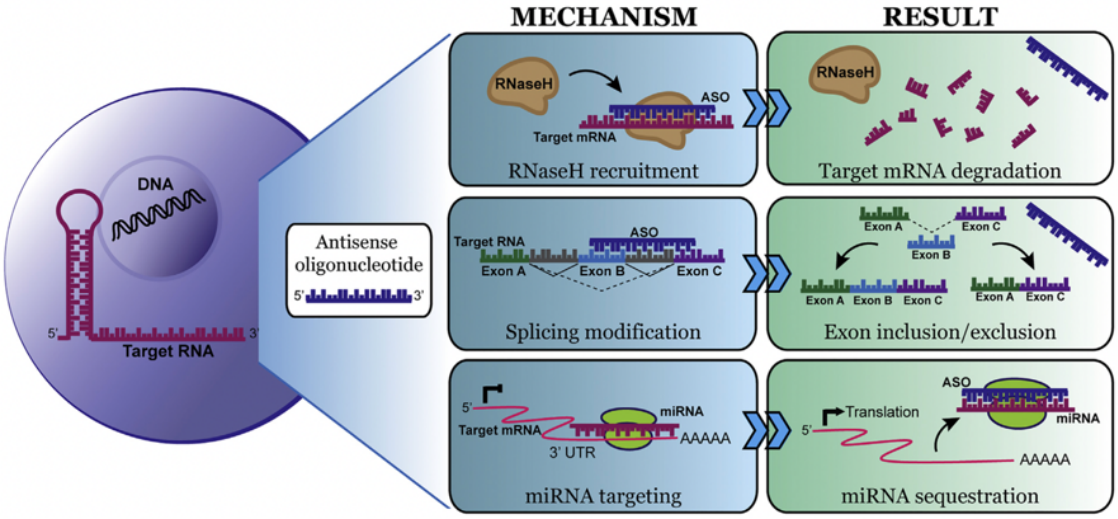

Figure 1.18: ASO mechanisms of action. (Schoch & Miller, 2017)

Recently, three human clinical trials testing the safety and efficacy of ASO-based agents have been terminated. The non-allele specific ASO described by Kordasiewicz and colleagues (Kordasiewicz et al., 2012) was being tested by Roche/Ionis Pharmaceuticals (tominersen) in a phase 3 clinical trial (GENERATION HD1; NCT0376184). Previous phase 1/2 studies (NCT02519036 and NCT03342053) had shown no serious adverse events and the reduction of approximately 40% of mHTT protein levels in the CSF after four intrathecal administrations (Tabrizi et al., 2019). Despite post-treatment higher concentrations of NfL were observed in the CSF, levels drop after day 141 of treatment with the continued dosing with tominersen (Ducray et al., 2019). However, individuals receiving tominersen every 8 weeks started performing worse on clinical rating scales than the placebo group. In addition, subjects started experiencing more serious adverse events. This led to the termination of the trial by an independent monitoring committee. A post-hoc analysis of the trial advanced that lower and less frequent treatments may be beneficial to younger subjects with diminished disease burden, and Roche/Ionis Pharmaceuticals plans to continue the program in a Phase 2 study in these participants. The other two recently terminated clinical trials were run by Wave Life Sciences and aimed the testing

of safety and efficiency of two allele specific ASOs (WVE-120101 and WVE-120102) in a phase 1b/2a studies (PRECISION-HD1; NCT03225833), (PRECISION-HD2; NCT03225846). Both trials reported no statistically significant lowering of mutant huntingtin in the CSF and were therefore discontinued. Wave Life Sciences has continued their program by launching a new phase 1b/2a trial (NCT05032196) to test a novel allele-specific ASO (WVE-003) with a chemically improved backbone.

Compared to RNAi-based *HTT* lowering approaches, a main disadvantage of ASOs is the requirement for repetitive administrations to maintain therapeutic concentrations. Since intrathecal injections are quite invasive, ASO infusions are often associated with pain-related side effects on patient. In all the three halted clinical trials, more than 75% of the patients experienced adverse events (Rook & Southwell, 2022). In addition, intracranial RNAi-based administration, and intrathecal infusion of ASOs are expected to result in different regional distribution in the CNS. The first one involves the injection of the therapeutic drug directly in the striatum with diffusion and/or transport to other brain regions such as cortex (Valles et al., 2021). In contrast, intrathecal administration of ASOs results in higher ASO concentrations in brain regions adjacent to the CSF flow (cortex) and in lower concentrations in deeper brain structures (striatum) (Kordasiewicz et al., 2012; Southwell et al., 2018). Whether the reduction of mHTT in both cortex and striatum is necessary to induce therapeutic benefits is still unknown. The worsening of clinical trial outcomes with the non-allele specific ASO (tominersen) suggests that mHTT lowering in superficial brain structures may not be enough to improve HD phenotype. In addition, another plausible explanation for trial failure is the potential toxic effect of tominersen in lowering both *mHTT* and *wtHTT*. Since the trials testing the allele specific ASOs (WVE-120101 and WVE-120102) were discontinued for not showing target engagement, we are not able to compare the effect of non-allele versus allele-specific ASOs. Finally, similarly to RNAi-based AMT-130, none of these ASOs have been shown to knockdown incomplete splicing isoforms of *mHTT*, which can also limit therapeutic outcome.

1.8.3.3. Splicing modulation

The splicing modulator risdiplam has been recently approved for the treatment of spinal muscular atrophy (SMA) (Dhillon, 2020). This oral, brain-penetrant, small molecule boosts the ability of an alternative survival of motor neuron (*SMN*) *2* gene to produce full-length and functional SMN protein. Another splicing modulator molecule named branaplam is also being currently clinically tested for SMA by Novartis Pharmaceuticals (NCT02268552). Recently, Keller and colleagues observed that branaplam also modulates *HTT* splicing by promoting the inclusion of a pseudoexon between the exons 49 and 50 in the *HTT* transcript (pseudoexon 50a) (Keller et al., 2022). Furthermore, they noticed that the inclusion of the pseudoexon 50a generates multiple premature stop codons in the *HTT* transcript, which is then targeted to degradation by the intrinsic nonsense-mediated RNA decay (NMD) cellular mechanism. They then observed that branaplam

lowered wtHTT and mHTT protein levels in HD patients-derived cells and in the BACHD HD mouse model (Keller et al., 2022). Although Novartis Pharmaceuticals advanced with the clinical testing of branaplam (VIBRANT-HD; NCT05111249), this trial was recently halted for safety reasons. The lead has now been taken by PTC Therapeutics, which is recruiting for a phase 2 trial (NCT05358717) to test the safety and efficacy of another splicing modulator (PTC518) in HD subjects (Estevez-Fraga et al., 2022).

1.8.4. Targeting *mHTT* DNA

At the DNA level, artificial zinc-fingers (ZFs) proteins and Clustered Regularly Interspaced Short Palindromic Repeats/Cas (CRISPR/Cas) system have been used to target *mHTT* allele. These molecular tools display distinct features regarding the recognition of specific nucleic acid sequences. The major advantage of CRISPR/Cas-based tools over ZFs is the ease of engineering to recognize unique sequences (Duarte & Déglon, 2020). While the DNA-binding specificity of ZFs rely on protein-DNA interactions and require protein engineering to re-target different DNA sequences, the targeting specificity of CRISPR/Cas9 system is conferred by RNA molecules, which are easily and quickly produced. Genetic engineering using these tools involve the generation of double-strand breaks (DSBs), or gene editing, and the recruitment of epigenetic modifiers to specific genomic sites, or epigenetic editing.

Site-specific DNA cleavage activates cellular DNA repair pathways, which then delete, insert, or replace nucleotide sequences (Yeh et al., 2019). The two main DNA repair pathways for DSBs are the non-homologous end-joining (NHEJ) and homology-directed repair (HDR) pathways. NHEJ is error-prone, often introducing small insertions or deletions (indels), whereas HDR uses homologous sequences as a template, to ensure the correct repair of damaged DNA. The NHEJ pathway is frequently used to inactivate toxic genes Figure 1.19). The introduction of indels on the target gene results can induce frameshift mutations, generating premature stop codons. Signals for premature translation termination can either result in the production of a non-functional truncated protein or in the NMD of the altered transcript. Other applications include the disruption of aberrant splicing sites or the deletion of large fragments of DNA through the generation of two DSBs in the same chromosome (Figure 1.19). By contrast, the accuracy of the HDR pathway allows precise nucleotide insertions, deletions, or substitutions at the target site (Figure 1.19). This is achieved by using dsDNA or ssDNA templates containing the intended modification, flanked by homologous sequences. HDR can, thus, be used to correct both gain-of-function and loss-of-function mutations. Homology-directed recombination can also be exploited as an alternative approach to classical gene replacement, to improve control over the copy number of the gene of interest and to prevent insertional mutagenesis due to the random integration of viral vectors (Figure 1.19). The gene replacement involves the site-specific insertion of full transgenes (cDNA) at “safe harbor” locations, defined as sites within the genome at which

the addition of sequences does not interfere with the neighboring genes and results in safe robust transgene expression.

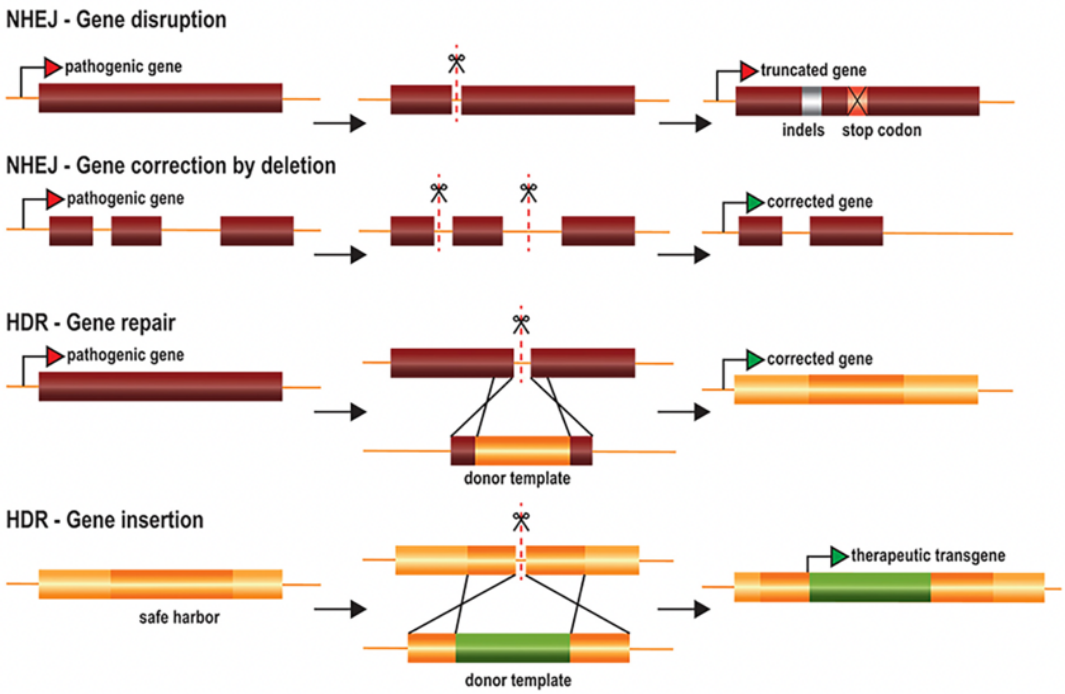

Figure 1.19: Therapeutic approaches using gene editing tools. (Duarte & Déglon, 2020)

In contrast, the recruitment of epigenetic factors to specific genomic sites modifies genetic expression profiles by altering the chromatin structure and/or accessibility of the transcription machinery (Figure 1.20). Epigenetic factors that have been used to modulate gene expression include transcriptional activators or repressors, histone (de)acetylases or (de)methylases, and DNA methylases (Duarte & Déglon, 2020).

1.8.4.1. Zinc Finger Repressors

Zinc finger motifs recognize specific trinucleotides and are present in multiple transcription factors. The combination of multiple ZF motifs in an array makes it possible to generate a DNA-binding protein recognizing specific sequences within the genome (Kim & Kini, 2017). The first application of ZFs for genome engineering were zinc finger nucleases (ZFNs). These tools were engineered by fusing the catalytic domain of the FokI nuclease to ZFs (Figure 1.21). FokI is a bipartite endonuclease that must dimerize to cleave the target sequence (Vanamee et al., 2001). ZFNs therefore have two fused FokI domains binding opposite strands of adjacent sequences in reverse orientations, to promote FokI dimerization and genome restriction. This technology showed promising results in preclinical studies, and it is currently being tested *in vivo* in humans for the treatment of mucopolysaccharidosis I (MPSI), MPSII and hemophilia B by Sangamo

therapeutics (Harmatz et al., 2022). These disorders are caused by a loss-of-function in different genes and the strategy consists of the integration of the corrective promoterless transgene into the albumin intron 1 “safe harbor” locus after the DSB is introduced by the ZFNs (Figure 1.19). Although no toxicity was associated to any of the treatments, it resulted in low levels of gene correction *in vivo* in the liver and the transgene integration did not induce long-term therapeutic effects (Harmatz et al., 2022).

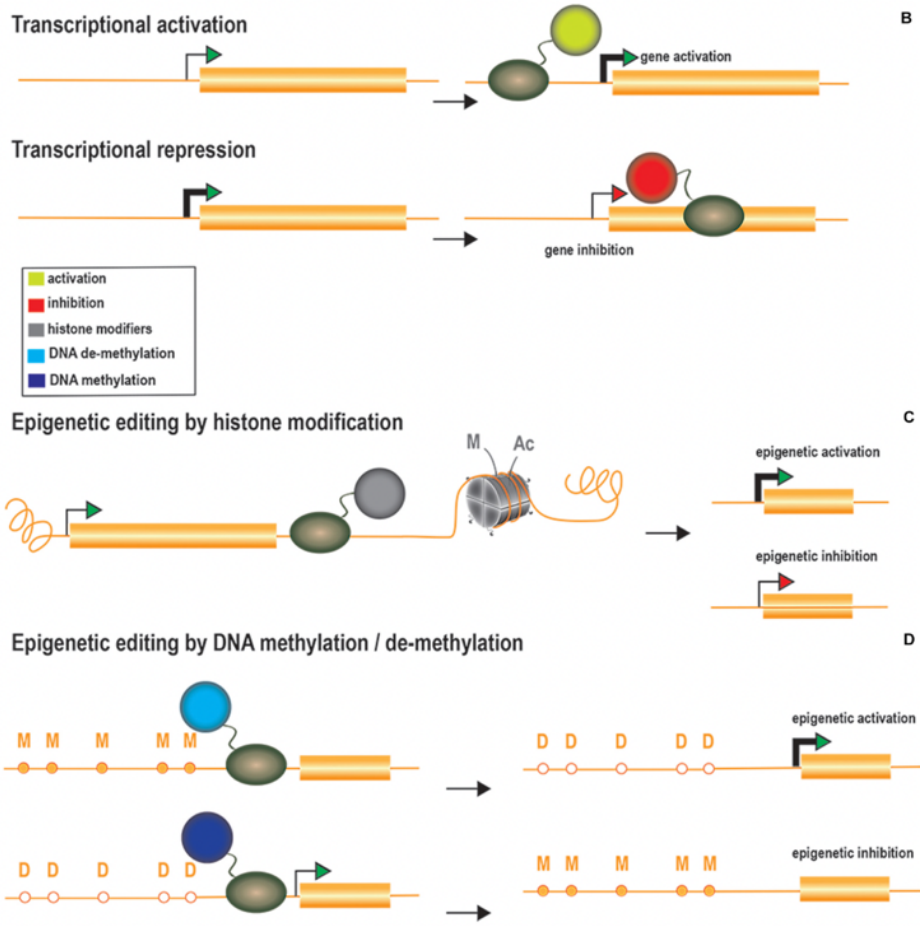

Figure 1.20: Therapeutic approaches using epigenetic editing tools. (Duarte & Déglon, 2020)

The application of zinc-fingers for the treatment of HD relies on the knockdown of *mHTT* expression by using a zinc finger protein fused to the KRAB domain of the human kox1 (ZF-KRAB), which confers strong transcriptional repressor activity. Garriga-Canut and colleagues attempted to design a CAG length-dependent ZF-KRAB exclusively targeting the *mHTT* allele (Garriga-Canut et al., 2012). This first tool established the proof-of-principle for *mHTT* repression *in vivo*, decreasing striatal *mHTT* mRNA levels by approximately 30% in the brains of R6/2 mice receiving AAV2/1-ZF-KRAB injections. Despite the achievement of repression *in vivo*, this zinc finger repressor was poorly tolerated *in vivo*. Later, Zeitler and coworkers extensively screened second-generation ZF-KRAB repressors that preferentially recognize physiological relevant pathogenic CAG repeats (Zeitler et al., 2019). They demonstrated almost complete *mHTT* suppression (>99%) along with the preservation of wtHTT expression (>86%) in HD patient-

derived cell lines. In addition, the striatal injection of AAV2/9 expressing the zinc finger repressor in R6/2 mice improved several aspects of the HD phenotype at 7 weeks post-treatment and no inflammation or adverse effects were observed after long-term expression. However, they also observed off-target knockdown of other CAG-containing genes, imposing some potential deleterious effects of this technology for the treatment of HD.

Compared to RNAi and ASOs, strategies repressing *mHTT* transcriptional activity hold great potential because they act upstream to *mHTT* transcription, immediately avoiding the expression of potential mRNA toxic species. In addition, this approach is expected to lower both full-length and incomplete spliced mRNA isoforms. Despite the targeting of more potentially mHTT toxic species, allele specific repressors based on the number of CAG repeats is likely to suppress additional genomic regions also containing CAG repeats. In addition, the design of allele specific zinc finger proteins based on *mHTT*-linked SNPs would be quite complex and require huge screening platforms. Therefore, it is likely that issues related to off-target repression may be holding this technology from being clinically tested in humans.

Figure 1.21: Illustration of mode of action of zinc finger nucleases. (Duarte & Déglon, 2020)

1.8.4.2. CRISPR/Cas9 system

The CRISPR/Cas system is an RNA guided nuclease system that allows adaptable immunity to bacteria (Makarova et al., 2020; Wright et al., 2016). The CRISPR/Cas-mediated bacterial immunity comprises three distinct steps: (1) adaptation by incorporation of foreign sequences, (2) biogenesis of the CRISPR RNAs (crRNAs) and (3) sequence-specific interference of subsequent invading viruses and/or plasmids. The CRISPR/Cas systems are extremely diverse, and they are classified into six distinct types accordingly to “signature proteins” (Makarova et al., 2020). These six types are further categorized into two main classes accordingly to the complexity of the interference effector. Class 1 systems (types I, III and IV) employ a large complex of several effector proteins while class 2 systems (types II, V and VI) use a single Cas protein to mediate the recognition and cleavage of foreign nucleic acids. The type II CRISPR/Cas9 system is the most popular and it has revolutionized the synthetic biology field over the past few years. Bacteria possessing this immunity system have a CRISPR locus flanked by *cas* genes and a sequence whose transcription generates a non-coding RNA named trans-activating CRISPR RNA (tracrRNA). In the CRISPR locus, the repeats are separated by specific foreign sequences

(called “spacers”) which were acquired during a previous infection and operate as an immune memory (Wright et al., 2016). The transcription of the CRISPR locus gives rise to the CRISPR RNA precursor (pre-crRNA), which is subsequently processed by the host RNase III enzyme. The pre-crRNA processing requires hybridization of several small tracrRNA, which contains a 24 nt complementary region to the repeats of the pre-crRNA. After base-pairing, the pre-crRNA:tracrRNA duplexes are recognized by Cas9 and the host RNase III enzyme cleaves the pre-crRNA into small crRNAs, each one containing a specific spacer and part of the CRISPR repeat. Finally, the Cas9 is guided by the crRNA:tracrRNA duplex to the cleave the target DNA, generating an end-blunted, double-stranded DNA break. The Cas9 DNA binding and interference are determined by the spacer sequence and the protospacer adjacent motif (PAM). The protospacer should be complementary to the crRNA spacer and located upstream to the PAM. The PAM allows the system to distinguish “self” versus “non-self” DNA, preventing it from cutting the bacterial chromosome.

Since the first application of CRISPR/Cas9 system from Streptococcus pyogenes (SpCas9) in eukaryotic cells (Cong et al., 2013; Jinek et al., 2012; Mali et al., 2013), this system has been extensively used for manipulation of the genome. Jinek and colleagues further simplified it by fusing the crRNA to part of the tracrRNA, named single guide RNA (sgRNA) (Jinek et al., 2012). The SpCas9 recognizes the PAM 5’-NGG-3’ in the non-target DNA strand and induces PAM-proximal blunt double-strand breaks in the target DNA (Figure 1.22). PAM requirements make it impossible to target all genomic sequences, but the use of different Cas9 orthologs with different PAM specifications has greatly expanded targeting capabilities (Cebrian-Serrano & Davies, 2017). Additionally, Cas9 proteins have been engineered to accept different and less restrictive PAMs, although sometimes compromising specificity (Hu et al., 2018; Walton et al., 2020). In contrast, other groups have restricted Cas9 binding parameters to increase specificity, which however often reduces editing efficiency (Kleinstiver et al., 2016; Kocak et al., 2019).

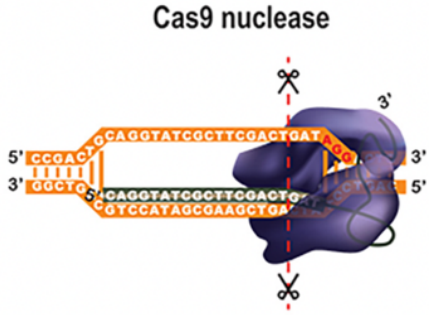

Figure 1.22: Illustration of mode of action of CRISPR/Cas9 system. (Duarte & Déglon, 2020)

1.8.4.2.1. Special considerations regarding gene editing in post-mitotic cells

Homology-directed recombination is a promising approach for therapeutic applications, but it is generally less efficient than NHEJ and mostly restricted to the G2 and S phases of the cell cycle (Yeh et al., 2019). This imposes additional challenges for the application of HDR-based gene repair in post-mitotic cells. Nishiyama and colleagues reported a high efficiency of HDR in the mouse brain (Nishiyama et al., 2017), but most groups have struggled to achieve such success with this approach. Several groups have proposed NHEJ-like strategies to overcome this limitation through precise gene editing in non-replicative cells by microhomology-mediated end-joining (MMEJ) (Yao et al., 2017a), homology-independent targeted integration (HITI) (Suzuki et al., 2016), and microhomology-dependent targeted integration (MITI) (Li et al., 2020). Other groups have explored HDR-like mechanisms, such as homology-mediated end joining (HMEJ) (Yao et al., 2017b) and single homology arm donor-mediated intron targeting integration (SATI) (Suzuki et al., 2019). These techniques have yielded significantly higher rates of gene insertion in post-mitotic cells, although the mechanisms involved are not fully understood. Other groups have even suggested approaches in which HDR repair is promoted by fusing the Cas9 nuclease to factors involved in the regulation of NHEJ/HDR pathways. For instance, p53-binding protein 1 (53BP1), which plays a major role in balancing NHEJ/HDR ratio, promotes DSB repair via the NHEJ pathway by preventing the DNA end resection required for HDR (Bunting et al., 2010). Cas9 fused to a dominant-negative 53BP1 enhanced HDR and inhibited NHEJ in a target-specific manner, without modifying cellular DNA repair mechanisms overall (Jayavaradhan et al., 2019). Efforts have also been made to improve HDR by fusing Cas9 to RecA (RAD51 in eukaryotes), which plays a key role in homologous recombination (Cai et al., 2019; Kurihara et al., 2020), or by altering the conformational checkpoints for Cas9 binding to DNA (Kato-Inui et al., 2018).

Another important aspect regarding gene editing in post-mitotic cells is the stable and permanent expression of Cas9 nuclease. While it may lead to higher levels of on-targeting editing, it can also increase the occurrence of off-target events and immunogenic responses. We and other have tried to overcome this limitation by developing CRISPR/Cas9 systems allowing transient Cas9 expression. We developed the KamiCas9 system which is based on a lentiviral vector with a larger cloning capacity than AAV (Merienne et al., 2017). It is composed of the SpCas9 nuclease, a sgRNA targeting *HTT* and a second sgRNA targeting the translation start site of the SpCas9 nuclease. High on-target efficiency and inactivation of the nuclease overtime are ensured by the use of a strong RNA Polymerase III promoter (H1) to drive the sgRNA for on-target gene and a weak promoter (7sk) to drive the sgRNA targeting the SpCas9 itself (sgCas9). We showed that striatal samples from mice receiving LV-KamiCas9 injections revealed an almost complete absence of the SpCas9 protein after 2 months by western blot analysis. Other AAV-based “self-deleting” systems have also used self-cleavage approaches to promote the transient expression of Cas9. These systems use a sgRNA targeting a sequence present in the AAV backbone but not in the coding sequence of the nuclease (Ibraheim et al., 2021; Krooss et al.,

2020; Li et al., 2018, 2021). Because cleaved non-integrated episomal AAV are vulnerable to cellular nucleases, the knockdown of Cas9 in these systems is induced by the degradation of AAV episomes rather than due to transgene inactivation by frameshifted mutations.

1.8.4.2.2. Gene editing in HD

Several studies have shown the non-allele specific *HTT* editing in multiple HD mouse models (Ekman et al., 2019; Liu et al., 2021a; Merienne et al., 2017; Yang et al., 2017). We demonstrated high levels of exogenous hHTT-82Q (20–35%) editing in a LV-based HD mouse model following the injection of our LV-KamiCas9 system expressing a sgRNA targeting the *HTT* translational starting site (Merienne et al., 2017). Yang and colleagues used two separate AAVs expressing neuronal SpCas9 and two sgRNAs targeting the flanking regions of the CAG repeat in a non-allele-specific manner in the HdhQ140 KI HD mouse model (Yang et al., 2017). The injection of neuron-specific AAV-Cas9-*HTT* resulted in the efficient transduction of medium spiny neurons, significantly decreasing the accumulation of striatal mHTT and mouse wtHTT of 9-months-old homozygous and heterozygous KI mice. The treated heterozygous mice demonstrated improved performance in the rotarod, beam and grip strength tests. Similarly, the injection of the same neuronal CRISPR system into the striatum of zQ175 KI HD mice delayed onset of striatal atrophy and slowed the progression of brain pathology and motor phenotype (Liu et al., 2021a). In another study, Ekman and colleagues used a smaller Cas9 orthologue from Staphylococcus aureus (SaCas9) to target the *HTT* translational site in R6/2 mice (Ekman et al., 2019). The AAV2/1-mediated delivery of SaCas9-*HTT* to striatal neurons halved the total HTT expression and decreased mHTT-positive neuronal inclusions about 40% at four weeks post-treatment. The treatment also improved motor functions up to 14 weeks after injection and increased mice survival compared to controls.

All these CRISPR/Cas9 studies used non-allele specific sgRNAs which would induce the inactivation of both *wtHTT* and *mHTT* in HD patients. As highlighted previously, the potential deleterious effects of reducing both wtHTT and mHTT are not fully elucidated. While partial reduction using RNA-targeting approaches may still permit wtHTT expression at non-deleterious levels, *HTT* gene editing results in the complete depletion of wtHTT expression in edited cells. Therefore, other gene editing strategies have focused on the design of sgRNAs targeting SNPs that generate novel PAM motifs in the mutant allele or delete PAM motifs from the wild-type allele (PAM-altering SNPs - PAS). These guides have great potential for allele discrimination since a single mismatch in the PAM site dramatically reduces the Cas9 editing efficiency (Hsu et al., 2013). Two distinct approaches have been proposed for allele-specific *mHTT* editing: (1) deletion of *mHTT* exon 1 by inducing simultaneous DSBs downstream and upstream to the exon 1 to prevent *mHTT* transcription (Fang et al., 2023; Monteys et al., 2017; Shin et al., 2016, 2022a) (Figure 1.19) or (2) generation of premature stop codons at downstream coding regions to induce degradation of *mHTT* transcript via NMD (Oikemus et al., 2022; Shin et al., 2022b). Although two

sgRNAs are required in the first approach, only one sgRNA needs to be allele-specific since exon 1 deletion only occurs in the presence of two simultaneous DSBs. However, a condition to maintain allele-specificity is that the DSB generated by the non-allele specific sgRNA should have minimal impact on wtHTT expression and/or function. As first proof-of-principle, two groups have demonstrated the feasibility in deleting specifically the *mHTT* exon 1 with several sgRNA combinations *in vitro* in HD-derived fibroblasts (Monteys et al., 2017; Shin et al., 2016). In particular, Monteys and colleagues demonstrated that the combination of the allele-specific sgHD1 targeting the *HTT* promoter (rs2857935) with a non-allele specific sgHDi3 targeting the intron 1 induced the deletion of the *mHTT* exon 1 and decreased *mHTT* expression in puromycin-selected HD-derived fibroblasts. They further showed that the AAV2/1-mediated delivery of this guide combination in the striatum of BACHD transgenic mice decreased striatal concentration of *mHTT* transcripts by 50% (Monteys et al., 2017). However, whether the decrease of *mHTT* expression was due to the deletion of *mHTT* exon 1 is unclear. These two groups have recently analyzed heterozygosity of PAS in novel genotype datasets attempting to demonstrate higher applicability of the deletion of *mHTT* exon 1 in HD patients (Fang et al., 2023; Shin et al., 2022a). Fang and colleagues analyzed novel potential PAS in the 10 kb around the *HTT* exon 1 in 319 HD samples from the French HD consortium and validated on 664 samples from the CHDI Foundation (Fang et al., 2023). Their analysis revealed only one extra novel prevalent PAS (rs3856973), which could be targeted by SaCas9 but not by SpCas9. They estimated that about 42% of HD patients could be targeted for allele-specific strategies, with 22% and 30.2% of the HD individuals being eligible for allele-specific editing by sgHD1 (rs2857935) and sgHD16 (rs3856973), respectively. Shin and colleagues performed a more extensive analysis in 8543 phased genotypes of HD subjects with European ancestry (Shin et al., 2022a). They identified 10 prevalent PAS in the 20 and 40 kb flanking regions upstream and downstream of the transcription starting site with at least 10% mutant specificity (i.e., proportion of HD subjects who carry the PAS only on the *mHTT* allele) (Figure 1.23). Among the SpCas9-sgRNAs targeting these 10 PAS, the guides L4 (rs2857935), R4 (rs16843804) and R6 (rs16843836) were selected for showing high levels of mutant specificity in two HD-derived iPSCs. Clonal analysis of iPSCs treated with L4-R4 or L4-R6 guide combinations indicated that large deletions had occurred specifically in the *mHTT* allele (29 kb and 38 kb, respectively), leading to the complete loss of *mHTT* expression. While these two combinations are eligible in less than 50% of HD patients, combining one of these three allele-specific sgRNAs with a non-allele specific sgRNA could be applied to approximately 60% of HD individuals. Nonetheless, approximately 30% of HD patients are still not eligible for an allele-specific targeting strategy based on any of the 10 PAS initially identified.

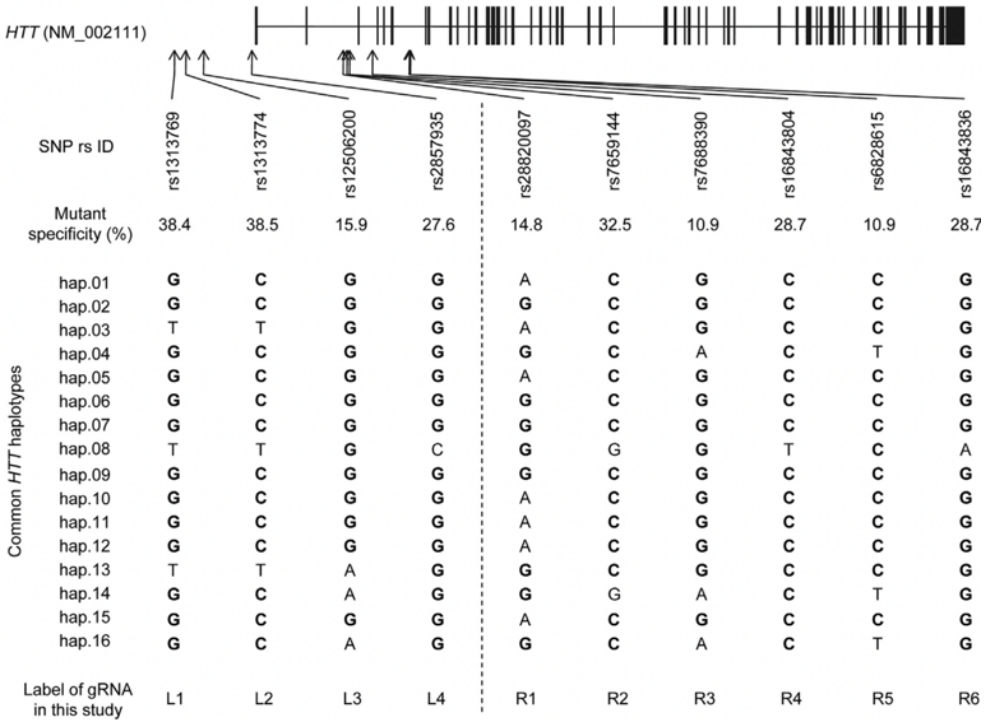

Figure 1.23: Ten candidate PAS on the 16 common HD haplotypes (Shin et al., 2022a)

The second strategy for lowering mHTT is to activate NMD by introducing premature stop codon into downstream exons of the *mHTT* transcript (Figure 1.24) (Oikemus et al., 2022; Shin et al., 2022c). Using the data from 1000 genomes project, Shin and colleagues identified 3 exonic PAS that generate SpCas9 PAM sites on some of the most common *HTT* haplotypes (rs1065745, rs363099 and rs362331) (Shin et al., 2022b). While PAS rs1065745 and rs362331 were estimated to have low levels of mutant specificity, about 22% of the HD subjects are eligible for allele-specific *mHTT* editing targeting the PAS rs363099 located in exon 29. The authors then confirmed high allele-specificity of the sgRNA targeting rs363099 in HD patient derived-NPCs and iPSCs. Subsequent analysis of RNA and protein samples from edited clonal cell lines containing premature stop codons in the *mHTT* allele demonstrated that *mHTT* mRNA was significantly reduced and mHTT protein was totally absent. In addition, no N-terminal truncated mHTT fragments were observed and RNA-sequencing analysis did not reveal any transcriptional changes in other genes. Similarly, Oikemus and coworkers demonstrated NMD of the *mHTT* transcript in primary neuronal cultures from the HU97/18 mice endogenously expressing SpCas9 by targeting the APS rs362331 located in the exon 50 (Oikemus et al., 2022). They further confirmed the specificity and efficiency of the approach *in vivo* by delivering an AAV expressing the sgRNA targeting the *mHTT* allele into the striatum of HU97/18 and HU18/18 mice. While no editing was detected in striatal samples from HU18/18, approximately 30% of indels were detected in HU97/18 samples four weeks after treatment. Protein analysis revealed a 4-fold decrease of mHTT protein levels in the striatum of treated BAC97 and no changes in the striatum of treated YAC18 compared to respective controls. Both studies illustrate the potential of NMD

approaches to specifically lower mHTT. Interestingly, while Shin and colleagues estimated that only 1.3% of HD patients were eligible for the allele-specific treatment when targeting rs362331, Oikemus and coworkers claim that 40–46% of patients could be treated using this approach (Oikemus et al., 2022; Shin et al., 2022c). Therefore, analysis of heterozygosity frequencies of APS in HD patients should be further investigated and homogenized between the research community for better consensus regarding feasibility of DNA-targeted approaches.

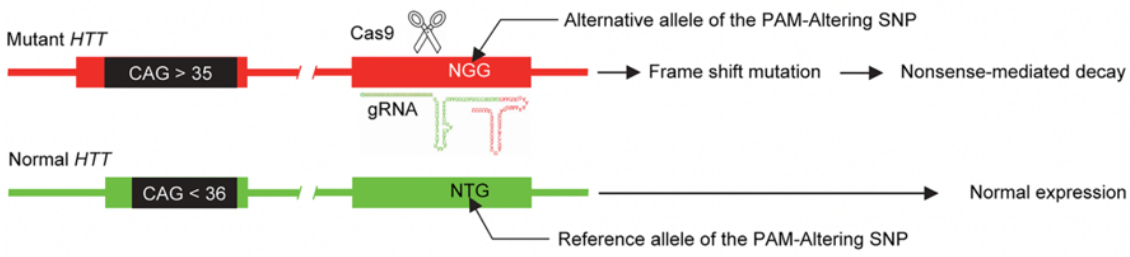

Figure 1.24: The concept of allele-specific NMD-CRISPR/Cas9 strategy. (Shin et al., 2022b)

In summary, multiple therapeutic strategies targeting the mHTT at protein, RNA and DNA levels have been proposed with some of them being tested clinically in HD patients. At the protein level, no current therapeutic approaches are being clinically tested and they have the disadvantage of not targeting other toxic *mHTT* species such as *mHTT* sense and anti-sense transcripts and RAN products. At the RNA level, dosing of the non-allele specific ASO (tominersen) was halted by worsening clinical trial outcomes. Plausible explanations may be drug-related toxicity, poor drug biodistribution in deeper brain structures such as striatum and/or toxic reduction of wtHTT expression levels in brain regions exposed to high concentrations of tominersen such as cortex. It would be interesting to compare clinical outcomes with the other two allele specific ASOs clinically tested, but their dosing was also stopped due to poor target engagement. Currently, the RNAi-based AAV5-AMT-130 is the only HTT lowering approach under clinical evaluation. In contrast to ASOs, this approach is advantageous by requiring a single administration and by promoting higher drug biodistribution in the striatum. However, drug target engagement at cortical regions may be compromised due to limited AAV diffusion/retrograde transport. In addition, AMT-130 does not discriminate *mHTT* from *wtHTT* and the long-term effects of reducing wtHTT in HD patients are still to be assessed. Antisense oligonucleotides have the additional limitation of not targeting incomplete spliced mRNA isoforms and/or RAN products. Lastly, at the DNA level, zinc fingers repressors prevent the activity of the transcriptional machinery at the *HTT* locus. Therefore, they hold great potential by targeting all toxic forms of mHTT. However, allele discrimination based on CAG repeat length induces off-targets in other genomic regions. A promising alternative approach is the modification of the *HTT* coding sequence using CRISPR/Cas system. While allele specific NMD-mediated *mHTT* lowering strategies only target the full-length *mHTT* transcript, the removal of the *mHTT* exon 1 completely depletes every potential toxic form of mHTT, including the CAG expansion itself. Nonetheless,

this strategy requires the combination of two sgRNAs that may enhance off-target events. This limitation may be overcome by delivery systems allowing the transient expression of Cas9 nuclease. Finally, novel therapeutic strategies to be clinically tested should aim at (1) efficient drug target engagement (all toxic mHTT forms); (2) reduced toxicity (allele-specificity and low off-target effects) and (3) coverage of all brain structures affected in HD.

1.9 Viral-mediated gene delivery

Since viruses have naturally evolved to infect cells, they are some of the most attractive tools to deliver genetic material (Kotterman et al., 2015).

1.9.1. Lentiviral Vectors

The most known and studied lentivirus is the highly pathogenic viral strain of the human immunodeficiency virus (HIV-1). It is an enveloped virus, and its genome consists in two positive-sense single-stranded (ssRNA) molecules (Engelman & Cherepanov, 2012; Ramdas et al., 2020; Sakuma et al., 2012). Briefly, the HIV-1 entries the cells by receptor-mediated envelope/membrane fusion (Figure 1.25). Once inside the cell, it is formed the preintegration complex (PIC), composed by viral RNA and proteins. At this stage, the viral ssRNA starts to be converted into double-stranded DNA (dsDNA) by the viral reverse transcriptase (RT). Besides the viral genome and the RT enzyme, the PIC is composed by other viral and cellular proteins, which are thought to mediate the nuclear importation and viral genome integration. After PIC nuclear import, the viral DNA integration into the host cell chromosomal DNA is catalyzed by the viral integrase (IN) and host repair enzymes. The integrated proviral DNA is then transcribed and translated using the host machinery. At this point, the viral genome is packaged into virions and the newly formed infectious particles exit the cell using the endosomal sorting complexes through a process called budding. This mechanism allows the viral particles to uptake specific host proteins in their envelope, facilitating subsequent cell infections.

The HIV-1 genome is ~ 9.6 kb and encodes for nine open reading frames (ORFs) (Engelman & Cherepanov, 2012; Ramezani & Hawley, 2002; Sakuma et al., 2012) (Figure 1.26). The genes can be divided into three groups: structural (gag, pol and env), regulatory (tat and rev) and accessory genes (vif, vpr, vpu and nef). The genes gag, pol and env encode for structural polyproteins which are subsequently cleaved into distinct proteins required for virus integration and replication (viral RT and IN enzymes) and proteins involved in viral envelope formation and virion maturation. The regulatory genes tat and rev encode for a transcription trans-activator which enhances the viral mRNA expression and for a protein involved in the viral mRNA transport to the cytoplasm, respectively. The accessory genes are not essential for viral replication but they specify virulent factors that enhance the replication *in vivo* (Milone & O'Doherty, 2018). Regarding

cis-acting elements, HIV-1 contains important components which includes two long terminal repeats (LTRs), the trans-activation response (TAR) element, the primer binding site (PBS), the retroviral psi packaging element (ψ) and the rev response element (RRE) (Figure 1.26). Each LTR flanking the proviral DNA genome consists of the U3 region, identical repeat (R) region and U5 region. The U3 region has promoter activity, the R region is important for viral integration and contains the polyadenylation signal, and the U5 region contains the TAR element. The TAR element is a RNA secondary-structure recognized by the regulatory tat protein. The PBS is essential for the binding of the tRNA-Lys, which is used as primer for reverse transcription. On the other hand, RRE and psi elements play a crucial role in the replication phase. RRE regulates the splicing and export of full-length viral mRNAs to the cytoplasm, while the psi element is essential for the packaging of the retroviral RNA genome into the viral capsid.

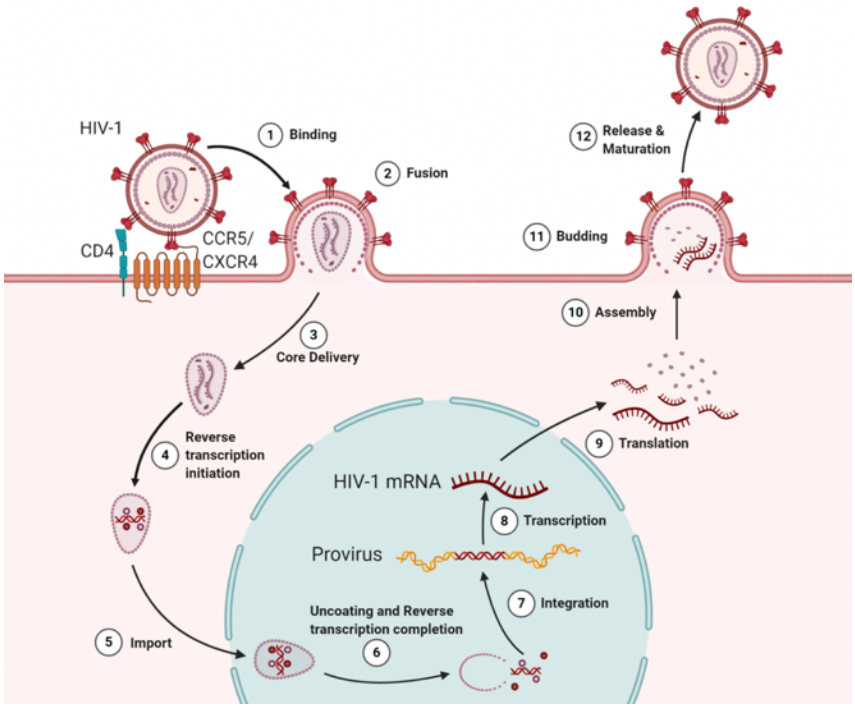

Figure 1.25: The HIV-1 lifecycle. (Ramdas et al., 2020)

The genome of HIV-1 has been used as a parental genome for the development of replication-defective lentivirus carrying a transgene expression cassette. Although these virions are unable to replicate, they are still able to integrate the genome of the infected cells (Engelman & Cherepanov, 2012; Ramezani & Hawley, 2002; Sakuma et al., 2012). The manufacture proceeding of lentiviral vectors has evolved and there are at least 3 generation systems (Figure 1.27). All of them consist in the co-transfection of multiple plasmids expressing different viral components to a producer cell line. The self-inactivating LVs (SIN) correspond to the last generation and contain modified cis-acting motifs allowing the packaging and integration of the transgene, but not its replication (Miyoshi et al., 1998; Zufferey et al., 1998). Briefly, the U3 region of the 5' LTR was replaced by the cytomegalovirus (CMV) promoter and deleted in the 3' LTR to

prevent recombination events that could result in replication-competent retroviruses (RCRs). The other components of the system consist of (i) packaging plasmid expressing HIV Gag (structural proteins) and Pol (reverse transcriptase and integrase components), (ii) a rev expressing plasmid, and (iii) an envelope plasmid expressing viral glycoproteins. Because HIV-1 envelope mainly recognizes the human CD4 receptor, viral glycoproteins are integrated in the LV envelope to expand the tropism and increase the rates of production (process named pseudotyping). The vesicular stomatitis virus G protein (VSV-G) has been widely used for LV pseudotyping. It binds to the LDL ubiquitous receptor, allowing transduction of a wider set of cells (Finkelshtein et al., 2013). In addition, other glycoproteins have been used to pseudotype LVs to confer neuronal retrograde transport features (Hirano et al., 2013; Kato et al., 2011, 2014).

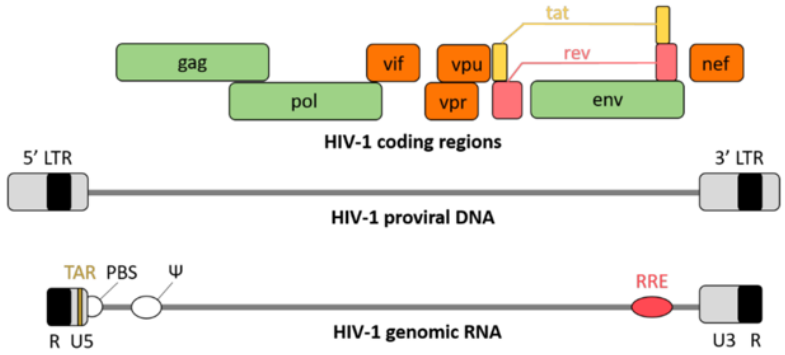

Figure 1.26: Structural features of the HIV-1 proviral DNA and genomic RNA. (Ramezani & Hawley, 2002)

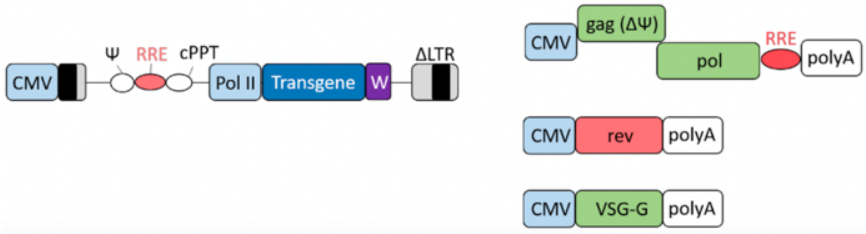

Figure 1.27: Schematic representation of the system for recombinant SIN lentiviral vector production. (Ramezani & Hawley, 2002)

1.9.2. Adeno-associated viral vectors

AAV is a small (25 nm), non-pathogenic and non-enveloped parvovirus that contains a ssDNA genome protected by an icosahedral capsid. AAV naturally infects humans and 12 naturally occurring AAV serotypes (AAV1 – AVV12) have been identified (Wang et al., 2019). AAV has evolved to specifically infect different cell types and each AAV serotype has a specific tissue tropism as a result of the interaction of the capsid proteins with different cellular molecules. The life cycle begins with the attachment of the AAV capsid to the receptor and co-receptor(s) on the cellular membrane which induces the viral uptake by endocytosis (Figure 1.28). Once inside

the cell, the viral particles need to escape endosomes in order to translocate to the nucleus. The lower pH of the endosomal compartment induces capsid structural modifications that promote the endosomal escape and retrograde transport to the nucleus. The nuclear translocation of the virion is still poorly understood. Once in the nucleus, the uncoated viral ssDNA is converted into dsDNA. AAV replication is dependent on co-infection by helper virus(es), such as adenovirus, herpes virus and vaccinia virus, which encode for proteins that activate the transcription of the AAV genes required for AAV replication. If the cell is not infected with helper virus(es), the AAV genome persists latently in the cell as an episomal molecule or integrates in the genome. In permissive conditions for replication, the AAV genome is actively transcribed, and the subsequent viral proteins mediate the AAV genome replication and encapsulation into viral particles (Figure 1.28).

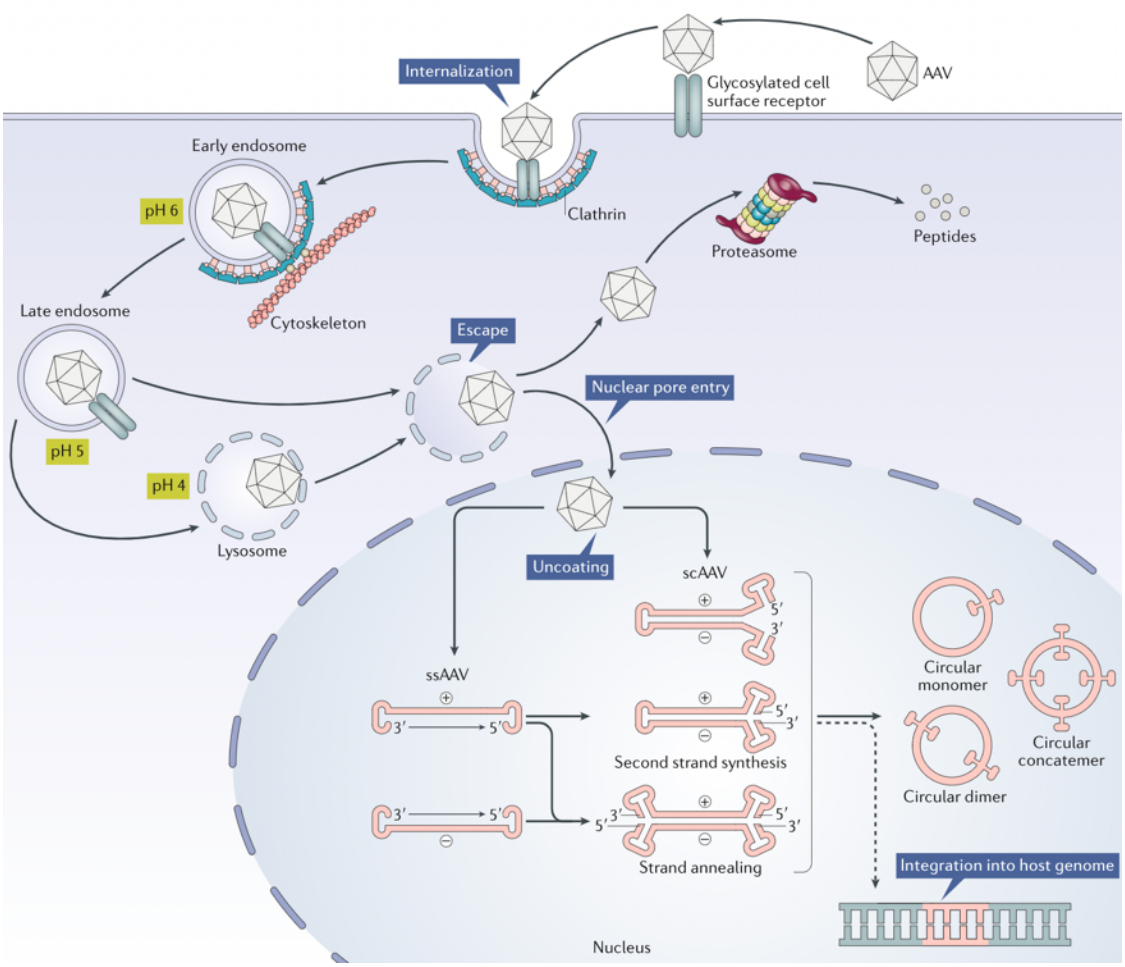

Figure 1.28: Illustration of AAV transduction mechanism. (Wang et al., 2019)

The AAV genome is approximately 4.7 kb and consists in 2 genes flanked by two inverted terminal repeat (ITR) sequences (Kotterman et al., 2015; Wang et al., 2019) (Figure 1.29). The rep gene encodes proteins involved in viral replication while cap gene encodes for capsid proteins. The rep gene is transcribed from two distinct promoters (P5 and P19) and encodes for 4 non-structural proteins (Rep78, Rep68, Rep52 and Rep40). The cap gene transcription is controlled exclusively by the P40 promoter, encoding three capsid proteins (VP1-3) and the

assembly-activating protein (app). Instead using distinct promoters to produce distinct mRNAs/proteins, the cap gene uses alternative start codons to translate different proteins from the same mRNA. The ITR sequence is 145 bp in length and contains a 125 bp palindromic sequence that has a T-shaped hairpin structure. This secondary structure possesses the origin of replication.

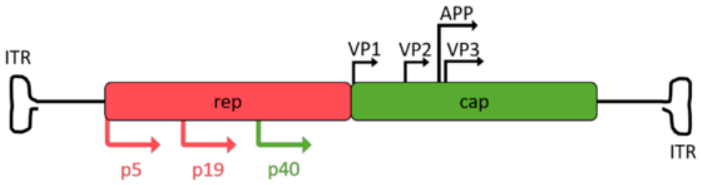

Figure 1.29: Schematic representation of the AAV genome. (Kotterman et al., 2015)

The generation of rAAV is usually achieved by transfecting a producer cell line with three plasmids (Kotterman et al., 2015) (Figure 1.30). The transfer plasmid contains the transgene expression cassette flanked by two intact ITRs. While the packaging plasmid contains the two ORFs of AAV parental genome, the helper plasmid encodes for additional genes required for AAV replication in the producer cells, such as E2A, E4 and VA RNA. Since the non-structural protein involved in AAV integration is encoded by rep gene and it is absent in the rAAV viral particle, these replication-deficient viral vectors do not tend to integrate the genome of the infected cells.

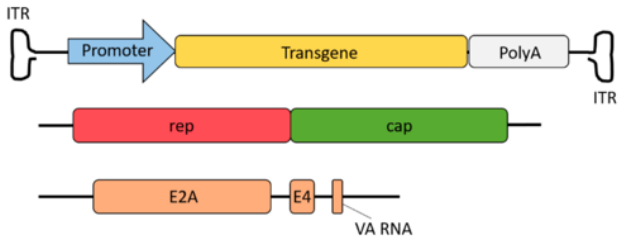

Figure 1.30: Schematic representation of the production system of recombinant AAV vectors. (Kotterman et al., 2015)

1.9.3. Toolbox of adeno-associated viral vectors for the CNS

Both lentiviral and adeno-associated vectors infect dividing and non-dividing cells (Kotterman et al., 2015) but they differ in the infectious mechanism. While rAAV persists mainly in episomal form in the infected cells, lentiviral vectors integrate the host chromosomal DNA. The random genomic insertion by LVs increases the oncogenic risk as insertional mutagenesis has the potential to disrupt crucial host genes. Nevertheless, this feature makes LVs a usefull tool for the transduction of dividing cells since they integrate in the genome and viral copies are not diluted as cells divide.

In contrast, AAVs have become the most prominent delivery vehicle for the CNS as they are non-pathogenic, present reduced immunogenicity and allow long-term gene expression without the need for genomic insertion (Challis et al., 2022; Zhu et al., 2021). In addition, the natural evolution of AAV into different AAV serotypes has enabled us to infect a wide range of cell types in a serotype-specific manner (Evers et al., 2018; Löw et al., 2013; Mondo et al., 2018). To date, two AAV-based gene therapies for the treatment of CNS disorders have been approved for SMA (Mendell et al., 2017) and aromatic L-amino acid decarboxylase (AADC) deficiency (Tai et al., 2022). In addition, many others are currently being clinically tested for several disorders, including Huntington's disease (Zhu et al., 2021). While most of them are based on gene replacement (i.e. delivery of cDNA expressing a deficient gene), Editas Medicine has tested a gene-editing approach to restore vision loss in Leber congenital amaurosis type 10 (LCA10) (Maeder et al., 2019). Unfortunately, the clinical trial has recently paused enrollment for disappointing efficacy with only 3 out of 14 patients presenting clinical improvements. Nevertheless, it was not observed any ocular serious adverse events related to the delivery of CRISPR to post-mitotic cells.

The treatment of localized organs such as the retina or inner ear are in an advantageous position for the development of gene-editing based therapies due to the reduced targeted area and easier accessibility. Indeed, one of the current major limitations of gene therapy for neurological disorders is the limited efficiency of delivery CNS. Adeno-associated viruses have been delivered into the CNS by intracranial or intravenous injection or by infusion into the CSF. Intracranial injection does not cover large or dispersed brain regions and produces a spatial gradient of transgene expression around the injection site. Intravenous administration requires high doses to transduce the CNS, increasing the risk for potential toxicity in the peripheric organs such as the liver. Finally, delivery into the CSF is invasive and most of the viral particles end on the systemic circulation. Therefore, huge efforts are taking place to identify AAV variants with precise transduction profiles and/or with the ability to cross the BBB. Multiple modern methods for capsid engineering based on rounds of selection of AAV variants have been developed. Among the huge list of discovered variants is the AAV-PHP.eB (Chan et al., 2017) with enhanced CNS targeting, AAV2.retro (Tervo et al., 2016) and AAV2-MNM004 (Davidsson et al., 2019) displaying high neuronal retrograde transport, and AAV-MG (Lin et al., 2022) which targets microglial cells more efficiently. The field of CNS drug delivery is developing at such a fast pace that new tools may be available soon to tackle some of the problems concerning gene delivery for the treatment of neurological disorders.

CHAPTER 2

Aim of the thesis

2. Aim of the thesis

The genetic cause of HD makes the *HTT* gene a promising target. Among the multiple huntingtin-lowering approaches, the use of the CRISPR/Cas9 gene editing tool to permanently inactivate the *mHTT* allele holds a huge therapeutic potential. The present project aimed at developing more efficient and safer gene editing strategies to inactivate the *mHTT* allele. This project is divided into two parts:

1 – Maximization of the therapeutic potential of gene therapy strategies for HD:

Although the striatum is the main region affected in HD, it is well known that the corticostriatal circuitry is affected at early stages of the disease. We have previously shown the proof-of-concept of *HTT* editing in the striatum by the LV-based KamiCas9 system, in which Cas9 nuclease is transiently expressed to minimize potential long-term toxic effects (Merienne et al., 2017). Here, we adapted the system for AAV delivery and combined the tropism features of these viral vectors to maximize the inactivation of the *HTT* gene in both striatal (SPNs) and cortical projection neurons (CPNs) affected in HD.

2 – *In vivo* assessment of the efficiency of allele specific strategies to inactivate *mHTT* allele:

It is still debatable whether the knockdown/knockout of wtHTT is deleterious in the context of the disease. The presence of SNPs linked to the expanded CAG represents a great opportunity to selectively target the *mHTT* allele with the CRISPR/Cas9 system. One strategy relies on the excision of the *mHTT* exon 1 containing the expanded CAG repeat. Although others have explored this approach, it is not clear how efficient this strategy is in the brain *in vivo* and whether it could be eventually translated into the clinic. Here, we revise this strategy by quantitatively assessing its efficiency *in vivo* using the adapted AAV-based KamiCas9 system.

CHAPTER 3

Maximization of therapeutic potential of gene therapy strategies for HD

Contribution

Writing of the manuscript

Preparation of the figures

Figure 3.1C-E – Design, injection, extractions, analysis

Figure 3.3 – Data analysis

Figure 3.4A-B – Design, injection, perfusion, imaging

Figure 3.4C-F – Design, injection, perfusion, imaging

Figure 3.5 – Design, injection, extractions, analysis

Figure S3.1A-B – Design, transfection, extractions, analysis

Figure S3.2C-D – Design, transduction, extractions, analysis

Figure S3.5 – Clonal line generation, extractions, analysis

Figure 3.6 – Extractions, analysis

3. Maximization of therapeutic potential of gene therapy strategies for HD

3.1. Duarte et al., 2023 (in revision)

Semi-automated workflows to quantify AAV transduction in various brain areas and predict gene editing outcome for neurological disorders

Fábio Duarte,[1,2] Mergim Ramosaj,[1,2,3] Ed Hasanovic,[1,2] Sara Regio,[1,2] Melanie Sipion,[1,2] Maria Rey[1,2] and Nicole Déglon[1,2]

[1]Lausanne University Hospital (CHUV) and University of Lausanne (UNIL), Department of Clinical Neurosciences (DNC), Laboratory of Cellular and Molecular Neurotherapies, Lausanne, Switzerland. [2]Lausanne University Hospital (CHUV) and University of Lausanne (UNIL), Neuroscience Research Center (CRN), Laboratory of Cellular and Molecular Neurotherapies (LCMN), Lausanne, Switzerland. [3]Department of Biomedical Sciences, Faculty of Biology and Medicine, University of Lausanne, Lausanne, Switzerland.

Correspondence should be addressed to N.D. (nicole.deglon@chuv.ch)

Lausanne, Vaud, Switzerland

Corresponding author:
Nicole Déglon
Lausanne University Hospital (CHUV)
Laboratory of Cellular and Molecular Neurotherapies
Pavillon 3, Avenue de Beaumont
1011 Lausanne
Switzerland
Phone: +41 21 314 21 20
E-mail: nicole.deglon@chuv.ch

In revision in: *Molecular Therapy - Methods and Clinical Development*

3.1.1. Abstract

One obstacle to the development of gene therapies for the central nervous system is the lack of workflows for quantifying transduction efficiency in affected neural networks and ultimately predicting therapeutic outcome. We integrated data from a brain cell atlas with 3D or 2D semi-automated quantification of transduced cells in segmented images to predict AAV transduction efficiency in multiple brain regions. We used this workflow to estimate the transduction efficiency of AAV2/rh.10 and AAV2.retro co-injection in the corticostriatal network affected in Huntington's disease. We then validated our pipeline in gene editing experiments targeting both human and mouse huntingtin genes in transgenic and wild-type mice, respectively. Our analysis predicted that 54% of striatal cells and 7% of cortical cells would be edited in highly transduced areas. Remarkably, in the treated animals, huntingtin gene inactivation reached 54.5% and 9.6%, respectively. These results demonstrate the power of this workflow to predict transduction efficiency and the likely efficacy of gene therapies in the central nervous system.

eTOC Synopsis

Using semi-automated quantification pipelines, the authors show that striatal co-injection of AAV2/rh.10 and AAV2.retro efficiently transduces the corticostriatal network affected in HD. Striatal and cortical transduction efficiency was predictive of *HTT* inactivation level in both regions, demonstrating the power of these pipelines to anticipate the potential of gene therapies.

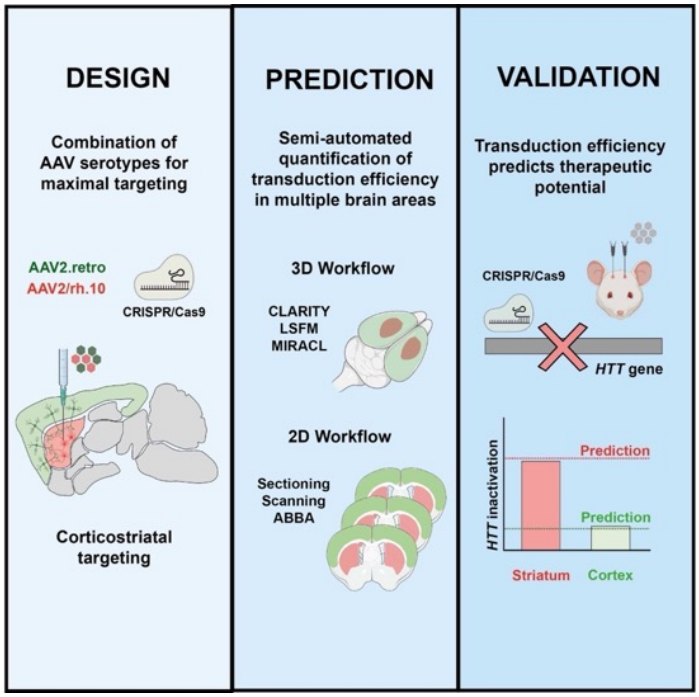

Keywords

CNS, Gene Therapy, Gene Editing, Semi-automated, Transduction Efficiency, Huntington's Disease

3.1.2. Introduction

Over the last decade, the concept of permanently treating neurological diseases by a single delivery of a therapeutic gene has driven the development of central nervous system (CNS) gene therapy (Hudry & Vandenberghe, 2019). This global effort has achieved a certain success, as attested by the recent approval of gene therapy products for spinal muscular atrophy (SMA) (Mendell et al., 2017) and aromatic L-amino acid decarboxylase (AADC) deficiency (Tai et al., 2022). However, notwithstanding these recent accomplishments, the development of CNS gene therapies remains challenging due to the complexity of neurodegenerative diseases. These diseases are often characterized by alterations to multiple neuronal networks in several brain regions, with a poor understanding of the underlying molecular mechanisms, associated with complex gene delivery. Adeno-associated viruses (AAVs) are the principal delivery vehicle for therapeutic gene delivery to the CNS (Hudry & Vandenberghe, 2019). The emergence of new AAV capsids has greatly increased transduction efficiency, but there is still a lack of semi-automated quantitative workflows for assessing the transduction profile and predicting therapeutic potential. Current workflows are based on the injection of AAVs expressing fluorescent reporter genes followed by the confocal imaging of immunolabeled tissue sections (Chan et al., 2017; Deverman et al., 2016; Hanlon et al., 2019; Smith et al., 2021). These methods are time-consuming, especially when large areas of the brain are transduced, and the manual parcellation of each brain region is required to assess transduction efficiency.

Here, we took advantage of 3D and 2D semi-automated workflows for evaluating transduction efficiency in multiple brain regions, with a view to predicting therapeutic outcome. This pipeline integrates data from a mouse brain cell atlas (Erö et al., 2018) to predict the pattern of transduction in various anatomical brain regions. It also makes use of recently developed methods for analyzing images from mice after AAV-GFP injection. 3D images from clarified brain (CLARITY) (Chung & Deisseroth, 2013) or 2D images from coronal brain sections (Bankhead et al., 2017; Chiaruttini et al., 2022; Schmidt et al., 2018) are co-registered with a mouse reference atlas (ARA) (Perens & Hecksher-Sørensen, 2022) to evaluate brain delivery performance.

We used these workflows to optimize gene editing approaches for Huntington's disease (HD), which is caused by a triplet repeat expansion in the huntingtin (*HTT*) gene. HD is characterized by a degeneration of spiny projection neurons (SPNs) in the striatum and neuronal dysfunction and cell death in the cerebral cortex and other areas of the brain (Johnson et al., 2021; Tabrizi et al., 2020). All gene editing strategies for HD to date have focused exclusively on the striatum (Ekman et al., 2019; Monteys et al., 2017; Oikemus et al., 2022; Yang et al., 2017). We developed an AAV platform based on our KamiCas9 system (Merienne et al., 2017) to target the corticostriatal neuronal network affected in HD. We delivered AAV2.retro (Tervo et al., 2016) which has strong retrograde properties, together with AAV2/rh.10 (Cearley & Wolfe, 2006; Gao et al., 2004) which efficiently transduces the striatum, to maximize *HTT* gene editing. We used our 3D and 2D workflows to estimate cortical and striatal transduction efficiency and to predict

the degree of *HTT* gene inactivation. We show that these semi-automated workflows provide accurate quantitative assessments of AAV profiles in various brain regions and demonstrate the power of these pipelines for predicting the likely therapeutic outcome of gene editing strategies.

3.1.3. Results

Development of an AAV-KamiCas9 system for CNS gene editing

We previously developed a lentiviral (LV)-based self-inactivating KamiCas9 system for gene editing (Merienne et al., 2017). Here, we adapted the system for AAV, which diffuse widely throughout the brain and yield high transduction efficiencies in various regions. As proof-of-principle, we first showed that the co-injection of AAV2/1-EFS-SpCas9 (Nishiyama et al., 2017) with an AAV2/1 expressing a sgRNA targeting the translational start site of GFP (sgGFP) led to a complete loss of GFP fluorescence in the transduced striatal area of Drd2-GFP transgenic mice (Gong et al., 2003; Kramer et al., 2011) (Figures 3.1A-B). We then focused on the *HTT* gene and developed two AAV-KamiCas9 systems (Figure S3.1A). The *HTT*-targeting sgRNA (sgHTT1) (Merienne et al., 2017) is under the control of the U6 promoter, whereas expression of the SpCas9 self-targeting sgRNA (sgCas9) is driven either by the U6 promoter (KamiCas9^{v1}) or by the 7sk promoter (KamiCas9^{v2}). High levels of *HTT* editing (42.5-57.9%) and SpCas9 self-editing (57.3-73.6%) were obtained with both systems in human embryonic kidney 293T (HEK293T) cells (Figure S3.1B). We selected the AAV2/1-CRISPR and AAV2/1-KamiCas9^{v1} for inactivation of the wild-type (WT) human *HTT* gene in the striatum of fully humanized HU18/18 transgenic mice (Southwell et al., 2013) (Figure 3.1C). The injection of AAV2/1-CRISPR and AAV2/1-KamiCas9^{v1} generated indels in 30.2 $\pm$ 6.3% and 21.0 $\pm$ 8.03% of *HTT* alleles (Figure 3.1D). We assessed SpCas9 self-editing, by analyzing DNA and RNA samples (Figure 3.1E). Löw and coworkers reported that large numbers of AAV genomes remained present as single-stranded AAV (ssAAV) several weeks after injection (Löw et al., 2013) (Figure 3.1F). By measuring SpCas9 self-editing at the RNA level, we avoided amplifying ssAAVs, which are not a substrate for SpCas9 (Figure 3.1F). We showed that 50.7 $\pm$ 7.7% of the SpCas9 transcripts contained indels, whereas only 29.0 $\pm$ 8.1% of AAV genomes had been edited (ssAAV and dsAAV) (Figures 3.1E-F). It has also been suggested that the failure of the DNA repair machinery to fix double-strand breaks (DSBs) on dsAAV episomes can lead to the degradation of these structures (Ibraheim et al., 2021; Krooss et al., 2020; Li et al., 2018, 2021) (Figure 3.1F). We tested this hypothesis, by determining whether *HTT* editing was affected by cleavage of the AAV expressing the sgHTT1 (Figure S3.1C). *HTT* editing efficiency was strongly decreased by the induction of AAV cleavage (7.1 $\pm$ 1.3%), resulting in levels much lower than for the uncleavable vector (28.2 $\pm$ 3.6%) (Figure S3.1D). This lower rate of *HTT* editing is explained by the lower levels of sgHTT1 due to the cleavage-induced partial degradation of the dsAAV expressing the sgHTT1. Translating these results to the KamiCas9 system, SpCas9 self-cleavage induces a partial degradation of dsAAVs expressing SpCas9,

thereby decreasing SpCas9 expression. Other AAV self-deleting systems rely exclusively on AAV degradation (Ibraheim et al., 2021; Krooss et al., 2020; Li et al., 2018, 2021) but our AAV-KamiCas9 efficiently inactivates SpCas9 even when the DSBs are successfully repaired (Figure 3.1F), further decreasing the risk of off-target events. In summary, we show here that the AAV-KamiCas9 system induces high levels of target gene editing with the effective self-activation of SpCas9.

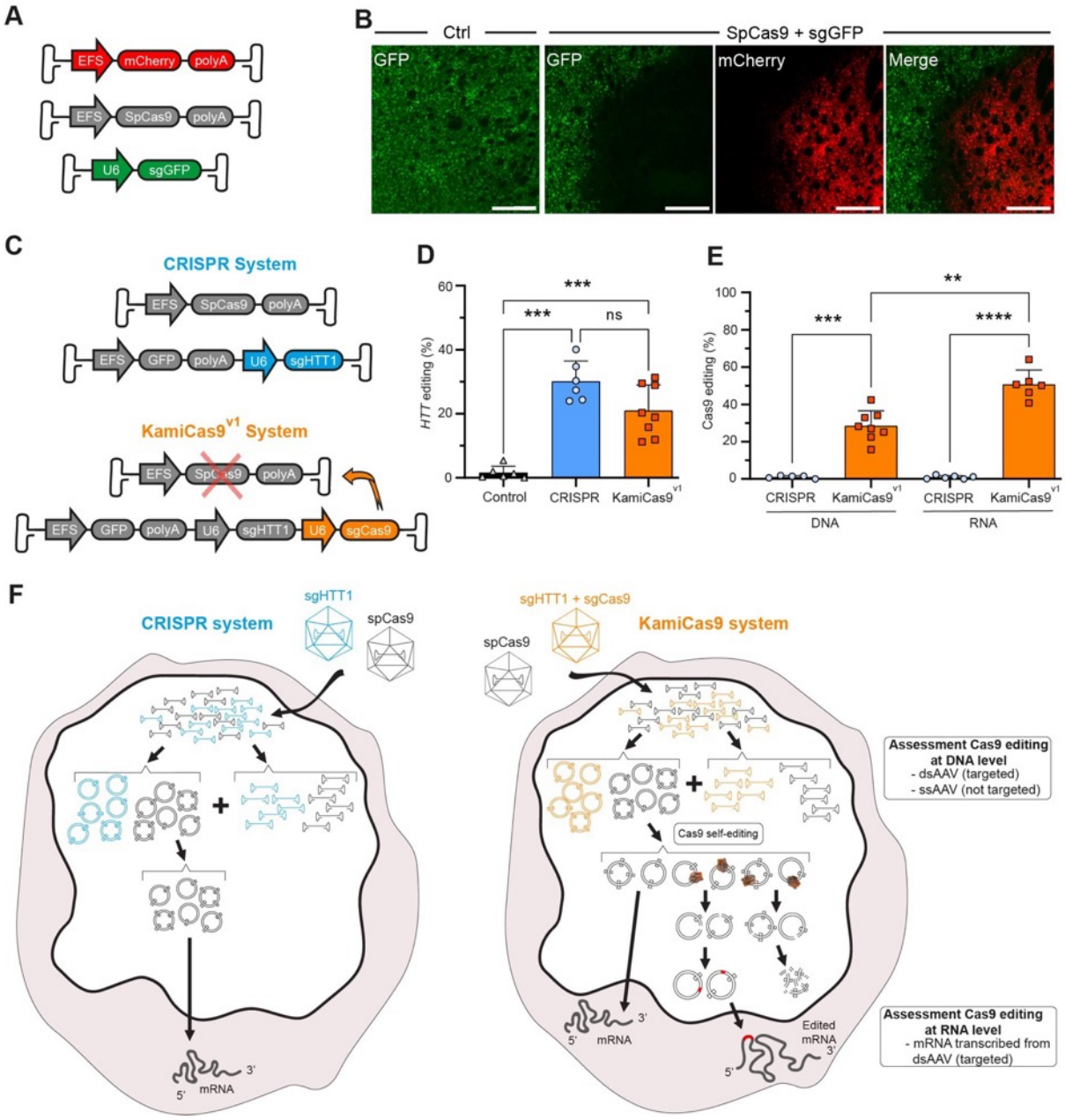

Figure 3.1: Development of an AAV-KamiCas9 system for *in vivo* gene editing. (A) Schematic representation of the AAV-CRISPR-GFP used for *in vivo* gene editing. The first two AAV2/1 express mCherry or the spCas9 under the control of the short elongation factor 1α promoter (EFS). The third vector expresses a sgRNA targeting the translational start site of GFP (sgGFP) under the control of the U6 promoter. **(B)** Representative images of the striatum of Drd2-GFP mice with and without injection of the CRISPR-GFP system. Scale bar: 200 µm. **(C)** Schematic representation of AAV2/1-CRISPR and AAV2/1-KamiCas9^{v1} used to inactivate the human *HTT* gene in the striatum of HU18/18 transgenic mice. The sgRNA targeting the translational start site of the human *HTT* gene (sgHTT1) (Merienne et al., 2017) is under the control of the U6 promoter in both systems. In KamiCas9^{v1}, there is a second sgRNA targeting the translational start site of SpCas9 itself (sgCas9). **(D)** Eight weeks post-injection, striatal punch

specimens were collected from the GFP-positive area. The frequency of *HTT* indels was assessed by TIDE (Brinkman et al., 2014) in DNA extracts (n=6 hemispheres from 3 animals for control and CRISPR; n=8 hemispheres from 4 animals for KamiCas9^{v1}). **(E)** The frequency of indels in the SpCas9 transgene was assessed in DNA (n=6 hemispheres from 3 animals for CRISPR; n=8 hemispheres from 4 animals for KamiCas9^{v1}) and RNA (n=6 hemispheres from 3 animals for CRISPR; n=6 hemispheres from 4 animals for KamiCas9^{v1}) extracts. **(F)** Diagrams illustrating the progressive inactivation of nuclease activity in the AAV-KamiCas9 system. Most AAV genomes are not self-targeted because they are present as ssAAV. The amplification of ssAAV-SpCas9 during TIDE analysis does not reflect the functional, actively transcribed AAV-SpCas9 genome population. By contrast, TIDE analysis for the SpCas9 transgene in RNA samples detects indels only in actively transcribed dsAAV-SpCas9 genomes. Data are represented as mean ± SD.

Development of semi-automated workflows for quantifying transduction efficiency in multiple brain areas

CNS disorders are complex and often associated with alterations to the neuronal networks in multiple brain regions. New therapeutic strategies and genetic tools for the treatment of CNS disorders are continually being developed, but effective gene delivery to affected brain regions remains a major challenge. Transduction efficiency depends on the specific features of each AAV serotype (e.g., tropism, diffusion, and transport properties), the amount of AAV injected (e.g., dose, volume, and flow rate) and the surgical procedure used (e.g., cannulas, coordinates, and procedure variability). All these parameters can be optimized to maximize gene delivery, but there are currently no automated quantitative workflows for measuring transduction efficiency in various regions of the brain. As a means of optimizing CNS gene delivery and facilitating the development of new therapies, we used semi-automated 3D and 2D fluorescence-based workflows for quantifying transduction efficiency in multiple brain areas (Figure 3.2). The first step in this pipeline is the estimation of the maximum theoretical number of cells that can be targeted in each brain region based on the specific characteristics of the vector, such as its tropism and retrograde transport. This estimate integrates information from the Blue Brain Cell Atlas (Erö et al., 2018). For example, a vector with a neuronal tropism can potentially target 88% of the cells in the cerebellum but only 74% of the cells in the hippocampus. Once the maximum number of cells that can be targeted is known, it is possible to quantify the number of cells actually transduced in a clarified brain (3D) or in coronal sections (2D). The 3D imaging-based workflow involves brain clarification (Chung & Deisseroth, 2013) followed by light sheet fluorescence microscopy (LSFM) imaging (Figure 3.2). The multimodal image registration and connectivity analysis (MIRACL) pipeline (Goubran et al., 2019) were then used to register against the Allen mouse brain common coordinate framework (CCFv3) reference atlas (Wang et al., 2020). The coordinates of all transduced cells are determined with fiji and catalogued on segmented brain images to quantify the number of cells transduced in each brain region using the recently published map objects to atlas (MOTA) pipeline (Scholler et al., 2022). In the 2D workflow, the DAPI signal from brain coronal sections is used for registration against the Allen CCFv3 reference atlas (Wang et al., 2020) with the aligning big brains and atlases (ABBA) plugin in fiji (Chiaruttini et al., 2022) (Figure 3.2). The segmented brain regions are then imported into QuPath software (Bankhead et al.,

2017) and the StarDist deep learning-based extension (Schmidt et al., 2018) is used to quantify the number of transduced cells in the various regions.

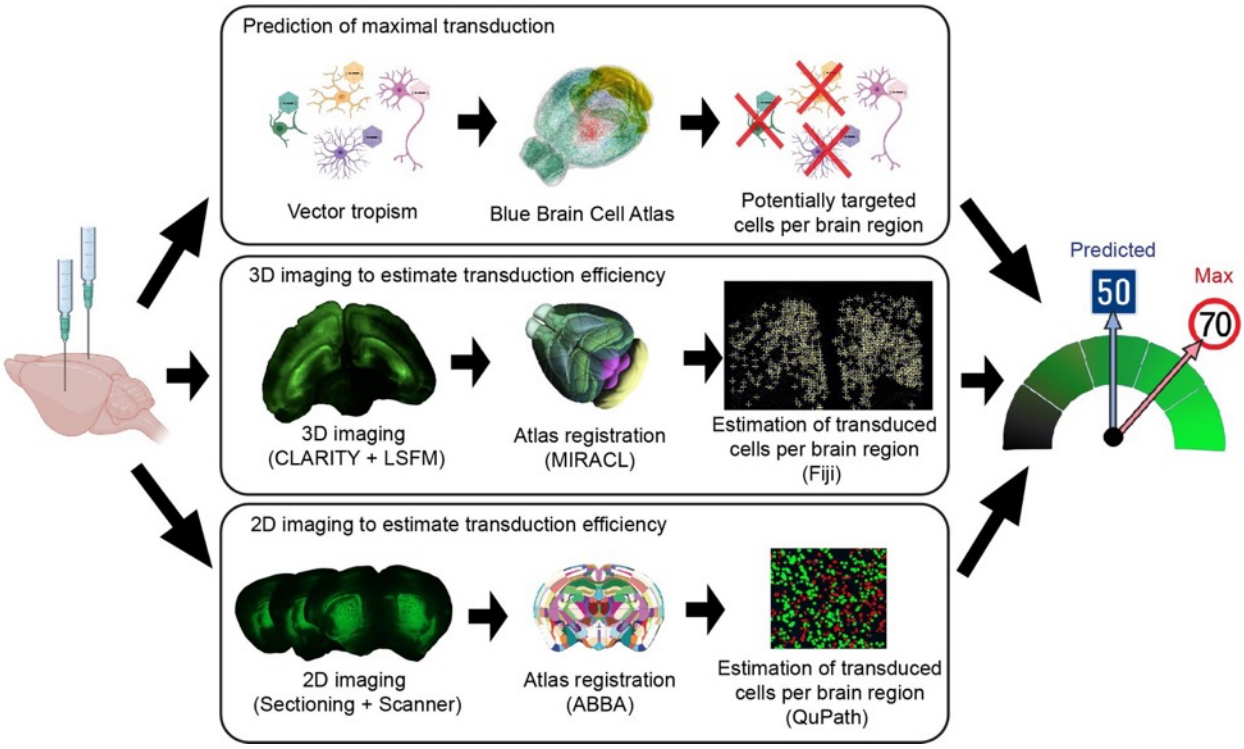

Figure 3.2: Diagram of the 2D and 3D fluorescence-based quantitative workflows for estimating transduction efficiencies in multiple brain regions. The first step of the pipeline is estimation of the theoretical maximum number of cells that can be transduced based on data from the Blue Brain Cell Atlas and the specific features of the vector (tropism, retrograde transport). The second step is quantification of the cells transduced, with either the 3D or the 2D imaging workflow. In the 3D workflow, the whole-mount brain is clarified and imaged by LSFM. The MIRACL pipeline (Goubran et al., 2019) is then used to register the 3D images against the Allen CCFv3 reference atlas (Wang et al., 2020) which contains 662 annotated structures. The coordinates of every GFP-positive cell are determined in fiji and catalogued on the registered images with the MOTA pipeline (Scholler et al., 2022). In the 2D workflow, 25 μm-thick brain coronal sections are subjected to whole-slide scanning. The images are aligned with the Allen CCFv3 reference atlas (Wang et al., 2020) with the ABBA plugin (Chiaruttini et al., 2022) in fiji. QuPath software (Bankhead et al., 2017) and the StarDist plugin (Schmidt et al., 2018) are then used to identify DAPI (4',6-diamidino-2-phenylindole) signals and to quantify GFP-positive signals with a cell classifier.

Gene editing strategies for HD to date have been evaluated only in the striatum (Ekman et al., 2019; Monteys et al., 2017; Oikemus et al., 2022; Yang et al., 2017). However, a loss of striatal SPNs is not the only sign of HD; other regions of the brain are also affected in this disease, including, in particular, the corticostriatal projecting neurons (CPNs) (Johnson et al., 2021; Tabrizi et al., 2020). We made use of the retrograde transport properties of AAV2.retro to achieve a broad delivery distribution and to target brain circuits affected in HD (Tervo et al., 2016). We injected AAV2.retro-CBA-GFP into the striatum and then used our 3D and 2D pipelines to assess the pattern of CPN transduction (Figure 3.3A). We first estimated the maximum theoretical numbers of neurons that could be transduced in each isocortical region. Almost all CPNs are excitatory neurons present in cortical layers II/III, V and VI (Assous & Tepper, 2019); only these cortical cells can be transduced by AAV2.retro (Figure 3.3A). According to the Blue Brain Cell Atlas, the

proportion of excitatory neurons in layers II/III, V and VI differs between isocortical regions (ranging from 22% to 49%) (Table S3.1). For example, AAV2.retro can potentially target 31.4% of the neurons in the orbital area (ORB), but only 22% of those in somatomotor areas (MO).

We investigated whether AAV2.retro transduction was optimal or whether the delivery parameters needed to be modified, by quantifying the cells transduced in a 3D clarified brain and in 2D coronal sections (Figures 3.3B-C and S3.2, and Video S3.1). The 3D and 2D analyses revealed that there were 417,579 and 507,408 GFP-positive neurons, respectively, in the isocortex (Table S3.1). Both analyses indicated that most of the transduced neurons were in more frontal cortical areas, such as the frontal pole (FRP), prelimbic area (PL), MO, ORB, agranular insular area (AI), gustatory area (GU), anterior cingulate area (ACA) and infralimbic area (ILA) (Table S3.1). AAV2.retro transduced 19% of the excitatory neurons in the 10 most transduced isocortical regions (Figure 3.3D). Remarkably, about half of the neurons that could be targeted were transduced in the FRP and 30% of those in the PL and MO areas (Figure 3.3D). These results are consistent with mouse corticostriatal connectome data, demonstrating a high degree of connectivity between the dorsolateral striatum and the prefrontal and motor cortices (Hintiryan et al., 2016). In summary, we demonstrated that the 2D and 3D pipelines yielded similar quantitative outcomes, and that both accurately estimated transduction efficiency.

Maximizing the targeting of the neuronal circuitry affected in HD

We have shown that AAV2.retro efficiently transduces CPNs from isocortical areas implicated in HD, such as the MO and ACA (Johnson et al., 2021). However, AAV2.retro transduction at the site of injection (the striatum) was very limited, as previously reported (Cai et al., 2021; Tervo et al., 2016; Weiss et al., 2020) (data not shown). As a means of maximizing the targeting of the neuronal circuitry affected in HD, we tested the co-injection of AAV2.retro-CBA-GFP and AAV2/rh.10-CBA-mCherry (Figure 3.4A). We also modified the stereotaxic coordinates, injecting the vectors bilaterally at a single striatal site per hemisphere, to reduce the variability associated with the surgical procedure and increase transduction efficacy. As expected, AAV2/rh.10-CBA-mCherry extensively transduced the striatum, whereas AAV2.retro-CBA-GFP predominantly transduced distant CPNs (Figure 3.4B). The minimal overlap between the fluorescent signals obtained suggests that the two AAV serotypes have complementary tropisms. We prevented confounding due to GFP-positive neuropil signals and facilitated the detection and quantification of transduced cells in the striatum, by performing a new experiment with AAV2.retro and AAV2/rh.10 expressing a nuclear green fluorescent protein (AcGFPnuc) (Figures 3.4C-D). The 2D workflow revealed that 927,725 $\pm$ 337,650 striatal cells were AcGFPnuc-positive (Figure S3.3), corresponding to the transduction of 32.2 $\pm$ 14.1% of the DAPI-positive nuclei (Figure 3.4E). An analysis of highly transduced regions in the dorsal striatum (around the injection site) indicated that 53.9 $\pm$ 5.4% of the DAPI-positive nuclei were AcGFPnuc-positive (Figure 3.4F). Overall, we

found that the simultaneous delivery of AAV2.retro and AAV2/rh.10 into the striatum resulted in the transduction of both CPNs and SPNs, the principal neuronal cells affected in HD.

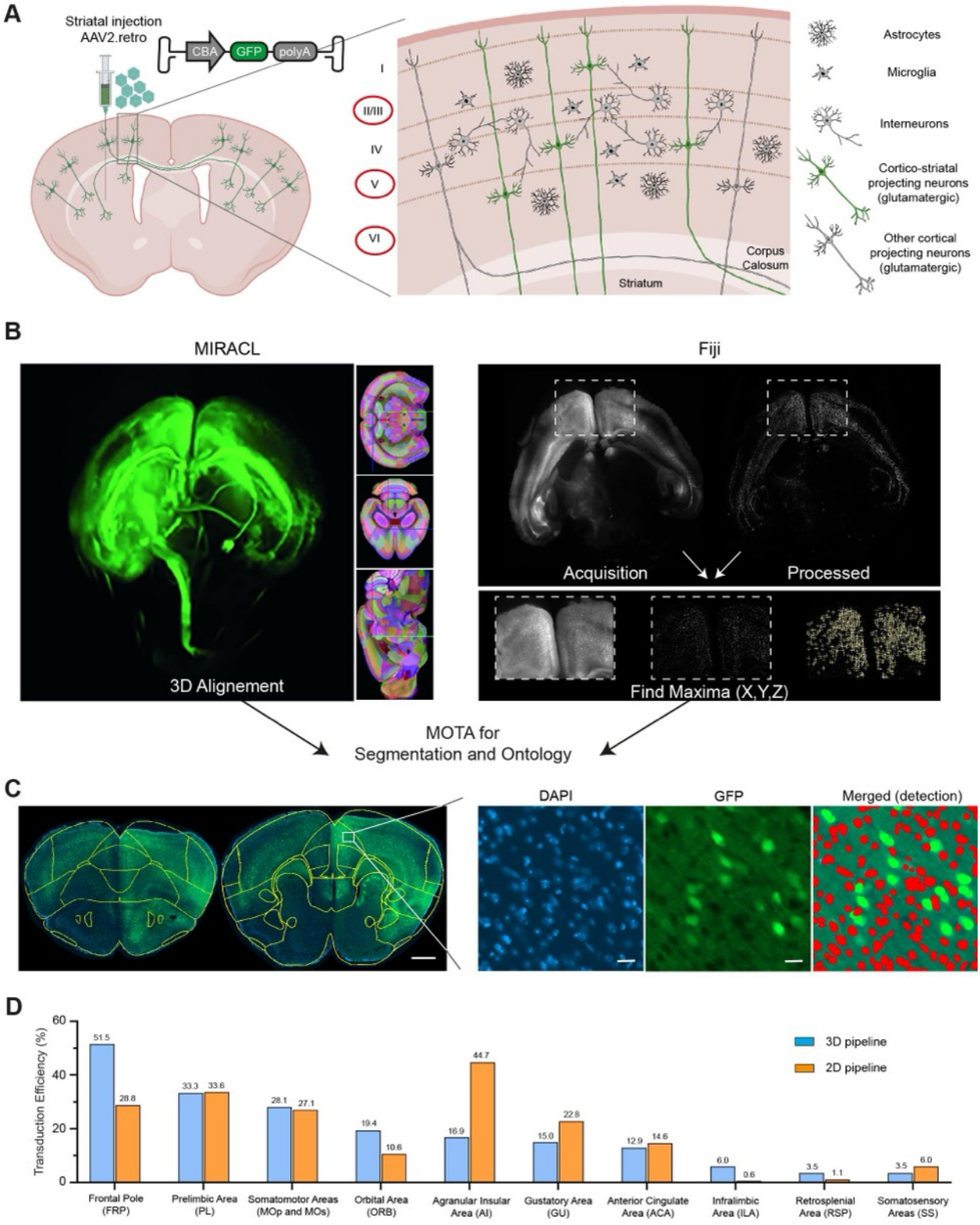

Figure 3.3: 3D and 2D workflows for quantifying transduction in various cortical regions. (A) Diagram illustrating the pipeline for determining the theoretical maximal number of excitatory neurons that could be transduced in the cortex of animals following the injection of AAV2.retro-CBA-GFP. The numbers of excitatory neurons in layers II/III, V and VI of the cortex were determined with information from the Blue Brain Cell Atlas. These neurons correspond to the cells that could be transduced with AAV2.retro-CBA-GFP. **(B)** Dorso-ventral light sheet acquisitions of clarified brain were subjected to MIRACL pipeline for

registration against the Allen CCFv3 reference atlas. Light sheet acquisitions were also processed in Fiji in parallel to determine X,Y,Z coordinates of each transduced cells using Find Maxima function. Both resulting outputs were combined using MOTA to get proper segmentation of cells within each brain region ontology. **(C)** Coronal brain sections were registered against the Allen CCFv3 reference atlas in fiji with the ABBA plugin, and then transferred to QuPath. The DAPI-positive nuclei were detected with StarDist, a deep learning-based 2D nucleus detection method trained with a set of fluorescent nucleus images (dsb2018_heavy_augment.pb). A cell classifier was trained to detect transduced GFP-positive cells throughout the entire section. A script was finally generated to run the analysis on all images for the project. Scale bar for low magnification: 800 µm. Scale bar for high magnification: 20 µm. **(D)** 3D and 2D data showing the percentage of GFP^+ excitatory neurons (hence, transduction efficiency) in the 10 isocortical regions most transduced with AAV2.retro-CBA-GFP.

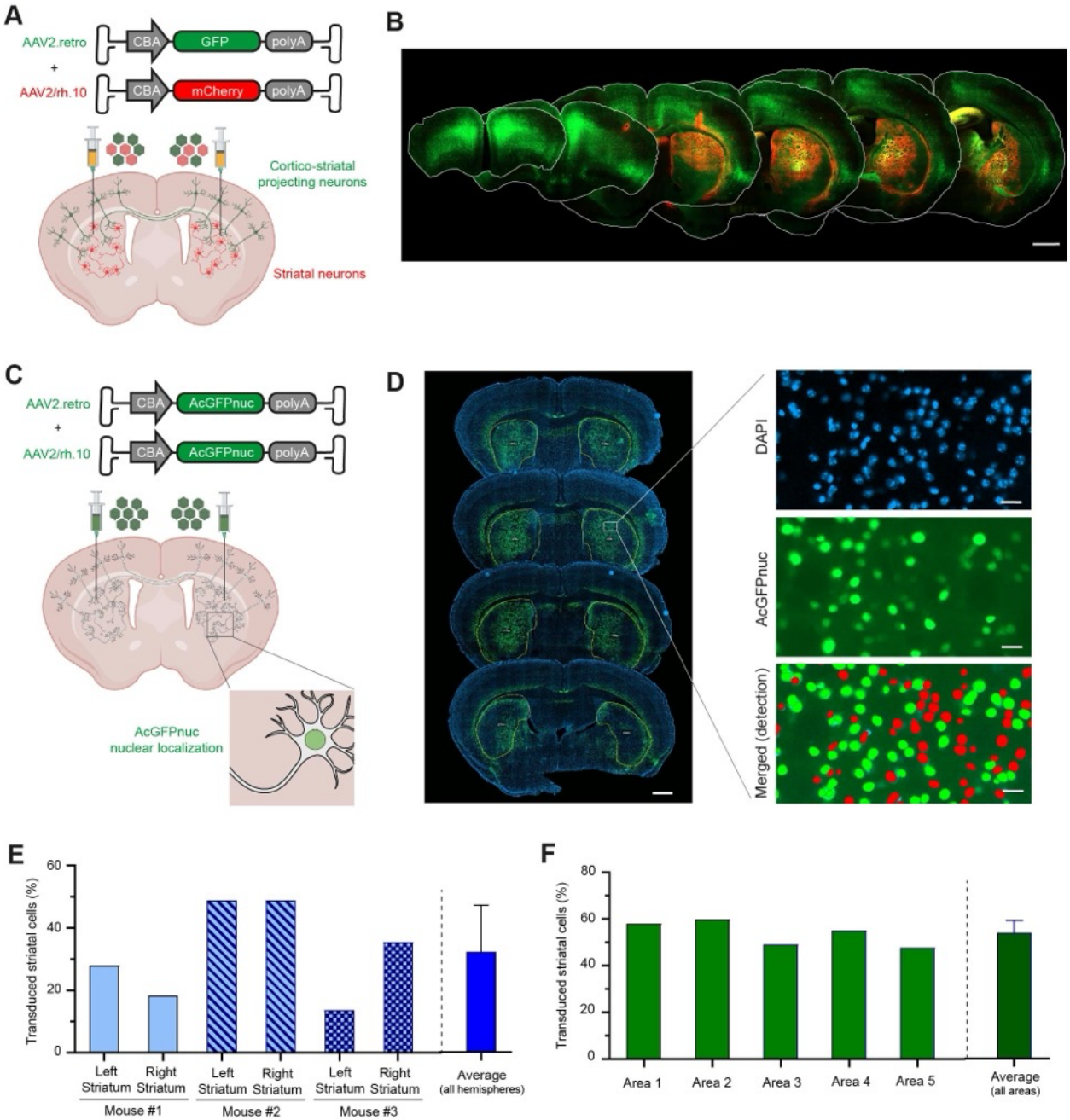

Figure 3.4: Optimized gene delivery following the co-injection of AAV2.retro and AAV2/rh.10. (A) Schematic representation of the experimental setting. AAV2.retro-CBA-GFP and AAV2/rh.10-CBA-GFP were co-injected bilaterally into the dorsolateral striatum of mice to favor retrograde transport in the cortex and striatal transduction. **(B)** Dense cortical layers of GFP-positive CPNs are observed throughout the rostro-caudal axis, whereas mCherry-positive cells are widely distributed throughout the striatum. Scale bar: 1000 µm. **(C)** Schematic representation of the experimental setting. AAV2.retro-CBA-AcGFPnuc and

AAV2/rh.10-CBA- AcGFPnuc were co-injected bilaterally into the dorsolateral striatum for the quantification of striatal transduction efficiency. **(D)** Coronal sections were co-registered against the Allen CCFv3 reference atlas to identify the striatum, and the 2D workflow described in Figure 3.3 was applied. Scale bar for low magnification: 800 µm. Scale bar for high magnification: 20 µm. **(E)** Quantitative analysis showing the percentage of DAPI-positive cells expressing AcGFPnuc in the left and right striatum of three animals. The mean transduction efficiency for the whole striatum is indicated. **(F)** Quantitative analysis showing the percentage of DAPI-positive cells expressing AcGFPnuc in five representative highly transduced areas of the dorsolateral striatum. The mean transduction efficiency in the highly transduced regions is indicated. Data are represented as mean ± SD.

Quantitative workflows accurately predict the outcome of a gene editing strategy targeting the corticostriatal circuitry affected in HD

We assessed the predictive value of the workflow, by evaluating *HTT* gene editing in fully humanized HU97/18 mice (Southwell et al., 2013) (Figure 3.5A). Three months after the co-injection of AAV2.retro- and AAV2/rh.10-KamiCas9^{v2}, the animals were killed, and cortical and striatal punch specimens were collected from the GFP-positive areas (Figure S3.4A). We predicted a maximum theoretical editing level of 31.2 ± 3.6% for the cells in the mediodorsal frontal cortical regions (Figure S3.4A and Table S3.1). The 3D and 2D transduction data indicated that, on average, there were 24.6± 18% (3D) and 17.6± 13.5 % (2D) GFP-positive cortical neurons, corresponding to 7.3 ± 4.9% (3D) and 5.1 ± 3.6% (2D) of all cells in a punch specimen. In the striatum, only SPNs were included in the theoretical prediction, because the EFS promoter driving SpCas9 expression displays neuronal tropism (Figure S3.4B). The predicted maximum theoretical number of cells that could be transduced in the striatum was 70 ± 0.4% (Matamales et al., 2009) and based on the 2D workflow, we expected to target 53.9 ± 5.4% of all cells in the dorsolateral striatum (Figure 3.5C).

The bilateral injection of the AAV-KamiCas9^{v2} system into HU97/18 transgenic mice with AAV2.retro and AAV2/rh.10 resulted in the inactivation of 5.2 ± 2.1% and 34.7 ± 10.6% of the *HTT* alleles in the cortex and striatum, respectively (Figures 3.5A-C). We investigated whether the *HTT* indels resulted in an inactivation of HTT translation, by analyzing HTT protein levels in a capillary-based western-blot assay (Figures 3.5D-E). We found that the level of *HTT* gene editing was correlated with the loss of striatal HTT protein (Figure 3.5F). The editing efficiencies actually achieved were slightly lower than the predictions from our 3D and 2D workflows, probably due to the presence of multiple, tandem copies of the human *HTT* (4 copies of mutant and 4 copies of WT HTT gene) in the HU97/18 transgenic mouse model (Figure S3.6), as recently highlighted by Shin and coworkers (Shin et al., 2022c).

We tested this hypothesis, by using our predictive pipeline in WT FVB mice and targeting the two copies of the mouse *HTT* gene (Figure 3.5G). There is a nucleotide mismatch between the human and mouse *HTT* sequences in the region targeted by sgHTT1 (Merienne et al., 2017). We therefore replaced sgHTT1 with sgHTT51, the sequence of which is identical to that of the mouse *HTT* gene. The injection of the AAV-KamiCas9^{v2} system expressing sgHTT51 into WT mice induced indels in 9.6 ± 6.7% and 54.4 ± 5.3% of the mouse *HTT* genes in the cortex and

striatum, respectively (Figures 3.5H-I). These editing efficiencies are consistent with the predictions of our 3D and 2D workflows and confirm the impact of multiple copies of the *HTT* gene on editing efficiencies.

In summary, we demonstrate that our semi-automated quantitative workflows can be used not only to estimate transduction efficiency, but also to optimize gene delivery and to predict gene editing outcomes in brain circuits affected by neurodegenerative disorders.

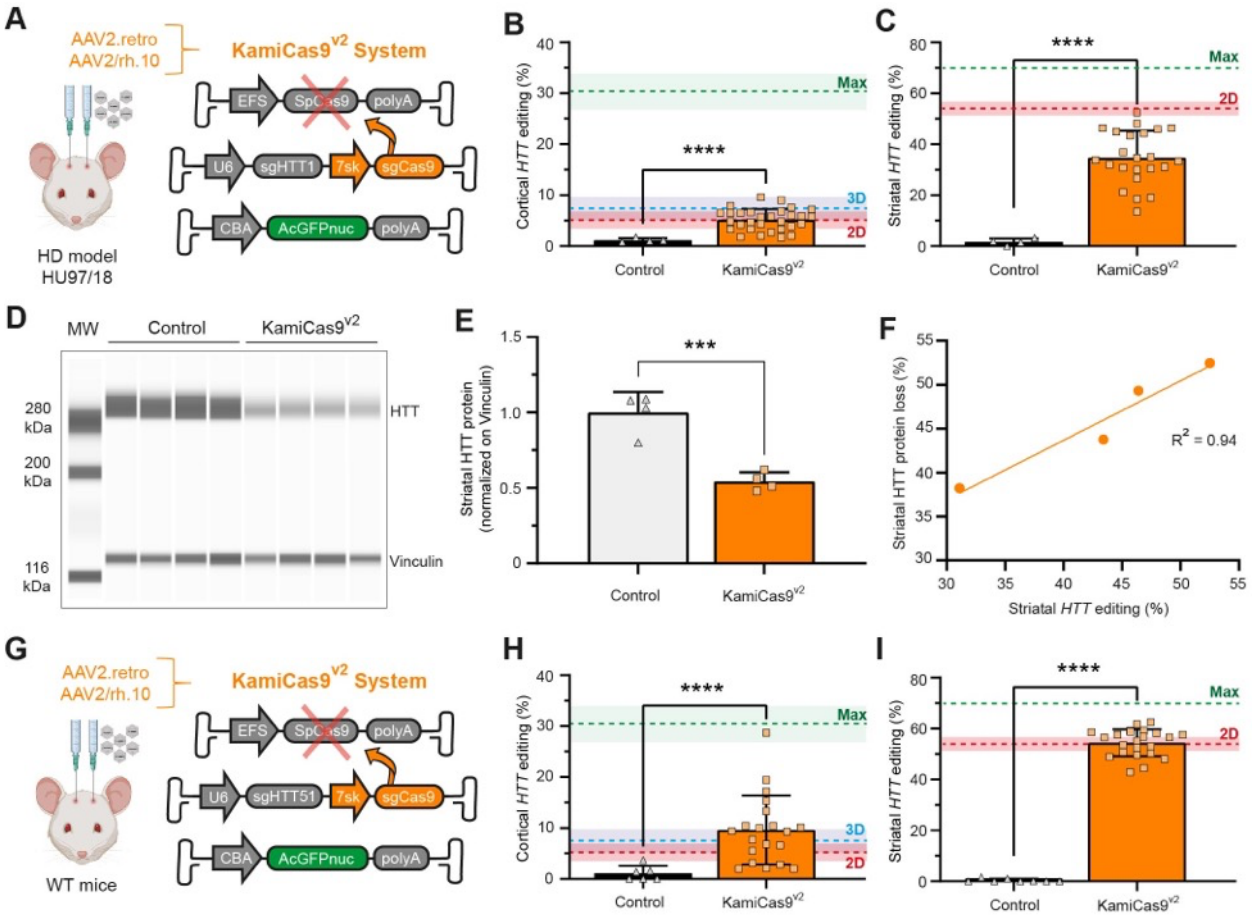

Figure 3.5: Validation of the workflow with a gene editing experiment targeting the *HTT* gene. (A) AAV2.retro- and AAV2/rh.10 KamiCas9^{v2} expressing the sgHTT1 and sgCas9 were injected bilaterally into fully humanized HU97/18 HD mice. Mice were killed three months post-injection and punch specimens were collected from the GFP-positive cortical and striatal areas (Figure S3.4). **(B and C)** Cortical (n=4 punch specimens from 2 animals for the control and n=30 punch specimens from 5 animals for KamiCas9^{v2}) and striatal (n=4 punch specimens from 2 animals for the control and n=23 punch specimens from 5 animals for KamiCas9^{v2}) editing was assessed by TIDE on DNA extracts from the punch specimens. The green dashed line indicates the theoretical maximum for transduction, and the predicted editing efficiency based on the 2D and 3D workflows is indicated by the blue and red dashed lines, respectively. **(D, E and F)** Capillary-based immunoassay showing that HTT editing leads to a proportional decrease in HTT protein levels (4C8 antibody). The vinculin antibody was used as an internal standard for the quantitative analysis (n=4 punch specimens from 2 animals for the control and n=6 punch specimens from 3 animals for KamiCas9^{v2}). **(G)** AAV2.retro- and AAV2/rh.10 KamiCas9^{v2} expressing sgHTT51 and sgCas9 were bilaterally injected into FVB mice. Mice were killed five months post-injection and the analysis was performed as in **(A)**. **(H and I)** Cortical (n=6 punch specimens from 2 animals for the control and n=20 punch specimens from 4 animals for KamiCas9^{v2}) and striatal (n=8 punch specimens from 2 animals for the control and n=23 punch specimens from 4 animals for KamiCas9^{v2}) editing was assessed as in panels **(B)** and **(C)**. Data are represented as mean ± SD.

3.1.4. Discussion

Despite intensive research to improve gene delivery to the CNS and the refinement of genetic tools to tackle neurological disorders, semi-automated analytic pipelines for evaluating gene delivery performance and therapeutic outcome are still lacking. The co-registration of a reference atlas and 3D images of clarified brains have been used to study drug distribution (Salinas et al., 2018) neuronal activity (Hansen et al., 2021; Renier et al., 2016; Salinas et al., 2018) and pathological disease mechanisms (Detrez et al., 2019; Goubran et al., 2019; Liebmann et al., 2016). Despite their considerable potential, these methods have been largely overlooked in the development of gene therapy products. Lopes and coworkers recently used registered LSFM-acquired images to evaluate the biodistribution of AAV2/9 transduction in the brain after intravenous (IV) administration (Lopes et al., 2022). However, their analysis was limited to the measurement of the area of each brain region positive for GFP. This measurement is a good indicator of AAV biodistribution, but provides no information about AAV transduction efficiency.

We therefore used a cell atlas and the Allen Reference Atlas (ARA) for the brain to develop a semi-automated workflow. The Blue Brain Cell Atlas provides information about cellular composition for 86 regions of the mouse brain (Erö et al., 2018). By considering specific characteristics of the delivery system — in this case, AAV tropism, retrograde transport, and site of injection into the brain — it is possible to estimate the maximum number of cells that can be targeted in a particular brain region. This theoretical maximum number of target cells can then be compared with experimental data, to determine the actual transduction efficiency.

In this study, we tested 3D and 2D semi-automated workflows for determining the efficiency of CPN transduction with AAV2.retro-CBA-GFP injected into the striatum. We estimated that AAV2.retro would be able to transduce 19% of the excitatory CPNs in the top 10 transduced cortical regions, corresponding to approximately 5.5% of the total number of cells in these regions. Similar cortical profiles were obtained for the two workflows, and AAV2.retro transduction efficiency was consistent between several cortical regions. One advantage of the 2D workflow is that it can be performed in most laboratories, whereas the 3D imaging pipeline requires LSFM and a high computational power for atlas co-registration. Conversely, the preparation of individual brain sections is time-consuming and can result in tissue deformations, which complicates registration to the reference atlas. For the 3D workflow, we used whole-brain imaging to quantify the total number of GFP-positive cells, rather than a subset of images of coronal sections. Our results indicated that the number of GFP-positive cells was consistent between the 3D and 2D workflows. The use of 2D imaging may currently be more appropriate than 3D whole-mount imaging for the examination of deeper brain structure, due to light scattering and possible incomplete brain clearing. The resolution of superficial areas (e.g., cortical areas) of the 3D-imaged cleared brain was higher than that for deeper brain structures (e.g., the striatum) (data not shown). Zhang and coworkers recently achieved constant image resolution across the whole brain with multi-scale LSFM (Zhang et al., 2021), which automatically removes brain areas once

they have been imaged, to ensure that the acquisition field of view is always close to the surface and to prevent light scattering through the tissue. The use of fluorescence proteins that localize to the nucleus, thereby preventing interference from neuropil signals, together with nuclear staining and StarDist-like machine learning algorithms, would also facilitate the implementation of the 3D workflow by the scientific community. Finally, although GFP fluorescence has been shown to be compatible with clearing methods (Chung & Deisseroth, 2013; Lopes et al., 2022) and to allow successful quantification for AAV2.retro-transduced cells, brighter, more photostable reporters, such as StayGold (Hirano et al., 2022) could also be used to improve the detection of cells with weak fluorescent signals.

The current version of the Blue Brain Cell Atlas is limited to cell composition in terms of oligodendrocytes, astrocytes, microglia, and excitatory and inhibitory neurons (parvalbumin (PV^+), somatostatin (SST^+), vasoactive intestinal peptide (VIP^+) and residual (RES) GABAergic neurons). These workflows cannot, therefore, be applied to vectors yielding transgene expression restricted to a subset of cells within a brain structure. For example, the proportion of striatal Drd1/Drd2 neurons in the striatum is not yet described in the atlas. Similarly, connectome data (Hintiryan et al., 2016) are not yet integrated in the 3D cell atlas but international initiatives (Muñoz-Castañeda et al., 2021) will provide more complex and complete atlases in the future.

CNS disorders are often associated with alterations to multiple neuronal networks across the brain and the targeting of various brain regions is complex. In recent years, AAV serotypes able to cross the blood-brain barrier have been characterized (Liu et al., 2021b) and intravenous (IV) administration has been considered as an option for targeting multiple brain regions. However, the IV delivery of AAVs to target the CNS requires the systemic administration of large doses, potentially leading to liver toxicity (“High-Dose AAV Gene Therapy Deaths,” 2020) and the transduction in deep brain structures remains suboptimal. Intraparenchymal delivery requires lower doses of AAV, but it can be difficult to target multiple brain regions by this approach. Here, we show that combining the potent retrograde transport properties of AAV2.retro (Tervo et al., 2016) with the broad striatal diffusion of AAV2/rh.10 (Cearley & Wolfe, 2006; Gao et al., 2004) makes it possible to target CPNs and striatal cells. This combinatorial approach could be particularly useful for the treatment of neurodegenerative diseases in which large areas of the brain are affected, such as Alzheimer's disease. In addition to making it possible to transduce multiple brain regions, the use of a combination of AAV serotypes also makes it possible to target different cell types. Lin and coworkers recently produced an AAV variant capable of efficiently transducing microglia with minimal immune activation (AAV-MG) (Lin et al., 2022). This work is paving the way for the combination of serotypes targeting neurons, astrocytes, and microglial cells. As these and other CNS delivery strategies are explored, the integration of semi-automated quantitative pipelines, such as those presented here, will be essential for the evaluation of their potential.

In the last part of the study, we validated our workflow for the codelivery of AAV2.retro and AAV2/rh.10-KamiCas9 vectors targeting the *HTT* gene. Based on the transduction efficiencies of AAV2.retro and AAV2/rh.10, we expected about 6% and 54% of the *HTT* alleles to be edited in the cortical and striatal regions, respectively. Rates of human *HTT* gene inactivation were relatively low in HU97/18 mice, but well within the predicted range for WT mice. HU97/18 mice are generated by crossing mice transgenic for the bacterial artificial chromosome (BACHD) (Gray et al., 2008) and yeast artificial (YAC18) (Hodgson et al., 1999) systems. As a result, it contains multiple copies of the human *HTT* gene in tandem. This artificial genomic structure of the human *HTT* loci in these mice probably accounts for the differences in *HTT* editing efficiency between the two models. These results suggest that genome editing studies should be performed preferentially in knock-in models, to prevent confounding due to genome structure-related factors.

In summary, we present here powerful semi-automated 2D and 3D quantitative workflows for the estimation of transduction efficiency throughout the mouse brain. We also demonstrate that such estimates can be used to predict editing outcomes. In addition, we propose the combination of AAV serotypes to expand gene delivery in the brain and to maximize gene editing in the corticostriatal network affected in HD.

3.1.5. Material and Methods

Plasmid production

Several fluorescence reporter constructs were used to the different AAV serotypes and to assess their transduction efficiency. The pAAV2ss-EFS-GFP-synPolyA and pAAV2ss-EFS-mCherry-SynPolyA plasmids were generated by replacing the SpCas9 with the GFP and mCherry transgenes in pAAV2ss-EFS-SpCas9-synPolyA (a gift from Ryohei Yasuda; RRID: Addgene 104588) (Nishiyama et al., 2017) after AgeI and EcoRI digestion. The pAAV2ss-CBA-EGFP-WPRE-bGH plasmid was kindly provided by Prof. During, Ohio, USA. Two other reporter plasmids, pAAV2ss-CBA-AcGFPnuc-WPRE-bGH and pAAV2ss-CBA-mCherry-WPRE-bGH, were generated by transferring the AcGFPnuc and mCherry coding sequences from the entry plasmids, pENTR4-AttL1-AcGFPnuc-AttL2 and pENTR4-AttL1-mCherry-AttL2, to an AAV destination transfer vector, pAAV2ss-CBA-Gateway-WPRE-bGH.

For the development of the AAV-KamiCas9 system, we ordered, from GeneArt, a universal entry plasmid, pMK-AttL1-NotI/BamHI-U6-BsaI-tracrRNAopt-BamHI-U6-SapI-tracrRNAopt-NotI/XbaI-7sk-BsmBI-tracrRNA-XbaI-AttL2 containing three sgRNA expression cassettes, to make it possible to adopt a flexible cloning strategy for multiple sgRNAs. The U6-driven expression cassettes contain an optimized tracrRNA described by Dang and coworkers (Dang et al., 2015) whereas the 7sk-driven expression cassette is associated with the original tracrRNA (Merienne et al., 2017). Unique restriction sites (NotI, BamHI and XbaI) were strategically placed between the cassettes to facilitate the removal of every possible cassette combination. The spacer sequence of each sgRNA was inserted into the universal entry plasmid

with overhang-compatible annealed oligos after digestion of the plasmid with type IIS restriction enzymes (BsaI, SapI or BsmBI). The sgGFP targeting the GFP transgene was cloned by SapI digestion and insertion of the annealed oligomers 5'-CACCGGGCGAGGAGCTGTTCACCG-3' and 5'-AAACCGGTGAACAGCTCCTCGCCC-3' to generate the pMK-AttL1-U6-sgGFP-AttL2 plasmid. Similarly, sgHTT1 and sgHTT51 were cloned by BsaI digestion and annealing of the oligos 5'-CACCGACCCTGGAAAAGCTGATGA-3' and 5'-AAACTCATCAGCTTTTCCAGGGTC-3' or 5'-CACCGAACCCTGGAAAAGCTGATGA-3' and 5'-AAACTCATCAGCTTTTCCAGGGTTC-3', respectively. A new sgCas9_2 (hereafter called sgCas9) targeting the 5' end of the open reading frame present in the pAAV2ss-EFS-SpCas9-synPolyA was inserted downstream from the 7sk promoter by BsmBI digestion and insertion of the annealed oligos 5'-CCTCGTCGCCGAAGAAAAAGCGCA-3' and 5'-AAACTGCGCTTTTTCTTCGGCGAC-3' (plasmids pMK-AttL1-U6-sgHTT1-7sk-sgCas9-AttL2 and pMK-AttL1-U6-sgHTT51-7sk-sgCas9-AttL2), or downstream from the U6 promoter by SapI digestion and annealing of the oligos 5'-ACCGTCGCCGAAGAAAAAGCGCA-3' and 5'-AACTGCGCTTTTTCTTCGGCGAC-3' (plasmid pMK-AttL1-U6-sgHTT1-U6-sgCas9-AttL2). The AAV plasmids expressing only sgRNAs, pAAV2ss-U6-sgGFP, pAAV2ss-U6-sgHTT1-7sk-sgCas9 and pAAVss-U6-sgHTT51-7sk-sgCas9, were produced by transferring the sgRNA expression cassettes from the entry plasmids into an AAV destination vector, pAAV2ss-Gateway-bGH. The AAV plasmids expressing sgRNAs together with the GFP reporter, pAAV2ss-EFS-GFP-synPolyA-U6-sgHTT1 and pAAV2ss-EFS-GFP-synPolyA-U6-sgHTT1-U6-sgCas9, were produced by classical restriction/ligation cloning with the NotI enzyme.

We also used the SIN-cPPT-PGK-SpCas9-WPRE (Addgene #87886), SIN-cPPT-U6-sgHTT1-PGK-mCherry-WPRE and SIN-cPPT-PGK-mCherry-WPRE plasmids to generate an *HTT*-KO clonal HEK293T cell line and an HEK293T cell line stably expressing SpCas9.

Human embryonic kidney 293T (HEK293T) cells

HEK293T cells (mycoplasma-negative, ATCC, LGC Standards GmbH, Wessel, Germany) were cultured in DMEM-Glutamax supplemented with 10% FBS and 1% penicillin/streptomycin (Gibco, Life Technologies, Zug, Switzerland) at 37°C under an atmosphere containing 5% CO_2. For routine culture, cells were passaged twice weekly after trypsin treatment for dissociation (Gibco, Life Technologies, Zug, Switzerland) and plated at a density of $2x10^6$ cells/cm^2 in T175 flasks.

Production of lentiviral vectors

The LV vectors were produced by the calcium phosphate-mediated transfection of HEK-293T cells with a four-plasmid system (Hottinger et al., 2000). Human immunodeficiency virus type 1 (HIV-1) vectors were pseudotyped with the vesicular stomatitis virus glycoprotein (VSV-G) envelope, concentrated by ultracentrifugation and resuspended in phosphate-buffered saline (PBS, Gibco, Life Technologies, Zug, Switzerland) supplemented with 1% bovine serum albumin

(BSA, Sigma-Aldrich, Buchs, Switzerland). The viral particle content of each batch was determined in a p24 antigen enzyme-linked immunosorbent assay (p24 ELISA, RETROtek, Kampenhout, Belgium). Viral stocks were stored at -80°C until use.

Production of adeno-associated vectors

AAVs were also produced in HEK293T cells by calcium phosphate-mediated transfection. The cells were transfected with the pAAV2ss containing the transgene of interest together with the pAd Helper-AAV (Agilent Technologies kit #240071) and pAAV-rh10_Rep_Cap (Penn Vector Core, University of Pennsylvania, School of Medicine, Philadelphia, USA) or pAAV2.retro (a gift from Alla Karpova & David Schaffer RRID: Addgene_81070). For AAV2/1, the cells were transfected with the pAAV2ss containing the transgene of interest together with the pDP1rs-RFP plasmid encoding helper functions (Plasmid Factory plasmid PF401). The cell suspension was centrifuged at 360 x *g* for 10 minutes at 4°C 72 hours post-transfection. The supernatant was supplemented with 10 mM PEG (Roth, Arlesheim, Switzerland) and 0.5 M NaCl (Merck, Nottingham, UK) and was incubated at 4°C for at least 2 hours. Cell pellets were pooled and incubated in lysis buffer (0.15 M NaCl, Merck, Nottingham, UK; 50 mM Tris-HCl, pH 8.5, Sigma-Aldrich, Buchs, Switzerland) for 3 consecutive freeze/thaw cycles (30 minutes in dry ice/ethanol followed by 30 minutes at 37°C). After the initial two-hour incubation period, the PEG-containing supernatant was centrifuged at 3700 x *g* for 20 minutes at 4°C and the supernatant was discarded. Cell lysate was added to the pellets and the mixture was incubated at 37°C for 1 hour to ensure that the pellets were fully homogenized. The lysate was then treated with 50 U/mL Benzonase (Sigma-Aldrich, Buchs, Switzerland) and 10 mM $MgCl_2$ (Sigma-Aldrich, Buchs, Switzerland) at 37°C for 30 minutes. The treated lysate was clarified by centrifugation at 3700 x *g* for 20 minutes at 4°C. AAVs were separated by iodixanol (AxonLab, Le Mont sur Lausanne, Switzerland) gradient ultracentrifugation at 255,690 g (70Ti rotor, Beckman-Coulter, Nyon, Switzerland) for 90 minutes at 20°C. The AAV-containing phase was harvested and loaded on an Amicon Ultra-15 PL 100 column (Millipore, Zug, Switzerland) with 0.001% Pluronic F68 D-PBS (Gibco, Thermo Fisher Scientific, Waltham, USA, Zug, Switzerland) for iodixanol cleaning and viral particle concentration. The tubes were first centrifuged at 4000 x *g* at 4°C until all the solution had passed through the column. Two additional washes with 0.001% Pluronic F68 D-PBS were performed and the AAV were finally suspended in 120-150 µL 0.001% Pluronic F68 D-PBS. The viral genome content (vg/mL) for each AAV was assessed by *Taq*man qPCR with primers recognizing the inverted terminal repeats of the AAV2 viral genome (forward primer: 5'-GGAACCCCTAGTGATGGAGTT-3', reverse primer: 5'-CGGCCTCAGTGAGCGA-3', *Taq*man probe: 5'- FAM-CACTCCCTCTCTGCGCGCTCG-TAMRA-3') and the KAPA probe fast qPCR universal kit (Sigma-Aldrich, Buchs, Switzerland). AAV vectors were stored at -80°C until use.

Transfection of HEK293T cells

For the transfection experiment (Figures S3.1A-B), we plated $5x10^5$ cells per well in six-well plates the day before transfection. We mixed 1150 fmol plasmids (150 fmol pAAV2ss-EFS-GFP-synPolyA, 250 fmol pAAV2ss-EFS-SpCas9-synPolyA and 750 fmol sgRNA(s)-expressing plasmids) in 0.25 M $CaCl_2$ solution and the mixture was then added dropwise to HEPES saline buffer (Sigma-Aldrich, Buchs, Switzerland, CaCl2-H2O:HEPES ratio 1:1). Cells not treated with the sgRNA-expressing plasmid were used as a negative control. The mixture was incubated at room temperature for five minutes and added dropwise to the cells (10% of the culture volume). The medium was completely replaced 6 hours after transfection. We evaluated the efficiency of *HTT* editing by SpCas9 four days post-transfection.

Production of a clonal huntingtin knockout (*HTT*-KO) HEK293T cell line

For the generation of an *HTT*-KO clonal HEK293T cell line (Figures S3.4B-C), we plated $5x10^6$ cells in a 10 cm Petri dish the day before transfection. We mixed 30 µg of plasmids (15 µg SIN-cPPT-PGK-SpCas9-WPRE and 15 µg SIN-cPPT-U6-sgHTT1-PGK-mCherry-WPRE) in 0.25 M $CaCl_2$ solution and the mixture was then added dropwise to HEPES saline buffer (Sigma-Aldrich, Buchs, Switzerland, CaCl2-H2O:HEPES ratio 1:1). The mixture was incubated at room temperature for five minutes and added dropwise to the cells (10% of the culture volume). The medium was completely replaced six hours after transfection. Five days post-transfection, the cells were dissociated with trypsin and serial dilutions were plated in 96-well plates. The cell clones that grew at the highest dilution conditions were sequentially expanded in 48-well plates, 24-well plates and, finally, six-well plates. We screened several clonal cell lines by Sanger sequencing and selected a single clone in which the *HTT* alleles had an extra adenosine nucleotide (+1, A) immediately downstream from the ATG at the sgHTT1 target site. This clonal cell line (clone F10) was then expanded and frozen in liquid nitrogen.

Transduction of HEK293T cells

For the transduction experiment (Figures S3.1C-D), we first generated a cell line stably expressing the SpCas9. We plated $5x10^5$ cells per well in six-well plates the day before LV transduction. We mixed 300 ng of LV (150 ng SIN-cPPT-PGK-SpCas9-WPRE and 150 ng SIN-cPPT-PGK-mCherry-WPRE) in DMEM medium and then added the mixture dropwise to the cells (10% of the culture volume). The medium was completely replaced 24 hours after transduction and the cells were passaged twice weekly. Two weeks after LV infection, we plated $1.2x10^5$ cells per well in 24-well plates. Cells were infected with $1.5x10^9$ vg of AAV2/1 ($7.5x10^8$ vg AAV2/1-EFS-GFP-SynPolyA-U6-sgHTT1 and $7.5x10^8$ vg AAV2/1-U6-sgGFP5) the next day. Cells incubated without AAV2/1-U6-sgGFP5 were used as a negative control. The medium was replaced 24 hours after transduction and *HTT* editing efficiency was evaluated seven days post-AAV transduction.

Animals

Adult male and female mice (9-15 weeks) were used for the *in vivo* experiments. Wild-type C57BL/6 and FVB mice were obtained from Janvier (Le Genest-Saint-Isle, France). Drd2-EGFP transgenic mice (Tg(Drd2-EGFP)S118Gsat/Mmnc, RRID:MMRRC_000230-UNC) were acquired from the Mutant Mouse Resource and Research Center (MMRRC) at the University of North Carolina at Chapel Hill. Transgenic mice expressing the full-length human wild-type *HTT* gene (HU18/18; YAC18++; Hdh-/-) or wild-type and mutant *HTT* gene (HU97/18; BACHD+;YAC18++; Hhd-/-) were kindly provided by Prof. Hayden (Vancouver, Canada) (Southwell et al., 2013) and BAC-GLT1-eGFP transgenic mice expressing eGFP specifically in astrocytes were provided by Prof. J Rothstein (Baltimore, MD, USA) (Regan et al., 2007). Mice were housed in a specific pathogen-free (SPF) facility with IVC cages GM500 (Tecniplast) or rat R.BTM.U x /R.ICV.6 cages (Innovive, Paris, France) and Innorack rats, simple face (cat# RS.5.8.40) containing corn cob bedding, with no more than five mice per cage. The animals were maintained in a controlled-temperature room (22±1°C), under a 14-hour light/10-hour dark cycle. The following enrichments were provided: 2 pieces of wipes, 1 cardboard tunnel, 1 cardboard or polysulfide house with 2 entrances/exits. Food (SAFE® 150, Safe, Rosenberg, Germany) and water were provided *ad libitum*. All experimental procedures were performed in strict accordance with Swiss regulations concerning the care and use of laboratory animals (veterinary authorizations 3447 and 3682).

Measurement of HTT gene copy number

Genomic DNA was extracted from HEK293T, neural progenitor cells (NPCs) (derived from Coriell GM03621), BACHD (Gray et al., 2008), HU18/18 and HU97/18 mice (Southwell et al., 2013) using the 500µl TRIzol® reagent (Life Technologies, Zug, Switzerland) according to the manufacturer's protocol. Concentration and quality of DNA were evaluated using a NanoDrop ultraviolet spectrophotometer (Thermo Fisher Scientific, Reinach, Switzerland). The absolute number of human *HTT* copies was quantified by digital PCR (QIAcuity® digital PCR, Qiagen, Basel, Switzerland) in QIAcuity 24-well Nanoplates with 8500 partitions. Separated Taqman assays targeting the SNP rs362331 (C/T) in exon 50 of the *HTT* gene were generated from the C_2231945_10 ThermoFisher assay (custom designed, ThermoFisher Scientific, Reinach, Switzerland) to individually analyze the number of *HTT* alleles containing a cytosine (VIC) or a thymine (FAM). We used the assay described by Christodoulou and colleagues targeting the poly(rC)-binding protein 2 (*PCBP2*) gene (Christodoulou et al., 2016) to normalize *HTT* amplification signals to the amount of gDNA. *HTT*-FAM and *HTT*-VIC signals were normalized to *PCBP2*-VIC (probe VIC-CCCTCTCCTGGCTCTAAATGTTGTGT-BHQ1) and *PCBP2*-FAM signals (FAM-CCCTCTCCTGGCTCTAAATGTTGTGT-BHQ1), respectively (Microsynth, Balgach, Switzerland). Each reaction was set up accordingly to the manufacturer's instructions in a 12 µL sample volume containing 3µL of 4x QIAcuity probe PCR mastermix (Qiagen, Basel,

Switzerland), 1X Taqman *HTT* custom assay, 0.8 µM of *PCBP2* forward and reverse primers, 0.4 µM *PCBP2*-labeled probes (Microsynth, Balgach, Switzerland), 3 units of EcoRI-HF restriction enzyme, and 100 nanograms genomic DNA. Loaded plates were incubating 10 minutes at RT for EcoRI-HF digestion followed by DNA amplification: initial denaturation at 95°C for 2min, 40 amplification cycles at 95°C, 60°C and 72°C for 15 sec each, and a final step at 40°C for 5 min. Finally, data analysis was performed with the QIAcuity Software Suite 2.0.20 (Qiagen, Basel, Switzerland).

Stereotaxic Injections

Anesthesia and surgical procedures were performed as previously described (Merienne et al., 2017). A total volume of 4-6 µL AAV per hemisphere (between $4.0x10^8$ and $1.75x10^9$ vg/hemisphere) was administered to the mouse striatum at a rate of 0.5 µL/min. AAVs administered bilaterally at a single striatal site per hemisphere were injected at the coordinates +1 ; ±1.8 ; -3.5 (+1 mm rostral to Bregma; ±1.8 mm lateral to midline; and 3.5 mm ventral from the skull surface, with the tooth bar set at -3.3 mm) in mice with a C57Bl/6 background mice, and at the coordinates +0.7 ; ±1.9 ; -3.0 in mice with an FVB background. For unilateral AAV delivery to two striatal sites, we used the coordinates +1.2 ; ±2.0 ; -3.2 (site 1) and +0.26 ; ±2.8 ; -3.2 (site 2) (Humbel et al., 2020). The needles were left in place for five minutes after the injection and were then slowly removed. During surgery, body temperature was controlled with a warming blanket (CMA 450 Temperature Controller, Phymep, Paris, France) and the eyes were protected with 0.2% Viscotears liquid gel (Novartis, Basel, Switzerland). Post-surgery analgesic treatment (acetaminophen, Dafalgan Upsa 1000 mg/750 mL) was administered in drinking water for 72 hours.

As a proof-of-concept for gene editing (Figures 3.1A-B), we injected $3.0x10^8$ vg AAV2/1-EFS-SpCas9-SynPolyA, $3.0x10^8$ vg AAV2/1-U6-sgGFP5 and $1.0x10^8$ vg AAV2/1-EFS-mCherry-SynPolyA bilaterally, at one site per hemisphere, in Drd2-EGFP mice. Mice not receiving the SpCas9 transgene were used as a negative control. Mice were killed three weeks after the injection, for histological processing.

For comparisons of the efficiency of AAV-CRISPR and AAV-KamiCas9 to edit the human *HTT* gene (Figures 3.1C-E), we injected $4.0x10^8$ vg AAV2/1-EFS-SpCas9-SynPolyA with $4.0x10^8$ vg AAV2/1-EFS-GFP-SynPolyA-U6-sgHTT1 or $4.0x10^8$ vg AAV2/1-EFS-GFP-SynPolyA-U6-sgHTT1-U6-sgCas9 bilaterally, at one site per hemisphere, in HU18/18 mice. Mice not receiving such injections were used as a negative control. Mice were killed eight weeks post-injection for the extraction of DNA and RNA.

For the establishment of the pipeline (Figures 3.3B-D, S3.2 and Video S3.1), we injected $1.3x10^9$vg (high dose) or $3.2x10^8$vg (low dose) of AAV2.retro-CBA-EGFP-WPRE-bGH into wild-type C57Bl/6 mice unilaterally, at two sites. Mice were killed three weeks post-injection, for histological processing (low dose) or CLARITY (high dose).

We maximized the targeting of the circuitry affected in HD (Figures 3.4A-B), by injecting $2.0x10^8$ vg AAV2/RH.10-CBA-mCherry-WPRE-bGH and $3.0x10^8$ vg AAV2/RH.10-CBA-EGFP-WPRE-bGH bilaterally, at one site per hemisphere, in HU18/18 mice. The mice were killed three weeks post-injection for histological processing.

For the estimation of striatal transduction efficiency (Figures 3.4C-E and S3.3), we injected $4.5x10^8$ vg AAV2/RH.10-U6-sgHTT51-7sk-sgCas9, $1.5x10^7$ vg AAV2/RH.10-CBA-AcGFPnuc-WPRE-bGH, $6.7x10^8$ vg AAV2.retro-U6-sgHTT51-7sk-sgCas9 and $1.5x10^7$ vg AAV2.retro-CBA-AcGFPnuc-WPRE-bGH bilaterally, at one site per hemisphere, in wild-type FVB mice. Mice were killed 24 weeks post-injection, for histological processing.

We checked the neuronal tropism of the AAV2/RH.10 and/or EFS promoters (Figure S3.4B), by injecting $4.0x10^8$ vg AAV2/RH.10-EFS-mCherry-synPolyA bilaterally into BAC-GLT-eGFP mice, at one site per hemisphere. Mice not receiving such injections were used as a negative control. Mice were killed three weeks post-injection, for histological processing.

For the evaluation of mutant *HTT* editing efficiency in both the striatum and cortex (Figures 3.5A-C, S3.4D-E), we injected $2.0x10^8$ vg AAV2/RH.10-EFS-SpCas9-SynPolyA, $4.0x10^8$ vg AAV2/RH.10-U6-sgHTT1-7sk-sgCas9, $1.0x10^8$ vg AAV2/RH.10-CBA-AcGFPnuc-WPRE-bGH, $3.0x10^8$ vg AAV2.retro-EFS-SpCas9-SynPolyA, $6.0x10^8$ vg AAV2.retro-U6-sgHTT1-7sk-sgCas9 and $1.5x10^8$ vg AAV2.retro-CBA-AcGFPnuc-WPRE-bGH bilaterally into HU97/18 mice, at one site per hemisphere. Mice not receiving SpCas9 transgene injections were used as a negative control. Mice were killed 14 weeks post-injection, for DNA and protein extraction.

For the evaluation of mouse *HTT* editing efficiency in both the striatum and cortex (Figures 3.5D-H), we injected $1.5x10^8$ vg AAV2/RH.10-EFS-SpCas9-SynPolyA, $4.5x10^8$ vg AAV2/RH.10-U6-sgHTT51-7sk-sgCas9, $1.5x10^7$ vg AAV2/RH.10-CBA-AcGFPnuc-WPRE-bGH, $2.3x10^8$ vg AAV2.retro-EFS-SpCas9-SynPolyA, $6.7x10^8$ vg AAV2.retro-U6-sgHTT51-7sk-sgCas9 and $1.5x10^7$ vg AAV2.retro-CBA-AcGFPnuc-WPRE-bGH bilaterally into FVB mice, at one site per hemisphere. Mice not receiving SpCas9 transgene injections were used as a negative control. Mice were killed 19 weeks post-injection, for DNA and protein extraction.

CLARITY, 3D light-sheet imaging and MIRACL analysis

For estimation of the transduction efficiency of AAV2.retro with the 3D quantitative workflow (Figure 3.3B and Video S3.1), mice were killed by sodium pentobarbital overdose three weeks post-injection and transcardially perfused with PBS followed by 4% paraformaldehyde (4% PFA) (Fluka, Sigma, Buchs, Switzerland). The brain was removed, post-fixed by incubation in 4% PFA for 24 hours and washed in PBS. CLARITY sample preparation and light-sheet imaging were performed as previously described (Humbel et al., 2020) . The clarified brain was analyzed with fiji software (Version 2.0.0-rc-69/1.52p) followed by the MIRACL registration pipeline (Goubran et al., 2019). CLARITY acquisition was followed by exportation as an image sequence to generate one tif file per stack, ordered numerically and dorsoventrally. This image sequence tif file was

duplicated and processed in parallel in fiji and MIRACL. In fiji, it was post-processed to determine the numbers and coordinates of GFP-positive cells after subtract background on the whole stack. GFP-positive cells can be found outside of the focal plane due to epifluorescence limitation. We therefore used only one in every six consecutive stacks (every 30 µm) to localize the cells and to ensure that the same cell was not considered twice. We obtained the coordinates of all GFP-positive cells, by using the Find Maxima/ List function of fiji and merging all coordinates into a single csv file. In parallel, the MIRACL pipeline (Goubran et al., 2019) was run on all image sequence tif files. Briefly, the images were initially subjected to processing with the changeValue function of fiji and manual editing to enhance co-registration quality and to decrease the discrepancy between transduced and non-transduced areas. The co-registration was performed on the 25 µm Allen Regional Atlas template. ITKsnap (*http*://www.itksnap.org) was used to visualize MIRACL outputs. Finally, the csv coordinates of GFP-positive cells and MIRACL co-registered brain were used to map segmented cells to the Allen Regional Atlas according to the recently described MOTA pipeline (Scholler et al., 2022).

Histological processing and imaging acquisition for 2D analysis

For the characterization of AAV serotype transduction patterns and tropisms (Figures 3.1A-B, 3.4A-B and S3.4B), the animals were killed by sodium pentobarbital injection three weeks post-injection and transcardially perfused with PBS followed by 4% paraformaldehyde (4% PFA) (Fluka, Sigma, Buchs, Switzerland). The brains of the animals were removed, post-fixed by incubation in 4% PFA for 24 hours and cryoprotected by two consecutive incubations in 20% and 30% sucrose (Sigma-Aldrich, Buchs, Switzerland) for 12 hours each. A cryostat (CM1850, Leica Biosystems, Muttenz, Switzerland) with a freezing stage at −20°C (SM2400; Leica Microsystems AG,Glattbrugg, Switzerland) was used to cut 25 µm-thick coronal brain sections. Sections were collected and stored in anti-freeze solution (0.2 M sodium phosphate buffer, 25% glycerol, 30% ethylene glycol) in 96-well plates at −20°C until use. If no immunohistochemical staining was to be performed, the brain sections were mounted directly on slides, in Vectashield supplemented with DAPI (Reactolab, Servion, Switzerland). Brain sections for immunohistochemical staining were rinsed in TBS (3 × 10 min) at room temperature and blocked by incubation for 1 hour in TBS-T (TBS, 0.1% Triton X-100) supplemented with 5% BSA (Sigma-Aldrich, Buchs, Switzerland). For AcGFPnuc immunoblotting (Figures 3.4C-E), sections were incubated overnight at 4°C with a goat polyclonal GFP primary antibody (AB0020-500, Sicgen) diluted 1/250 in TBST supplemented with 1% BSA. They were washed three times with TBS (3 × 10 min) and were then incubated with the Alexa Fluor®568-conjugated donkey anti-goat secondary antibody (A-11057, Life Technologies, Zug, Switzerland) diluted 1/1000 in TBS-T supplemented with 1% BSA for 1 hour at room temperature. For the mCherry immunoblotting (Figure S3.4B), sections were incubated overnight at 4°C with a goat polyclonal mCherry primary antibody (AB0040-500, Sicgen) diluted 1/250 in TBS-T supplemented with 1% BSA. They were washed three times with

TBS (3 × 10 min) and then incubated with the Alexa Fluor®568-conjugated donkey anti-goat secondary antibody (A-11057, Life Technologies, Zug, Switzerland) diluted 1/1000 in TBS-T supplemented with 1% BSA for 1 hour at room temperature. Finally, for all immunoblots, the brain sections were washed three times in TBS (3 × 10 min) and mounted on slides, in Vectashield supplemented with DAPI (Reactolab, Servion, Switzerland).

Images of the full brain sections were obtained with a digital camera (3CCD Hitachi HV-F202SCL) on a slide scanner microscope (×20 objective, Zeiss axioscan Z1).

QuPath and ABBA analysis

For estimation of the cortical transduction efficiency of AAV2.retro (Figure 3.3C) and the striatal transduction efficiency of AAV2.retro and AAV2/rh.10 (Figures 3.4C-E) with the 2D quantitative workflow, images of the brain sections were obtained with a digital camera (3CCD Hitachi HV-F202SCL) on a slide scanner microscope (×20 objective, Zeiss Axioscan Z1). We then used a fiji and QuPath workflow to estimate the number of transduced cells in various brain regions. We co-registered the coronal brain sections and the Allen CCFv3 reference atlas (Wang et al., 2020) in fiji, with the Aligning Big Brains & Atlases (ABBA) plugin (Chiaruttini et al., 2022) and exported the data in QuPath (*htt*ps://biop.github.io/ijp-imagetoatlas/). The QuPath bioimage analysis software and StarDist extension (Schmidt et al., 2018), a deep learning-based method of nucleus detection with pretrained models, were then used to identify nuclei on the basis of DAPI staining (Bankhead et al., 2017). Finally, a cell classifier was used to quantify GFP-positive cells and to export the data.

DNA, RNA and protein extraction

For *in vitro* experiments (Figure S3.1), DNA was extracted from HEK293T cells with QuickExtract® DNA extraction solution (QE09050, Lubioscience, Zürich, Switzerland), according to the manufacturer's recommendations. Briefly, cells were dissociated with trypsin (Gibco, Life Technologies, Zug, Switzerland) and washed in PBS. Genomic DNA from approximately $3x10^5$ cells was extracted by mixing the cells with 100 µL QuickExtract solution and incubating at 65°C and 98°C for 10 and 2 minutes, respectively. In addition, protein was extracted from wild-type and *HTT*-KO HEK293T cells in RIPA buffer (R0278, Sigma) supplemented with a 1/200 dilution of protease inhibitor cocktail (P8340, Sigma-Aldrich, Buchs, Switzerland) and 5 µM Z-VAD-FMK (HY-16658B, Chemie Brunschwig, Basel, Switzerland), hereafter referred to as $RIPA^+$ buffer. Approximately $1x10^6$ cells were washed in PBS and 50 µl of $RIPA^+$ buffer was added to the cell pellet. The pellet was homogenized with a pellet mixer (VWR, Dietikon, Switzerland) and left on ice for 30 minutes. The protein extract was then centrifuge at 18000 x g for 15 minutes at 4°C and the supernatant containing solubilized proteins was collected into a new tube and stored at -80°C.

For *in vivo* experiments, mice were sacrificed by isoflurane overdose and brains were collected and cut into 1 mm-thick coronal slices. For the comparison of AAV-CRISPR and AAV-

KamiCas9 systems (Figures 3.1C-E), we collected 5-6 punches (~ 1.5 mm^3 each) from the GFP-positive striatum and merged them by hemisphere. The DNA and RNA from each transduced striatal hemisphere was extracted with 500 µl TRIzol® reagent (Life Technologies, Zug, Switzerland) according to the manufacturer's protocol. DNA was resuspended by incubation overnight in water at RT and it was then stored at -20°C. RNA samples were first treated with RQ1 RNase-free DNase (Promega, Dübendorf, Switzerland) and then converted into cDNA using the RNA with Superscript II (Thermo Fisher, Reinach, Switzerland) according to the manufacturer's instructions. RNA and cDNA samples were then stored at -80°C. For the evaluation of human and mouse *HTT* editing in both the cortex and striatum (AAV2.retro and AAV2/RH.10) (Figures 3.5, S3.4D-E), we collected four to six striatal punch specimens and six to 10 cortical punch specimens from the transduced areas. The striatal punch specimens were then split into two tubes for the extraction of both DNA and protein. DNA was extracted from each individual punch specimen with the AllPrep DNA/RNA/miRNA Universal Kit (Qiagen, Hombrechtikon, Switzerland) according to the manufacturer's recommendations. The DNA was stored at -20°C. The protein from each striatal punch specimen was extracted in 30 µL $RIPA^+$ buffer, as described for protein extraction from HEK293T cells.

TIDE analysis

HTT and SpCas9 editing efficiencies were assessed by performing Tracking of Indels by Decomposition (TIDE) analysis (Brinkman et al., 2014) on amplified gDNA or cDNA. The indel size range was set to 10 and the size of the decomposition window was adapted for reads of low quality or containing repetitive sequences. The significance cutoff was set to 0.05 (*htt*ps://tide.nki.nl/). Nucleic acid amplification was performed on 100 ng of gDNA or 5 ng of cDNA with the KAPA HiFi Hotstart kit (KAPA Biosystems, Labgene) according to the manufacturer's recommendations. The primers 5'-TTGCTGTGTGAGGCAGAACCTGCGG-3' (h*HTT*_fwd/seq) and 5'-TGCAGCGGCTCCTCAGCCAC-3' (h*HTT*_rev) were used to amplify the sgHTT1 target site of the human *HTT* gene from DNA samples from HEK293T cells and HD transgenic mice (Merienne et al., 2017). TIDE analysis was performed on chromatograms for wild-type *HTT* amplicons sequenced with the primer h*HTT*_fwd primer, or chromatograms for mutant *HTT* amplicons sequenced with the 5'-GCGGGATCCATAACTTCGTA-3' (mut*HTT*_seq) primer. For the mouse *HTT* gene, the sgHTT51 target site was amplified from WT mouse DNA samples with the primers 5'-CCTCCTCACTTCTTTTCTATCG-3' (*mHTT*_fwd) and 5'-AGCATTATGTCATCCACTACC-3' (*mHTT*_rev), with a melting temperature of 56°C and an extension period of 90 seconds. The mouse *HTT* amplicons were sequenced with the primer 5'-CTGTCAATTCTGCGGGTCTG-3' (*mHTT*_seq) to generate the chromatograms for indel analysis. Finally, the sgCas9 target site in AAV-SpCas9 was amplified from both DNA and cDNA with the primers 5'-TTTTTCGCAACGGGTTTGCC-3' (SpCas9_fwd) and 5'-AGAAGCTGTCGTCCACCTTG-3' (SpCas9-rev/seq), using a melting temperature of 65°C and

an extension period of 25 seconds. The efficiency of sgCas9 editing was evaluated by TIDE on analysis on amplicons sequenced with the SpCas9_rev/seq primer.

Virtual western blot

Protein concentration was assessed with a BCA kit (Thermo Fisher Scientific, Reinach, Switzerland) according to the recommended procedure. After dilution in 0.1x SB (ProteinSimple, Bio-Techne), 0.6 µg of total protein extract was size-separated with the Jess capillary-based immunoassay system. Samples were processed according to the manufacturer's instructions, with the 66-440 kDa separation module (SM-W008). The primary anti-huntingtin antibody clone 1HU-4C8 (MAB2166, Zug, Switzerland) (diluted 1/500) and the anti-vinculin antibody clone 3M13 (ZRB1089, Merck, Nottingham, UK) (diluted 1/50) were used to target the HTT and vinculin proteins, respectively. HTT and vinculin were then detected by chemiluminescence with the anti-rabbit-HRP conjugate (043-026, ProteinSimple, Bio-Techne AG, Zug Switzerland) diluted 1/20 in the ready-to-use anti-mouse-HRP conjugate (DM-002, ProteinSimple, Bio-Techne AG, Zug, Switzerland). Compass software (version 6.1) was used for the analysis. Peaks were determined with the dropped line method and HTT and vinculin signals were used to calculate the HTT/vinculin ratios.

Statistical methods

For the statistical analyses, we tested the hypotheses of normally distributed data and equal variances to determine the most appropriate statistical test. Post-hoc analyses were performed with GraphPad Prism 9.1.0 software. ANOVA was used for comparisons of more than two groups and *t*-tests were used for comparisons between two groups. The results of statistical tests were considered significant if the *p* value obtained was below 5%. No specific method was used for sample randomization, sample-size estimation, or data inclusion/exclusion. All results are presented as the mean ± SD. *$p < 0.05$, **$p < 0.01$, and ***$p < 0.001$.

For *HTT* editing in HU18/18 mice in Figure 3.1D, *p* values were calculated for Brown-Forsythe and Welch ANOVA, with F*(DFn, DFd): 111.9(2.0, 11.9). For SpCas9 editing in HU18/18 mice in Figure 3.1E, *p* values were calculated by Brown-Forsythe and Welch ANOVA, with F*(DFn, DFd): 100.2(3.0, 11.0).

For *HTT* editing in transfected HEK293T cells in Figure S3.1B, the *p* values were calculated by ordinary one-way ANOVA with F(DFn, DFd): 386.1(3, 8). For SpCas9 editing in transfected HEK293T cells in Figure S3.1B, the *p* values were calculated by ordinary one-way ANOVA with F(DFn, DFd): 3343(2, 6). For *HTT* editing in transduced HEK293T cells in Figure S3.1D, the *p* values were calculated by ordinary one-way ANOVA with F(DFn, DFd): 205.9(2,7).

For cortical *HTT* editing in HU97/18 mice in Figure 3.5B, *p* values were calculated in one-tailed unpaired *t*-tests with Welch's correction (*t* value: 9.3; DF: 28.1). For striatal *HTT* editing in HU97/18 mice in Figure 3.5C, *p* values were calculated in one-tailed unpaired *t* tests with Welch's

correction (*t* value: 14.4; DF: 24.7). For cortical *HTT* editing in wild-type mice in Figure 3.5E, *p* values were calculated in one-tailed unpaired *t* tests with Welch's correction (*t* value: 5.3; DF: 23.3). For striatal *HTT* editing in wild-type mice in Figure 3.5F, *p* values were calculated in one-tailed unpaired *t* tests with Welch's correction (*t* value: 48.3; DF: 23.7). For the striatal HTT protein in wild-type mice in Figure 3.5H, *p* values were calculated in one-tailed unpaired *t* tests (*t* value: 11.0; DF: 8).

For the striatal HTT protein in HU97/18 mice in Figure S3.5D, *p* values were calculated in one-tailed unpaired *t* tests (*t* value: 6.1; DF: 6).

3.1.6. Supplemental information

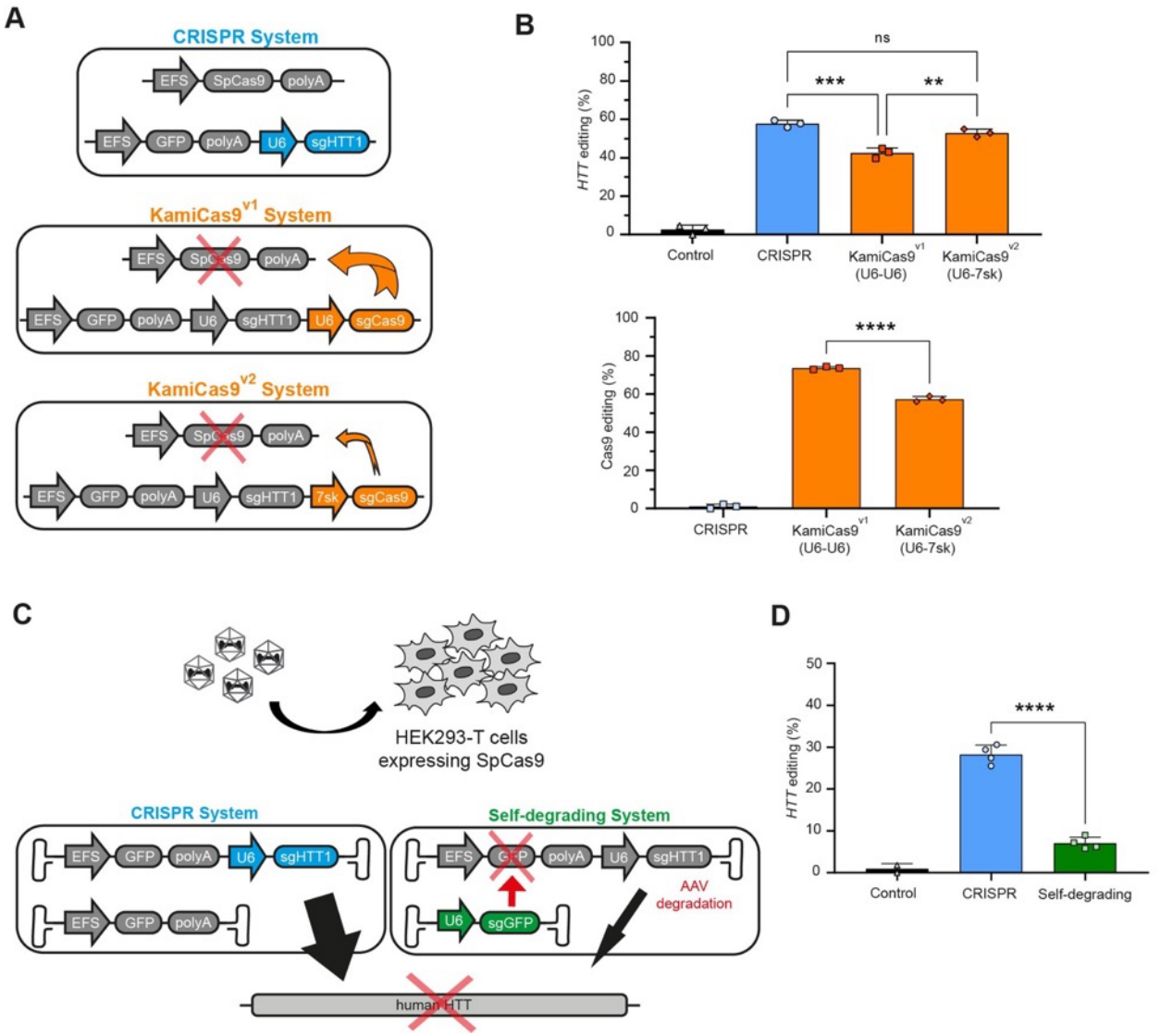

Figure S3.1: Characterization of the AAV-KamiCas9 system targeting the *HTT* gene in HEK293T cells, related to Figure 3.1 (A) Schematic representation of the CRISPR, KamiCas9^{v1} and KamiCas9^{v2} systems. All systems express a sgRNA targeting the translational start site of the human *HTT* gene (sgHTT1) but the two KamiCas9 systems express an additional sgRNA targeting the translational start site of SpCas9 itself (sgCas9). The expression of sgCas9 is driven by the strong U6 promoter in the KamiCas9^{v1} system and by the weaker 7sk promoter in the KamiCas9^{v2} system. **(B)** The frequency of indels in the *HTT* and SpCas9 genes was assessed four days post-transfection, by TIDE (n=3 replicates/group). **(C)** HEK293T cells stably expressing SpCas9 were transduced with AAV2/1 encoding the CRISPR system or a self-degrading system. The self-degrading system induces the cleavage of the AAV2/1 expressing the sgHTT1. **(D)** The *HTT* indel frequency measured by TIDE analysis seven days post-transduction showed that *HTT* editing levels were lower in the self-degrading group, suggesting that at least a fraction of cleaved AAV episomes are degraded (n=2 replicates for the control; n=4 replicates for CRISPR and the self-deleting system). Data are represented as mean ± SD.

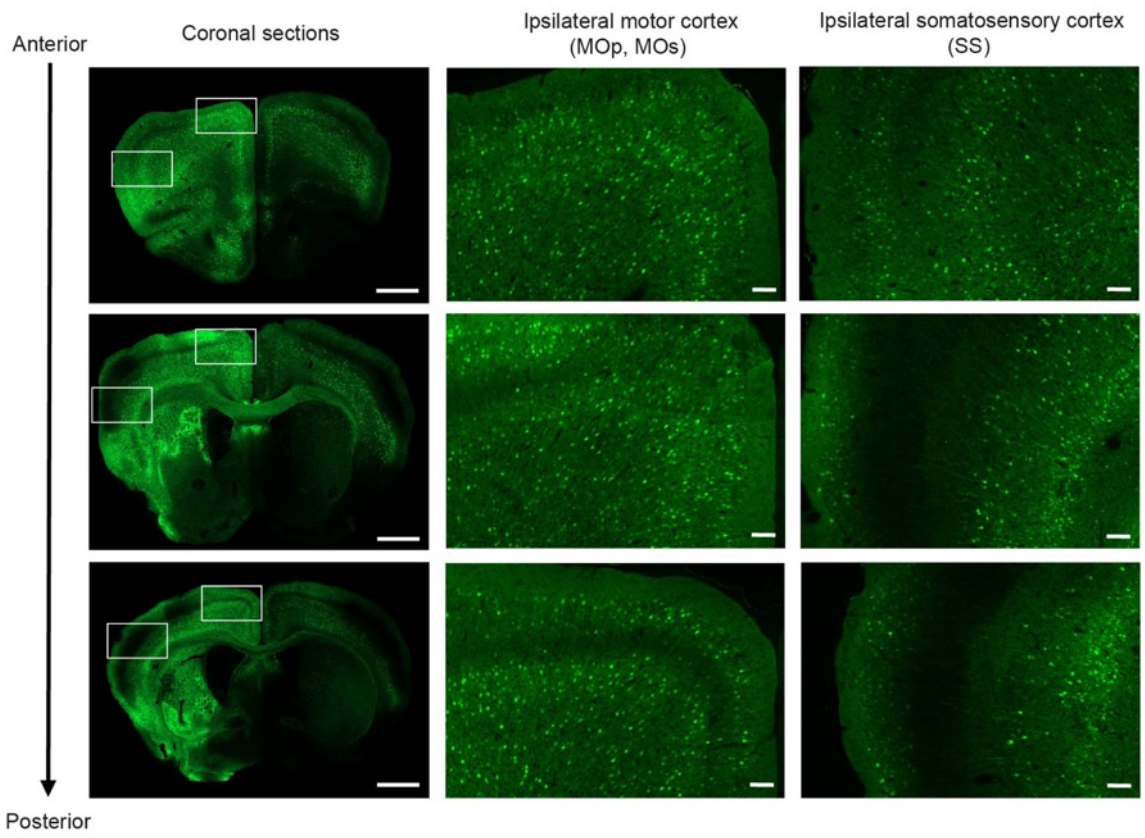

Figure S3.2: AAV2.retro transduction pattern following a unilateral intrastriatal injection, related to Figure 3.3. Rostro-caudal images showing retrograde transport in the cortex and, in particular, massive transduction of the ipsilateral motor cortex (Mop, Mos) and, to a lesser extent, the somatosensory cortex (SS). Scale bar for low magnification: 1000 µm. Scale bar for high magnification: 100 µm.

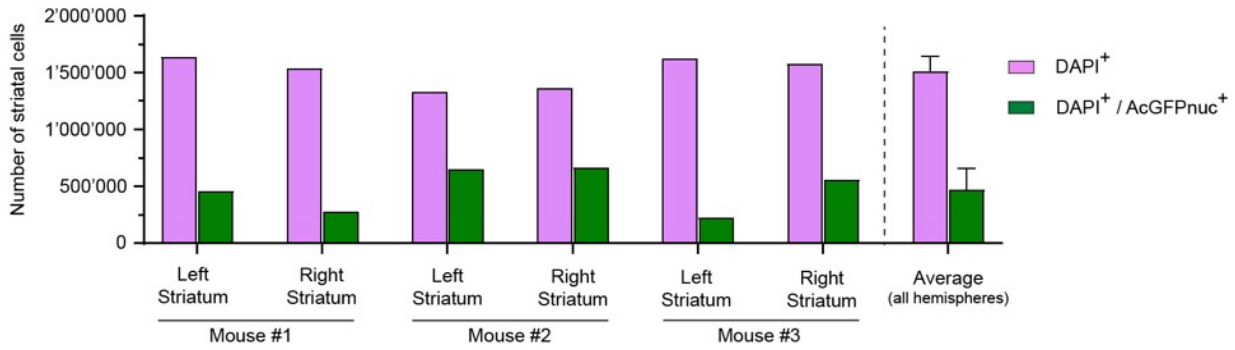

Figure S3.3: Quantification of the number of transduced cells in the striatum using the 2D pipeline, related to Figure 3.4. Graph showing the total number of striatal cells detected in the QuPath/Stardist analysis (DAPI staining) and the number of AcGFPnuc$^+$/DAPI$^+$ cells in the 3 animals analyzed. Data are represented as mean ± SD.

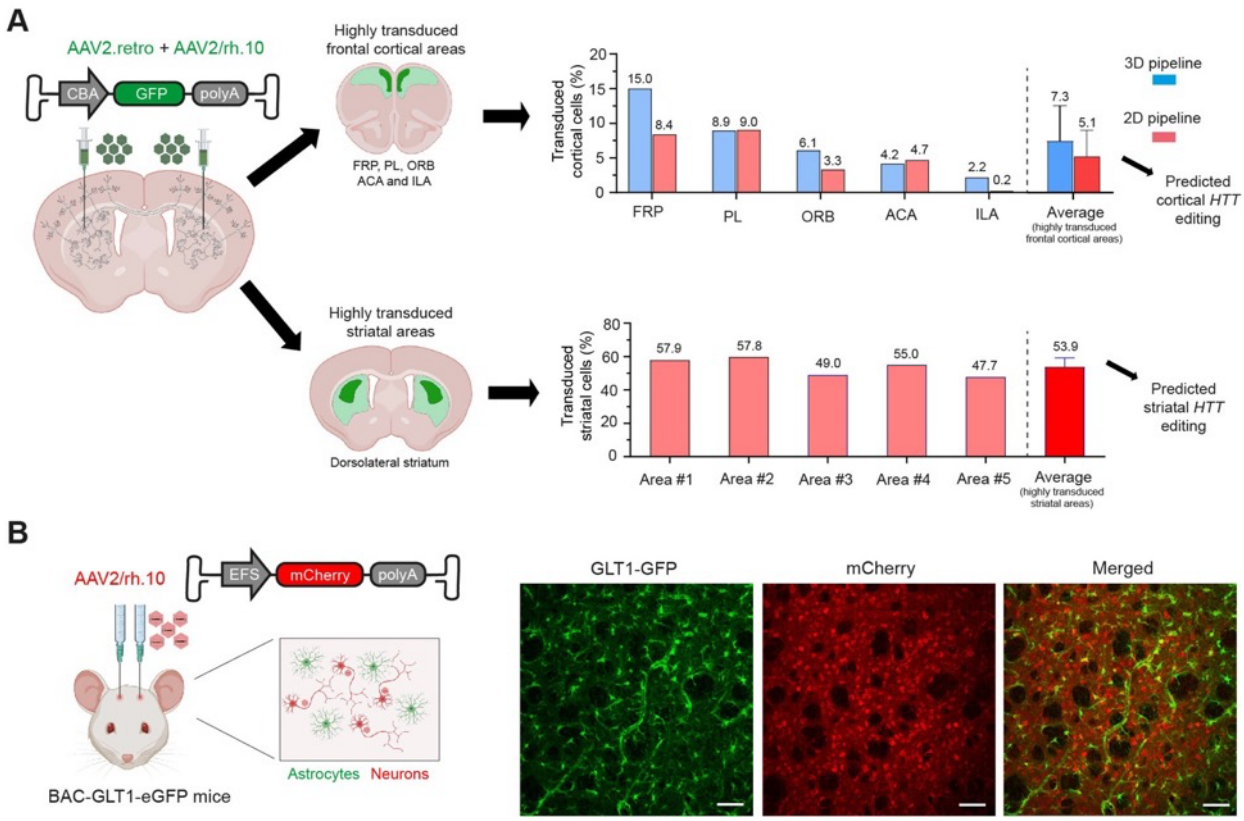

Figure S3.4: Prediction of *HTT* editing based on transduction efficiency and cell tropism, related to Figure 3.5. (A) For the *HTT* editing analysis, punch specimens were taken from the highly GFP-positive cortical and striatal areas. Because all cell types are present in the brain punches, we calculated the proportion of transduced cells over the total number of cells (neurons in Figure 3.3) at the most transduced areas to predict *HTT* editing outcome. Regarding the cortex, we focused on mediodorsal frontal cortical regions (including the FRP, PL, ORB, ACA, and ILA) as these were the areas with stronger GFP signal. Regarding the striatum, we used the previous quantification of the highly transduced striatal areas (Figure 3.4F). **(B)** The AAV2/rh.10 expressing mCherry under the control of EFS promoter was injected in BAC-GLT1-GFP transgenic mice. These mice endogenously express GFP in astrocytes. The poor localization between signals suggests that the AAV2/rh.10-EFS-mCherry (hence, AAV2/rh.10-EFS-SpCas9) has a strong neuronal tropism. Data are represented as mean ± SD.

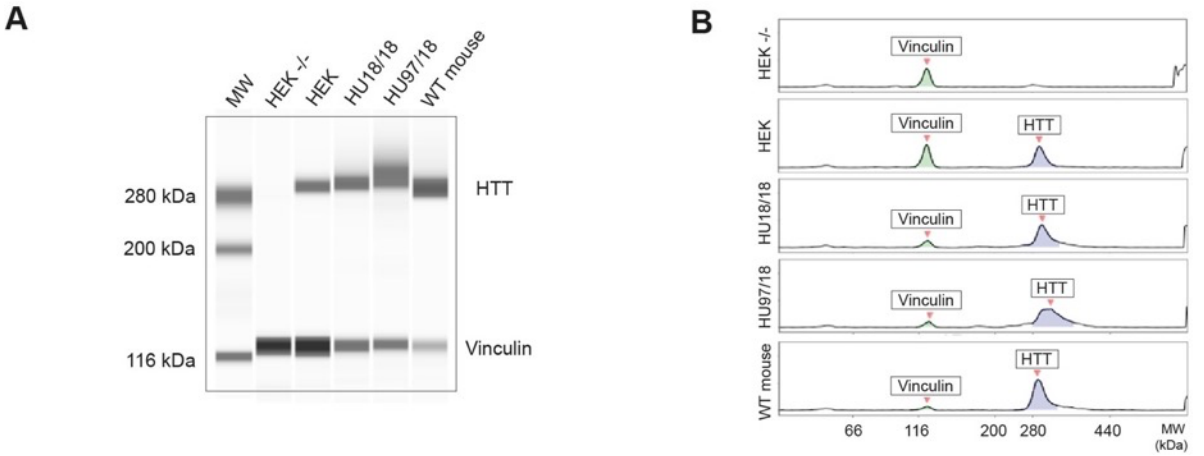

Figure S3.5: Validation of the capillary-based immunoassay for detecting HTT, related to Figure 3.5. (A) Validation of the immunoassay for the specific detection of HTT protein (4C8 antibody). Both mouse and human HTT proteins are detected by the 4C8 antibody. The selectivity of the signal was demonstrated in samples from *HTT*$^{-/-}$ HEK cells (knockout). The differences between samples for HTT protein migration were expected because HU97/18 mice express the mutant HTT with 97 CAG repeats. **(B)** Peak analysis with Compass software confirmed the specificity of the assay. The vinculin antibody was used as internal standard for the quantitative analysis.

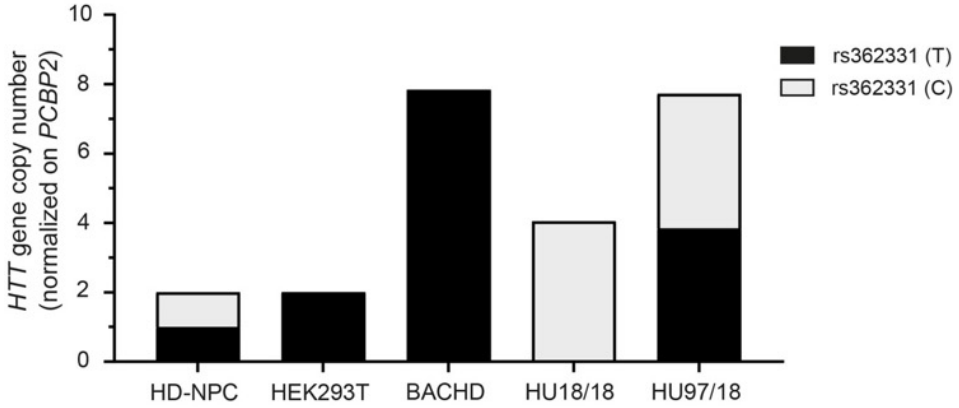

Figure S3.6: Absolute quantification of the *HTT* gene copy number by QIAcuity digital PCR, related to Figure 3.5. The HD transgenic mouse model HU97/18 is heterozygous for the SNP rs362331 (C/T) in the exon 50 of the *HTT* gene. While the cytosine is linked to the *wtHTT* allele, the thymine is associated to the *mHTT* allele. Taqman assays with FAM/VIC probes targeting the SNP rs362331 (C/T) were used to determine the number of copies of *wtHTT* and *mHTT* alleles in HU97/18 mice. As a reference gene, we used the previously described Taqman assay targeting the poly(rC)-binding protein 2 (*PCBP2*) gene (Christodoulou et al., 2016). Genomic DNA from HD-derived neuronal precursor cells (HD-NPCs) was used to normalize quantifications as they are also heterozygous for the SNP rs362331 and contain two copies of the *HTT* gene (one *wtHTT* allele and one *mHTT* allele). Genomic DNA from HEK293T cells were used to control copy number analysis since they are expected to have two *HTT* alleles. In addition, genomic DNA from BACHD and HU18/18 were used to control probe specificity because they are homozygous for the SNP rs362331.

Video S3.1: AAV2.retro transduction profile analyzed by LSFM.

Table S3.1: Quantification of cortical AAV2.retro transduction with the 3D and 2D imaging workflows, related to Figures 3 and S4. Frontal pole (FRP), prelimbic area (PL), orbital area (ORB), anterior cingulate area (ACA), infralimbic area (ILA), primary and secondary somatomotor area (Mop, MOs), agranular insular area (AI), gustatory area (GU), restrosplenial area (RSP), somatosensory area (SS).

Brain Regions		Blue Brain Cell Atlas (BBCAv2)			3D Imaging workflow			2D Imaging workflow		
		Total cells (all layers)	Total excitatory neurons (Layers II/III, V and VI)	Targetable cells (%)	GFP+ cells	Transduction efficiency (%) (all layers)	Transduction efficiency (%) (excitatory neurons layers II/III, V and VI)	GFP+ cells	Transduction efficiency (%) (all layers)	Transduction efficiency (%) (excitatory neurons layers II/III, V and VI)
Isocortex		20'003'896	6'754'869	33.77	417'579	2.09	6.18	507'408	2.54	7.51
Isocortical Areas	Frontal pole (FRP)	28'248	8'225	29.12	4'233	14.99	51.47	2'368	8.38	28.79
	Prelimbic area (PL)	261'181	70'128	26.85	23'366	8.95	33.32	23'592	9.03	33.64
	Orbital area (ORB)	599'296	188'191	31.40	36'465	6.08	19.38	19'864	3.31	10.56
	Anterior cingulate area (ACA)	770'227	247'010	32.07	31'954	4.15	12.94	36'096	4.69	14.61
	Infralimbic area (ILA)	283'406	103'015	36.35	6'134	2.16	5.95	632	0.22	0.61
	Somatomotor areas (MOp and MOs)	2'927'777	646'633	22.09	181'718	6.21	28.10	174'936	5.98	27.05
	Agranular insular area (AI)	508'275	180'042	35.42	30'372	5.98	16.87	80'528	15.84	44.73
	Gustatory area (GU)	242'804	72'478	29.85	10'899	4.49	15.04	16'504	6.80	22.77
	Retrosplenial area RSP)	1'662'829	506'644	30.47	17'948	1.08	3.54	5'664	0.34	1.12
	Somatosensory areas (SS)	6'088'444	1'482'205	24.34	52'333	0.86	3.53	88'248	1.45	5.95
			AVERAGE	29.8	39'542	5.5	19.0	44'843	5.6	19.0
			AVERAGE (FRP, PL, ORB, ACA and ILA)	31.2	20'430	7.3	24.6	16'510	5.1	17.6

CHAPTER 4

Assessment of allele-specific exon 1 deletion to inactivate the *mHTT* allele

Contribution

Writing of the manuscript

Preparation of the figures

Figure 4.1E – Data analysis

Figure 4.3 - Design, transfection, extraction, analysis

Figure 4.4 - Design, transduction, extraction, analysis

Figure 4.5 - Design, injection, extractions, analysis

Figure 4.6 - Design, injection, extractions, analysis

Figure S4.2 – Clone generation, extraction, analysis

Figure S4.3 - Design, transduction, extractions, analysis

Figure S4.4 – Design, transduction, extractions, analysis

Figure S4.5 – Design, transduction, extractions, analysis

Figure S4.6 – Design, extractions, analysis

Figure S4.7 - Design, transfection, extraction, analysis

4. Assessment of allele-specific exon 1 deletion to inactivate *mHTT* allele

4.1. Duarte, Vachey et al., 2023 (in preparation)

Dual sgRNA CRISPR-based systems display limited efficiency to excise genomic regions *in vivo*

Fábio Duarte,[1,2] Gabriel Vachey,[1,2] Melanie Sipion,[1,2] Maria Rey[1,2], Anselme Perrier[3,4] and Nicole Déglon[1,2]

[1]Lausanne University Hospital (CHUV) and University of Lausanne (UNIL), Department of Clinical Neurosciences (DNC), Laboratory of Cellular and Molecular Neurotherapies, Lausanne, Switzerland. [2]Lausanne University Hospital (CHUV) and University of Lausanne (UNIL), Neuroscience Research Center (CRN), Laboratory of Cellular and Molecular Neurotherapies (LCMN), Lausanne, Switzerland. [3]Université Paris-Saclay, CEA, CNRS, Laboratoire des Maladies Neurodégénératives: mécanismes, thérapies, imagerie, Fontenay-aux-Roses, France. [4]Université Paris-Saclay, CEA, Molecular Imaging Research Center, Fontenay-aux-Roses, France

Correspondence should be addressed to N.D. (nicole.deglon@chuv.ch)

Corresponding author:
Nicole Déglon
Lausanne University Hospital (CHUV)
Laboratory of Cellular and Molecular Neurotherapies
Pavillon 3, Avenue de Beaumont
1011 Lausanne
Switzerland
Phone: +41 21 314 21 20
E-mail: nicole.deglon@chuv.ch

4.1.1. Abstract

Huntington's disease (HD) is a fatal neurodegenerative disorder caused by a toxic gain-of-function CAG expansion in the first exon of the huntingtin (*HTT*) gene. The monogenic nature of HD makes *HTT* inactivation a promising therapeutic strategy. Nevertheless, it is still unclear to which extent the loss of the wild-type *HTT* (*wtHTT*) normal functions may impact on disease progression. Single nucleotide polymorphisms (SNPs) frequently associated to the expanded CAG have been explored to selectively inactivate the mutant *HTT* (*mHTT)* allele with the CRISPR/Cas9 system. One of the current approaches consists of the excision of the first exon of *mHTT* by inducing simultaneous double-strand breaks at upstream and downstream positions of the *mHTT* exon 1. The removal of the first exon of *mHTT* deletes the CAG expansion and important transcription regulatory sites, consequently ceasing *mHTT* expression. However, the therapeutic potential of this strategy is yet to be assessed *in vivo*. To date, the single study testing *mHTT* exon 1 excision *in vivo* in BACHD mice focused the analysis exclusively on the *mHTT* expression levels with no quantification of the frequency of deletion events. While exon 1 was expected to be deleted only in *mHTT* transgenes, both *wtHTT* and *mHTT* expression levels were decreased, suggesting that *mHTT* knockdown was not necessarily induced by deletion events. Here, we designed an optimized allele specific strategy which has no impact on *wtHTT* expression and developed accurate digital PCR-based quantitative assays to precisely assess the efficiency of *mHTT* exon 1 deletion *in vivo* in fully humanized HU97/18 mice. Our results suggest that approaches to delete *HTT* exon 1 are efficient *in vitro*, but their application *in vivo* is far more challenging.

KEYWORDS

Huntington's disease, Haplotypes, SNP, Allele-specific, Gene Editing.

4.1.2. Introduction

Huntington's disease (HD) is a fatal neurodegenerative disorder caused by a CAG expansion in the exon 1 of the huntingtin (*HTT)* gene (MacDonald et al., 1993). The age of HD onset and disease progression are inversely correlated with the CAG tract size with a full penetrance above 40 repeats. Clinical manifestations arise between the ages of 35 and 50, with death occurring within the next 15 to 20 years. Symptoms in HD are strongly associated with the dysfunction and degeneration of spiny projecting neurons (SPNs) in the basal ganglia, which are important relay in voluntary motor functions and various cognitive loops, including attention and memory (Bates et al., 2015; Ross et al., 2014). The expanded CAG repeat encodes a longer polyglutamine (polyQ) domain present at the N-terminus of the HTT protein. This feature modifies the mutant HTT (mHTT) conformation and induces aggregation. Mutant HTT-mediated toxicity includes the dysregulations of several cellular pathways such as axonal transport, transcription, translation, and mitochondrial and synaptic functions. In addition to toxic oligomeric forms of mHTT, other evidence suggest that the contribution of expanded CAG repeats to HD phenotype may be beyond the encoding the polyQ peptides, including toxicity mediated by the RNAs containing the CUG expansion (Chung et al., 2011; Nalavade et al., 2013) and RAN proteins (Bañez-Coronel et al., 2015).

To date, there are no available therapies modifying the disease progression. Considering that the CAG expansion is a toxic gain-of-function mutation, strategies targeting the primary toxic features in HD such as the CAG expansion and/or their subsequent products hold great therapeutic potential. They may prevent downstream toxic effects at both molecular and cellular levels, potentially slowing or stopping the disease progression. Because wild-type HTT (wtHTT) is ubiquitously expressed and it is involved in multiple cellular processes, a current topic of discussion is whether strategies should specifically address the mHTT in order to maintain wtHTT functions (Kaemmerer & Grondin, 2019). In addition, the recently premature termination of a clinical trial testing a non-allele-specific antisense oligonucleotide to reduce HTT expression has raised even more concerns regarding non-allele-specific strategies (Rook & Southwell, 2022).

Patients carrying the *mHTT* share common ancestors and, therefore, sets of single nucleotide polymorphisms (SNPs) are more strongly associated to the expanded *HTT* alleles (Chao et al., 2017; Kay et al., 2015, 2019; Lee et al., 2012, 2015; Warby et al., 2009, 2011). The association of specific SNPs with the CAG expansion provides a unique opportunity to discriminate the two *HTT* alleles. In parallel, the emergence of the CRISPR/Cas9 system has boosted the design of multiple approaches to permanently and specifically inactivate the *mHTT* allele as a therapeutic option for HD (Fang et al., 2023; Monteys et al., 2017; Oikemus et al., 2022; Shin et al., 2016, 2022a, 2022c). These studies have focused on the design of sgRNAs targeting SNPs that generate novel protospacer adjacent motifs (PAM) in the mutant allele or delete PAM motifs from the wild-type allele (PAM-altering SNPs - PAS). In this way, it is ensured that only the *mHTT* allele is cleaved by the Cas9 nuclease. One of the approaches involves the

combination of two single guide RNAs (sgRNAs) to promote the simultaneous cleavage at upstream and downstream locations of the *mHTT* exon 1 to excise the expanded CAG repeat out of the genome (Fang et al., 2023; Monteys et al., 2017; Shin et al., 2016, 2022a).All of the *in vitro* studies have shown the feasibility of the approach by analyzing puromycin-enriched or clonal lines of induced pluripotent cells from HD patients (HD-iPSCs). In addition, Monteys and colleagues tested their strategy *in vivo* in the transgenic BACHD mouse model (Monteys et al., 2017). In this study, the authors combined an allele-specific sgRNA targeting the SNP rs2857935 located at the *HTT* promoter with a non-allele specific sgRNA targeting the *HTT* intron 1 to induce the specific deletion of the human *mHTT* exon 1. They showed a 55% decrease of the human *mHTT* mRNA levels in the striatum of treated BACHD mice, but did not quantify the frequency of deletion events (Monteys et al., 2017). Since puromycin-selected cells transfected with the intronic non-allele-specific sgRNA alone decreased *HTT* expression up to 40%, one cannot conclude that the reduction on *mHTT* expression *in vivo* was exclusively due to the deletion of the *mHTT* exon 1. Moreover, authors also observed that mouse *wtHTT* expression levels in BACHD were almost halved in the injected striatal hemispheres. They presumed that the mouse *wtHTT* knockdown could be the result of off-target cleavage of the mouse gene by the intronic non-allele-specific sgRNA, which differs from the human homologue sequence by only two nucleotides. Nevertheless, such effects of the intronic sgRNA alone on the expression of both *wtHTT* and *mHTT* indicates that the strategy is not allele-specific and, therefore, *mHTT* expression levels cannot be used to draw conclusions regarding the efficiency of *mHTT* exon 1 deletion.

Here, we designed an intronic non-allele-specific sgRNA with no impact on the *HTT* expression to precisely assess the functional outcomes related to *HTT* exon 1 deletion at the mRNA and protein levels. Because the constitutive expression of SpCas9 may favor potential unspecific cleavage at multiple genomic regions, we adapted the strategy to our previously established KamiCas9 systems (Merienne et al. 2017; Duarte et al., 2023 – in revision). We confirmed that the constitutive and transient SpCas9 expression induce *HTT* exon 1 deletion in both HEK293T and neuronal progenitor cells from HD patients (HD-NPCs). Finally, we developed a digital PCR-based quantitative assay to accurately evaluate the efficiency of *HTT* exon 1 deletion *in vitro* and *in vivo* in fully humanized HD mice (Southwell et al., 2013).

4.1.3. Results

Design and *in vitro* validation of allele-specific sgRNAs

To selectively excise the *mHTT* exon 1 containing the expanded CAG, we identified frequently occurring SNPs located 2 kb upstream and 1.3 kb downstream of the *HTT* transcription start site (GRCh38, chr4:3072744-3076049). According to the phase 3 of the 1000 genomes project, this region contains 6 SNPs located upstream to the CAG repeat with a minor allele

frequency (MAF) in the global population superior to 10% (Table 4.1). These variants are also amongst the most common SNPs associated to mutant *HTT* allele in this region (Fang et al., 2023; Shin et al., 2022a). In particular, Shin and colleagues estimated that the variant rs2857935 is heterozygous in 27.6% of the HD patients, making it one of the most promising targets for the development of allele-specific therapeutic strategies based on *mHTT* exon 1 deletion (Shin et al., 2022a). This variant is also a SpCas9 PAS, meaning that it eliminates the PAM on the *wtHTT* allele and prevents its cleavage. We designed two PAM-based selective sgRNAs targeting this PAS (sgHTT8P_L and sgHTT8P_S), which differ in the length of the protospacer sequence (22 nt and 17 nt, respectively) (Table 4.1). For the other variants, the sgRNAs were designed to target the SNP close to the seed region of the sgRNA sequence (sgHTT25, sgHTT6, sgHTT10 and sgHTT2) since mismatches in this region have been shown to highly affect DNA binding and SpCas9 activity (Boyle et al., 2021; Bravo et al., 2022; Ivanov et al., 2020; Zhang et al., 2020). We did not design a sgRNA targeting the SNP rs9996199 because it was previously shown to induce poor on-target cleavage (Monteys et al., 2017). Since *mHTT* allele should be simultaneously cleaved upstream and downstream of the CAG expansion to promote *mHTT* exon 1 deletion, we designed a sgRNA targeting a sequence in the first intron conserved between the *wtHTT* and *mHTT* alleles (sgHTT4) (Table 4.1), whose cleavage is expected to be well tolerated with minor or no impact on *HTT* expression.

We first assessed the efficiency and selectivity of each individual sgRNA in transfected HEK293T cells. While PAS have been shown to abort the SpCas9 activity (Fang et al., 2023; Monteys et al., 2017; Oikemus et al., 2022; Shin et al., 2016, 2022a, 2022c), sgRNA targeting SNPs in the seed region still have the potential to induce indels in the non-targeted allele (i.e. *wtHTT*). Since HEK293T cells are homozygous for all of the identified SNPs (Table 4.1), we designed sgRNAs harboring the respective mismatch sequence at the SNP (hereafter called mismatch sgRNAs) to assess selectivity by simulating the SNP on the non-targeted allele (Figure 4.1A-B). The gene editing efficiency of each individual sgRNA was determinated by tracking of indels by decomposition (TIDE) in HEK293T cells transfected with three plasmids separately encoding for SpCas9, sgRNA and GFP (Figure 4.1C). Cells transfected only with the plasmids encoding SpCas9 and GFP were used as negative control. Among the sgRNAs targeting SNPs upstream to the CAG, the sgHTT25 generated low levels of indels whereas sgHTT6T, sgHTT10C and sgHTT2G induced indels in more than 10% of *HTT* alleles (Figure 4.1C). All of these sgRNAs generated significantly more indels than the respective sgRNAs containing the mismatch sequence in the seed region, with the sgHTT6T targeting the SNP rs28431418 displaying the highest selectivity. In addition, the PAM-based sgHTT8P_L and sgHTT8P_S targeting the PAS rs2857935 also generated high levels of indels in the *HTT* gene (16.5 ± 0.9% and 19.6 ± 0.8%, respectively). Finally, the non-allele-specific sgHTT4 located in intron 1 showed relatively high editing efficiency (13.8 ± 1.0%) (Figure 4.1C). We then evaluated the impact of indels generated by these sgRNA candidates on the *HTT* mRNA expression. To ensure high level of editing by

each sgRNA, we modified the sgRNA backbone (tracrRNA) to the one described by Dang and colleagues (Dang et al., 2015), which was shown to promote higher sgRNA expression levels and higher editing efficiencies. In addition, we used lentiviral vectors (LVs) to maximize the delivery of the CRISPR system into HEK293T cells.

Table 4.1: Design of sgRNA targeting the *HTT* promoter, exon 1 and intron 1. We selected single nucleotide polymorphisms (SNPs) located 2 kb upstream and 1.3 kb downstream of the HTT transcription start site with a minor allele frequency (MAF) superior to 10%, according to the 1000 genomes project phase 3. The sgHTT8P_L and sgHTT8P_S target the PAM-altering SNP (PAS) rs2857935 (PAM-based selectivity). The sgHTT25 (rs762855), sgHTT6 (rs28431418), sgHTT10 (rs13122415) and sgHTT2 (rs13102260) target SNPs located in target sequence of the sgRNAs (mismatch-based selectivity). The sgHTT4 targets the HTT intron 1 and does not discriminate the wild-type and mutant alleles. Human embryonic kidney cells 293T (HEK293T) are homozygous for all selected SNPs. Neuronal progenitor cells derived from HD-patient cells (HD-NPCs) (Coriell – line GM03621) and HU97/18 mice (Southwell et al., 2013) are heterozygous for the rs762855 and rs2857935 variants.

SNP	Mutation	MAF	HEK-293T genotype	HD-NPCs genotype	HU97/18 genotype	*HTT* region	sgRNA name	SNP position	sgRNA sequence (5' to 3')
rs762855	G>A	A=0.48	A/A	A/G	A/G	Promoter	sgHTT25	3	GACAGCAGAGAAACAGCTGT
rs9996199	C>G	G=0.16	C/C	C/C	C/C	Promoter	---	---	----------
rs28431418	T>C	C=0.14	T/T	T/T	T/T	Promoter	sgHTT6	2	CAGGGCTGTCCGGGTGAGTA
rs2857935	G>C	C=0.23	G/G	C/G	C/G	Promoter	sgHTT8P_L	PAM	GCCCCGCTCCAGGCGTCGGCGG
							sgHTT8P_S	PAM	GCTCCAGGCGTCGGCGG
rs13122415	C>G	G=0.11	C/C	C/C	C/C	Promoter	sgHTT10	4	GGGGCTCAACGGAGAGGGGGA
rs13102260	G>A	A=0.16	G/G	G/G	G/G	Exon 1	sgHTT2	3	ACCCGTCCCGGCAGCCCCCA
						Intron1	sgHTT4	No SNP	GTGGATGACATAATGCTTTT

At three weeks post-transduction, all sgRNAs demonstrated higher editing efficiencies (between 70% and 91%) compared to transfection (Figure 4.1D). Regarding the impact on *HTT* mRNA expression, the sgHTT2G was the only sgRNA inducing a decrease on *HTT* mRNA levels compared to control ($p<0.0001$) (Figure 4.1E). The sgHTT2G targets the transcription start site and indels at this position (rs13102260) may disrupt important transcription factor binding sites and/or destabilize the nascent *HTT* mRNA. Importantly, despite the high levels of gene editing (91.2 ± 3.4%), the intronic non-allele-specific sgHTT4 did not show any significant impact on *HTT* transcription compared to control ($p=0.9986$) (Figure 4.1E). In summary, the sgHTT6T, sgHTT8P_S and sgHTT8P_L presented high editing efficiencies while maintaining strong selectivity criteria for the targeted allele. In addition, indels generated by the non-allele-specific sgHTT4 in the first intron have no major impact on *HTT* transcription. These results support the combination of the allele-specific sgRNAs targeting the *HTT* promoter with the intronic

non-allele-specific sgHTT4 to selectively delete the *mHTT* exon 1 without influencing *wtHTT* expression. Finally, prediction of off-target sites using the CRISPRSeek package (Zhu et al., 2014) indicated few potential off-target sites for the sgHTT6T, sgHTT8P_L and sgHTT4 at genomic coding regions (Figure S4.1), further encouraging the use of these sgRNAs candidates for the development of allele specific *HTT* exon 1 deletion strategies.

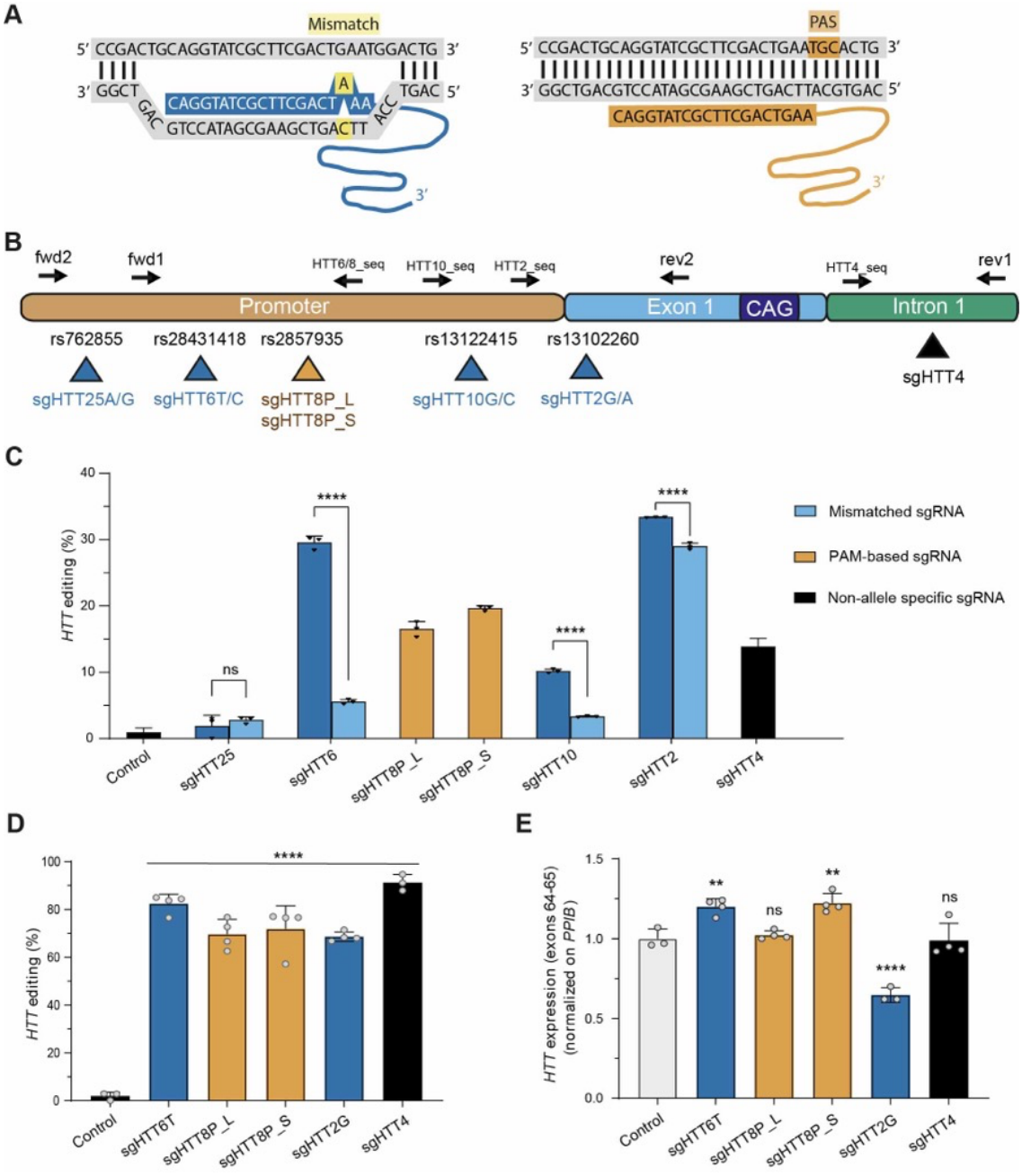

Figure 4.1: Design and screening of sgRNA targeting the *HTT* promoter, exon 1 and intron 1. (A) Illustration of the specificity basis of sgRNAs targeting single nucleotide polymorphisms (SNPs) in the seed sequence of the sgRNA (mismatch-based selectivity) (left) or in the protospacer adjacent motif (PAM-based selectivity) (right). **(B)** Schematic representation of the *HTT* promoter, exon 1 and intron 1 is depicted. The sgHTT25, sgHTT6, sgHTT10, sgHTT2 and sgHTT12 are mismatch-based selective sgRNAs (blue) whereas sgHTT8P_S and sgHTT8P_L target a PAM-altering SNP (PAS) (brown). The sgHTT4 targets the intron 1 of both wild-type and mutant *wtHTT* alleles (black). The primers used for *HTT* amplification and sequencing are illustrated in the scheme and described on the Table S4.3. **(C)** Editing efficiency of each sgRNA in HEK293T cells quantified by TIDE at four days post-transfection. Cells were transfected with two plasmids separately encoding for SpCas9 and GFP under the control of the PGK promoter together with

an extra plasmid encoding for a sgRNA targeting the *HTT* gene. Cells transfected with only the plasmid encoding SpCas9 and GFP were used as negative control. Because HEK293T cells are homozygous for all tested SNPs (Table 4.1), we generated two versions of the mismatched-based sgRNAs to facilitate the evaluation of sgRNA selectivity: one corresponding to the homologous reference sequence and the other corresponding to mismatched sgRNA. The sgHTT8P_L and sgHTT8P_S have no mismatched variant since they target a PAS. Results are presented as mean ± SD (N=1, n=3). Statistics: two-way ANOVA and multiple-comparisons to control with Sidak's correction; ∗∗∗∗ :p<0.0001. **(D-E)** HEK293T cells were co-transduced with one LV encoding for SpCas9 under the control of the PGK promoter and another LV expressing an optimized sgRNA (Dang et al., 2015) and for mCherry by the U6 and PGK promoters, respectively. Cells transduced with LVs separately encoding for SpCas9 and GFP with no sgRNAs were used as negative control. Editing efficiency and *HTT* expression were analyzed at 3 weeks post lentiviral (LV) transduction. **(D)** Gene editing efficiency was analyzed by TIDE and **(D)** *HTT* expression normalized on the expression of peptidylprolyl isomerase B (*PPIB*) was evaluated by QIAcuity digital RT-PCR. Results are presented as mean ± SD (N=1, n=3/4). Statistics: one-way ANOVA and multiple-comparisons to control with Dunnet's correction; ∗∗∗∗ :p<0.0001; ∗∗ :p<0.01.

Combining allele-specific sgRNAs with sgHTT4 to delete the *HTT* exon 1 in HEK293T cells

To investigate whether simultaneous editing in the promoter and intron 1 of *HTT* could induce the deletion of the *HTT* exon 1, we delivered constructs encoding for SpCas9 and for the sgRNA combinations sgHTT8P_L/sgHTT4, sgHTT8P_S/sgHTT4 and sgHT6T/sgHTT4 (Figure 4.2A). These constructs were delivered into HEK293T cells by transfection or by lentiviral vectors. Gene editing outcomes were analyzed 4 or 21 days after delivery, respectively. To detect the occurrence of *HTT* exon 1 deletion events, we amplified genomic DNA using the primer set 1 (Figure 4.2A). Full-length amplicons of 2732 bp result from the amplification of the *HTT* alleles containing the exon 1 whereas smaller amplicons of 974 bp and 1053 bp result are expected to be generated from the amplification of exon 1-depleted *HTT* alleles by the sgHTT6T/sgHTT4 and sgHTT8P/sgHTT4 combinations, respectively. We observed the amplification of smaller amplicons with the expected sizes for exon 1 deletion in all conditions expressing the two sgRNAs (Figure 4.2B). Semiquantitative analysis of the bands present in the agarose gels indicated that the combination of the sgHTT4 with the sgHTT6T and sgHTT8P_L induced the highest levels of deletion in both transfected and transduced HEK293T cells (Figure 4.2C). In addition to the deletion of exon 1, the non-simultaneous cleavage of the *HTT* gene by the two sgRNAs can also generate indels in non-deleted *HTT* alleles. To evaluate the frequency of *HTT* alleles that had been cleaved by the SpCas9 despite the unsuccessful excision of the exon 1, we sequenced the full-length amplicons and assessed the presence of indels at the sgRNA target sites by TIDE analysis. While only 10-20% of the *HTT* alleles containing the exon 1 had been edited in transfected cells, most of the full-length *HTT* alleles of transduced cells contained indels at the sgRNA target sites (Figure 4.2D). These results indicate that the exon 1 is not depleted in all edited *HTT* alleles. We next characterized the deletion events induced by the sgHTT8P_L/sgHTT4 combination in transfected HEK293T clonal cell lines (Figure S4.2). Amplification of genomic DNA with the primer set 1 indicated that 6 out of 13 clones (46%) contained deleted sequences in the amplified region (Figure S4.2A). None of the clonal cell lines presented deletions in both *HTT* alleles. In addition, we observed deletions of different sizes,

suggesting heterogeneous repair of the double-strand breaks after the excision of the *HTT* exon 1. The clones I-D9, II-E2, II-E11 and II-H8 presented deletions with expected sizes (around 1670 bp), whereas the clones I-C12 and II-E5 displayed shorter and longer deletions than expected, respectively. We then used Sanger sequencing to characterize the exon 1-deleted amplicons from the clones I-C12, II-E5 and II-H8 (Figure S4.2B). The clone II-H8 carries a deletion of 1660 bp with breaking points close to the sgHTT8P_L and sgHTT4 targeting sites. The clone II-E5 carries a longer deletion of 1983 bp due to the loss of an extra portion of the *HTT* promoter. The 492 bp deletion in the clone I-C12 also excised the *HTT* exon 1 but it was accompanied by complex rearrangements at the promoter region, involving inversion and exchange of sequences. RNA expression analysis by RT-qPCR indicated that *HTT* mRNA levels were decreased in all clones carrying *HTT* exon 1 deletions compared to wild-type HEK293T cells (Figure S4.2C). Protein expression analysis by capillary-based western blot also indicated a 40% and 15% reduction on the HTT protein levels in the clones II-H8 and II-E5 compared to control, respectively (Figure S4.2D-E). Overall, these results suggest that the association of the intronic sgHTT4 with the sgHTT6T or sgHTT8P_L targeting the *HTT* promoter are the most efficient sgRNA combinations deleting the *HTT* exon 1. Similarly to others (Monteys et al., 2017), we observed that *HTT* exon 1 excision reduces *HTT* mRNA expression levels. In addition, our results indicate that deletion events can result in in heterogenous editing outcomes and that suggest that the exon 1 is not depleted from all edited *HTT* alleles.

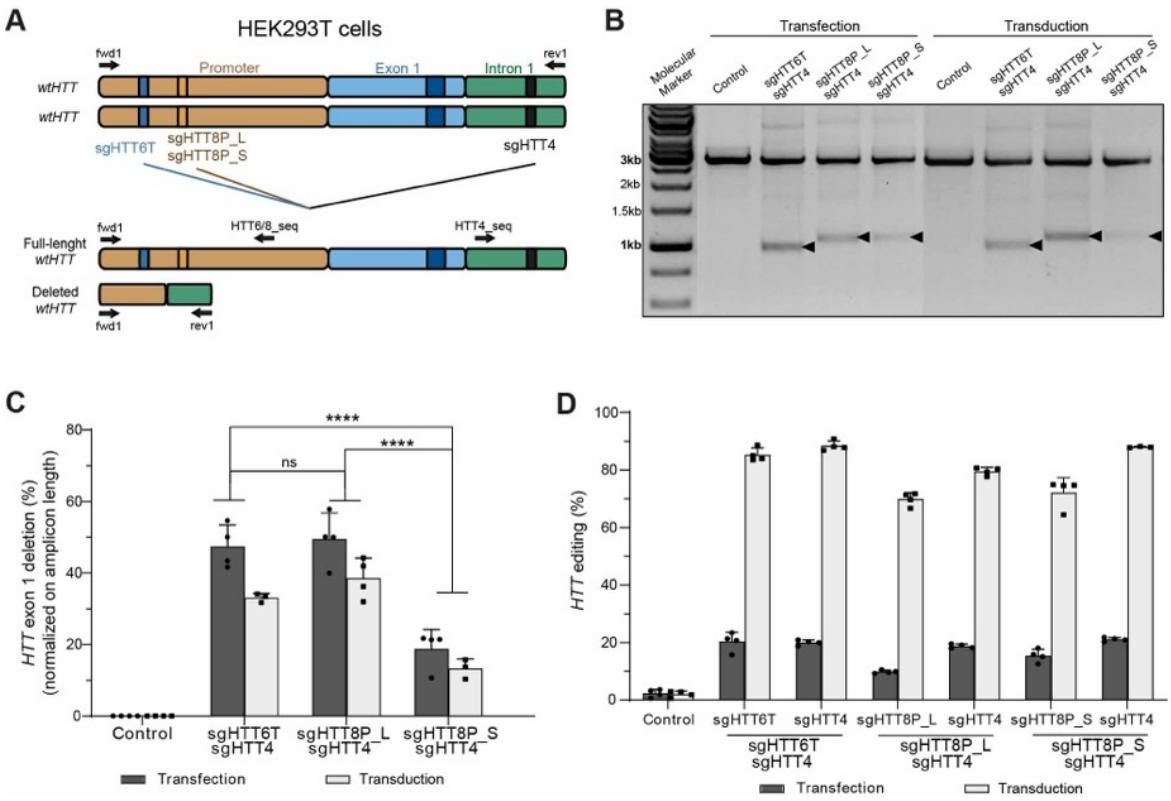

Figure 4.2: Deletion of the *HTT* exon 1 in transfected HEK293T cells. (A) Schematic representation of the *HTT* exon 1 deletion in HEK293T cells using the sgHTT6T, sgHTT8P_L or sgHTT8P_S combined with the sgHTT4. Amplification using the primer set 1 generates amplicons of 2732 bp when the full HTT gene is intact. The exon 1 deletion induced by sgHTT6T/sgHTT4 and sgHTT8P_L/sgHTT4 or

sgHTT8P_S/sgHTT4 generates amplicons of 974 bp and 1053 bp. The primers used to analyze the extent of indels induced in the non-deleted *HTT* alleles are represented in the Figure 4.2B. **(B-E)** Two constructs separately expressing the SpCas9 and the sgRNA combinations (sgHT6T/sgHTT4, sgHTT8P_L/sgHTT4 and sgHTT8P_S/sgHTT4) with the mCherry reporter were delivered into HEK293T cells by calcium transfection or by lentiviral transduction. Cells receiving only the SpCas9 and GFP transgenes with no sgRNAs were used as negative control. Transfected and transduced cells were analyzed at 4 and 21 days after the delivery of the CRISPR components, respectively. **(B)** Representative images of the agarose gels displaying the amplification of *HTT* gene using the primer set 1. **(C)** Semiquantitative analysis of the agarose gel images to estimate the efficiency of *HTT* exon 1 excision. After the normalization of the optical densities to amplicon size, deletion efficiency was calculated by dividing the intensity of the exon1-deleted amplicons by the sum of the intensity of the full-length and exon1-deleted amplicons. Results are presented as mean ± SD (N=1, n=3/4). Statistics: two-way ANOVA and multiple-comparisons to control with Tukey's correction; **** :p<0.0001. **(D)** Proportion of indels at the sgRNA target sites in the non-deleted *HTT* alleles in each condition measured by TIDE analysis. Results are presented as mean ± SD (N=1, n=3/4).

Transient SpCas9 expression excises the *HTT* exon 1 in HEK293T and in HD-NPCs

In the previous experiments, the *HTT* exon 1 deletion was achieved by constitutively expressing the SpCas9. However, the long-term SpCas9 nuclease expression increases the likelihood for the occurrence of off-target events. We have previously developed the lentiviral-based KamiCas9 system for transient SpCas9 expression, which is composed of the SpCas9 nuclease, a sgRNA targeting *HTT* and a second sgRNA targeting the translation start site of the SpCas9 nuclease itself (Merienne et al., 2017). Therefore, we adapted the system to promote the deletion of the *HTT* exon 1 by adding an extra sgRNA expression cassette (Figure 4.3A). In addition, to improve the kinetic of the system, we incorporated an optimized version of the tracrRNA (Dang et al., 2015) in the two *HTT*-targeting sgRNAs and replaced the H1 promoter by the stronger U6 promoter to boost their expression. The sgCas9 expression cassette was not modified. We next compared the efficiency of the constitutive (sgHTT6T or sgHTT8P_L with sgHTT4) and adapted KamiCas9 versions (sgHTT6T or sgHTT8P_L with sgHTT4 and sgCas9) in deleting the *HTT* exon 1 in transfected HEK293T cells (Figure 4.3A). At 4 days post-transfection, PCR amplification indicated that both constitutive and KamiCas9 systems expressing the two sgRNA combinations successfully deleted the exon 1 from the *HTT* gene (Figure 4.3B). Semiquantitative analysis of the gel agarose bands suggested a slight decrease on the efficiency of KamiCas9 system in excising the *HTT* exon 1 compared to the constitutive system (Figure 4.3C). TIDE analysis indicated that more than 60% of the SpCas9 transgenes had been self-inactivated (Figure 4.3D). These results suggest that the transient expression of SpCas9 slightly decreases the deletion efficiency in both sgRNA combinations when compared to the constitutive expression of SpCas9. Given the potential toxic effects related to the permanent SpCas9 expression, we considered that the high levels of nuclease self-inactivation offer a positive equilibrium between safety and editing efficiency.

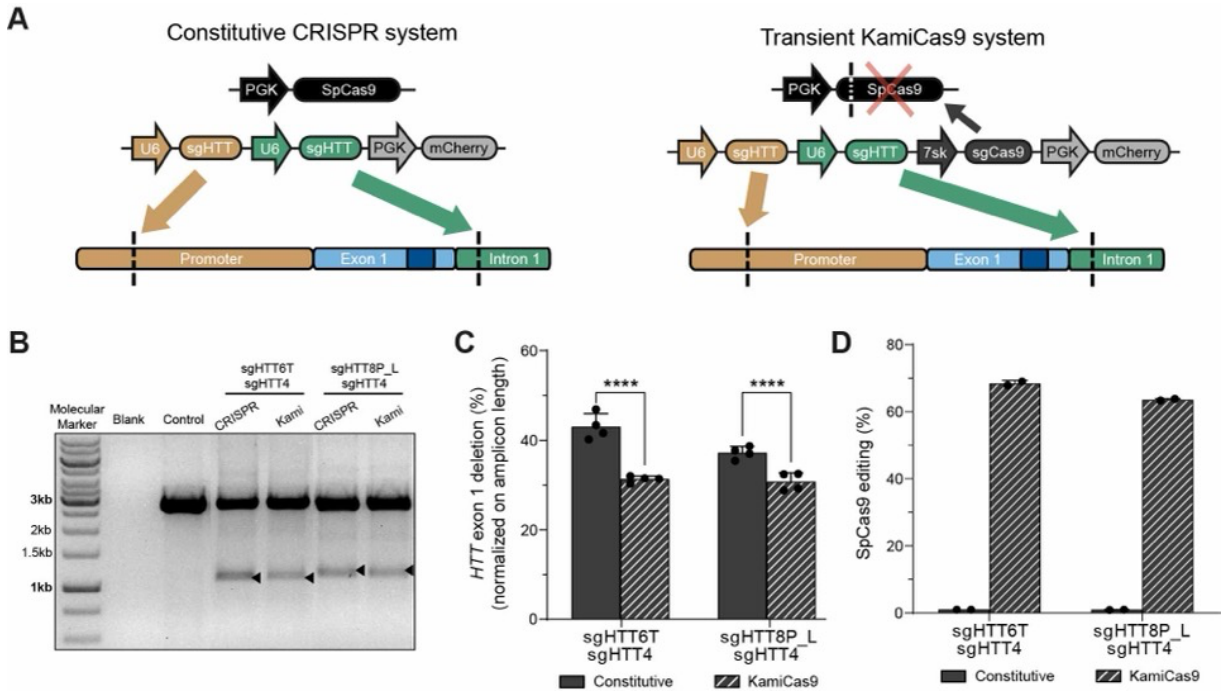

Figure 4.3: Deletion of the *HTT* exon 1 using the KamiCas9 system in transfected HEK293T cells. **(A)** Schematic representation of the constitutive and KamiCas9 system for *HTT* exon 1 deletion. In both systems, the sgRNAs targeting the *HTT* gene (sgHTT6T or sgHTT8P_L and sgHTT4) contain an optimized sgRNA tracrRNA (Dang et al., 2015) and their expression is driven by the U6 promoter. In the KamiCas9 system, an extra sgRNA (sgCas9) with no optimized sequences is expressed by the weaker 7sk promoter (Merienne et al., 2017) to promote gradual SpCas9 self-editing at the translational start site. **(B-D)** HEK293T cells were transfected with two plasmids separately expressing the SpCas9 and the constitutive sgRNA combinations (sgHT6T/sgHTT4 or sgHTT8P_L/sgHTT4) or KamiCas9 sgRNA combinations (sgHT6T/sgHTT4/sgCas9 or sgHTT8P_L/sgHTT4/sgCas9). Cells transfected with plasmids encoding for SpCas9 and mCherry were used as negative control. Gene editing outcomes were analyzed at 4 days post-transfection. **(B)** Representative images and **(C)** semiquantitative analysis of the agarose gels displaying the amplification of *HTT* gene using the primer set 1. Results are presented as mean ± SD (N=1, n=4). Statistics: two-way ANOVA and multiple-comparisons between constitutive and KamiCas9 conditions with Sidak's correction; **** :p<0.0001. **(D)** Editing efficiency of the sgCas9 quantified by TIDE. Results are presented as mean ± SD (N=1, n=2).

We next evaluated the constitutive and KamiCas9 systems in deleting the *HTT* exon 1 in neuronal progenitor cells derived from HD patients (HD-NPCs). We started by optimizing transduction conditions to favor maximal editing efficiency (Figure S4.3). Then, we co-transduced HD-NPCs with LVs expressing the SpCas9-BPNLS and the sgHTT6T/sgHTT4 or sgHTT8P_L/sgHTT4 in the constitutive or KamiCas9 settings (plus sgCas9) (Figure 4.4). Since these cells are heterozygous for rs2857935 (targeted by sgHTT8P_L) and homozygous for the rs28431418 (targeted by sgHTT6T) (Table 4.1), the sgHTT8P_L/sgHTT4 exclusively targets the exon 1 of the mutant *HTT* allele whereas the sgHTT6T/sgHTT4 is expected to delete the exon 1 in both alleles (Figure 4.4A). In addition, as in Figure 4.1, we also transduced HD-NPCs with an LV expressing the sgHTT4 combined with the mismatch sgHTT6C to simulate off-target exon 1 deletion at the non-targeted allele. Two weeks post-transduction, agarose gel electrophoresis semiquantitative analysis show that all sgRNA combinations induced *HTT* deletions, including the sgHTT6C(mismatch)/sgHTT4 combination (Figure 4.4B). Importantly, *HTT* exon 1 deletion efficiency was drastically reduced by the transient SpCas9 expression in the

sgHTT6C(mismatch)/sgHTT4 condition ($p<0.0001$) but not in the sgHTT6T/sgHTT4 condition ($p=0.153$) (Figure 4.4C), despite similar levels of SpCas9 self-editing (Figure 4.4D). In addition, efficiency of sgHTT8P_L/sgHTT4 in excising the exon 1 of the mutant *HTT* allele was just slightly decreased even though more than 50% of SpCas9 transgenes were inactivated (Figure 4.4C-D). These results suggest that KamiCas9 system greatly reduces off-target *HTT* exon 1 deletion induced by the sgHTT6C(mismatch)/sgHTT4 while having no major impact on the on-target deletion induced by the sgHTT6T/sgHTT4 and sgHTT8P_L/sgHTT4. We isolated and sequenced the *wtHTT* and *mHTT* full-length amplicons to evaluate the editing outcomes in the non-deleted *HTT* alleles (Figure S4.4). As expected, sgHTT6T and mismatch sgHTT6C did not discriminate between *HTT* alleles as similar rates of indels were observed in both *mHTT* and *wtHTT* (Figure 4.4E). Contrarily, indels at the sgHTT8P_L target site were only detected in the *mHTT* allele. Similar to the effect of KamiCas9 on deletion efficiency (Figure 4.4B-C), the transient SpCas9 expression only reduced the frequency of indels generated by the mismatch sgHTT6C ($p<0.0001$) (Figure 4.4E). Surprisingly, editing efficiency of sgHTT8P_L was lower than the sgHTT6T. These results differ from previous analysis of transduced HEK293T cells, which indicated that sgHTT6T, sgHTT8P_L and sgHTT8P_S induced comparable rates of indels at their respective targeted sites (Figures 4.1D and 4.2D). We further confirmed the reduced editing efficiency of sgHTT8P_L in a second experiment transducing HD-NPCs with LVs expressing exclusively the sgHTT6T, sgHTT8P_L, sgHTT8P_S or sgHTT4 (Figure S4.5). The distinct gene editing efficiencies of sgHTT8P_L and sgHTT8P_S in HEK293T cells and HD-NPCs may be related to differences in the genomic architecture of the *HTT* gene at the targeted locus.

In summary, we showed that the KamiCas9 system can be adapted to delete the *HTT* exon 1 in both HEK293T cells and HD-NPCs. The value of KamiCas9 is highlighted by the reduced off-target cleavage of the mismatch sgHTT6C but not by sgHTT6T. In agreement with previous studies (Fang et al., 2023; Monteys et al., 2017; Oikemus et al., 2022; Shin et al., 2022a, 2022b), we showed that PAM-based allele specific sgRNAs exhibit high levels of specificity as demonstrated by the sgHTT8P_L in HD-NPCs. We demonstrated that editing efficiencies of individual sgRNAs are cell type-dependent, as sgHTT8P_L and sgHTT8P_S generated high frequency of indels in HEK293T cells but low levels in HD-NPCs. Finally, despite the KamiCas9 system slightly decreased the efficiency of *HTT* exon 1 deletion, we considered that it offers a positive equilibrium between safety and efficiency.

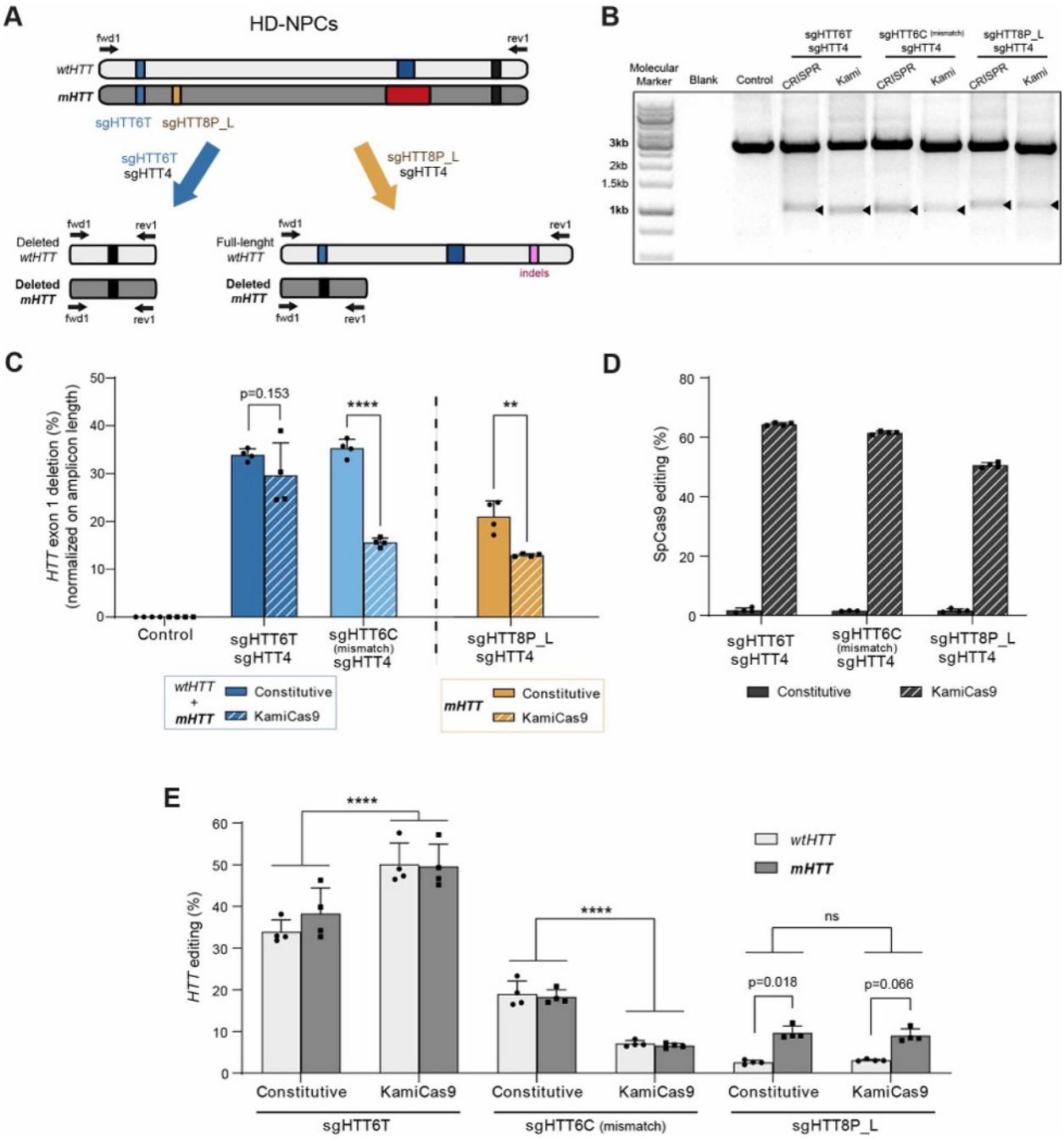

Figure 4.4: Deletion of the *HTT* exon 1 using the KamiCas9 system in transduced HD-NPCs. (A) HD-NPCs were transduced with two LVs separately expressing the SpCas9-BPNLS and the constitutive sgRNA combinations (sgHT6T/sgHTT4, sgHTT6C/sgHTT4 or sgHTT8P_L/sgHTT4) or KamiCas9 sgRNA combinations (sgHT6T/sgHTT4/sgCas9, sgHTT6C/sgHTT4/sgCas9 or sgHTT8P_L/sgHTT4/sgCas9). Cells transduced with LVs encoding for SpCas9-BPNLS and mCherry were used as negative control. Gene editing outcomes were analyzed at 2 weeks post-transduction. **(B)** Representative images and **(C)** semiquantitative analysis of the agarose gels displaying the amplification of *HTT* gene using the primer set 1. Results are presented as mean ± SD (N=1, n=4). Statistics: two-way ANOVA and multiple-comparisons between constitutive and KamiCas9 conditions with Sidak's correction; **** :p<0.0001. **(D)** Editing efficiency of the sgCas9 quantified by TIDE. Results are presented as mean ± SD (N=1, n=4). **(E)** TIDE analysis was performed on sequencing chromatograms from isolated full-length amplicons of *wtHTT* and *mHTT*. Results are presented as mean ± SD (N=1, n=4). Statistics: two-way ANOVA and multiple-comparisons between *wtHTT* and *mHTT* with Sidak's correction; and two-way ANOVA and multiple comparisons between constitutive and KamiCas9 with Tukey's correction; **** :p<0.0001.

Adapting the AAV-KamiCas9 for the deletion of the *mHTT* exon 1 *in vivo*

After *in vitro* validation, we next sought in investigating efficiency and specificity of mutant *HTT* exon 1 deletion *in vivo* in the fully humanized HU97/18 HD mouse model (Southwell et al., 2013). This mouse model was generated by crossbreeding mice transgenic for the bacterial artificial (BACHD) (Gray et al., 2008) and yeast artificial (YAC18) chromosomes (Hodgson et al., 1999) mice on a background strain lacking the mouse homolog *HTT* gene. The presence of both *wtHTT* and *mHTT* human sequences make these mice more suitable to test allele-specific strategies. In addition, wild-type and mutant *HTT* transgenes are heterozygous for the variant rs2857935 (Table 4.1), allowing the evaluation of sgHTT8P_L/sgHTT4 to specifically excise the *mHTT* exon 1 *in vivo*. Nonetheless, a disadvantage of this transgenic model is the presence of 8 copies of the human *HTT* transgene (4 *wtHTT* and 4 *mHTT*) (Duarte et al. 2023 – in revision). Because transgenes in transgenic models are often repeated in tandem, the cleavage of multiple target sites in the same chromosome can potentially induce complex rearrangements, including the deletion of larger chromosomal portions. These events are likely to not be captured using the semiquantitative agarose gel approach. In addition, while semiquantitative analysis of agarose gel bands is useful to detect deletion events, it does not accurately assess their frequency due to bias introduced by the amplification of fragments with different sizes. To overcome these limitations, we developed two QIAcuity digital PCR-based assays to accurately quantify the overall loss of *HTT* exon 1 copies (intronic assay) or the specific loss of mutant *HTT* exon 1 copies (FLOX assay) (Figure S4.6). The FLOX assay amplifies the FLOX sequence which is present only in the 5'UTR of *mHTT* transgenes of HU97/18, whereas the intronic assay amplifies an intronic sequence in both *wtHTT* and *mHTT* transgenes immediately upstream to the exon 1 (Figure S4.6A). Both assays quantify exon 1 deletion based on the loss of amplification signals after normalization to the signals from the amplification of the reference poly(rC)-binding protein 2 (*PCBP2*) gene. To validate the assays, we mixed gDNA from wild-type and HU97/18 mice in increasing ratios to simulate the loss of human *HTT* exon 1. Both the intronic (Figure S4.6B) and FLOX assays (Figure S4.6C) accurately predicted the relative loss of human *HTT* exon 1 in the different mixes compared to the parental genomic sample from HU97/18 mice, validating their use for the quantification of *HTT* exon 1 deletion.

Because our previously described AAV-KamiCas9 system induced high gene editing efficiencies in the mouse brain (Duarte et al. 2023 – in revision), we adapted the allele-specific strategy for AAV-mediated delivery. After verifying the functionality of the system in transfected HEK293T cells (Figure S4.7), we co-injected the striatum of HU97/18 mice with AAV2/rh.10 separately expressing the $SpCas9^{AAV}$ (3.3×10^9 vg/hemisphere) and the $sgHTT8P\_L/sgHTT4/sgCas9^{AAV}$ KamiCas9 plus a nuclear GFP reporter (6.6×10^9 vg/hemisphere) for visualization of the transduced cells (Figure 4.5A). Control mice were injected with the same doses but the AAV2/rh.10 expressing the sgRNAs combination was replaced by AAV2/rh.10 expressing only the nuclear GFP reporter. Since HU97/18 mice are heterozygous for

rs2857935 (targeted by sgHTT8P_L) (Table 4.1), the sgHTT8P_L/sgHTT4 is expected to exclusively delete the exon 1 of the *mHTT* allele (Figure 4.5B). The animals were sacrificed at 10 weeks post-injection and striatal punches were collected from the GFP-positive areas for DNA extraction. Genomic DNA amplification using the primer set 1 indicated that the human *HTT* exon 1 had been deleted in the animals injected with the KamiCas9 system (Figure 4.5C). We then used the intronic and FLOX assays to quantify deletion events and assess allele-specificity. As previously mentioned, HU97/18 mice carry equal number of *mHTT* and *wtHTT* transgenes (4 copies of each) (Duarte et al. 2023 – in revision). Therefore, the specific deletion of exon 1 in the *mHTT* transgenes is expected to induce a two-fold loss of FLOX signals compared to intronic signals. The intronic and FLOX assays indicated that *HTT* exon 1 had been excised in 1.6 ± 3.9% of the total *HTT* transgenes (p=0.321) (Figure 4.5D) and in 3.2 ± 1.7% of the mutant *HTT* transgenes in the treated mice (p=0.012) (Figure 4.5E). These results demonstrate that *HTT* exon 1 deletion events were very rare *in vivo*. Nevertheless, the more pronounced loss of FLOX signals compared to intronic signals (1.9-fold) suggests that deletion events mainly occurred at the *mHTT* transgenes. The low number of *HTT* exon 1 deletion events could be due the lower intrinsic activity of the sgHTT8P_L (as in Figure 4.4E and S4.5) and/or to the gradual self-inactivation of the SpCas9. Therefore, we took one step back and tested the efficiency of the constitutive CRISPR system expressing the sgHTT6T/sgHTT4 combination in HU97/18 mice. We also increased the ratio sgRNAs:SpCas9^{AAV} to 1:3 to ensure maximal efficiency. The striatum of HU97/18 mice was then injected with three AAV2/rh.10 vectors: one expressing the SpCas9^{AAV} (2.5 x 10^9 vg/hemisphere), other expressing the sgHTT6T/sgHTT4 constitutive combination (7.5 x 10^9 vg/hemisphere) and the last vector expressing the nuclear GFP reporter (5.0 x 10^8 vg/hemisphere) (Figure 4.6A). Control mice were not injected with the AAV2/rh.10 expressing the SpCas9^{AAV}. Contrarily to the previous experiment, HU97/18 mice are heterozygous for rs28431418 (targeted by sgHTT6T) (Table 4.1), and therefore the sgHTT6T/sgHTT4 targets both wild-type and mutant human *HTT* transgenes (Figure 4.6B). At 4 weeks post-injection, genomic DNA amplification indicated that *HTT* exon 1 deletion had occurred in treated but not in control animals (Figure 4.6C). Similar to the previous experiment, analysis by the intronic assay also indicated poor efficiency of the strategy, with *HTT* exon 1 being deleted in only 4.8 ± 4.0% of the total *HTT* transgenes (p=0.017) (Figure 4.6D). As expected, we did not observe any greater loss of FLOX signal compared to intronic signals (Figure 4.6E), supporting that deletion occurred in both wild-type and mutant *HTT* transgenes.

In summary, we showed the sgHTT8P_L/sgHTT4 combination excised the exon 1 from 25-30% of *HTT* alleles in transfected HEK293T cells (Figure S4.7D) whereas merely 3% of the mutant HTT transgenes were targeted for exon 1 deletion in the striatum of HU97/18 mice. Additionally, we demonstrated that the sgHTT6T/sgHTT4 combination targeting both *wtHTT* and *mHTT* alleles also resulted in rare deletion events *in vivo*, with just approximately 5% of *HTT* alleles lacking the exon 1. Overall, these results suggest that approaches to delete *HTT* exon 1

are relatively efficient *in vitro*, but their application to excise the *HTT* exon 1 *in vivo* is far more challenging.

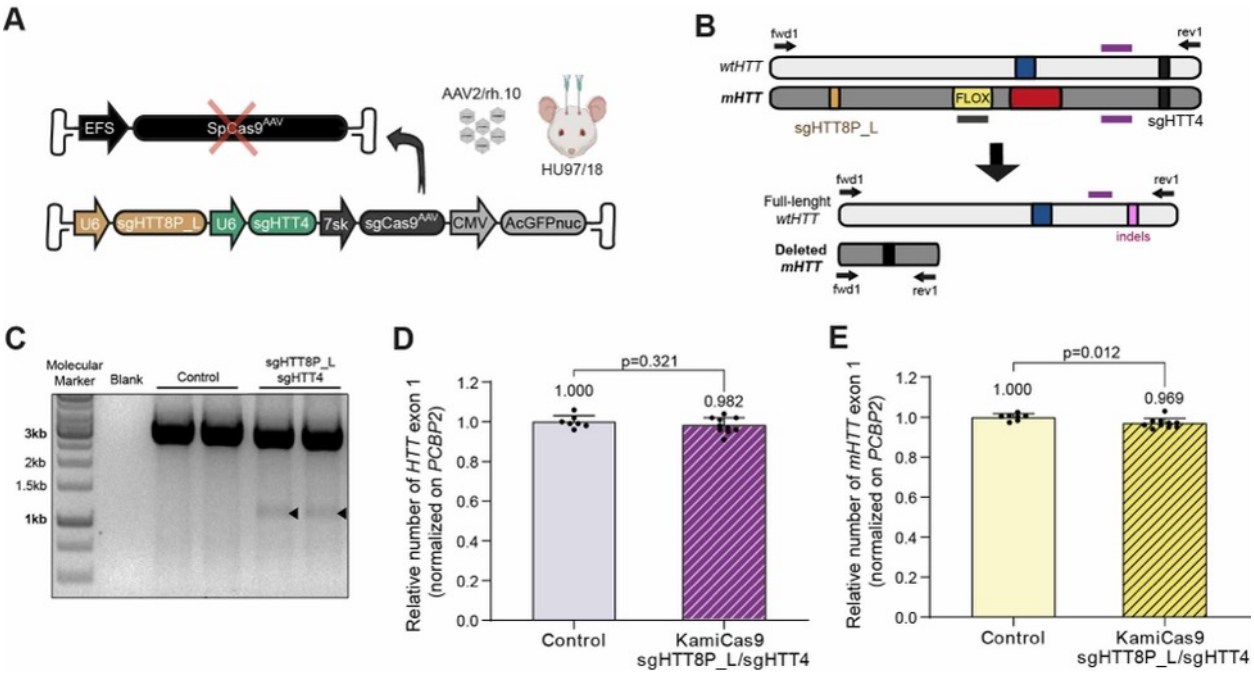

Figure 4.5: Allele-specific deletion of the *mHTT* exon 1 in HU97/18 by the AAV-KamiCas9 system expressing the sgHTT8P_L/sgHTT4 combination. (A) The striatum of HU97/18 mice was bilaterally injected with an AAV2/rh.10 expressing the $SpCas9^{AAV}$ (3.3×10^9 vg/hemisphere) plus another AAV2/rh.10 expressing the sgHTT8P_L/sgHTT4/$sgCas9^{AAV}$ KamiCas9 combination with a nuclear GFP reporter (6.6×10^9 vg/hemisphere). Control mice were injected with the same doses but the AAV2/rh.10 expressing the sgRNAs combination was replaced by AAV2/rh.10 expressing only the nuclear GFP reporter. **(B)** The treatment is expected to induce deletions exclusively in the *mHTT* transgene. At 10 weeks post-injection, 4 to 5 punches/mice were taken from the GFP-positive striatal areas for gDNA extraction. **(C)** Agarose gel demonstrating the presence of exon 1-deleted *HTT* amplicons with the expected size. Quantification of *HTT* exon 1 deletion events using the **(B)** intronic and **(C)** FLOX QIAcuity-based assays. Results are presented as mean ± SD (N=1, n=7 punch specimens from 2 animals for the control and n=10 punch specimens from 2 animals for KamiCas9). Statistics: two-tailed unpaired t-tests with Welch's correction.

4.1.4. Discussion

Among the therapeutic strategies aiming at lowering *mHTT*, gene editing using the CRISPR/Cas9 system offers the possibility to permanently inactivate the *HTT* gene. Given the wide-range functions of wtHTT, it is still unclear whether the loss of wtHTT activity may induce long-term deleterious effects (Kaemmerer & Grondin, 2019). Therefore, alternative strategies are under development to specifically inactivate the *mHTT* allele by targeting PAS associated to the expanded CAG. One of the approaches consists of the specific excision of the *mHTT* exon 1 (Fang et al., 2023; Monteys et al., 2017; Shin et al., 2016, 2022a). Shin and colleagues selected several allele-specific sgRNA combinations targeting upstream and downstream PAS to the expanded CAG repeat to delete large portions of the *mHTT* allele (> 22 kb) (Shin et al., 2016, 2022a). A disadvantage of this strategy is the low combined heterozygosity of two targetable SNPs in HD subjects, which

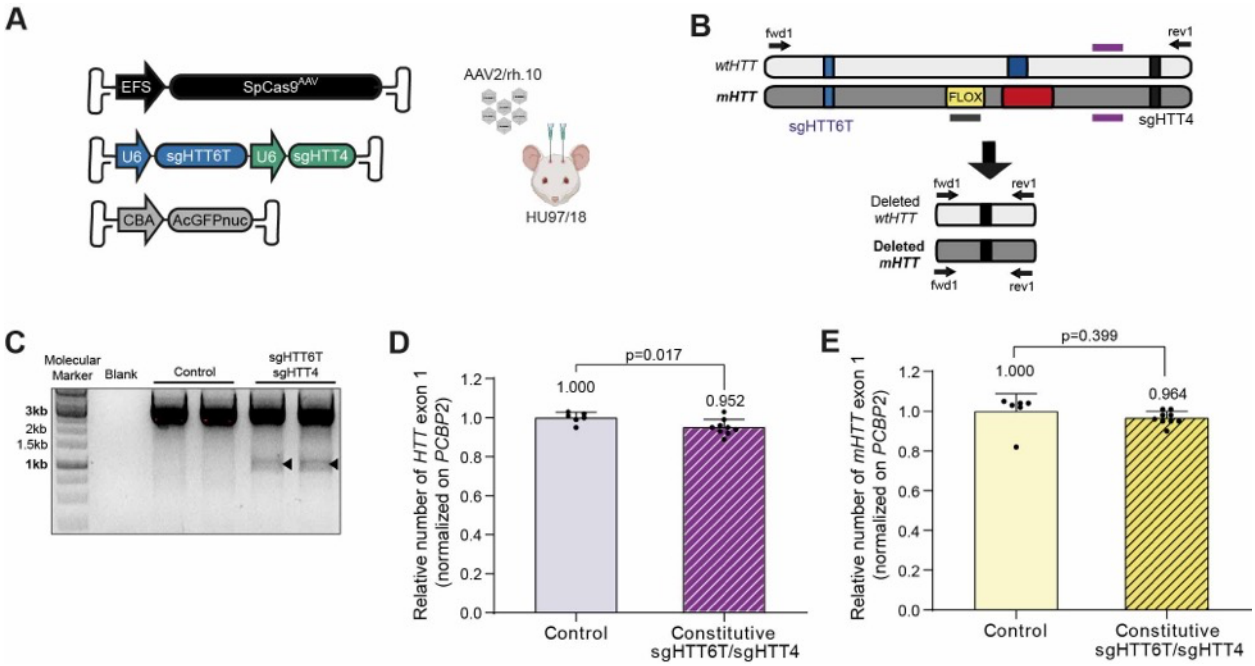

Figure 4.6: Deletion of both *mHTT* and *wtHTT* exon 1 in HU97/18 with constitutive CRISPR system expressing the sgHTT6T/sgHTT4 combination. (A) The striatum of HU97/18 mice was bilaterally injected with three AAV2/rh.10 vectors: one expressing the $SpCas9^{AAV}$ (2.5×10^9 vg/hemisphere), other expressing the sgHTT6T/sgHTT4 constitutive combination (7.5×10^9 vg/hemisphere) and the last vector expressing the nuclear GFP reporter (5.0×10^8 vg/hemisphere). Control mice were not injected with the AAV2/rh.10 expressing the $SpCas9^{AAV}$. **(B)** The treatment is expected to induce deletions in both *mHTT* and *wtHTT* transgenes. At 4 weeks post-injection, 4 to 5 punches/mice were taken from the GFP-positive striatal areas for gDNA extraction. (**C)** Agarose gel demonstrating the presence of exon 1-deleted *HTT* amplicons with the expected size. Quantification of HTT exon 1 deletion events using the **(B)** intronic and **(C)** FLOX QIAcuity-based assays. Results are presented as mean ± SD (N=1, n=6 punch specimens from 2 animals for the control and n=9 punch specimens from 3 animals for KamiCas9). Statistics: two-tailed unpaired t-tests with Welch's correction.

limits the number of eligible patients for *mHTT* exon 1 deletion. To overcome this limitation, Monteys and colleagues combined an allele-specific sgRNA with a non-allele-specific sgRNA (Monteys et al., 2017). However, indels generated by their selected non-allele-specific sgRNA decreased the human and mouse *wtHTT* expression up to 40% *in vitro* and *in vivo*, respectively, indicating that the strategy did not target exclusively the *mHTT* allele. Here, we designed an optimized intronic non-allele-specific sgRNA (sgHTT4) whose cleavage has no impact on *HTT* expression to ensure allele-specificity of the approach. Among the sgRNAs targeting frequent SNPs in the *HTT* promoter region, the allele-specific sgRNAs targeting the variants rs28431418 (sgHTT6T) and rs2857935 (sgHTT8P_L) were selected based on their selectivity and efficiency performances. While the first variant is not in close linkage to the expanded CAG (Fang et al., 2023), the PAS rs2857935 is estimated to be present exclusively in the mutant allele in 27.6% of the HD patients (Shin et al., 2022a). While all sgRNAs demonstrated similar editing efficiency in HEK293T cells, the sgHTT8P_L and sgHTT8P_S targeting the most promising variant rs2857935 displayed reduced gene editing efficiency in HD-NPCs compared to the other sgRNAs. Likewise, relative low levels of gene editing at this locus was also recently reported by Shin and colleagues in transfected HD-iPSCs, who detected a 2-fold lower proportion of indels (6%) compared to other

sgRNAs (12-14%) (Shin et al., 2022a). Reduced chromatin accessibility at the rs2857935 locus caused by the presence of an expanded CAG tract in HD-derived cells could explain the lower editing efficiencies in these cell models (Verkuijl & Rots, 2019). These results suggest that sgRNAs efficiency cannot be generalized to multiple models. Despite differences in the gene editing efficiencies, we demonstrated that the allele-specific sgHTT6T and sgHTT8P_L excised the *HTT* exon 1 in both HEK293T and HD-NPCs when combined with the intronic non-allele-specific sgHTT4. Consistent with previous reports (Fang et al., 2023; Monteys et al., 2017; Shin et al., 2016, 2022a), we confirmed that the *HTT* exon 1 excision prevents HTT mRNA and protein expression.

In the studies testing *HTT* exon 1 deletion *in vitro* (Fang et al., 2023; Monteys et al., 2017; Shin et al., 2016, 2022a), allele-specific *mHTT* deletion has been exclusively demonstrated in HD-iPSCs lines after clonal or puromycin selection. In the study testing *HTT* exon 1 deletion *in vivo*, Monteys and colleagues confirmed *mHTT* exon 1 deletion in the striatum of BACHD mice by agarose gel analysis (Monteys et al., 2017). The authors inferred that the 50% decrease of *mHTT* mRNA expression in the treated striatum was the result of *mHTT* exon 1 deletion events. However, indels generated by individual sgRNAs decrease *HTT* expression up to 40% in HEK293T cells and HD-iPSCs. In addition, while no deletion was expected to occur in the endogenous mouse *wtHTT* gene, its expression was reduced by 35% in the treated striatum. Taken together, analysis of *mHTT* expression levels is not sufficient to draw conclusions regarding the efficiency of *mHTT* exon 1 deletion. Moreover, here we show that agarose gel analysis greatly overestimates the extent of *mHTT* exon 1 events due to PCR bias towards the amplification of smaller fragments. meaning that the overall efficiency of *HTT* exon 1 deletion strategy was never evaluated *in vitro* nor *in vivo.*

Given the ultimate goal of applying this strategy for the treatment of HD, it is critical to accurately assess its efficacy to determine therapeutic potential. Therefore, here we developed digital PCR-based assays to accurately quantify the frequency of deletion events. We observed that deletion events were relatively frequent *in vitro* (approximately 30% in non-selected transfected HEK293T cells), but extremely rare in the striatum of HU97/18 mice (less than 5% in the transduced areas). The poor frequency of deletion events *in vivo* was confirmed using sgRNA combinations targeting exclusively the *mHTT* transgene (sgHTT8P_L/sgHTT4) and both *wtHTT* and *mHTT* transgenes (sgHTT6T/sgHTT4). The *HTT* exon 1 deletion in HU18/18 mice also yielded disappointing results (data not shown). Recently, Simpson and collaborators highlighted the challenges of dual sgRNA strategies to delete genomic sequences in the brain (Simpson et al., 2023). By combining two sgRNAs to eliminate the expanded CAG from the human *ATXN2* transgene in two SCA2 mouse models, the authors observed that AAV fragment integrations (22-26%) and indels (22-30%) occurred much more frequently than CAG deletions (1-4%). Additionally, a small proportion of inversions (1-2%) and complex rearrangements involving the removal of multiple transgenes in tandem (< 1%) were also detected. Another study that

attempted a deletion of the exon 23 of the *DMD* gene *in vivo* also observed heterogeneous editing outcomes (AAV integration, indels, deletions and inversions) after the systemic delivery of the CRISPR system (Nelson et al., 2019). Nevertheless, deletion events were almost absent in all analyzed organs with exception of the liver, where the *DMD* exon 23 was deleted in approximately 5% of the alleles. These data suggest that most of the gene editing outcomes induced by dual sgRNA-based approaches are not deletions. Although we have not yet analyzed the frequency of indels at the targeted sites in the latest *in vivo*, unpublished experiments from the lab using lower AAV doses and a different AAV serotype (AAV2/1 – serotype 1) revealed that sgHTT6T and sgHTT4 induced indels in 27.2 ± 6.0% and 9.1 ± 3.7% of the human *HTT* transgenes, whereas lower indel frequencies were observed at the sgHTT8P_L target site (5.4 ± 0.4%) (data not shown). Similarly to HD-NPCs, it indicates that the sgHTT8P_L is less efficient than sgHTT6T. In addition, the frequency of indels at the sgHTT4 target site was decreased in HU97/18 compared to HD-NPCs and HEK293T cells. Future indel profiling in the latest experiments will provide further insights regarding individual efficiency of the sgRNAs under optimized *in vivo* transduction conditions. Overall, the low frequency of deletion events detected in HD mice is supported by previous studies indicating poor efficiency of dual sgRNA-based strategies to induce deletion events *in vivo*.

A dual sgRNA deletion strategy is being tested clinically for the treatment of Leber congenital amaurosis type 10 (LCA10) (EDIT-101 - NCT03872479). The therapeutic approach consists of the subretinal delivery of an AAV2/5 expressing SaCas9 and a pair of sgRNAs to remove or invert the IVS26 mutation in the *CEP290* gene, preventing the inclusion of on alternative exon containing a premature stop codon (Maeder et al., 2019). The injection of EDIT-101 was estimated to induce deletion/inversions events in 3 to 28% of the *CEP290* alleles of retinal photoreceptor cells of primates (Maeder et al., 2019). Even though the frequency of these events was highly variable between treated samples, clinical trial was launched because low levels of gene correction (10%) were estimated to be required to induce phenotypic improvements (Maeder et al., 2019). This trial has recently paused enrollment for disappointing efficacy, with only 3 out of 14 patients presenting clinical improvements. Whether these disappointing results are due to poor *CEP290* gene correction in the photoreceptor cells of the patients is unknown. Nevertheless, these results highlight the therapeutic challenges regarding dual sgRNA strategies aiming at deleting genomic sequences *in vivo* even when low frequency of edited events are required to induce phenotypic benefit.

In addition to the low deletion efficiencies, one of the major drawbacks of allele-specific excision of *mHTT* exon 1 is the requirement for the presence of CAG-associated SNPs proximal to the *mHTT* exon 1. Shin and colleagues identified 10 variants with high mutant specificity altering the NGG PAM of SpCas9 at the 5' region of the *HTT* gene in a large genotype dataset of European-descendent HD subjects (Shin et al., 2022a). However, most of these SpCas9-PAS are located far away from the *mHTT* exon 1 (> 10 kb) and deletion efficiency has been shown to

decrease with deletion size (Canver et al., 2014; Monteys et al., 2017). Furthermore, approximately 30% of the HD subjects are still not eligible for *mHTT* exon 1 deletion strategies using any of these PAS (Shin et al., 2022a). An alternative CRISPR/Cas9-mediated strategy is to promote the specific degradation of the *mHTT* transcript by nonsense-mediated mRNA decay (NMD) (Oikemus et al., 2022; Shin et al., 2022c). Contrarily to deletion strategies, NMD-mediated approaches require only one sgRNA targeting the exonic sequences of *mHTT* allele to induce frameshift mutations which generate downstream premature stop codons. However, a disadvantage of NMD-based strategies is non-targeting of the short transcript *HTT1*α*,* which is translated into highly toxic exon 1 mHTT truncated forms (Neueder et al., 2017; Sathasivam et al., 2013). Allele-specific strategies based on deletion and NDM have mainly focused on PAS as SpCas9 has a lower tolerance to mismatches at PAM sites (Hsu et al., 2013). Nevertheless, the targeting of other SNP variants that do not alter PAM sites but are still linked to the expanded CAG repeat would maximize the applicability of allele-specific strategies to more HD patients. Here, we demonstrate that the transient SpCas9 expression using our previously described LV-KamiCas9 system not only prevents off-target events (Merienne et al., 2017) but also greatly improves sgRNA specificity. These results encourage the use of the KamiCas9 system to maximize allele discrimination options by designing allele-specific sgRNAs targeting SNPs located at both the seed sequence and the PAM sites. Future analysis of HD genotype datasets including not only PAS but all variants linked to the expanded CAG will provide additional options to introduce allele-specific modifications in the *HTT* gene.

In summary, we present novel insights regarding the *in vivo* applicability of dual sgRNA deletion approaches. While the field has mainly relied on PCR amplification followed by agarose gel analysis to evaluate gene editing outcomes, we show that these methods greatly overestimate the frequency of deletion events. In addition, we demonstrate that excision events are frequent *in vitro* but very rare *in vivo*. Despite the huge efforts to establish dual sgRNA-based deletion strategies for the treatment of HD and other neurodegenerative disorders, our results do not support their application *in vivo*.

4.1.5. Material and Methods

Plasmid production

The sgHTT25A/G, sgHTT6T/C, sgHTT10C/G, sgHTT2G/A and sgHTT4 were initially ordered as gene strand (IDT, LEuven, Belgium ; Table S4.1) and cloned into the pENTR221 plasmid as previously described (Merienne et al., 2017). The lead candidates (sgHTT6T/C, sgHTT8P_L, sgHTT8P_S, sgHTT2G and sgHTT4) were then clones into optimized expression cassettes. We ordered a universal entry plasmid (pMK-AttL1-NotI/BamHI-U6-BsaI-tracrRNAopt-BamHI/NcoI-U6-SapI-tracrRNAopt-NotI/NcoI/XbaI-7sk-BsmBI-tracrRNA-XbaI-AttL2) containing three sgRNA expression cassettes, to make it possible to adopt a flexible cloning strategy for

multiple sgRNAs. The U6-driven expression cassettes contain an optimized tracrRNA described by Dang and coworkers (Dang et al., 2015) whereas the 7sk-driven expression cassette is associated with the original tracrRNA (Merienne et al., 2017). Unique restriction sites (NotI, BamHI, XbaI and NcoI) were strategically placed between the cassettes to facilitate the removal of every possible cassette combination. The spacer sequence of each sgRNA was then inserted into the universal entry plasmid with overhang-compatible annealed oligos after digestion of the plasmid with type IIS restriction enzymes (BsaI, SapI or BsmBI). The oligomers used to clone each sgRNA is described on the Table S4.2. We then generated the entry plasmids expressing different combination of sgRNAs. Briefly, we first generated the KamiCas9 entry plasmids, which contain the allele-specific sgRNA (sgHTT6T/C, sgHTT8P_L, sgHTT8P_S, or sgHTT2G) in first cassette, the sgHTT4 in the second cassette and the sgCas9 in the last cassette (U6-sgHTT"X"-U6-sgHTT4-7sk-sgCas9). The entry constitutive plasmids expressing two HTT-targeting sgRNAs were generated by removing the last 7sk-sgCas9 cassette by XbaI digestion. Finally, the entry plasmids expressing only one HTT-target sgRNA were subsequently produced by removing the first or second U6-driven expression cassettes by BamHI or NcoI digestion, respectively. The SIN or pAAV2ss plasmids were then produced by transferring the sgRNA expression cassettes from the entry plasmids into a LV (SIN-cPPT-Gateway-PGK-mCherry-WPRE) or AAV destination vector (pAAV2ss-Gateway-WPRE-bGH), respectively.

Regarding SIN plasmids expressing the SpCas9, we used the SIN-cPPT-PGK-SpCas9-WPRE (Addgene #87886) (Merienne et al., 2017) for editing assessment in HEK293T cells. For HD-NPCs, we generated the SIN-cPPT-PGK-SpCas9-BPNLS-WPRE plasmid after replacing the SRAD and SV40-NLS of the previous construct by a glycine-serine linker (Zhao et al., 2016) and the bipartite NLS (BPNLS) (Suzuki et al., 2016; Wu et al., 2009). For the AAV-based systems, we used the pAAV2ss-EFS-SpCas9-synPolyA (a gift from Ryohei Yasuda; Addgene #104588) (Nishiyama et al., 2017). Additionally, we used the pAAV2ss-CBA-EGFP-WPRE-bGH plasmid was kindly provided by Prof. During, Ohio, USA. Another plasmid expressing a nuclear GFP (pAAV2ss-CBA-AcGFPnuc-WPRE-bGH) was generated by transferring the AcGFPnuc coding sequence from the entry plasmid pENTR4-AttL1-AcGFPnuc-AttL2 to the pAAV2ss-CBA-Gateway-WPRE-bGH destination vector.

Human embryonic kidney 293T (HEK293T) cells

HEK293T cells (mycoplasma-negative, ATCC, LGC Standards GmbH, Wessel, Germany) were cultured in DMEM-Glutamax supplemented with 10% FBS and 1% penicillin/streptomycin (Gibco, Life Technologies, Zug, Switzerland) at 37°C under an atmosphere containing 5% CO_2. For routine culture, cells were passaged twice weekly after trypsin treatment for dissociation (Gibco, Life Technologies, Zug, Switzerland) and plated at a density of $2x10^6$ cells/cm^2 in T175 flasks.

HD-derived Neuronal precursor cells (HD-NPCs)

Patient-derived neuronal progenitor cells (HD-NPCs) were generated from hPSCs line GM03621 (Coriell) and provided by Dr. Anselme Perrier (I-Stem, Evry, France). Differentiation and culture protocols were previously described (Gribaudo et al., 2019; Nicoleau et al., 2013). After amplification, HD-NPCs were banked in vials of $4x10^6$ cells and stored in liquid nitrogen. For each experiment, cells were defrost and resuspended in N2B27 medium (1:1 ratio of DMEM-F12-Glutamax:Neurobasal, 1% N2 supplement, 2% B27 supplement and 0.1% Gentamicin - Gibco, Life Technologies, Zug, Switzerland). Cells were centrifuged at 300 x g for 5 minutes to remove any trace of FBS and DMSO. Cell pellet was resuspended in 1 mL of N2B27 medium and counted with an hemocytometer. For cell expansion, approximately $1.5x10^6$ and $10x10^6$ of cells were plated in 6-wells plates or in 10 cm dishes, respectively, in N2B27 medium supplemented with 10 ng/mL FGF (Bio-techne, Zug, Switzerland), 10 ng/mL EFG (Peprotech, Zug, Switzerland) and 20 ng/mL BDNF (Peprotech, Zug, Switzerland). Prior plating, wells/dishes were coated with 1:6 poly-L-ornithine (Sigma-Aldrich, Buchs, Switzerland) in H_2O for 24 hour and then with 2 µg/mL laminin (Sigma-Aldrich, Buchs, Switzerland) in H_2O for 24 hours. Medium was completely changed twice a week and cells were passed once a week.

Production of lentiviral vectors

The LV vectors were produced by the calcium phosphate-mediated transfection of HEK293T cells with a four-plasmid system (Hottinger et al., 2000). Human immunodeficiency virus type 1 (HIV-1) vectors were pseudotyped with the vesicular stomatitis virus glycoprotein (VSV-G) envelope, concentrated by ultracentrifugation and resuspended in phosphate-buffered saline (PBS, Gibco, Life Technologies, Zug, Switzerland) supplemented with 1% bovine serum albumin (BSA, Sigma-Aldrich, Buchs, Switzerland). The viral particle content of each batch was determined in a p24 antigen enzyme-linked immunosorbent assay (p24 ELISA, RETROtek, Kampenhout, Belgium). Viral stocks were stored at -80°C until use.

Production of adeno-associated vectors

AAVs were produced in HEK293T cells by calcium phosphate-mediated transfection. The cells were transfected with the pAAV2ss containing the transgene of interest together with the pAd Helper-AAV (Agilent Technologies kit #240071) and pAAV-rh10_Rep_Cap (Penn Vector Core, University of Pennsylvania, School of Medicine, Philadelphia, USA). The cell suspension was centrifuged at 360 x *g* for 10 minutes at 4°C 72 hours post-transfection. The supernatant was supplemented with 10 mM PEG (Roth, Arlesheim, Switzerland) and 0.5 M NaCl (Merck, Nottingham, UK) and was incubated at 4°C for at least 2 hours. Cell pellets were pooled and incubated in lysis buffer (0.15 M NaCl, Merck, Nottingham, UK; 50 mM Tris-HCl, pH 8.5, Sigma-Aldrich, Buchs, Switzerland) for 3 consecutive freeze/thaw cycles (30 minutes in dry ice/ethanol followed by 30 minutes at 37°C). After the initial two-hour incubation period, the PEG-containing

supernatant was centrifuged at 3700 x *g* for 20 minutes at 4°C and the supernatant was discarded. Cell lysate was added to the pellets and the mixture was incubated at 37°C for 1 hour to ensure that the pellets were fully homogenized. The lysate was then treated with 50 U/mL Benzonase (Sigma-Aldrich, Buchs, Switzerland) and 10 mM $MgCl_2$ (Sigma-Aldrich, Buchs, Switzerland) at 37°C for 30 minutes. The treated lysate was clarified by centrifugation at 3700 x *g* for 20 minutes at 4°C. AAVs were separated by iodixanol (AxonLab, Le Mont sur Lausanne, Switzerland) gradient ultracentrifugation at 255,690 g (70Ti rotor, Beckman-Coulter, Nyon, Switzerland) for 90 minutes at 20°C. The AAV-containing phase was harvested and loaded on an Amicon Ultra-15 PL 100 column (Millipore, Zug, Switzerland) with 0.001% Pluronic F68 D-PBS (Gibco, Thermo Fisher Scientific, Waltham, USA, Zug, Switzerland) for iodixanol cleaning and viral particle concentration. The tubes were first centrifuged at 4000 x *g* at 4°C until all the solution had passed through the column. Two additional washes with 0.001% Pluronic F68 D-PBS were performed and the AAV were finally suspended in 120-150 µL 0.001% Pluronic F68 D-PBS. The viral genome content (vg/mL) for each AAV was assessed by *Taq*Man qPCR with primers recognizing the inverted terminal repeats of the AAV2 viral genome (forward primer: 5'-GGAACCCCTAGTGATGGAGTT-3', reverse primer: 5'-CGGCCTCAGTGAGCGA-3', *Taq*Man probe: 5'- FAM-CACTCCCTCTCTGCGCGCTCG-TAMRA-3') and the KAPA probe fast qPCR universal kit (Sigma-Aldrich, Buchs, Switzerland). AAV vectors were stored at -80°C until use.

Transfection of HEK293T cells

For the transfection experiments (Figures 4.1C, 4.2, 4.3 and S4.7), we plated $5x10^5$ cells per well in six-well plates the day before transfection. We mixed the plasmids in 0.25 M $CaCl_2$ solution and the mixture was then added dropwise to HEPES saline buffer (Sigma-Aldrich, Buchs, Switzerland, CaCl2-H2O:HEPES ratio 1:1). The mixture was incubated at room temperature for five minutes and added dropwise to the cells (10% of the culture volume). The medium was completely replaced 6 hours after transfection. Transfected cells were lysed for DNA and/or RNA extraction at four days post-transfection.

To evaluate the efficiency and/or selectivity of the sgRNAs (Figure 4.1C), HEK293T cells were transfected with 0.5 µg of SIN-cPPT-PGK-GFP-WPRE, 2 µg of SIN-cPPT-PGK-SpCas9-WPRE, and 2 µg of pENTR221 plasmids expressing the sgRNA. The sgRNA expression is under the control of H1 promoter for all sgRNAs but sgHTT4, which expression was driven by the U6 promoter. All sgRNAs present the backbone (tracrRNA) used in Merienne et al., 2017. Cells transfected only with the plasmid encoding SpCas9 and GFP were used as negative control.

To compare HTT exon 1 deletion efficiency between transfected and transduced cells (Figure 4.2), HEK293T cells were transfected with 2 µg of SIN-cPPT-PGK-Cas9-WPRE and 2 µg of SIN plasmids expressing two sgRNAs plus mCherry. All sgRNAs contained the optimized tracrRNA sequence described by Dang et al., 2015 and their expression was driven by the U6

promoter. The expression of mCherry was driven by the PGK promoter. Cells transfected with only SIN plasmids encoding for SpCas9 and GFP were used as negative control.

To compare HTT exon 1 deletion efficiency between the LV-based constitutive and KamiCas9 systems (Figure 4.3), HEK293T cells were transfected with 1.6 ug of SIN-cPPT-PGK-Cas9-WPRE and 1.3 µg of SIN plasmids expressing two (constitutive) or three sgRNAs (KamiCas9) plus mCherry. The sgRNAs targeting the HTT gene contained the optimized tracrRNA sequence described by Dang et al., 2015 and their expression was driven by the U6 promoter. The expression cassette of the sgRNA targeting the LV-SpCas9 (sgCas9) was identical to the one used in Merienne et al., 2017. The expression of mCherry was driven by the PGK promoter. Cells transfected with SIN plasmids encoding for SpCas9 and mCherry with no sgRNAs were used as negative control.

To compare HTT exon 1 deletion efficiency between the AAV-based constitutive and KamiCas9 systems (Figure S4.7), HEK293T cells were transfected with 0.6 ug of pAAV2ss-CBA-GFP-WPRE-bGH, 1.1 ug pAAV2ss-EFS-myc-SV40-spCas9-SV40-synPolyA and 2.1 ug of pAAV2ss plasmids expressing sgHTT8P_L/sgHTT4 (constitutive) or sgHTT8P_L/sgHTT4/sgCas9^{AAV} (KamiCas9) (SpCas9:sgRNA molar ratio of 1:3). The features of the sgRNA expression cassettes were identical to the ones used in the LV-based systems tested in the Figure 4.3. Cells transfected only with pAAV2ss plasmids encoding for SpCas9 and GPF were used as negative control.

Generation of clonal HEK293T cell lines with *HTT* exon 1 deletion

For the clonal analysis of HEK293T cell containing deletion of the exon 1 in the HTT gene (Figures S4.2), 5x10^6 cells in 10 cm dish were transfected 24 hours after seeding with 30 µg of plasmids (15 µg SIN-cPPT-PGK-SpCas9-WPRE and 15 µg SIN-U6-sgHTT8P_L-U6-sgHTT4-PGK-mCherry). Five days post-transfection, the cells were dissociated with trypsin and serial dilutions were plated in 96-well plates. The cell clones that grew at the highest dilution conditions were sequentially expanded in 48-well plates, 24-well plates, and six-well plates. Finally, we screened the clonal cell lines for the presence of exon 1 deletion in the HTT gene by PCR amplification.

Transduction of HEK293T cells

For the transduction experiments in HEK293T cells (Figures 4.1D-E and 4.2), we plated 5x10^5 cells per well in six-well plates the day before transduction. The cells were transduced with 200 ng of LVs (100 ng of SIN-cPPT-PGK-Cas9-WPRE and 100 ng of LV expressing the sgRNAs plus mCherry reporter) diluted in DMEM medium added dropwise to the cells (5% of the culture volume). Cells transduced with LVs encoding for SpCas9 and mCherry with no sgRNAs were used as negative control. The medium was completely replaced 24 hours after transduction.

Transduced cells were then passed once a week and lysed for DNA and RNA extraction at three weeks post-transduction.

Transduction of HD-NPCs

For the transduction experiments in HD-NPCs (Figures 4.4, S4.3 and S4.5), we plated $8x10^5$ cells per well in six-well plates the day before transduction. The cells were transduced with LVs diluted in N2B27 medium added dropwise to the cells (5% of the culture volume). The medium was completely replaced 24 hours after transduction. Transduced cells were then passed once a week and lysed for DNA and RNA extraction at two weeks post-transduction.

To optimize transduction conditions in HD-NPCs (Figure S4.3), cells were transduced with 200, 300 or 400 ng of LVs expressing the SpCas9 or SpCas9-BPNLS with LVs expressing the sgHTT1 (Merienne et al., 2017) in a ratio 1:1. Cells transduced with LVs encoding for SpCas9 and mCherry with no sgRNAs were used as negative control.

To compare HTT exon 1 deletion efficiency between the LV-based constitutive and KamiCas9 systems (Figure 4.4), cells were transduced with 200 ng of LVs expressing the SpCas9-BPNLS and 200 ng of LVs expressing the sgRNA combinations. Cells transduced with LVs encoding for SpCas9 and mCherry with no sgRNAs were used as negative control.

To assess individual editing efficiency of each sgRNA (Figure S4.5), cells were transduced with 200 ng of LVs expressing the SpCas9-BPNLS and 200 ng of LVs expressing each sgRNA. Cells transduced with LVs encoding for SpCas9 and mCherry with no sgRNAs were used as negative control.

Animals

Transgenic mice expressing the full-length human wild-type and mutant *HTT* gene (HU97/18; BACHD+;YAC18++; Hhd-/-) were kindly provided by Prof. Hayden (Vancouver, Canada) (Southwell et al., 2013). Adult male and female transgenic mice (> 9 weeks-old) were used for the *in vivo* experiments. Mice were housed in a specific pathogen-free (SPF) facility with IVC cages GM500 (Tecniplast) or rat R.BTM.U x /R.ICV.6 cages (Innovive, Paris, France) and Innorack rats, simple face (cat# RS.5.8.40) containing corn cob bedding, with no more than five mice per cage. The animals were maintained in a controlled-temperature room (22 ± 1°C), under a 14-hour light/10-hour dark cycle. The following enrichments were provided: 2 pieces of wipes, 1 cardboard tunnel, 1 cardboard or polysulfide house with 2 entrances/exits. Food (SAFE® 150, Safe, Rosenberg, Germany) and water were provided *ad libitum*. All experimental procedures were performed in strict accordance with Swiss regulations concerning the care and use of laboratory animals (veterinary authorizations 3447 and 3682).

Stereotaxic Injections

Anesthesia and surgical procedures were performed as previously described (Merienne et al., 2017). The mice striata was bilaterally injected with 4 µL of AAV2/rh.10 ($1.00 x10^{10}$ vg) per

hemisphere at a rate of 0.5 µL/min at the coordinates +0.8 ; ±1.9 ; -3.3 (+0.8 mm rostral to Bregma; ±1.9 mm lateral to midline; and 3.3 mm ventral from the skull surface, with the tooth bar set at -3.3 mm). The needles were left in place for five minutes after the injection and were then slowly removed. During surgery, body temperature was controlled with a warming blanket (CMA 450 Temperature Controller, Phymep, Paris, France) and the eyes were protected with 0.2% Viscotears liquid gel (Novartis, Basel, Switzerland). Post-surgery analgesic treatment (acetaminophen, Dafalgan Upsa 1000 mg/750 mL) was administered in drinking water for 72 hours.

DNA, RNA, and protein extraction

For *in vitro* experiments, genomic DNA and RNA were extracted with Trizol Reagent (Life Technologies, Zug, Switzerland), according to the manufacturer's instructions. Briefly, the culture medium was removed, and the cells were washed three times with PBS (Gibco, Life Technologies, Zug, Switzerland). The cells were lysed directly in the well with 1 mL of Trizol. The gDNA was precipitated and purified in accordance with the protocol provided by the supplier. The final DNA pellet was then resuspended in nuclease-free water (Gibco, Life Technologies, Zug, Switzerland) by passive homogenization in increasing volumes of water for 24-72 hours at room temperature. For the experiments containing RNA analysis, the RNA was precipitated from the aqueous phase and purified in accordance with the protocol supplied by the supplier. The final RNA pellet was then resuspended in nuclease-free water (Gibco, Life Technologies, Zug, Switzerland) by passive homogenization and then vortexing. Finally, both gDNA and RNA concentrations were determined with a Nanodrop spectrophotometer (Thermo Fisher Scientific, Reinach, Switzerland). The gDNA and RNA were kept at –20°C and –80°C for long-term storage, respectively. In addition, protein was extracted from wild-type and clonal HEK293T cell lines in RIPA buffer (R0278, Sigma) supplemented with a 1/200 dilution of protease inhibitor cocktail (P8340, Sigma-Aldrich, Buchs, Switzerland) and 5 µM Z-VAD-FMK (HY-16658B, Chemie Brunschwig, Basel, Switzerland), hereafter referred to as RIPA$^+$ buffer. Briefly, approximately 1x10^6 cells were washed in PBS and 50 µl of RIPA$^+$ buffer was added to the cell pellet. The pellet was homogenized with a pellet mixer (VWR, Dietikon, Switzerland) and left on ice for 30 minutes. The protein extract was then centrifuge at 18000 x g for 15 minutes at 4°C and the supernatant containing solubilized proteins was collected into a new tube and stored at -80°C.

For *in vivo* experiments, mice were sacrificed by isoflurane overdose and brains were collected and cut into 1 mm-thick coronal slices. We collected 5-6 punch specimens/animal (~ 1.5 mm^3 each) from the GFP-positive striatal area. Genomic DNA was extracted from each individual punch specimen with the AllPrep DNA/RNA/miRNA Universal Kit (Qiagen, Hombrechtikon, Switzerland) according to the manufacturer's recommendations. The gDNA was stored at -20°C.

PCR and TIDE analysis

The editing efficiencies of the sgRNAs targeting *HTT* and SpCas9 were assessed by Tracking of Indels by Decomposition (TIDE) analysis (Brinkman et al., 2014) on Sanger sequencing chromatograms of amplified DNA. The indel size range was set to 10 and the size of the decomposition window was adapted for reads of low quality or containing repetitive sequences. The significance cutoff was set to 0.05 (*htt*ps://tide.nki.nl/). Nucleic acid amplification was performed on 100 ng of gDNA (extracted by Trizol) or 10 ng gDNA (extracted with AllPrep DNA/RNA/miRNA Universal Kit) with the KAPA HiFi Hotstart kit (KAPA Biosystems, Labgene) according to the manufacturer's recommendations. The human HTT gene was amplified with teo sets of PCR primers. The set 1 amplifies a region of 2732 bp containing all sgRNA target sites except the sgHTT25 target site, whereas the set 2 amplifies a region of 2037 bp containing all sgRNA target sites except the sgHTT4 target site. PCR reaction with the primer set 1 consists of the primers 5'-CTCCCAAGAACTGGGAACTAAC-3' (fwd1) and 5'-ACCACCGTGATCATGAACTAAA-3' (rev1), with a melting temperature of 55°C and an extension period of 90 seconds. PCR reaction with the primer set 2 consists of the primers 5'-TCGAACTCCTGACCTCTGGT-3' (fwd2) and 5'-CTGCTGGAAGGACTTGAGGG-3' (rev2), with a melting temperature of 65°C and an extension period of 60 seconds. The LV-SpCas9 transgene was amplified with the primers 5'-AATGGAAGTAGCACGTCTCACTAG-3' and 5'-GTTGATCGGGTTCTCTTCGAAAAG-3', with a melting temperature of 60°C and an extension period of 30 seconds (Merienne et al., 2017). The AAV-SpCas9 transgene was amplified with the primers 5'-TTTTTCGCAACGGGTTTGCC-3' and 5'-AGAAGCTGTCGTCCACCTTG-3', with a melting temperature of 65°C and an extension period of 25 seconds. The primers used to generate Sanger sequencing chromatograms for each sgRNA target site are described in the Table S4.3.

Measurement of HTT exon 1 deletion

For the semiquantification of HTT exon 1 deletion on agarose gel, HTT gene was amplified using the primer set 1. We measured the optical density of the different PCR bands on the agarose gel with fiji software. The optical density of each band was then normalized on the length of the amplicon. Finally, for each sample, the length-normalized optical density of the exon1-deleted amplicon was divided by the sum of length-normalized optical densities of the deleted and non-deleted amplicons.

The quantification of HTT exon 1 deletion using the intronic and FLOX assays was performed by digital PCR in QIAcuity 24-well Nanoplates with 8500 partitions (QIAcuity® digital PCR, Qiagen, Basel, Switzerland). The intronic assay is based on EvaGreen signal of amplified amplicons by the primers 5'-TCGCAGGATGCGAAGAGTTG-3' and 5'-GTTAAAAGAACCCCCGCCCT-3'. The FLOX assay is a Taqman-based assay to detect the amplification of the FLOX sequence in HU97/18 mice using the primers 5'-GCGGGATCCATAACTTCGTA-3' and 5'-ACTCGAAGGCCTTCATCAGC-3' with the probe 5'-

FAM-ATTAATCGAGGTCGACCGCC-BHQ1-3'. EvaGreen-intronic and FAM-FLOX signals were normalized on VIC signals generated by the amplification of the poly(rC)-binding protein 2 (*PCBP2*) gene with the primers 5'-TTGTGTCTCCAGTCTGCTTG-3' and 5'-AGGTGGTGGTGGTGGTA-3' (Christodoulou et al., 2016), and the probe 5'-VIC-CCCTCTCCTGGCTCTAAATGTTGTGT-BHQ1-3'. Two different reactions were set up accordingly to the manufacturer's instructions in a 12 µL volume with 42 ng of gDNA. The reaction amplifying the HTT intronic region contained 4 µL of 3x QIAcuity EvaGreen PCR master mix (Qiagen, Basel, Switzerland), 0.4 µM of each primer, and 3 units of EcoRI-HF restriction enzyme. The second reaction simultaneously amplifying the FLOX sequence and PCBP2 gene contained 3 µL of 4x QIAcuity Probe PCR master mix (Qiagen, Basel, Switzerland), 0.8 µM of each primer, 0.4 µM of each probe, and 3 units of EcoRI-HF restriction enzyme. Loaded plates were incubating 10 minutes at RT for EcoRI-HF digestion followed by DNA amplification: initial denaturation at 95°C for 2min, 40 amplification cycles at 95°C, 60°C and 72°C for 15 sec each, and a final step at 40°C for 5 min. Finally, data analysis was performed with the QIAcuity Software Suite 2.0.20 (Qiagen, Basel, Switzerland).

RNA expression analysis

One thousand nanograms of RNA were first treated with RNase-free DNase (RQ1, Promega, Dubendorf, Switzerland) according to the manufacturer's protocol to remove any trace of genomic DNA and diluted to 20 ng/µL. The cDNA was generated from 200 ng DNase treated-RNA with the Superscript II (Thermo Fisher, Reinach, Switzerland) according to the manufacturer's guidelines. Two sets of primers were used to evaluate HTT mRNA expression. One set was comprised by the primers 5'-AGTGATTGTTGCTATGGAGCGG-3' and 5'-GCTGCTGGTTGGACAGAAACTC-3' (targeting HTT exon 64 and 65, respectively) (Cambon et al., 2017). The other set consists of the primers 5'-CTGCACCGACCAAAGAAAGAAC-3' and 5'-CATAGCGATGCCCAGAAGTTTC-3' (targeting the HTT exon1/2 junction and exon 3, respectively) (Cambon et al., 2017) . As a reference gene quantification analysis, we amplified the peptidylprolyl isomerase B (*PPIB*) gene with the primers 5'-TTCCATCGTGTAATCAAGGACTTC-3' (targeting PPIB exon 3) and 5'-GCTCACCGTAGATGCTCTTTC-3' (targeting PPIB exon 4) (Kirschneck et al., 2017). Real-time quantitative PCR (RT-qPCR) was used to assess HTT expression in the clonal cell lines (Figure S4.2C) with the KAPA SYBR Fast qPCR master mix (Sigma-Aldrich, Buchs, Switzerland) according to the manufacturer's protocol, using the Rotor gene (Qiagen, Basel, Switzerland) and the following cycle parameters: 95°C for 180 seconds, then 40 cycles of 95°C for 3 seconds, 60°C for 10 seconds. Digital PCR in QIAcuity 24-well Nanoplates with 8500 partitions (QIAcuity® digital PCR, Qiagen, Basel, Switzerland) was used to evaluate the impact of indels (Figure 4.1E) on HTT expression in transduced HEK293T cells. Each reaction was set up accordingly to the manufacturer's instructions in a 12 µL volume containing 4µL of 3x QIAcuity EvaGreen PCR

master mix (Qiagen, Basel, Switzerland), 0.4 µM of *HTT* or *PPIB* forward and reverse primers and 40 ng of cDNA. Loaded plates were then subjected to the following temperature cycling: initial denaturation at 95°C for 2min, 40 amplification cycles at 95°C, 60°C and 72°C for 15 sec each, and a final step at 40°C for 5 min. Finally, data analysis was performed with the QIAcuity Software Suite 2.0.20 (Qiagen, Basel, Switzerland).

Virtual western blot

Protein concentration was assessed with a BCA kit (Thermo Fisher Scientific, Reinach, Switzerland) according to the recommended procedure. After dilution in 0.1x SB (ProteinSimple, Bio-Techne), 0.6 µg of total protein extract was size-separated with the Jess capillary-based immunoassay system. Samples were processed according to the manufacturer's instructions, with the 66-440 kDa separation module (SM-W008). The primary anti-huntingtin antibody clone 1HU-4C8 (MAB2166, Zug, Switzerland) (diluted 1/750) and the anti-vinculin antibody clone 3M13 (ZRB1089, Merck, Nottingham, UK) (diluted 1/50) were used to target the HTT and vinculin proteins, respectively. Huntingtin and vinculin were then detected by chemiluminescence with the anti-rabbit-HRP conjugate (043-026, ProteinSimple, Bio-Techne AG, Zug Switzerland) diluted 1/20 in the ready-to-use anti-mouse-HRP conjugate (DM-002, ProteinSimple, Bio-Techne AG, Zug, Switzerland). Compass software (version 6.1) was used for the analysis. Peaks were determined with the gaussian fit method and HTT and vinculin signals were used to calculate the HTT/vinculin ratios.

Bioinformatic analysis

Potential off-target sites were assessed with the Bioconductor package CRISPRseek (Zhu et al., 2014) with a maximum of mismatch set to 4. Off-targets with a score ≥1 was considered as potential off-target sites.

Statistical methods

For the statistical analyses, we tested the hypotheses of normally distributed data and equal variances to determine the most appropriate statistical test. Post-hoc analyses were performed with GraphPad Prism 9.1.0 software. ANOVA was used for comparisons of more than two groups and *t*-tests were used for comparisons between two groups. No specific method was used for sample randomization, sample-size estimation, or data inclusion/exclusion. All results are presented as the mean ± SD. *$p < 0.05$, **$p < 0.01$, ***$p < 0.001$, and ****$p < 0.0001$.

4.1.6. Supplemental information

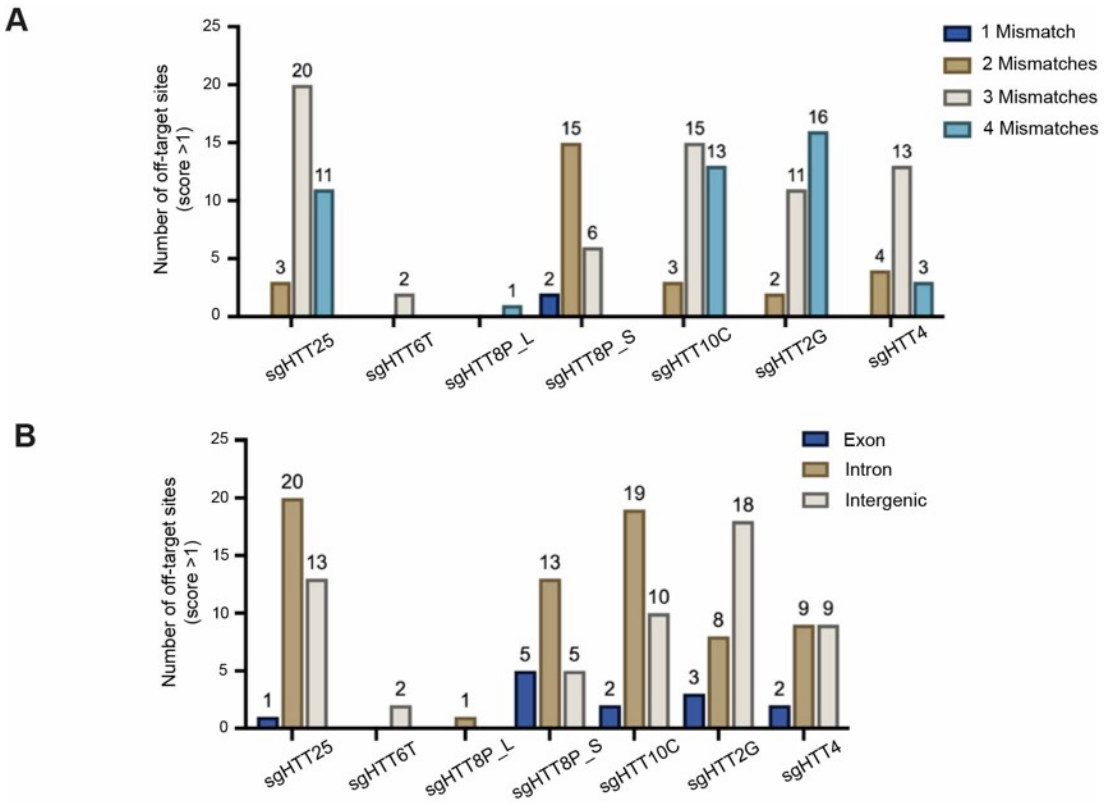

Figure S4.1: Off-target analysis, related to Figure 4.1. (A) Bioinformatic analysis with CRISPRSeek package (Zhu et al., 2014) revealed potential off-target sites for the different sgRNAs. The analysis was conducted by searching for off-target sites with a maximum of 4 mismatches and the threshold for off-target cleavage score was set to 1 (≥ 1, range from 0 to 100). **(B)** Localization of the off-target sites in the human genome.

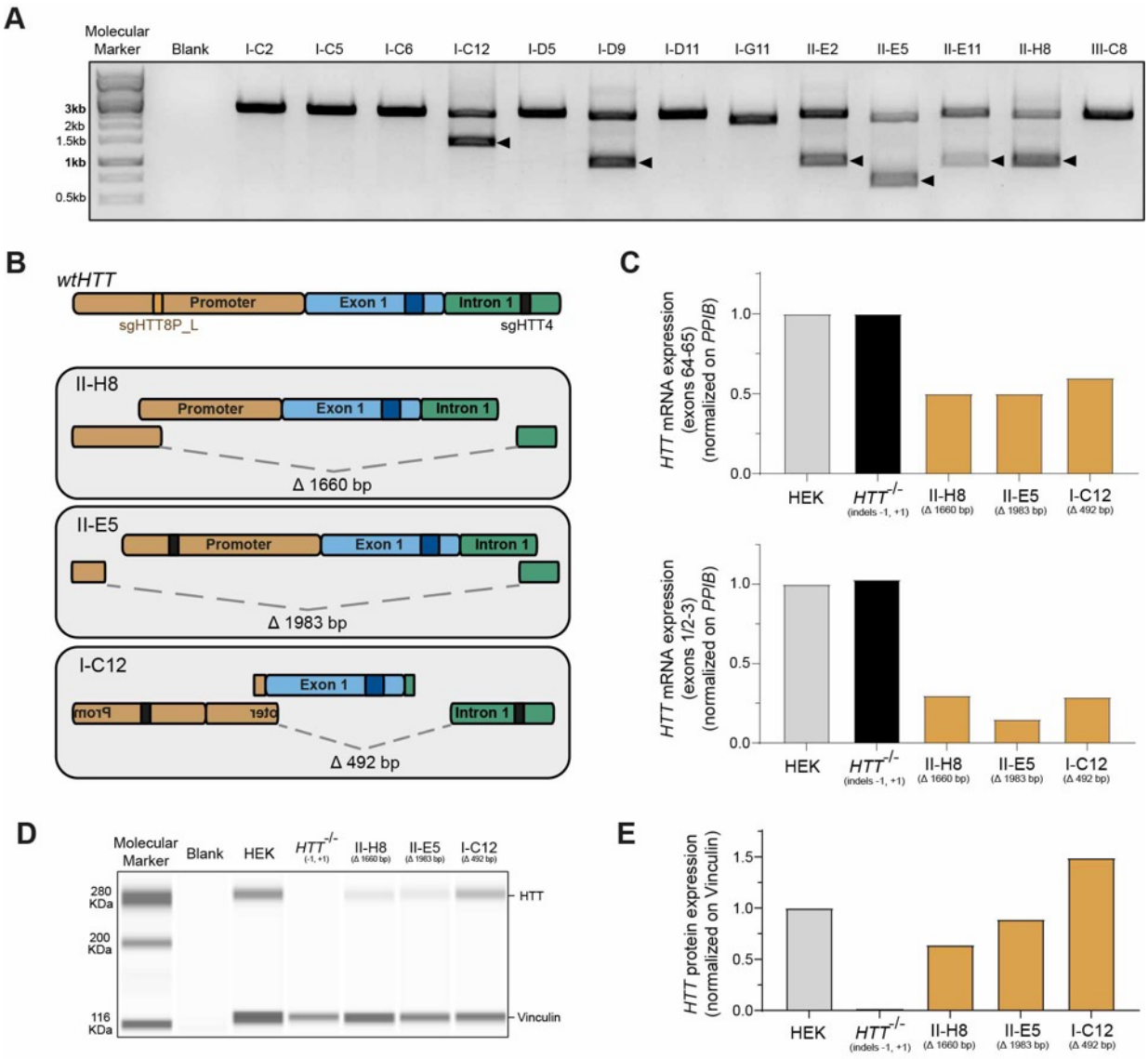

Figure S4.2: Deletion of *HTT* exon 1 in HEK293T clonal cell lines, related to Figure 4.2. Cells were transfected with plasmids encoding for SpCas9 and sgRNA combination (sgHTT8P_L/sgHTT4) and subsequently cloned in individual cell lines by dilution cloning. **(A)** After clone expansion, clonal lines were screened for *HTT* exon 1 deletion using the primer set 1. The upper fragment in the agarose gel results from the amplification of non-deleted *HTT* alleles (2732 bp) whereas lower fragments correspond to the amplification of exon 1-depleted *HTT* alleles. **(B)** Illustration of the predicted rearrangements occurred in the *HTT* alleles depleted of exon 1 based on Sanger sequencing. **(C)** *HTT* expression normalized to *PPIB* expression levels was evaluated by RT-qPCR in the non-treated HEK293T cells, *HTT* knockout clonal cell line carrying indels at the translational start site (Duarte et al., 2023 – in revision) and in the three selected clones II-H8, II-E5 and I-C12 (N=1, n=1). **(D)** Capillary-based immunoassay representative image and **(E)** quantification of HTT protein levels (4C8 antibody). The vinculin antibody was used as an internal standard for the quantitative analysis (N=1, n=1).

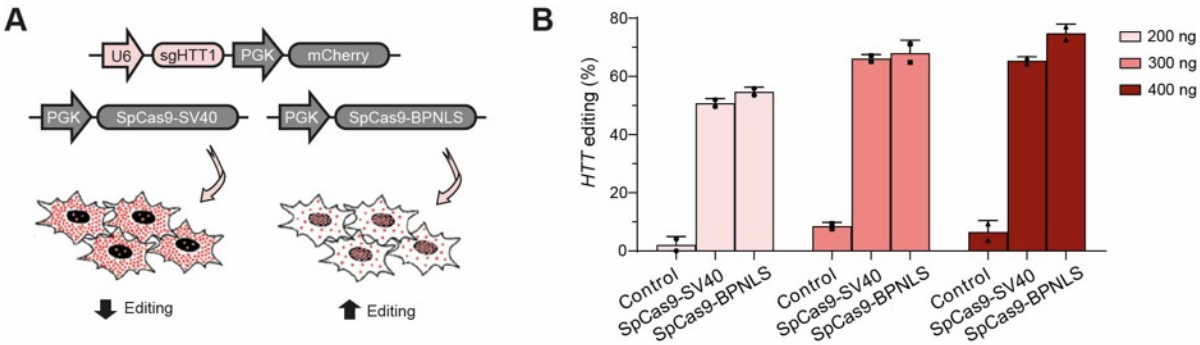

Figure S4.3: Optimization of the conditions for HD-NPCs transduction, related to Figure 4.4. (A) We evaluated whether another SpCas9 variant with improved nuclear localization (SpCas9-BPNLS) could enhance sgHTT1 editing efficiency. This SpCas9-BPNLS variant differs from the original SpCas9 construct (Mali et al., 2013) on the linker and nuclear localization signal (NLS). Original SpCas9 contains a SRAD linker and SV40-NLS whereas SpCas9-BPNLS bears a glycine-serine linker (Zhao et al., 2016) and the bipartite NLS (BPNLS) (Suzuki et al., 2016; Wu et al., 2009). **(B)** Proportion of indels measured by TIDE in transduced neuronal progenitor cells derived from HD patients (HD-NPCs) with different doses of LVs separately encoding for SpCas9 and sgHTT1 in a 1:1 ratio (200 ng, 300 ng or 400 ng) at 2 weeks post-transduction. Results are presented as mean ± SD (N=1, n=2).

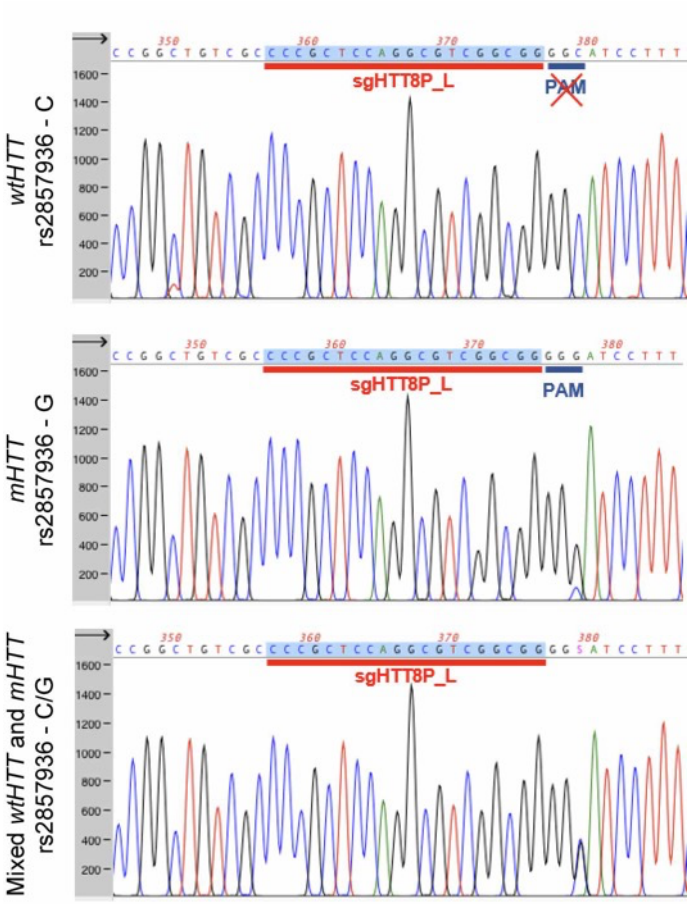

Figure S4.4: Validation of separation of amplicons from *wtHTT* and *mHTT* for analysis of editing efficiency, related to Figure 4.4. Representative chromatograms of the sequencing of wild-type, mutant or both (bulk) *HTT* alleles showing different signals at the SNP rs2857935 site.

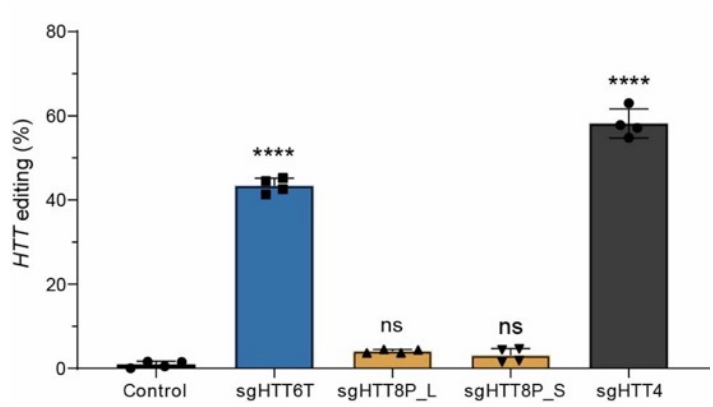

Figure S4.5: Single cut efficiency of the sgHTT6T, sgHTT8P_L, sgHTT8P_S and sgHTT4 in HD-NPCs, related to Figure 4.4. HD-NPCs were transduced with two LVs separately expressing the SpCas9 and the sgRNA targeting *HTT* gene (sgHT6T, sgHTT8P_L, sgHTT8P_S and sgHTT4). Cells transduced with LVs encoding for SpCas9 and mCherry were used as negative control. Gene editing outcomes were analyzed at 2 weeks post-transduction. Results are presented as mean ± SD (N=1, n=4). Statistics: one-way ANOVA and multiple-comparisons to control with Dunnet's correction; **** :p<0.0001.

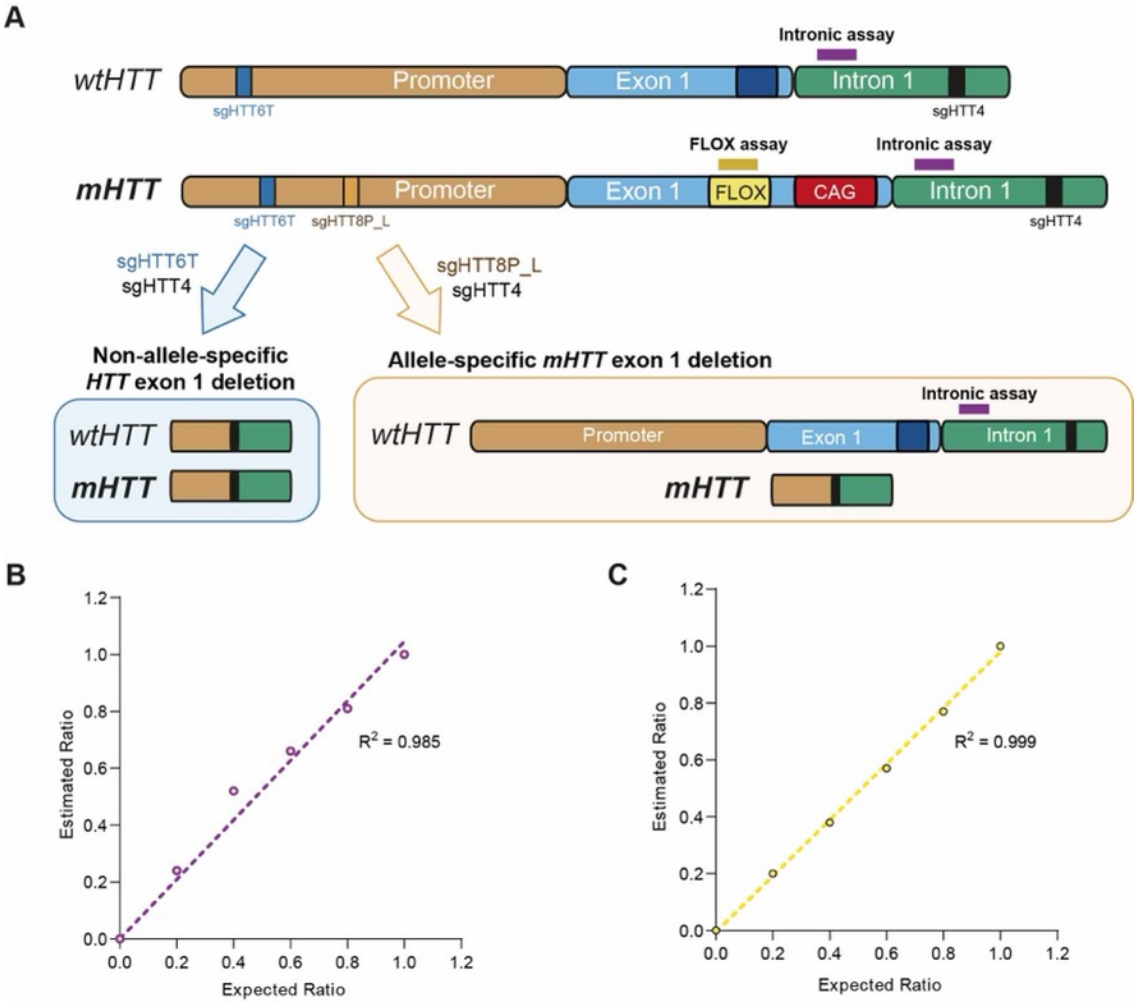

Figure S4.6: Validation of QIAcuity digital PCR-based assays for quantification of *HTT* exon 1 deletion, related to Figures 4.5 and 4.6. (A) Schematic representation of the quantitative assays. The transgenic HU97/18 mice (Southwell et al., 2013) carries 8 copies of the human *HTT* transgenes (4 copies of *mHTT* and 4 copies of *wtHTT*) and no homolog mouse *HTT* gene (Duarte et al., 2023 – in revision). The *mHTT* transgene derived from the BACHD mice (Gray et al., 2008) contains 97 trinucleotide repeats (CAG-CAA) coding for an expanded polyglutamine and a FLOX sequence at the 5'UTR. The *wtHTT* transgene derives from YAC18/18 (Hodgson et al., 1999) and carries 18 CAG repeats. The FLOX assay consists of

a TaqMan-based assay amplifying the sequence FLOX on the *mHTT* transgenes whereas the intronic assay consists of a EvaGreen-based assay amplifying an intronic sequence in both *wtHTT* and *mHTT* transgenes immediately upstream to the *HTT* exon 1. Amplification signals of both FLOX and intronic assays are then normalized to the amplification signals of a TaqMan-based assay targeting the poly(rC)-binding protein 2 (*PCBP2*) gene (Christodoulou et al., 2016). The loss of *PCBP2*-normalized FLOX signals indicate that the exon 1 of the *mHTT* allele has been deleted. An equal loss of *PCBP2*-normalized intronic and FLOX signals indicates deletion in both *mHTT* and *wtHTT* transgenes. In the case of specific *mHTT* exon 1 deletion, the loss of *PCBP2*-normalized FLOX signal is expected to be higher than the loss of signals from the intronic assay. (B-C) Wild-type mice do not carry human *HTT* transgenes but do carry the reference *PCBP2* gene, and therefore it is possible to simulate the loss of the FLOX and human HTT intronic sequences by mixing gDNA from these two strains in different ratios. To validate the two assays, we mixed 20 ng or 30 ng of gDNA from these two mice strains in increasing ratios and observed high correlation between expected and estimated amplification ratios using the **(B)** intronic assay (R^2=0.985) and **(C)** FLOX assay (R^2=0.999). These results validate the use of these assays for the quantification of *HTT* exon 1 deletion.

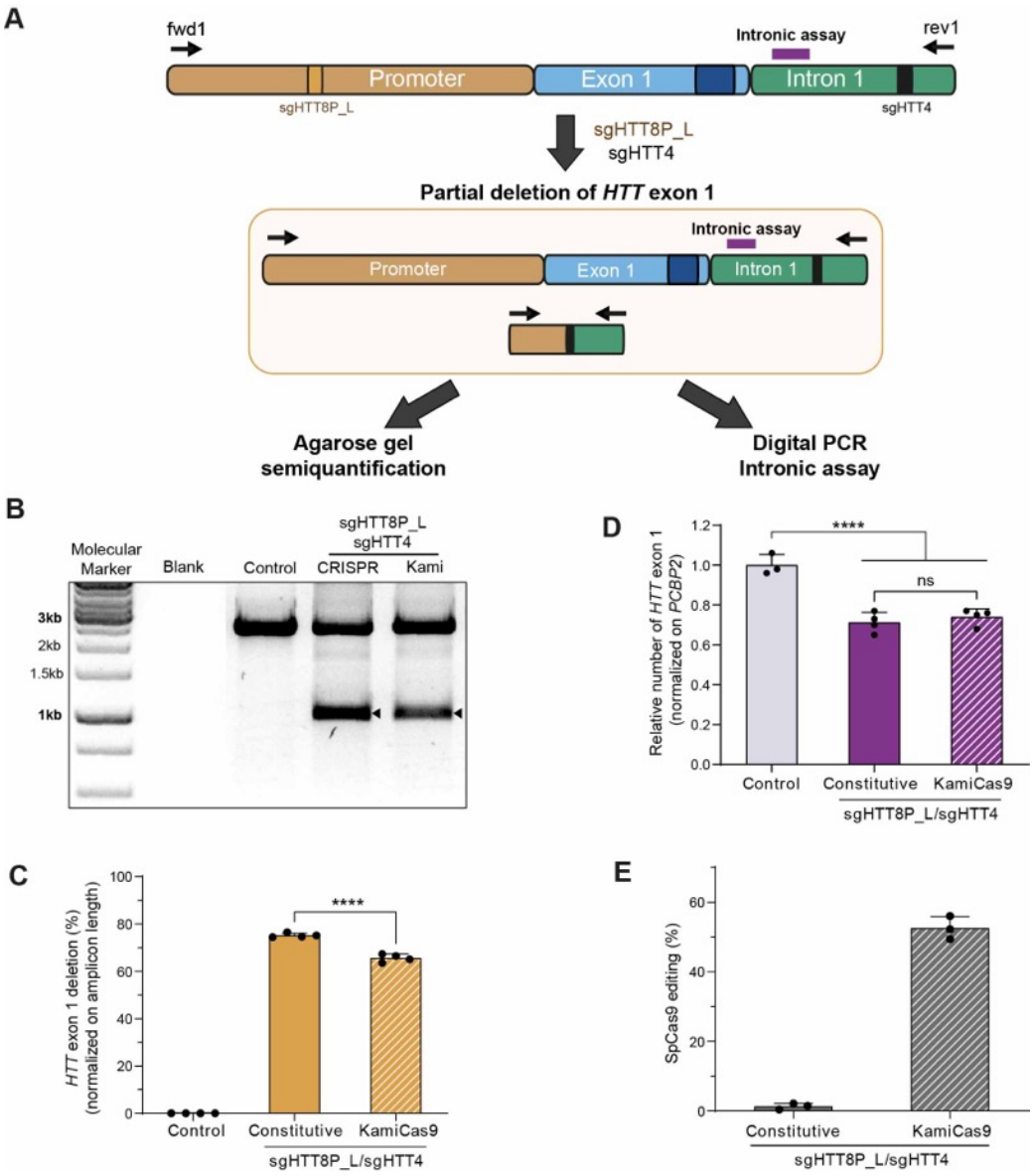

Figure S4.7: Validation of the AAV-KamiCas9 system for *HTT* exon 1 deletion in transfected HEK293T cells, related to Figures 4.5 and 4.6. (A) HEK293T cells were transfected with the AAV-constitutive or KamiCas9 systems (Duarte et al., 2023 – in revision) adapted for *HTT* exon 1 deletion, composed by 3 plasmids separately expressing $SpCas9^{AAV}$, GFP, and sgHTT8P_L/sgHTT4 (constitutive) or sgHTT8P_L/sgHTT4/$sgCas9^{AAV}$ (KamiCas9). At 4 days-post transfection, *HTT* exon 1 deletion was evaluated by gel agarose semiquantitative analysis and by the QIAcuity digital PCR-based intronic assay.

(B) Representative images and **(C)** semiquantitative analysis of the agarose gels after amplification of *HTT* gene using the primer set 1. Results are presented as mean ± SD (N=1, n=4). Statistics: one-way ANOVA and multiple-comparisons between conditions with Tukey's correction; ∗∗∗∗ :p<0.0001. **(D)** Quantification of the relative number of *HTT* exon 1 normalized to the number of *PCBP2* alleles in control and treated samples. Results are presented as mean ± SD (N=1, n=4). Statistics: one-way ANOVA and multiple-comparisons between conditions with Tukey's correction; ∗∗ :p<0.01. **(E)** Editing efficiency of the sgCas9^{AAV} quantified by TIDE. Results are presented as mean ± SD (N=1, n=3).

Table S4.1: List of sgRNAs ordered as gene strands and cloned into pENTR221 plasmids.

sgRNA name	Gene strand sequence
sgHTT25A	GTTCTGTATGAGACCACAGATCTGACAGCAGAGAAACAGCTGTGTTTTAGAGCTAGAAATAGCAA GTTAAAATAAGGCTAGTCCGTTATCAACTTGAAAAAGTGGCACCGAGTCGGTGCTTTTTTAGATCG GATCCAAGCTTCCAGGCTAGTCCGTTATCAACTTGAAAAAGTGGCACCGAGTCGGTGCTTTTTTAG ATCGGATCCAAGCTTCCA
sgHTT25G (mismatch)	GTTCTGTATGAGACCACAGATCTGACAGCAGAGAAACAGCCGTGTTTTAGAGCTAGAAATAGCAA GTTAAAATAAGGCTAGTCCGTTATCAACTTGAAAAAGTGGCACCGAGTCGGTGCTTTTTTAGATCG GATCCAAGCTTCCAGGCTAGTCCGTTATCAACTTGAAAAAGTGGCACCGAGTCGGTGCTTTTTTAG ATCGGATCCAAGCTTCCA
sgHTT6T	ACAAGATCTCAGGGCTGTCCGGGTGAGTAGTTTCAGAGCTATGCTGGAAACAGCATAGCAAGTTG AAATAAGGCTAGTCCGTTATCAACTTGAAAAAGTGGCACCGAGTCGGTGCTTTTTTAGATCGGATC CAAGCTTACATAGTCCGTTATCAACTTGAAAAAGTGGCACCGAGTCGGTGCTTTTTTAGATCGGAT CCAAGCTTACA
sgHTT6C (mismatch)	ACAAGATCTCAGGGCTGTCCGGGTGAGCAGTTTCAGAGCTATGCTGGAAACAGCATAGCAAGTTG AAATAAGGCTAGTCCGTTATCAACTTGAAAAAGTGGCACCGAGTCGGTGCTTTTTTAGATCGGATC CAAGCTTACATAGTCCGTTATCAACTTGAAAAAGTGGCACCGAGTCGGTGCTTTTTTAGATCGGAT CCAAGCTTAC
sgHTT10C	GTTCTGTATGAGACCACAGATCTGGGGCTCAACGGAGAGGGGAGTTTTGAGCTAGAAATAGCAAG TTAAAATAAGGCTAGTCCGTTATCAACTTGAAAAAGTGGCACCGAGTCGGTGCTTTTTTAGATCGG ATCCAAGCTCCAGGCTAGTCCGTTATCAACTTGAAAAAGTGGCACCGAGTCGGTGCTTTTTTAGAT CGGATCCAAGCTTCCA
sgHTT10G (mismatch)	GTTCTGTATGAGACCACAGATCTGGGGCTCAACGGAGAGCGGAGTTTTAGAGCTAGAAATAGCAA GTTAAAATAAGGCTAGTCCGTTATCAACTTGAAAAAGTGGCACCGAGTCGGTGCTTTTTTAGATCG GATCCAAGCTTCCAGGCTAGTCCGTTATCAACTTGAAAAAGTGGCACCGAGTCGGTGCTTTTTTAG ATCGGATCCAAGCTTCCA
sgHTT2G	GTTCTGTATGAGACCACAGATCTACCCGTCCCGGCAGCCCCCAGTTTTAGAGCTAGAAATAGCAA GTTAAATAAGGCTAGTCCGTTATCAACTTGAAAAAGTGGCACCGAGTCGGTGCTTTTTTAGATCGG ATCCAAGCTTCCAGGCTAGTCCGTTATCAACTTGAAAAAGTGGCACCGAGTCGGTGCTTTTTTAGA TCGGATCCAAGCTTCCA
sgHTT2A (mismatch)	GTTCTGTATGAGACCACAGATCTACTCGTCCCGGCAGCCCCCAGTTTTAGAGCTAGAAATAGCAA GTTAAAATAAGGCTAGTCCGTTATCAACTTGAAAAAGTGGCACCGAGTCGGTGCTTTTTTAGATCG GATCCAAGCTTCCAGGCTAGTCCGTTATCAACTTGAAAAAGTGGCACCGAGTCGGTGCTTTTTTAG ATCGGATCCAAGCTTCCA
sgHTT4	GGACTATCATATGCTTACCGTAACTTGAAAGTATTTCGATTTCTTGGGTTTATATATCTTGTGGAAA GGACGAAACACCGTGGATGACATAATGCTTTGTTTTAGAGCTAGAAATAGCAAGTTAAAATAAGGC TAGTCCGTTATCAACTTGAAAAAGTGGCACCGAGTCGGTGCTTTTTTCATAGCCATGGGCGGCCG CTCTAGACACCGTGGATGACATAATGCTTTGTTTTAGAGCTAGAAATAGCAAGTTAAAATAAGGCT AGTCCGTTATCAACTTGAAAAAGTGGCACCGAGTCGGTGCTTTTTTCATAGCCATGGGCGGCCGC TCTAGA

Table S4.2: List of sgRNAs ordered as oligonucleotides and cloned into pMK entry plasmids. The generated overhangs after oligonucleotide annealing are underlined. In some sgRNA, an extra guanine was added at the 5' to facilitate U6-driven expression. The enzymes used for the cloning of the annealed oligos and position of the cassette in the universal pMK entry plasmid are indicated in the second column.

sgRNA name	Enzyme # cassette	Forward oligo (5' – 3')	Reverse oligo (5' – 3')
sgHTT6T	BsaI #1	CACC**G**CAGGGCTGTCCGGGTGAGTA	AAACTACTCACCCGGACAGCCCTG**C**
sgHTT6C (mismatch)	BsaI #1	CACC**G**CAGGGCTGTCCGGGTGAGCA	AAACTGCTCACCCGGACAGCCCTG**C**
sgHTT8P_L	BsaI #1	CACCGCCCCGCTCCAGGCGTCGGCGG	AAACCCGCCGACGCCTGGAGCGGGGC
sgHTT8P_S	BsaI #1	CACCGCTCCAGGCGTCGGCGG	AAACCCGCCGACGCCTGGAGC
sgHTT2G	BsaI #1	CACCGTGGGGGCTGCCGGGACGGGT	AAACACCCGTCCCGGCAGCCCCCAC
sgHTT4	SapI #2	ACCGTGGATGACATAATGCTTTT	AACAAAAGCATTATGTCATCCAC
sgCas9	BsmBI #3	CCTCAATGGAGTACTTCTTGTCCA	AAACTGGACAAGAAGTACTCCATT
sgCas9^{AAV}	BsmBI #3	CCTCGTCGCCGAAGAAAAAGCGCA	AAACTGCGCTTTTTCTTCGGCGAC

Table S4.3: List of primers used for Sanger sequencing and respective targeted sequencing sites.

sgRNA target site	Amplification primer set	Sequencing primer	Primer sequence (5' – 3')
sgHTT25	Set 2 (fwd2/rev2)	HTT25_seq / fwd2	TCGAACTCCTGACCTCTGGT
sgHTT6 sgHTT8P_L sgHTT8P_S	Set 1 (fwd1/rev1)	HTT6/8_seq	GACTGCATGGTAAGGGAGGC
sgHTT10	Set 1 (fwd1/rev1)	HTT10_seq	GCCCCCACGGCGCCTTGCGTCC
sgHTT2	Set 1 (fwd1/rev1)	HTT2_seq	TGCTGCTGGAAGGACTTGAG
sgHTT1	Set 1 (fwd1/rev1)	HTT1_seq	GCCTGTCCTGAATTCACCGA
sgHTT4	Set 1 (fwd1/rev1)	HTT4_seq	TTGCTGTGTGAGGCAGAACCTGCGG

CHAPTER 5

Conclusions and Future Perspectives

5. Conclusions and Future Perspectives

Facilitating quantification of AAV transduction in the brain

Gene therapy represents a great window of opportunity for the treatment of CNS disorders. One obstacle to the development of CNS gene therapies is the lack of automated workflows to facilitate evaluation of transduction efficiency in the brain. Single-cell RNA sequencing (scRNA-seq) has been used to estimate transduction efficiency *in vivo* (Brown et al., 2021; Davidsson et al., 2019; Maturana et al., 2021). However, this methodology is expensive and it usually evaluates transduction efficiency on a brain subregion rather than in the whole brain tissue. The current approaches to evaluate transduction efficiency at the whole-brain level mainly rely on the quantification of the proportion of fluorescent cells on brain images upon delivery of a reporter transgene (Chan et al., 2017; Deverman et al., 2016; Hanlon et al., 2019; Smith et al., 2021). These methods require the manual parcellation of each brain region, which can be time-consuming. Semi-automatic co-registration of brain images to reference atlas has been used to speed evaluation of drug distribution across multiple brain areas (Lopes et al., 2022; Salinas et al., 2018). However, transduction efficiency cannot be deduced from distribution analysis due to differences in the cell density and composition among different brain regions. In here we explored 3D and 2D semi-automated pipelines to facilitate the quantification of the number of transduced cells in multiple brain areas. We cross-validated the 3D and 2D quantitative workflows by demonstrating that both approaches yielded similar numbers of transduced cells. We then integrated information regarding cellular density and composition from the Blue Brain Cell Atlas (Erö et al., 2018) to calculate the proportion of transduced cells in each brain region. Finally, we showed that the proportion of transduced cells accurately predicted the extent of *HTT* inactivation. In summary, the quantitative workflows here presented represent valuable tools to assess AAV transduction efficiency across multiple brain regions and can be used to estimate therapeutic potential of CNS gene therapies.

Nevertheless, we observed that quantification of fluorescent cells using the 3D workflow is more challenging in deep brain structures due to the lower resolution of LSFM-acquired 3D images. The use of microscopy techniques avoiding light scattering throughout the tissue to allow the capture of high-resolution images of deeper brain structures (Zhang et al., 2021) should be used in future applications to improve 3D-based quantification. In addition, the use of nuclear reporters will simplify detection of fluorescent cells by preventing interference signals from neuropil. Recently, a study evaluating liver transduction observed that the number of fluorescent hepatocytes was 4-fold lower than the number of hepatocytes carrying AAV-induced genome modifications (Lang et al., 2019). The authors reasoned that the quantification of fluorescent cells underestimates the absolute number of transduced cells because cells transiently expressing the reporter transgene and/or cells expressing low levels of the transgene are often below the

detection fluorescence threshold. Given the much more limited cellular turnover in the brain compared to the liver (Heinke et al., 2022), it is unlikely that transduced cells would escape fluorescence detection due to dilution of transgene expression during cell division. Contrary, we cannot discard the possibility that our quantitative workflows may fail to capture some transduced cells with lower reporter transgene expression. Nonetheless, the high correlation between the frequency of *HTT* editing events and proportion of fluorescent cells suggests that our fluorescence-based workflows accurately quantified the number of transduced cells. Altogether, this data suggests that the use of fluorescent reporters to estimate transduction efficiency can accurately quantify the number of transduced cells with low turnover capacity, but it might underestimate the number of transduced cells in replicative cells.

Efficient KamiCas9-mediated *HTT* inactivation in the cortico-striatal neuronal circuitry affected in HD

Among the therapeutic strategies aiming at lowering *mHTT*, gene editing using the CRISPR/Cas9 system offers the possibility to permanently inactivate the *HTT* gene. We and others have successfully used the CRISPR/Cas9 system to inactivate the *HTT* gene in the striatum of HD models (Ekman et al., 2019; Merienne et al., 2017; Monteys et al., 2017; Oikemus et al., 2022; Yan et al., 2023; Yang et al., 2017) resulting in the improvement of HD motor-like symptoms and lifespan. Despite these promising results, it still unknown whether the exclusive treatment of the striatum will be sufficient to induce therapeutic benefit in HD patients as cortical neurons are also highly affected at early stages of the disease (Aylward et al., 2013; Johnson et al., 2021). The targeting of both striatal and cortical neurons will likely improve therapeutic benefit. Nevertheless, the targeting of multiple brain regions is challenging. Yan and colleagues recently demonstrated that the intravenous administration of an AAV2/9 expressing two sgRNAs targeting the exon 1 of the human *mHTT* transgene reduced HTT protein levels in several brain areas in a KI minipig HD model (Yan et al., 2023). However, such results were achieved with the injection of high doses of AAVs in neonatal piglets before the full establishment of the BBB. While this strategy may be compatible with the treatment of newborn HD carriers, its application at adult stages will be limited by the diminished brain transduction due to difficulties to transpose the BBB. Moreover, high systemic AAV doses increase the risk for potential toxic effects in peripheral tissues, especially in the liver. Therefore, despite its invasiveness, intracranial delivery is still the most efficient administration route to transduce brain cells. Nonetheless, a drawback of this delivery method is that it usually restricts transgene expression to the injected areas. To maximize therapeutic efficacy for HD, we reasoned to combine the retrograde transport properties of the AAV2.retro (Tervo et al., 2016) with the broad striatal diffusion of the AAV2/rh.10 (Cearley & Wolfe, 2006; Gao et al., 2004) to simultaneously inactivate the *HTT* gene in both CPNs and SPNs upon intrastriatal injection. Additionally, *HTT* inactivation in the striatum has been previously

achieved by constitutively expressing the Cas9 nuclease (Ekman et al., 2019; Monteys et al., 2017; Oikemus et al., 2022; Yan et al., 2023; Yang et al., 2017), increasing the likelihood for the occurrence of off-target events and immunogenic responses. Here, we show that the transient AAV-KamiCas9 system simultaneously delivered by the AAV2/rh.10 and AAV2.retro efficiently inactivates the *HTT* gene in both striatal and cortical neurons. In summary, we propose a safer gene editing strategy based on the transient SpCas9 expression maximized to inactivate the *HTT* gene in the corticostriatal network affected in HD.

Despite the complexity of the approach (based on 6 AAVs), our results suggest that the *HTT* gene was successfully edited in nearly all transduced cells. This is in agreement with a recent report demonstrating that multiple AAV vectors expressing for different transgenes can efficiently co-express in the same cells in the brain (Maturana et al., 2021). Nevertheless, we acknowledge that the simplification of this strategy to fewer AAV components would likely improve cell targeting and facilitate clinical translation. The use of smaller orthologue Cas9 nucleases would allow the package of both nuclease and sgRNAs in the same vector. In addition, the development of new AAV variants with combined diffusion and retrograde transport properties will allow the efficient targeting of both SPNs and CPNs using a single AAV serotype. Recently, Lin and colleagues developed the AAV2/9-retro, which can retrogradely transduce projection neurons with an efficiency comparable to AAV2.retro while retaining AAV2/9 diffusion properties (Lin et al., 2020). This new AAV variant could be a valuable alternative for the maximal targeting of the corticostriatal network affected in HD.

Limited *in vivo* efficiency to selectively inactivate *mHTT* through exon 1 deletion

The potential deleterious effects of reducing both wtHTT and mHTT are still not fully elucidated in the context of the disease. Therefore, alternative strategies are under development to specifically inactivate the *mHTT* allele by targeting SNPs associated to the expanded CAG. One of the approaches consists of the specific excision of the *mHTT* exon 1 (Fang et al., 2023; Monteys et al., 2017; Shin et al., 2016, 2022a). Nevertheless, these studies reporting *mHTT* exon 1 deletion *in vitro* and *in vivo* HD models have merely relied on the amplification of exon 1-deleted *mHTT* alleles to demonstrate strategy feasibility, without providing any absolute quantitative measures. Likewise, similar dual sgRNA deletion strategies have been proposed for other CNS disorders with no reports available regarding their efficiency (Piao et al., 2022). Given the ultimate goal for clinical application, it is critical to accurately assess the efficacy of these dual sgRNA-based strategies to determine therapeutic potential. Therefore, here we developed digital PCR-based assays to accurately quantify the frequency of *HTT* exon 1 deletion events. We observed that deletion events were frequent *in vitro*, but extremely rare in the striatum of HU97/18 (less than 5% in the transduced areas) and HU18/18 mice (data not shown). These results are supported by other two studies in SCA1 and DMD mouse models, which demonstrated that most of the gene editing outcomes induced by dual sgRNA-based approaches *in vivo* do not

correspond to the intended deletions. Additionally, the clinical trial testing a pair of sgRNAs to remove or invert the IVS26 mutation in the *CEP290* gene for the treatment of LCA10 has recently paused enrollment due to disappointing efficacy. In summary, our results do not support the application of dual sgRNA-based deletion strategies for the *in vivo* treatment of HD and other CNS disorders. In addition, we highlight that the current methodologies based on agarose gel analysis of PCR amplicons containing the intended modifications greatly overestimate the frequency of such gene editing events. For instance, Yan and colleagues recently reported the Cas9-mediated replacement of expanded CAG repeats in a KI minipig HD model (Yan et al., 2023). However, this claim was solely based on the positive amplification of the expected replaced fragment. Moreover, not only HTT alleles containing the corrected number of CAG repeats were poorly amplified beforehand indicating poor efficiency, but also only 15-20% of the cloned PCR fragments contained the intended modification. Overall, we pretend to encourage the scientific community to adopt more quantitative methods when analyzing such complex gene editing events to avoid misleading conclusions concerning the applicability of such therapeutic strategies *in vivo*.

An alternative CRISPR/Cas9-mediated strategy to selectively silence the *mHTT* allele is the specific degradation of the *mHTT* transcript by NMD (Oikemus et al., 2022; Shin et al., 2022c). Contrarily to deletion strategies, NMD-mediated approaches require only one sgRNA targeting the exonic sequences of *mHTT* allele to induce frameshift mutations which generate downstream premature stop codons. Nonetheless, a disadvantage of NMD-based strategies compared to exon 1 deletion strategies is non-targeting of the short transcript *HTT1α,* which is translated into highly toxic exon 1 mHTT truncated forms (Neueder et al., 2017; Sathasivam et al., 2013). Oikemus and coworkers selected the PAS rs362331 to demonstrate *mHTT* allele-specific NMD in HU97/18 mice (Oikemus et al., 2022) based on previous estimations of patient eligibility provided by Pfister et al. (40-46%) (Pfister et al., 2009). In contrast, Shin and colleagues estimated that 1,3% and 20,4% of European HD subjects are eligible for allele-specific NMD-mediated strategies targeting of the PAS rs362331 and rs363099, respectively (Shin et al., 2022c). Both studies provided important proof-of-concept insights regarding the applicability of allele-specific NMD-mediated approaches for HD. However, the inconsistent estimation of the proportion of HD patients eligible for strategies targeting the variant rs362331 highlight the urgent need to generate a consensus regarding patient eligibility for allele-specific strategies.

6. References

Albin, R. L., Reiner, A., Anderson, K. D., Dure, L. S., Handelin, B., Balfour, R., Whetsell, W. O., Penney, J. B., & Young, A. B. (1992). Preferential loss of striato-external pallidal projection neurons in presymptomatic Huntington's disease. *Annals of Neurology*, *31*(4), 425–430. https://doi.org/10.1002/ANA.410310412

Ambrose, C. M., Duyao, M. P., Barnes, G., Bates, G. P., Lin, C. S., Srinidhi, J., Baxendale, S., Hummerich, H., Lehrach, H., Altherr, M., Wasmuth, J., Buckler, A., Church, D., Housman, D., Berks, M., Micklem, G., Durbin, R., Dodge, A., Read, A., … MacDonald, M. E. (1994). Structure and expression of the Huntington's disease gene: Evidence against simple inactivation due to an expanded CAG repeat. *Somatic Cell and Molecular Genetics 1994 20:1*, *20*(1), 27–38. https://doi.org/10.1007/BF02257483

Andrew, S. E., Goldberg, Y. P., Kremer, B., Telenius, H., Theilmann, J., Adam, S., Starr, E., Squitieri, F., Lin, B., Kalchman, M. A., Graham, R. K., & Hayden, M. R. (1993). The relationship between trinucleotide (CAG) repeat length and clinical features of Huntington's disease. *Nature Genetics 1993 4:4*, *4*(4), 398–403. https://doi.org/10.1038/ng0893-398

Arrasate, M., Mitra, S., Schweitzer, E. S., Segal, M. R., & Finkbeiner, S. (2004). Inclusion body formation reduces levels of mutant huntingtin and the risk of neuronal death. *Nature 2004 431:7010*, *431*(7010), 805–810. https://doi.org/10.1038/nature02998

Arteaga-Bracho, E. E., Gulinello, M., Winchester, M. L., Pichamoorthy, N., Petronglo, J. R., Zambrano, A. D., Inocencio, J., De Jesus, C. D., Louie, J. O., Gokhan, S., Mehler, M. F., & Molero, A. E. (2016). Postnatal and adult consequences of loss of huntingtin during development: Implications for Huntington's disease. *Neurobiology of Disease*, *96*, 144–155. https://doi.org/10.1016/J.NBD.2016.09.006

Assous, M., & Tepper, J. M. (2019). Excitatory extrinsic afferents to striatal interneurons and interactions with striatal microcircuitry. *Eur J Neurosci*, *49*(5), 593–603. https://doi.org/https://doi.org/10.1111/ejn.13881

Atwal, R. S., Xia, J., Pinchev, D., Taylor, J., Epand, R. M., & Truant, R. (2007). Huntingtin has a membrane association signal that can modulate huntingtin aggregation, nuclear entry and toxicity. *Human Molecular Genetics*, *16*(21), 2600–2615. https://doi.org/10.1093/HMG/DDM217

Auerbach, W., Hurlbert, M. S., Hilditch-Maguire, P., Wadghiri, Y. Z., Wheeler, V. C., Cohen, S. I., Joyner, A. L., MacDonald, M. E., & Turnbull, D. H. (2001). The HD mutation causes progressive lethal neurological disease in mice expressing reduced levels of huntingtin. *Human Molecular Genetics*, *10*(22), 2515–2523. https://doi.org/10.1093/HMG/10.22.2515

Aylward, E. H., Harrington, D. L., Mills, J. A., Nopoulos, P. C., Ross, C. A., Long, J. D., Liu, D., Westervelt, H. K., Paulsen, J. S., Cross, S., Ryan, P., Epping, E. A., Chiu, E., Preston, J., Goh, A., Antonopoulos, S., Loi, S., Raymond, L., Decolongon, J., … Wyse, R. (2013). Regional Atrophy Associated with Cognitive and Motor Function in Prodromal Huntington Disease. *Journal of Huntington's Disease*, *2*(4), 477–489. https://doi.org/10.3233/JHD-130076

Aylward, E. H., Nopoulos, P. C., Ross, C. A., Langbehn, D. R., Pierson, R. K., Mills, J. A., Johnson, H. J., Magnotta, V. A., Juhl, A. R., & Paulsen, J. S. (2011). Longitudinal change in regional brain volumes in prodromal Huntington disease. *Journal of Neurology, Neurosurgery & Psychiatry*, *82*(4), 405–410. https://doi.org/10.1136/JNNP.2010.208264

Bachoud-Lévi, A. C., Ferreira, J., Massart, R., Youssov, K., Rosser, A., Busse, M., Craufurd, D., Reilmann, R., De Michele, G., Rae, D., Squitieri, F., Seppi, K., Perrine, C., Scherer-Gagou, C., Audrey, O., Verny, C., & Burgunder, J. M. (2019). International guidelines for the treatment of Huntington's disease. *Frontiers in Neurology*, *10*(JUL), 710. https://doi.org/10.3389/FNEUR.2019.00710/BIBTEX

Bakels, H. S., Roos, R. A. C., van Roon-Mom, W. M. C., & de Bot, S. T. (2022). Juvenile-Onset Huntington Disease Pathophysiology and Neurodevelopment: A Review. *Movement Disorders*, *37*(1), 16–24. https://doi.org/10.1002/MDS.28823

Baldo, B., Sajjad, M. U., Cheong, R. Y., Bigarreau, J., Vijayvargia, R., McLean, C., Perrier, A. L., Seong, I. S., Halliday, G., Petersén, Å., & Kirik, D. (2018). Quantification of Total and Mutant Huntingtin Protein Levels in Biospecimens Using a Novel alphaLISA Assay. *ENeuro*, *5*(4). https://doi.org/10.1523/ENEURO.0234-18.2018

Bañez-Coronel, M., Ayhan, F., Tarabochia, A. D., Zu, T., Perez, B. A., Tusi, S. K., Pletnikova, O., Borchelt,

D. R., Ross, C. A., Margolis, R. L., Yachnis, A. T., Troncoso, J. C., & Ranum, L. P. W. (2015). RAN Translation in Huntington Disease. *Neuron*, *88*(4), 667–677. https://doi.org/10.1016/J.NEURON.2015.10.038

Bankhead, P., Loughrey, M. B., Fernández, J. A., Dombrowski, Y., McArt, D. G., Dunne, P. D., McQuaid, S., Gray, R. T., Murray, L. J., Coleman, H. G., James, J. A., Salto-Tellez, M., & Hamilton, P. W. (2017). QuPath: Open source software for digital pathology image analysis. *Scientific Reports*, *7*(1), 1–7. https://doi.org/https://doi.org/10.1038/s41598-017-17204-5

Barnat, M., Le Friec, J., Benstaali, C., & Humbert, S. (2017). Huntingtin-Mediated Multipolar-Bipolar Transition of Newborn Cortical Neurons Is Critical for Their Postnatal Neuronal Morphology. *Neuron*, *93*(1), 99–114. https://doi.org/10.1016/J.NEURON.2016.11.035

Bates, G. P., Dorsey, R., Gusella, J. F., Hayden, M. R., Kay, C., Leavitt, B. R., Nance, M., Ross, C. A., Scahill, R. I., Wetzel, R., Wild, E. J., & Tabrizi, S. J. (2015). Huntington disease. *Nature Reviews Disease Primers 2015 1:1*, *1*(1), 1–21. https://doi.org/10.1038/nrdp.2015.5

Bates, G. P., MacDonald, M. E., Baxendale, S., Youngman, S., Lin, C., Whaley, W. L., Wasmuth, J. J., Gusella, J. F., & Lehrach, H. (1991). Defined physical limits of the Huntington disease gene candidate region. *American Journal of Human Genetics*, *49*(1), 7. /pmc/articles/PMC1683226/?report=abstract

Baxa, M., Hruska-Plochan, M., Juhas, S., Vodicka, P., Pavlok, A., Juhasova, J., Miyanohara, A., Nejime, T., Klima, J., Macakova, M., Marsala, S., Weiss, A., Kubickova, S., Musilova, P., Vrtel, R., Sontag, E. M., Thompson, L. M., Schier, J., Hansikova, H., … Motlik, J. (2013). A Transgenic Minipig Model of Huntington's Disease. *Journal of Huntington's Disease*, *2*(1), 47–68. https://doi.org/10.3233/JHD-130001

Becher, M. W., Kotzuk, J. A., Sharp, A. H., Davies, S. W., Bates, G. P., Price, D. L., & Ross, C. A. (1998). Intranuclear Neuronal Inclusions in Huntington's Disease and Dentatorubral and Pallidoluysian Atrophy: Correlation between the Density of Inclusions andIT15CAG Triplet Repeat Length. *Neurobiology of Disease*, *4*(6), 387–397. https://doi.org/10.1006/NBDI.1998.0168

Benchoua, A., Trioulier, Y., Zala, D., Gaillard, M. C., Lefort, N., Dufour, N., Saudou, F., Elalouf, J. M., Hirsch, E., Hantraye, P., Déglon, N., & Brouillet, E. (2006). Involvement of mitochondrial complex II defects in neuronal death produced by N-terminus fragment of mutated huntingtin. *Molecular Biology of the Cell*, *17*(4), 1652–1663. https://doi.org/10.1091/MBC.E05-07-0607/ASSET/IMAGES/LARGE/ZMK0040675920007.JPEG

Benraiss, A., Wang, S., Herrlinger, S., Li, X., Chandler-Militello, D., Mauceri, J., Burm, H. B., Toner, M., Osipovitch, M., Jim Xu, Q., Ding, F., Wang, F., Kang, N., Kang, J., Curtin, P. C., Brunner, D., Windrem, M. S., Munoz-Sanjuan, I., Nedergaard, M., & Goldman, S. A. (2016). Human glia can both induce and rescue aspects of disease phenotype in Huntington disease. *Nature Communications 2016 7:1*, *7*(1), 1–13. https://doi.org/10.1038/ncomms11758

Bertoglio, D., Verhaeghe, J., Miranda, A., Wyffels, L., Stroobants, S., Mrzljak, L., Khetarpal, V., Skinbjerg, M., Liu, L., Dominguez, C., Munoz-Sanjuan, I., Bard, J., & Staelens, S. (2022). Longitudinal preclinical evaluation of the novel radioligand [11C]CHDI-626 for PET imaging of mutant huntingtin aggregates in Huntington's disease. *European Journal of Nuclear Medicine and Molecular Imaging*, *49*(4), 1166–1175. https://doi.org/10.1007/S00259-021-05578-8/FIGURES/5

Blumenstock, S., & Dudanova, I. (2020). Cortical and Striatal Circuits in Huntington's Disease. *Frontiers in Neuroscience*, *14*, 82. https://doi.org/10.3389/FNINS.2020.00082/BIBTEX

Boatz, J. C., Piretra, T., Lasorsa, A., Matlahov, I., Conway, J. F., & van der Wel, P. C. A. (2020). Protofilament Structure and Supramolecular Polymorphism of Aggregated Mutant Huntingtin Exon 1. *Journal of Molecular Biology*, *432*(16), 4722–4744. https://doi.org/10.1016/J.JMB.2020.06.021

Boudreau, R. L., McBride, J. L., Martins, I., Shen, S., Xing, Y., Carter, B. J., & Davidson, B. L. (2009a). Nonallele-specific Silencing of Mutant and Wild-type Huntingtin Demonstrates Therapeutic Efficacy in Huntington's Disease Mice. *Molecular Therapy*, *17*(6), 1053–1063. https://doi.org/10.1038/MT.2009.17

Boudreau, R. L., Martins, I., & Davidson, B. L. (2009b). Artificial MicroRNAs as siRNA Shuttles: Improved Safety as Compared to shRNAs In vitro and In vivo. *Molecular Therapy*, *17*(1), 169–175. https://doi.org/10.1038/MT.2008.231

Boyle, E. A., Becker, W. R., Bai, H. B., Chen, J. S., Doudna, J. A., & Greenleaf, W. J. (2021). Quantification of Cas9 binding and cleavage across diverse guide sequences maps landscapes of target engagement. *Science Advances*, *7*(8), 5496.

https://doi.org/10.1126/SCIADV.ABE5496/SUPPL_FILE/ABE5496_TABLES_S1_TO_S19.XLSX
Bradford, J., Shin, J. Y., Roberts, M., Wang, C. E., Li, X. J., & Li, S. (2009). Expression of mutant huntingtin in mouse brain astrocytes causes age-dependent neurological symptoms. *Proceedings of the National Academy of Sciences of the United States of America*, *106*(52), 22480–22485. https://doi.org/10.1073/PNAS.0911503106/SUPPL_FILE/SM1.MOV
Bravo, J. P. K., Liu, M. Sen, Hibshman, G. N., Dangerfield, T. L., Jung, K., McCool, R. S., Johnson, K. A., & Taylor, D. W. (2022). Structural basis for mismatch surveillance by CRISPR–Cas9. *Nature 2022 603:7900*, *603*(7900), 343–347. https://doi.org/10.1038/s41586-022-04470-1
Brinkman, E. K., Chen, T., Amendola, M., & Van Steensel, B. (2014). Easy quantitative assessment of genome editing by sequence trace decomposition. *Nucleic Acids Research*, *42*(22), 168–168. https://doi.org/https://doi.org/10.1093/nar/gku936
Brown, D., Altermatt, M., Dobreva, T., Chen, S., Wang, A., Thomson, M., & Gradinaru, V. (2021). Deep Parallel Characterization of AAV Tropism and AAV-Mediated Transcriptional Changes via Single-Cell RNA Sequencing. *Frontiers in Immunology*, *12*, 4117. https://doi.org/10.3389/FIMMU.2021.730825/BIBTEX
Browne, S. E., Bowling, A. C., MacGarvey, U., Baik, M. J., Berger, S. C., Muqit, M. M. K., Bird, E. D., & Beal, M. F. (1997). Oxidative damage and metabolic dysfunction in Huntington's disease: Selective vulnerability of the basal ganglia. *Annals of Neurology*, *41*(5), 646–653. https://doi.org/10.1002/ANA.410410514
Buckler, A. J., Chang, D. D., Graw, S. L., David Brook, J., Haber, D. A., Sharp, P. A., & Housman, D. E. (1991). Exon amplification: a strategy to isolate mammalian genes based on RNA splicing. *Proceedings of the National Academy of Sciences*, *88*(9), 4005–4009. https://doi.org/10.1073/PNAS.88.9.4005
Bunner, K. D., & Rebec, G. V. (2016). Corticostriatal dysfunction in Huntington's disease: The basics. *Frontiers in Human Neuroscience*, *10*, 317. https://doi.org/10.3389/FNHUM.2016.00317/BIBTEX
Bunting, S. F., Callén, E., Wong, N., Chen, H. T., Polato, F., Gunn, A., Bothmer, A., Feldhahn, N., Fernandez-Capetillo, O., Cao, L., Xu, X., Deng, C. X., Finkel, T., Nussenzweig, M., Stark, J. M., & Nussenzweig, A. (2010). 53BP1 Inhibits Homologous Recombination in Brca1-Deficient Cells by Blocking Resection of DNA Breaks. *Cell*, *141*(2), 243–254. https://doi.org/10.1016/J.CELL.2010.03.012
Byrne, L. M., Rodrigues, F. B., Johnson, E. B., Wijeratne, P. A., De Vita, E., Alexander, D. C., Palermo, G., Czech, C., Schobel, S., Scahill, R. I., Heslegrave, A., Zetterberg, H., & Wild, E. J. (2018). Evaluation of mutant huntingtin and neurofilament proteins as potential markers in Huntington's disease. *Science Translational Medicine*, *10*(458), 7108. https://doi.org/10.1126/SCITRANSLMED.AAT7108/SUPPL_FILE/AAT7108_SM.PDF
Cai, Y., Cheng, T., Yao, Y., Li, X., Ma, Y., Li, L., Zhao, H., Bao, J., Zhang, M., Qiu, Z., & Xue, T. (2019). In vivo genome editing rescues photoreceptor degeneration via a Cas9/RecA-mediated homology-directed repair pathway. *Science Advances*, *5*(4). https://doi.org/10.1126/SCIADV.AAV3335/SUPPL_FILE/AAV3335_SM.PDF
Cai, Zheng, N., Thompson, G. J., Wu, Y., Nie, B., Lin, K., Su, P., Wu, J., Manyande, A., Zhu, L. Q., Wang, J., & Xu, F. (2021). Longitudinal neural connection detection using a ferritin-encoding adeno-associated virus vector and in vivo MRI method. *Human Brain Mapping*, *42*(15), 5010–5022. https://doi.org/https://doi.org/10.1002/hbm.25596
Cambon, K., Zimmer, V., Martineau, S., Gaillard, M. C., Jarrige, M., Bugi, A., Miniarikova, J., Rey, M., Hassig, R., Dufour, N., Auregan, G., Hantraye, P., Perrier, A. L., & Déglon, N. (2017). Preclinical Evaluation of a Lentiviral Vector for Huntingtin Silencing. *Molecular Therapy - Methods & Clinical Development*, *5*, 259–276. https://doi.org/10.1016/J.OMTM.2017.05.001
Canver, M. C., Bauer, D. E., Dass, A., Yien, Y. Y., Chung, J., Masuda, T., Maeda, T., Paw, B. H., & Orkin, S. H. (2014). Characterization of Genomic Deletion Efficiency Mediated by Clustered Regularly Interspaced Palindromic Repeats (CRISPR)/Cas9 Nuclease System in Mammalian Cells,. *Journal of Biological Chemistry*, *289*(31), 21312–21324. https://doi.org/10.1074/JBC.M114.564625
Caron, N. S., Dorsey, E. R., & Hayden, M. R. (2018). Therapeutic approaches to Huntington disease: from the bench to the clinic. *Nature Reviews Drug Discovery 2018 17:10*, *17*(10), 729–750. https://doi.org/10.1038/nrd.2018.133
Castel, A. L., Tomkinson, A. E., & Pearson, C. E. (2009). CTG/CAG Repeat Instability Is Modulated by the

Levels of Human DNA Ligase I and Its Interaction with Proliferating Cell Nuclear Antigen: A DISTINCTION BETWEEN REPLICATION AND SLIPPED-DNA REPAIR. *Journal of Biological Chemistry*, *284*(39), 26631–26645. https://doi.org/10.1074/JBC.M109.034405

Cavazza, T., & Vernos, I. (2016). The RanGTP pathway: From nucleo-cytoplasmic transport to spindle assembly and beyond. *Frontiers in Cell and Developmental Biology*, *3*(JAN), 82. https://doi.org/10.3389/FCELL.2015.00082/BIBTEX

Cearley, C. N., & Wolfe, J. H. (2006). Transduction characteristics of adeno-associated virus vectors expressing cap serotypes 7, 8, 9, and Rh10 in the mouse brain. *Mol Ther*, *13*(3), 528–537. https://doi.org/https://doi.org/10.1016/j.ymthe.2005.11.015

Cebrian-Serrano, A., & Davies, B. (2017). CRISPR-Cas orthologues and variants: optimizing the repertoire, specificity and delivery of genome engineering tools. *Mammalian Genome*, *28*(7), 247–261. https://doi.org/10.1007/S00335-017-9697-4

Challis, R. C., Ravindra Kumar, S., Chen, X., Goertsen, D., Coughlin, G. M., Hori, A. M., Chuapoco, M. R., Otis, T. S., Miles, T. F., & Gradinaru, V. (2022). Adeno-Associated Virus Toolkit to Target Diverse Brain Cells. *Https://Doi.Org/10.1146/Annurev-Neuro-111020-100834*, *45*, 447–469. https://doi.org/10.1146/ANNUREV-NEURO-111020-100834

Chan, Jiang, J., Chen, Y., Li, C., Prucha, M. S., Hu, Y., Chi, T., Moran, S., Rahim, T., Li, S., Li, X., Zola, S. M., Testa, C. M., Mao, H., Villalba, R., Smith, Y., Zhang, X., & Bachevalier, J. (2015). Progressive Cognitive Deficit, Motor Impairment and Striatal Pathology in a Transgenic Huntington Disease Monkey Model from Infancy to Adulthood. *PLOS ONE*, *10*(5), e0122335. https://doi.org/10.1371/JOURNAL.PONE.0122335

Chan, K. Y., Jang, M. J., Yoo, B. B., Greenbaum, A., Ravi, N., Wu, W. L., Sánchez-Guardado, L., Lois, C., Mazmanian, S. K., Deverman, B. E., & Gradinaru, V. (2017). Engineered AAVs for efficient noninvasive gene delivery to the central and peripheral nervous systems. *Nature Neuroscience 2017 20:8*, *20*(8), 1172–1179. https://doi.org/10.1038/nn.4593

Chao, M. J., Gillis, T., Atwal, R. S., Mysore, J. S., Arjomand, J., Harold, D., Holmans, P., Jones, L., Orth, M., Myers, R. H., Kwak, S., Wheeler, V. C., MacDonald, M. E., Gusella, J. F., & Lee, J. M. (2017). Haplotype-based stratification of Huntington's disease. *European Journal of Human Genetics*, *25*(11), 1202–1209. https://doi.org/10.1038/ejhg.2017.125

Chen, S. S., Sun, L. W., Brickner, H., & Sun, P. Q. (2015). Downregulating galectin-3 inhibits proinflammatory cytokine production by human monocyte-derived dendritic cells via RNA interference. *Cellular Immunology*, *294*(1), 44–53. https://doi.org/10.1016/J.CELLIMM.2015.01.017

Chiang, C., Jacobsen, J. C., Ernst, C., Hanscom, C., Heilbut, A., Blumenthal, I., Mills, R. E., Kirby, A., Lindgren, A. M., Rudiger, S. R., McLaughlan, C. J., Bawden, C. S., Reid, S. J., Faull, R. L. M., Snell, R. G., Hall, I. M., Shen, Y., Ohsumi, T. K., Borowsky, M. L., … Talkowski, M. E. (2012). Complex reorganization and predominant non-homologous repair following chromosomal breakage in karyotypically balanced germline rearrangements and transgenic integration. *Nature Genetics 2012 44:4*, *44*(4), 390–397. https://doi.org/10.1038/ng.2202

Chiaruttini, N., Burri, O., Haub, P., Guiet, R., Sordet-Dessimoz, J., & Seitz, A. (2022). An Open-Source Whole Slide Image Registration Workflow at Cellular Precision Using Fiji, QuPath and Elastix. *Frontiers in Computer Science*, *3*, 130. https://doi.org/https://doi.org/10.3389/fcomp.2021.780026

Chongtham, A., Barbaro, B., Filip, T., Syed, A., Huang, W., Smith, M. R., & Marsh, J. L. (2018). Nonmammalian models of Huntington's disease. *Methods in Molecular Biology*, *1780*, 75–96. https://doi.org/10.1007/978-1-4939-7825-0_5/COVER

Christodoulou, I., Patsali, P., Stephanou, C., Antoniou, M., Kleanthous, M., & Lederer, C. W. (2016). Measurement of lentiviral vector titre and copy number by cross-species duplex quantitative PCR. *Gene Therapy*, *23*(1), 113–118. https://doi.org/https://doi.org/10.1038/gt.2015.60

Chung, D. W., Rudnicki, D. D., Yu, L., & Margolis, R. L. (2011). A natural antisense transcript at the Huntington's disease repeat locus regulates HTT expression. *Human Molecular Genetics*, *20*(17), 3467–3477. https://doi.org/10.1093/HMG/DDR263

Chung, & Deisseroth, K. (2013). CLARITY for mapping the nervous system. *Nature Methods*, *10*(6), 508–513. https://doi.org/https://doi.org/10.1038/nmeth.2481

Ciarmiello, A., Giovacchini, G., Orobello, S., Bruselli, L., Elifani, F., & Squitieri, F. (2012). 18F-FDG PET uptake in the pre-Huntington disease caudate affects the time-to-onset independently of CAG expansion size. *European Journal of Nuclear Medicine and Molecular Imaging*, *39*(6), 1030–1036.

https://doi.org/10.1007/S00259-012-2114-Z/FIGURES/2
Cleary, J. D., Pattamatta, A., & Ranum, L. P. W. (2018). Repeat-associated non-ATG (RAN) translation. *Journal of Biological Chemistry*, *293*(42), 16127–16141. https://doi.org/10.1074/JBC.R118.003237
Cloud, L. J., Rosenblatt, A., Margolis, R. L., Ross, C. A., Pillai, J. A., Corey-Bloom, J., Tully, H. M., Bird, T., Panegyres, P. K., Nichter, C. A., Higgins, D. S., Helmers, S. L., Factor, S. A., Jones, R., & Testa, C. M. (2012). Seizures in juvenile Huntington's disease: Frequency and characterization in a multicenter cohort. *Movement Disorders*, *27*(14), 1797–1800. https://doi.org/10.1002/MDS.25237
Coles, R., Caswell, R., & Rubinsztein, D. C. (1998). Functional Analysis of the Huntington's Disease (HD) Gene Promoter. *Human Molecular Genetics*, *7*(5), 791–800. https://doi.org/10.1093/HMG/7.5.791
Colin, E., Zala, D., Liot, G., Rangone, H., Borrell-Pagès, M., Li, X. J., Saudou, F., & Humbert, S. (2008). Huntingtin phosphorylation acts as a molecular switch for anterograde/retrograde transport in neurons. *The EMBO Journal*, *27*(15), 2124–2134. https://doi.org/10.1038/EMBOJ.2008.133
Cong, L., Ran, F. A., Cox, D., Lin, S., Barretto, R., Habib, N., Hsu, P. D., Wu, X., Jiang, W., Marraffini, L. A., & Zhang, F. (2013). Multiplex genome engineering using CRISPR/Cas systems. *Science*, *339*(6121), 819–823. https://doi.org/10.1126/SCIENCE.1231143/SUPPL_FILE/PAPV2.PDF
Cowan, C. M., & Raymond, L. A. (2006). Selective Neuronal Degeneration in Huntington's Disease. *Current Topics in Developmental Biology*, *75*, 25–71. https://doi.org/10.1016/S0070-2153(06)75002-5
Crotti, A., Benner, C., Kerman, B. E., Gosselin, D., Lagier-Tourenne, C., Zuccato, C., Cattaneo, E., Gage, F. H., Cleveland, D. W., & Glass, C. K. (2014). Mutant Huntingtin promotes autonomous microglia activation via myeloid lineage-determining factors. *Nature Neuroscience 2014 17:4*, *17*(4), 513–521. https://doi.org/10.1038/nn.3668
Cubo, E. (2016). Huntington disease: a journey through history. *Neurosciences and History*, *4*(4), 160–163. https://nah.sen.es/en/issues/lastest-issues/146-journals/volume-4/issue-4/346-huntington-disease-a-journey-through-history
Damiano, M., Diguet, E., Malgorn, C., D'Aurelio, M., Galvan, L., Petit, F., Benhaim, L., Guillermier, M., Houitte, D., Dufour, N., Hantraye, P., Canals, J. M., Alberch, J., Delzescaux, T., Déglon, N., Beal, F. M., & Brouillet, E. (2013). A role of mitochondrial complex II defects in genetic models of Huntington's disease expressing N-terminal fragments of mutant huntingtin. *Human Molecular Genetics*, *22*(19), 3869–3882. https://doi.org/10.1093/HMG/DDT242
Dang, Y., Jia, G., Choi, J., Ma, H., Anaya, E., Ye, C., Shankar, P., & Wu, H. (2015). Optimizing sgRNA structure to improve CRISPR-Cas9 knockout efficiency. *Genome Biology*, *16*(1), 1–10. https://doi.org/https://doi.org/10.1186/s13059-015-0846-3
Das, M. R., Chang, Y., Anderson, R., Saunders, R. A., Zhang, N., Tomberlin, C. P., Vale, R. D., & Jain, A. (2023). Repeat-associated non-AUG translation induces cytoplasmic aggregation of CAG repeat-containing RNAs. *Proceedings of the National Academy of Sciences of the United States of America*, *120*(3), e2215071120. https://doi.org/10.1073/PNAS.2215071120/SUPPL_FILE/PNAS.2215071120.SM05.AVI
Davidsson, M., Wang, G., Aldrin-Kirk, P., Cardoso, T., Nolbrant, S., Hartnor, M., Mudannayake, J., Parmar, M., & Björklund, T. (2019). A systematic capsid evolution approach performed in vivo for the design of AAV vectors with tailored properties and tropism. *Proceedings of the National Academy of Sciences of the United States of America*, *116*(52), 27053–27062. https://doi.org/10.1073/PNAS.1910061116/SUPPL_FILE/PNAS.1910061116.SM02.MOV
Davies, S. W., Turmaine, M., Cozens, B. A., DiFiglia, M., Sharp, A. H., Ross, C. A., Scherzinger, E., Wanker, E. E., Mangiarini, L., & Bates, G. P. (1997). Formation of Neuronal Intranuclear Inclusions Underlies the Neurological Dysfunction in Mice Transgenic for the HD Mutation. *Cell*, *90*(3), 537–548. https://doi.org/10.1016/S0092-8674(00)80513-9
De Almeida, L. P., Ross, C. A., Zala, D., Aebischer, P., & Déglon, N. (2002). Lentiviral-Mediated Delivery of Mutant Huntingtin in the Striatum of Rats Induces a Selective Neuropathology Modulated by Polyglutamine Repeat Size, Huntingtin Expression Levels, and Protein Length. *Journal of Neuroscience*, *22*(9), 3473–3483. https://doi.org/10.1523/JNEUROSCI.22-09-03473.2002
Déglon, N. (2017). From huntingtin gene to Huntington's disease-altering strategies. In *Disease-Modifying Targets in Neurodegenerative Disorders: Paving the Way for Disease-Modifying Therapies* (pp. 251–276). Academic Press. https://doi.org/10.1016/B978-0-12-805120-7.00010-5
Detrez, J. R., Maurin, H., Van Kolen, K., Willems, R., Colombelli, J., Lechat, B., Roucourt, B., Van Leuven, F., Baatout, S., Larsen, P., Nuydens, R., Timmermans, J. P., & De Vos, W. H. (2019). Regional

vulnerability and spreading of hyperphosphorylated tau in seeded mouse brain. *Neurobiology of Disease*, *127*, 398–409. https://doi.org/https://doi.org/10.1016/j.nbd.2019.03.010

Deverman, B. E., Pravdo, P. L., Simpson, B. P., Kumar, S. R., Chan, K. Y., Banerjee, A., Wu, W. L., Yang, B., Huber, N., Pasca, S. P., & Gradinaru, V. (2016). Cre-dependent selection yields AAV variants for widespread gene transfer to the adult brain. *Nature Biotechnology*, *34*(2), 204–209. https://doi.org/https://doi.org/10.1038/nbt.3440

Dhillon, S. (2020). Risdiplam: First Approval. *Drugs*, *80*(17), 1853–1858. https://doi.org/10.1007/S40265-020-01410-Z/METRICS

Diaz-Castro, B., Gangwani, M. R., Yu, X., Coppola, G., & Khakh, B. S. (2019). Astrocyte molecular signatures in Huntington's disease. *Science Translational Medicine*, *11*(514). https://doi.org/10.1126/SCITRANSLMED.AAW8546/SUPPL_FILE/AAW8546_SM.PDF

Díaz-Hernández, M., Hernández, F., Martín-Aparicio, E., Gómez-Ramos, P., Morán, M. A., Castaño, J. G., Ferrer, I., Avila, J., & Lucas, J. J. (2003). Neuronal Induction of the Immunoproteasome in Huntington's Disease. *Journal of Neuroscience*, *23*(37), 11653–11661. https://doi.org/10.1523/JNEUROSCI.23-37-11653.2003

Dietrich, P., Johnson, I. M., Alli, S., & Dragatsis, I. (2017). Elimination of huntingtin in the adult mouse leads to progressive behavioral deficits, bilateral thalamic calcification, and altered brain iron homeostasis. *PLOS Genetics*, *13*(7), e1006846. https://doi.org/10.1371/JOURNAL.PGEN.1006846

DiFiglia, M., Sapp, E., Chase, K. O., Davies, S. W., Bates, G. P., Vonsattel, J. P., & Aronin, N. (1997). Aggregation of huntingtin in neuronal intranuclear inclusions and dystrophic neurites in brain. *Science*, *277*(5334), 1990–1993. https://doi.org/10.1126/SCIENCE.277.5334.1990/ASSET/7433F340-81EB-4536-932B-F1DD8E97A9B0/ASSETS/GRAPHIC/SE3975752005.JPEG

DiFiglia, M., Sena-Esteves, M., Chase, K., Sapp, E., Pfister, E., Sass, M., Yoder, J., Reeves, P., Pandey, R. K., Rajeev, K. G., Manoharan, M., Sah, D. W. Y., Zamore, P. D., & Aronin, N. (2007). Therapeutic silencing of mutant huntingtin with siRNA attenuates striatal and cortical neuropathology and behavioral deficits. *Proceedings of the National Academy of Sciences of the United States of America*, *104*(43), 17204–17209. https://doi.org/10.1073/PNAS.0708285104/SUPPL_FILE/08285FIG9.JPG

Djoussé, L., Knowlton, B., Hayden, M., Almqvist, E. W., Brinkman, R., Ross, C., Margolis, R., Rosenblatt, A., Durr, A., Dode, C., Morrison, P. J., Novelletto, A., Frontali, M., Trent, R. J. A., McCusker, E., Gómez-Tortosa, E., Mayo, D., Jones, R., Zanko, A., … Myers, R. H. (2003). Interaction of normal and expanded CAG repeat sizes influences age at onset of Huntington disease. *American Journal of Medical Genetics Part A*, *119A*(3), 279–282. https://doi.org/10.1002/AJMG.A.20190

Donnelly, K. M., Coleman, C. M., Fuller, M. L., Reed, V. L., Smerina, D., Tomlinson, D. S., & Pearce, M. M. P. (2022). Hunting for the cause: Evidence for prion-like mechanisms in Huntington's disease. *Frontiers in Neuroscience*, *16*, 1380. https://doi.org/10.3389/FNINS.2022.946822/BIBTEX

Dragatsis, Efstratiadis, A., & Zeitlin, S. (1998). Mouse mutant embryos lacking huntingtin are rescued from lethality by wild-type extraembryonic tissues. *Development*, *125*(8), 1529–1539. https://doi.org/10.1242/DEV.125.8.1529

Dragatsis, I., Dietrich, P., Ren, H., Deng, Y. P., Del Mar, N., Wang, H. B., Johnson, I. M., Jones, K. R., & Reiner, A. (2018). Effect of early embryonic deletion of huntingtin from pyramidal neurons on the development and long-term survival of neurons in cerebral cortex and striatum. *Neurobiology of Disease*, *111*, 102–117. https://doi.org/10.1016/J.NBD.2017.12.015

Drouet, V., Perrin, V., Hassig, R., Dufour, N., Auregan, G., Alves, S., Bonvento, G., Brouillet, E., Luthi-Carter, R., Hantraye, P., & Déglon, N. (2009). Sustained effects of nonallele-specific Huntingtin silencing. *Annals of Neurology*, *65*(3), 276–285. https://doi.org/10.1002/ANA.21569

Duarte, F., & Déglon, N. (2020). Genome Editing for CNS Disorders. *Frontiers in Neuroscience*, *14*, 1039. https://doi.org/10.3389/FNINS.2020.579062/BIBTEX

Ducray, P. S., Frances, N., Smart, K., Norris, D., Kordasiewicz, H., Guenther, A., Wild, E., & Schobel, S. (2019). Translational Pharmacokinetic/Pharmacodynamic (PK/PD) Modeling Strategy to Support RG6042 Dose Selection in Huntington's Disease (HD) (S16.005). *Neurology*, *92*(15 Supplement).

Duyao, M. P., Ambrose, C., Myers, R., Novelletto, A., Persichetti, F., Frontali, M., Folstein, S., Ross, C., Franz, M., Abbott, M., Gray, J., Conneally, P., Young, A., Penney, J., Hollingsworth, Z., Shoulson, I., Lazzarini, A., Falek, A., Koroshetz, W., … Macdonald, M. (1993). Trinucleotide repeat length instability and age of onset in Huntington's disease. *Nature Genetics 1993 4:4*, *4*(4), 387–392. https://doi.org/10.1038/ng0893-387

Duyao, M. P., Auerbach, A. B., Ryan, A., Persichetti, F., Barnes, G. T., McNeil, S. M., Ge, P., Vonsattel, J. P., Gusella, J. F., Joyner, A. L., & MacDonald, M. E. (1995). Inactivation of the Mouse Huntington's Disease Gene Homolog Hdh. *Science*, *269*(5222), 407–410. https://doi.org/10.1126/SCIENCE.7618107

Ekman, F. K., Ojala, D. S., Adil, M. M., Lopez, P. A., Schaffer, D. V., & Gaj, T. (2019). CRISPR-Cas9-Mediated Genome Editing Increases Lifespan and Improves Motor Deficits in a Huntington's Disease Mouse Model. *Molecular Therapy - Nucleic Acids*, *17*, 829–839. https://doi.org/https://doi.org/10.1016/j.omtn.2019.07.009

Elias, S., Thion, M. S., Yu, H., Sousa, C. M., Lasgi, C., Morin, X., & Humbert, S. (2014). Huntingtin Regulates Mammary Stem Cell Division and Differentiation. *Stem Cell Reports*, *2*(4), 491–506. https://doi.org/10.1016/J.STEMCR.2014.02.011

Engelman, A., & Cherepanov, P. (2012). The structural biology of HIV-1: mechanistic and therapeutic insights. *Nature Reviews Microbiology 2012 10:4*, *10*(4), 279–290. https://doi.org/10.1038/nrmicro2747

Engqvist-Goldstein, Å. E. Y., Warren, R. A., Kessels, M. M., Keen, J. H., Heuser, J., & Drubin, D. G. (2001). The actin-binding protein Hip1R associates with clathrin during early stages of endocytosis and promotes clathrin assembly in vitro. *Journal of Cell Biology*, *154*(6), 1209–1223. https://doi.org/10.1083/JCB.200106089/VIDEO-1

Epping, E. A., Kim, J. I., Craufurd, D., Brashers-Krug, T. M., Anderson, K. E., McCusker, E., Luther, J., Long, J. D., & Paulsen, J. S. (2016). Longitudinal psychiatric symptoms in prodromal Huntington's disease: A decade of data. *American Journal of Psychiatry*, *173*(2), 187–192. https://doi.org/10.1176/APPI.AJP.2015.14121551/ASSET/IMAGES/LARGE/APPI.AJP.2015.14121551F1.JPEG

Erö, C., Gewaltig, M. O., Keller, D., & Markram, H. (2018). A cell atlas for the mouse brain. *Frontiers in Neuroinformatics*, *12*, 84. https://doi.org/https://doi.org/10.3389/fninf.2018.00084

Estevez-Fraga, C., Tabrizi, S. J., & Wild, E. J. (2022). Huntington's Disease Clinical Trials Corner: November 2022. *Journal of Huntington's Disease*, *11*(4), 351–367. https://doi.org/10.3233/JHD-229006

Evers, M. M., Miniarikova, J., Juhas, S., Vallès, A., Bohuslavova, B., Juhasova, J., Skalnikova, H. K., Vodicka, P., Valekova, I., Brouwers, C., Blits, B., Lubelski, J., Kovarova, H., Ellederova, Z., van Deventer, S. J., Petry, H., Motlik, J., & Konstantinova, P. (2018). AAV5-miHTT Gene Therapy Demonstrates Broad Distribution and Strong Human Mutant Huntingtin Lowering in a Huntington's Disease Minipig Model. *Molecular Therapy*, *26*(9), 2163–2177. https://doi.org/10.1016/J.YMTHE.2018.06.021/ATTACHMENT/57B7743D-30F7-4A08-9ADF-7EF146C8886C/MMC1.PDF

Faideau, M., Kim, J., Cormier, K., Gilmore, R., Welch, M., Auregan, G., Dufour, N., Guillermier, M., Brouillet, E., Hantraye, P., DéGlon, N., Ferrante, R. J., & Bonvento, G. (2010). In vivo expression of polyglutamine-expanded huntingtin by mouse striatal astrocytes impairs glutamate transport: a correlation with Huntington's disease subjects. *Human Molecular Genetics*, *19*(15), 3053–3067. https://doi.org/10.1093/HMG/DDQ212

Fang, L., Monteys, A. M., Dürr, A., Keiser, M., Cheng, C., Harapanahalli, A., Gonzalez-Alegre, P., Davidson, B. L., & Wang, K. (2023). Haplotyping SNPs for allele-specific gene editing of the expanded huntingtin allele using long-read sequencing. *Human Genetics and Genomics Advances*, *4*(1), 100146. https://doi.org/10.1016/J.XHGG.2022.100146

Farshim, P. P., & Bates, G. P. (2018). Mouse Models of Huntington's Disease. *Methods in Molecular Biology (Clifton, N.J.)*, *1780*, 97–120. https://doi.org/10.1007/978-1-4939-7825-0_6

Fazio, P., Fitzer-Attas, C. J., Mrzljak, L., Bronzova, J., Nag, S., Warner, J. H., Landwehrmeyer, B., Al-Tawil, N., Halldin, C., Forsberg, A., Ware, J., Dilda, V., Wood, A., Sampaio, C., & Varrone, A. (2020). PET Molecular Imaging of Phosphodiesterase 10A: An Early Biomarker of Huntington's Disease Progression. *Movement Disorders*, *35*(4), 606–615. https://doi.org/10.1002/MDS.27963

Feng, Z., Jin, S., Zupnick, A., Hoh, J., De Stanchina, E., Lowe, S., Prives, C., & Levine, A. J. (2005). p53 tumor suppressor protein regulates the levels of huntingtin gene expression. *Oncogene 2006 25:1*, *25*(1), 1–7. https://doi.org/10.1038/sj.onc.1209021

Fienko, S., Landles, C., Sathasivam, K., Mcateer, S. J., Milton, R. E., Osborne, G. F., Smith, E. J., Jones, S. T., Bondulich, M. K., Danby, E. C. E., Phillips, J., Taxy, B. A., Kordasiewicz, H. B., Bates, G. P., &

Bates, G. (2022). Alternative processing of human HTT mRNA with implications for Huntington's disease therapeutics. *Brain*, *145*(12), 4409–4424. https://doi.org/10.1093/BRAIN/AWAC241

Finkelshtein, D., Werman, A., Novick, D., Barak, S., & Rubinstein, M. (2013). LDL receptor and its family members serve as the cellular receptors for vesicular stomatitis virus. *Proceedings of the National Academy of Sciences of the United States of America*, *110*(18), 7306–7311. https://doi.org/10.1073/PNAS.1214441110/SUPPL_FILE/PNAS.201214441SI.PDF

Fodale, V., Boggio, R., Daldin, M., Cariulo, C., Spiezia, M. C., Byrne, L. M., Leavitt, B. R., Wild, E. J., MacDonald, D., Weiss, A., & Bresciani, A. (2017). Validation of Ultrasensitive Mutant Huntingtin Detection in Human Cerebrospinal Fluid by Single Molecule Counting Immunoassay. *Journal of Huntington's Disease*, *6*(4), 349–361. https://doi.org/10.3233/JHD-170269

Fodale, V., Pintauro, R., Daldin, M., Spiezia, M. C., MacDonald, D., & Bresciani, A. (2022). Quantifying Huntingtin Protein in Human Cerebrospinal Fluid Using a Novel Polyglutamine Length-Independent Assay. *Journal of Huntington's Disease*, *11*(3), 291–305. https://doi.org/10.3233/JHD-220527

Fusilli, C., Migliore, S., Mazza, T., Consoli, F., De Luca, A., Barbagallo, G., Ciammola, A., Gatto, E. M., Cesarini, M., Etcheverry, J. L., Parisi, V., Al-Oraimi, M., Al-Harrasi, S., Al-Salmi, Q., Marano, M., Vonsattel, J. P. G., Sabatini, U., Landwehrmeyer, G. B., & Squitieri, F. (2018). Biological and clinical manifestations of juvenile Huntington's disease: a retrospective analysis. *The Lancet Neurology*, *17*(11), 986–993. https://doi.org/10.1016/S1474-4422(18)30294-1

Gabery, S., Sajjad, M. U., Hult, S., Soylu, R., Kirik, D., & Petersén, Å. (2012). Characterization of a rat model of Huntington's disease based on targeted expression of mutant huntingtin in the forebrain using adeno-associated viral vectors. *European Journal of Neuroscience*, *36*(6), 2789–2800. https://doi.org/10.1111/J.1460-9568.2012.08193.X

Gao, G., Vandenberghe, L. H., Alvira, M. R., Lu, Y., Calcedo, R., Zhou, X., & Wilson, J. M. (2004). Clades of Adeno-Associated Viruses Are Widely Disseminated in Human Tissues. *Journal of Virology*, *78*(12), 6381–6388. https://doi.org/https://doi.org/10.1128/JVI.78.12.6381-6388.2004

Garcia, V. J., Rushton, D. J., Tom, C. M., Allen, N. D., Kemp, P. J., Svendsen, C. N., & Mattis, V. B. (2019). Huntington's disease patient-derived astrocytes display electrophysiological impairments and reduced neuronal support. *Frontiers in Neuroscience*, *13*(JUN), 669. https://doi.org/10.3389/FNINS.2019.00669/BIBTEX

Garriga-Canut, M., Agustín-Pavón, C., Herrmann, F., Sánchez, A., Dierssen, M., Fillat, C., & Isalan, M. (2012). Synthetic zinc finger repressors reduce mutant huntingtin expression in the brain of R6/2 mice. *Proceedings of the National Academy of Sciences of the United States of America*, *109*(45), E3136–E3145. https://doi.org/10.1073/PNAS.1206506109/-/DCSUPPLEMENTAL

Gauthier, L. R., Charrin, B. C., Borrell-Pagès, M., Dompierre, J. P., Rangone, H., Cordelières, F. P., De Mey, J., MacDonald, M. E., Leßmann, V., Humbert, S., & Saudou, F. (2004). Huntingtin Controls Neurotrophic Support and Survival of Neurons by Enhancing BDNF Vesicular Transport along Microtubules. *Cell*, *118*(1), 127–138. https://doi.org/10.1016/J.CELL.2004.06.018

Gil, J. M., & Rego, A. C. (2008). Mechanisms of neurodegeneration in Huntington's disease. *European Journal of Neuroscience*, *27*(11), 2803–2820. https://doi.org/10.1111/J.1460-9568.2008.06310.X

Godin, J. D., Colombo, K., Molina-Calavita, M., Keryer, G., Zala, D., Charrin, B. E. C., Dietrich, P., Volvert, M. L., Guillemot, F., Dragatsis, I., Bellaiche, Y., Saudou, F., Nguyen, L., & Humbert, S. (2010). Huntingtin Is Required for Mitotic Spindle Orientation and Mammalian Neurogenesis. *Neuron*, *67*(3), 392–406. https://doi.org/10.1016/J.NEURON.2010.06.027

Goldberg, Y. P., Kremer, B., Andrew, S. E., Theilmann, J., Graham, R. K., Squitieri, F., Telenius, H., Adam, S., Sajoo, A., Starr, E., Heiberg, A., Wolff, G., & Hayden, M. R. (1993). Molecular analysis of new mutations for Huntington's disease: intermediate alleles and sex of origin effects. *Nature Genetics 1993 5:2*, *5*(2), 174–179. https://doi.org/10.1038/ng1093-174

Gómez-Jaramillo, L., Cano-Cano, F., González-Montelongo, M. D. C., Campos-Caro, A., Aguilar-Diosdado, M., & Arroba, A. I. (2022). A New Perspective on Huntington’s Disease: How a Neurological Disorder Influences the Peripheral Tissues. *International Journal of Molecular Sciences 2022, Vol. 23, Page 6089*, *23*(11), 6089. https://doi.org/10.3390/IJMS23116089

Gong, S., Zheng, C., Doughty, M. L., Losos, K., Didkovsky, N., Schambra, U. B., Nowak, N. J., Joyner, A., Leblanc, G., Hatten, M. E., & Heintz, N. (2003). A gene expression atlas of the central nervous system based on bacterial artificial chromosomes. *Nature*, *425*(6961), 917–925. https://doi.org/https://doi.org/10.1038/nature02033

Goold, R., Flower, M., Moss, D. H., Medway, C., Wood-Kaczmar, A., Andre, R., Farshim, P., Bates, G. P., Holmans, P., Jones, L., & Tabrizi, S. J. (2019). FAN1 modifies Huntington's disease progression by stabilizing the expanded HTT CAG repeat. *Human Molecular Genetics*, *28*(4), 650–661. https://doi.org/10.1093/HMG/DDY375

Goubran, M., Leuze, C., Hsueh, B., Aswendt, M., Ye, L., Tian, Q., Cheng, M. Y., Crow, A., Steinberg, G. K., McNab, J. A., Deisseroth, K., & Zeineh, M. (2019). Multimodal image registration and connectivity analysis for integration of connectomic data from microscopy to MRI. *Nature Communications*, *10*(1), 1–17. https://doi.org/https://doi.org/10.1038/s41467-019-13374-0

Gray, M., Shirasaki, D. I., Cepeda, C., André, V. M., Wilburn, B., Lu, X. H., Tao, J., Yamazaki, I., Li, S. H., Sun, Y. E., Li, X. J., Levine, M. S., & Yang, X. W. (2008). Full-Length Human Mutant Huntingtin with a Stable Polyglutamine Repeat Can Elicit Progressive and Selective Neuropathogenesis in BACHD Mice. *J Neurosci*, *28*(24), 6182–6195. https://doi.org/https://doi.org/10.1523/jneurosci.0857-08.2008

Gribaudo, S., Tixador, P., Bousset, L., Fenyi, A., Lino, P., Melki, R., Peyrin, J. M., & Perrier, A. L. (2019). Propagation of α-Synuclein Strains within Human Reconstructed Neuronal Network. *Stem Cell Reports*, *12*(2), 230–244. https://doi.org/10.1016/J.STEMCR.2018.12.007

Grima, J. C., Daigle, J. G., Arbez, N., Cunningham, K. C., Zhang, K., Ochaba, J., Geater, C., Morozko, E., Stocksdale, J., Glatzer, J. C., Pham, J. T., Ahmed, I., Peng, Q., Wadhwa, H., Pletnikova, O., Troncoso, J. C., Duan, W., Snyder, S. H., Ranum, L. P. W., … Rothstein, J. D. (2017). Mutant Huntingtin Disrupts the Nuclear Pore Complex. *Neuron*, *94*(1), 93-107.e6. https://doi.org/10.1016/J.NEURON.2017.03.023

Grondin, R., Kaytor, M. D., Ai, Y., Nelson, P. T., Thakker, D. R., Heisel, J., Weatherspoon, M. R., Blum, J. L., Burright, E. N., Zhang, Z., & Kaemmerer, W. F. (2012). Six-month partial suppression of Huntingtin is well tolerated in the adult rhesus striatum. *Brain*, *135*(4), 1197–1209. https://doi.org/10.1093/BRAIN/AWR333

Gropp, M. H. M., Klaips, C. L., & Hartl, F. U. (2022). Formation of toxic oligomers of polyQ-expanded Huntingtin by prion-mediated cross-seeding. *Molecular Cell*, *82*(22), 4290-4306.e11. https://doi.org/10.1016/J.MOLCEL.2022.09.031

Group PHAROS Investigators. (2006). At Risk for Huntington Disease: The PHAROS (Prospective Huntington At Risk Observational Study) Cohort Enrolled. *Archives of Neurology*, *63*(7), 991–996. https://doi.org/10.1001/ARCHNEUR.63.7.991

Gu, M., Gash, M. T., Mann, V. M., Javoy-Agid, F., Cooper, J. M., & Schapira, A. H. V. (1996). Mitochondrial defect in Huntington's disease caudate nucleus. *Annals of Neurology*, *39*(3), 385–389. https://doi.org/10.1002/ANA.410390317

Gu, Richman, J., Langfelder, P., Wang, N., Zhang, S., Bañez-Coronel, M., Wang, H. Bin, Yang, L., Ramanathan, L., Deng, L., Park, C. S., Choi, C. R., Cantle, J. P., Gao, F., Gray, M., Coppola, G., Bates, G. P., Ranum, L. P. W., Horvath, S., … Yang, X. W. (2022). Uninterrupted CAG repeat drives striatum-selective transcriptionopathy and nuclear pathogenesis in human Huntingtin BAC mice. *Neuron*, *110*(7), 1173-1192.e7. https://doi.org/10.1016/J.NEURON.2022.01.006

Guo, Q., Huang, B., Cheng, J., Seefelder, M., Engler, T., Pfeifer, G., Oeckl, P., Otto, M., Moser, F., Maurer, M., Pautsch, A., Baumeister, W., Fernández-Busnadiego, R., & Kochanek, S. (2018). The cryo-electron microscopy structure of huntingtin. *Nature 2018 555:7694*, *555*(7694), 117–120. https://doi.org/10.1038/nature25502

Gusella, J. F., Wexler, N. S., Conneally, P. M., Naylor, S. L., Anderson, M. A., Tanzi, R. E., Watkins, P. C., Ottina, K., Wallace, M. R., Sakaguchi, A. Y., Young, A. B., Shoulson, I., Bonilla, E., & Martin, J. B. (1983). A polymorphic DNA marker genetically linked to Huntington's disease. *Nature*, *306*(5940), 234–238. https://doi.org/10.1038/306234a0

Gutekunst, C. A., Li, S. H., Yi, H., Mulroy, J. S., Kuemmerle, S., Jones, R., Rye, D., Ferrante, R. J., Hersch, S. M., & Li, X. J. (1999). Nuclear and Neuropil Aggregates in Huntington's Disease: Relationship to Neuropathology. *Journal of Neuroscience*, *19*(7), 2522–2534. https://doi.org/10.1523/JNEUROSCI.19-07-02522.1999

Ha, M., & Kim, V. N. (2014). Regulation of microRNA biogenesis. *Nature Reviews Molecular Cell Biology 2014 15:8*, *15*(8), 509–524. https://doi.org/10.1038/nrm3838

Hanlon, K. S., Meltzer, J. C., Buzhdygan, T., Cheng, M. J., Sena-Esteves, M., Bennett, R. E., Sullivan, T. P., Razmpour, R., Gong, Y., Ng, C., Nammour, J., Maiz, D., Dujardin, S., Ramirez, S. H., Hudry, E., & Maguire, C. A. (2019). Selection of an Efficient AAV Vector for Robust CNS Transgene Expression.

Molecular Therapy - Methods & Clinical Development, *15*, 320–332. https://doi.org/https://doi.org/10.1016/j.omtm.2019.10.007

Hansen, H. H., Perens, J., Roostalu, U., Skytte, J. L., Salinas, C. G., Barkholt, P., Thorbek, D. D., Rigbolt, K. T. G., Vrang, N., Jelsing, J., & Hecksher-Sørensen, J. (2021). Whole-brain activation signatures of weight-lowering drugs. *Molecular Metabolism*, *47*, 101171. https://doi.org/https://doi.org/10.1016/j.molmet.2021.101171

Haremaki, T., Deglincerti, A., & Brivanlou, A. H. (2015). Huntingtin is required for ciliogenesis and neurogenesis during early Xenopus development. *Developmental Biology*, *408*(2), 305–315. https://doi.org/10.1016/J.YDBIO.2015.07.013

Harjes, P., & Wanker, E. E. (2003). The hunt for huntingtin function: interaction partners tell many different stories. *Trends in Biochemical Sciences*, *28*(8), 425–433. https://doi.org/10.1016/S0968-0004(03)00168-3

Harmatz, P., Prada, C. E., Burton, B. K., Lau, H., Kessler, C. M., Cao, L., Falaleeva, M., Villegas, A. G., Zeitler, J., Meyer, K., Miller, W., Wong Po Foo, C., Vaidya, S., Swenson, W., Shiue, L. H., Rouy, D., & Muenzer, J. (2022). First-in-human in vivo genome editing via AAV-zinc-finger nucleases for mucopolysaccharidosis I/II and hemophilia B. *Molecular Therapy*, *30*(12), 3587–3600. https://doi.org/10.1016/j.ymthe.2022.10.010

Harper, S. Q., Staber, P. D., He, X., Eliason, S. L., Martins, I. H., Mao, Q., Yang, L., Kotin, R. M., Paulson, H. L., & Davidson, B. L. (2005). RNA interference improves motor and neuropathological abnormalities in a Huntington's disease mouse model. *Proceedings of the National Academy of Sciences*, *102*(16), 5820–5825. https://doi.org/10.1073/PNAS.0501507102

Harris, K. D., & Shepherd, G. M. G. (2015). The neocortical circuit: themes and variations. *Nature Neuroscience 2015 18:2*, *18*(2), 170–181. https://doi.org/10.1038/nn.3917

Hedreen, J. C., Peyser, C. E., Folstein, S. E., & Ross, C. A. (1991). Neuronal loss in layers V and VI of cerebral cortex in Huntington's disease. *Neuroscience Letters*, *133*(2), 257–261. https://doi.org/10.1016/0304-3940(91)90583-F

Heinke, P., Rost, F., Rode, J., Trus, P., Simonova, I., Lázár, E., Feddema, J., Welsch, T., Alkass, K., Salehpour, M., Zimmermann, A., Seehofer, D., Possnert, G., Damm, G., Druid, H., Brusch, L., & Bergmann, O. (2022). Diploid hepatocytes drive physiological liver renewal in adult humans. *Cell Systems*, *13*(6), 499-507.e12. https://doi.org/10.1016/J.CELS.2022.05.001

Hickman, R. A., Faust, P. L., Marder, K., Yamamoto, A., & Vonsattel, J. P. (2022). The distribution and density of Huntingtin inclusions across the Huntington disease neocortex: regional correlations with Huntingtin repeat expansion independent of pathologic grade. *Acta Neuropathologica Communications*, *10*(1), 1–12. https://doi.org/10.1186/S40478-022-01364-1/FIGURES/5

High-dose AAV gene therapy deaths. (2020). *Nature Biotechnology*, *38*, 910. https://doi.org/https://doi.org/10.1038/s41587-020-0642-9

Hintiryan, H., Foster, N. N., Bowman, I., Bay, M., Song, M. Y., Gou, L., Yamashita, S., Bienkowski, M. S., Zingg, B., Zhu, M., Yang, X. W., Shih, J. C., Toga, A. W., & Dong, H. W. (2016). The mouse cortico-striatal projectome. *Nature Neuroscience*, *19*(8), 1100–1114. https://doi.org/https://doi.org/10.1038/nn.4332

Hipp, M. S., Patel, C. N., Bersuker, K., Riley, B. E., Kaiser, S. E., Shaler, T. A., Brandeis, M., & Kopito, R. R. (2012). Indirect inhibition of 26S proteasome activity in a cellular model of Huntington's disease. *Journal of Cell Biology*, *196*(5), 573–587. https://doi.org/10.1083/JCB.201110093/VIDEO-3

Hirano, M., Ando, R., Shimozono, S., Sugiyama, M., Takeda, N., Kurokawa, H., Deguchi, R., Endo, K., Haga, K., Takai-Todaka, R., Inaura, S., Matsumura, Y., Hama, H., Okada, Y., Fujiwara, T., Morimoto, T., Katayama, K., & Miyawaki, A. (2022). A highly photostable and bright green fluorescent protein. *Nature Biotechnology*, *40*(7), 1132–1142. https://doi.org/https://doi.org/10.1038/s41587-022-01278-2

Hirano, M., Kato, S., Kobayashi, K., Okada, T., Yaginuma, H., & Kobayashi, K. (2013). Highly Efficient Retrograde Gene Transfer into Motor Neurons by a Lentiviral Vector Pseudotyped with Fusion Glycoprotein. *PLOS ONE*, *8*(9), e75896. https://doi.org/10.1371/JOURNAL.PONE.0075896

Hodges, A., Strand, A. D., Aragaki, A. K., Kuhn, A., Sengstag, T., Hughes, G., Elliston, L. A., Hartog, C., Goldstein, D. R., Thu, D., Hollingsworth, Z. R., Collin, F., Synek, B., Holmans, P. A., Young, A. B., Wexler, N. S., Delorenzi, M., Kooperberg, C., Augood, S. J., … Luthi-Carter, R. (2006). Regional and cellular gene expression changes in human Huntington's disease brain. *Human Molecular Genetics*, *15*(6), 965–977. https://doi.org/10.1093/HMG/DDL013

Hodgson, J. G., Agopyan, N., Gutekunst, C. A., Leavitt, B. R., Lepiane, F., Singaraja, R., Smith, D. J., Bissada, N., McCutcheon, K., Nasir, J., Jamot, L., Xiao-Jiang, L., Stevens, M. E., Rosemond, E., Roder, J. C., Phillips, A. G., Rubin, E. M., Hersch, S. M., & Hayden, M. R. (1999). A YAC Mouse Model for Huntington's Disease with Full-Length Mutant Huntingtin, Cytoplasmic Toxicity, and Selective Striatal Neurodegeneration. *Neuron*, *23*(1), 181–192. https://doi.org/https://doi.org/10.1016/S0896-6273(00)80764-3

Hosp, F., Vossfeldt, H., Heinig, M., Vasiljevic, D., Arumughan, A., Wyler, E., Landthaler, M., Hubner, N., Wanker, E. E., Lannfelt, L., Ingelsson, M., Lalowski, M., Voigt, A., Selbach, M., Harold, D., Abraham, R., Hollingworth, P., Sims, R., Gerrish, A., … Williams, J. (2015). Quantitative Interaction Proteomics of Neurodegenerative Disease Proteins. *Cell Reports*, *11*(7), 1134–1146. https://doi.org/10.1016/J.CELREP.2015.04.030

Hottinger, A. F., Azzouz, M., Deglon, N., Aebischer, P., & Zurn, A. D. (2000). Complete and Long-Term Rescue of Lesioned Adult Motoneurons by Lentiviral-Mediated Expression of Glial Cell Line-Derived Neurotrophic Factor in the Facial Nucleus. *J Neurosci*, *20*(15), 5587–5593. https://doi.org/https://doi.org/10.1523/jneurosci.20-15-05587.2000

Howland, D., Ellederova, Z., Aronin, N., Fernau, D., Gallagher, J., Taylor, A., Hennebold, J., Weiss, A. R., Gray-Edwards, H., & McBride, J. (2020). Large Animal Models of Huntington's Disease: What We Have Learned and Where We Need to Go Next. *Journal of Huntington's Disease*, *9*(3), 201–216. https://doi.org/10.3233/JHD-200425

Hsu, P. D., Scott, D. A., Weinstein, J. A., Ran, F. A., Konermann, S., Agarwala, V., Li, Y., Fine, E. J., Wu, X., Shalem, O., Cradick, T. J., Marraffini, L. A., Bao, G., & Zhang, F. (2013). DNA targeting specificity of RNA-guided Cas9 nucleases. *Nature Biotechnology 2013 31:9*, *31*(9), 827–832. https://doi.org/10.1038/nbt.2647

Hu, J. H., Miller, S. M., Geurts, M. H., Tang, W., Chen, L., Sun, N., Zeina, C. M., Gao, X., Rees, H. A., Lin, Z., & Liu, D. R. (2018). Evolved Cas9 variants with broad PAM compatibility and high DNA specificity. *Nature*, *556*(7699), 57–63. https://doi.org/10.1038/nature26155

Hubers, A. A. M., van Duijn, E., Roos, R. A. C., Craufurd, D., Rickards, H., Landwehrmeyer, B., Van Der Mast, R. C., Giltay, E. J., Bachoud-Lévi, A. C., Bentivoglio, A. R., Biunno, I., Bonelli, R. M., Burgunder, J. M., Dunnett, S. B., Ferreira, J. J., Handley, O. J., Heiberg, A., Illmann, T., Landwehrmeyer, G. B., … Quarrell, O. (2013). Suicidal ideation in a European Huntington's disease population. *Journal of Affective Disorders*, *151*(1), 248–258. https://doi.org/10.1016/J.JAD.2013.06.001

Hudry, E., & Vandenberghe, L. H. (2019). Therapeutic AAV Gene Transfer to the Nervous System: A Clinical Reality. *Neuron*, *101*(5), 839–862. https://doi.org/https://doi.org/10.1016/j.neuron.2019.02.017

Hughes, A. C., Mort, M., Elliston, L., Thomas, R. M., Brooks, S. P., Dunnett, S. B., & Jones, L. (2014). Identification of Novel Alternative Splicing Events in the Huntingtin Gene and Assessment of the Functional Consequences Using Structural Protein Homology Modelling. *Journal of Molecular Biology*, *426*(7), 1428–1438. https://doi.org/10.1016/J.JMB.2013.12.028

Humbel, M., Ramosaj, M., Zimmer, V., Regio, S., Aeby, L., Moser, S., Boizot, A., Sipion, M., Rey, M., & Déglon, N. (2020). Maximizing lentiviral vector gene transfer in the CNS. *Gene Therapy*, *28*(1), 75–88. https://doi.org/https://doi.org/10.1038/s41434-020-0172-6

Huntington, G. (1872). On chorea. *Med. Surg. Reporter*, *26*, 320–321.

Ibraheim, R., Tai, P. W. L., Mir, A., Javeed, N., Wang, J., Rodríguez, T. C., Namkung, S., Nelson, S., Khokhar, E. S., Mintzer, E., Maitland, S., Chen, Z., Cao, Y., Tsagkaraki, E., Wolfe, S. A., Wang, D., Pai, A. A., Xue, W., Gao, G., & Sontheimer, E. J. (2021). Self-inactivating, all-in-one AAV vectors for precision Cas9 genome editing via homology-directed repair in vivo. *Nature Communications*, *12*(1), 1–17. https://doi.org/https://doi.org/10.1038/s41467-021-26518-y

International Huntington Association. (1994). Guidelines for the molecular genetics predictive test in Huntington's disease. *Journal of Medical Genetics*, *31*(7), 555–559. https://doi.org/10.1136/JMG.31.7.555

Ivanov, I. E., Wright, A. V., Cofsky, J. C., Palacio Aris, K. D., Doudna, J. A., & Bryant, Z. (2020). Cas9 interrogates DNA in discrete steps modulated by mismatches and supercoiling. *Proceedings of the National Academy of Sciences of the United States of America*, *117*(11), 5853–5860. https://doi.org/10.1073/PNAS.1913445117/SUPPL_FILE/PNAS.1913445117.SAPP.PDF

Iyer, R. R., & Pluciennik, A. (2021). DNA Mismatch Repair and its Role in Huntington's Disease. *Journal of*

Huntington's Disease, *10*(1), 75–94. https://doi.org/10.3233/JHD-200438

Jacobsen, J. C., Bawden, C. S., Rudiger, S. R., McLaughlan, C. J., Reid, S. J., Waldvogel, H. J., MacDonald, M. E., Gusella, J. F., Walker, S. K., Kelly, J. M., Webb, G. C., Faull, R. L. M., Rees, M. I., & Snell, R. G. (2010). An ovine transgenic Huntington's disease model. *Human Molecular Genetics*, *19*(10), 1873–1882. https://doi.org/10.1093/HMG/DDQ063

Jacobsen, J. C., Erdin, S., Chiang, C., Hanscom, C., Handley, R. R., Barker, D. D., Stortchevoi, A., Blumenthal, I., Reid, S. J., Snell, R. G., MacDonald, M. E., Morton, A. J., Ernst, C., Gusella, J. F., & Talkowski, M. E. (2017). Potential molecular consequences of transgene integration: The R6/2 mouse example. *Scientific Reports 2017 7:1*, *7*(1), 1–7. https://doi.org/10.1038/srep41120

Jang, M., Lee, S. E., & Cho, I. H. (2018). Adeno-associated viral vector serotype DJ-mediated overexpression of N171-82Q-mutant huntingtin in the striatum of juvenile mice is a new model for Huntington's disease. *Frontiers in Cellular Neuroscience*, *12*, 157. https://doi.org/10.3389/FNCEL.2018.00157/BIBTEX

Jayavaradhan, R., Pillis, D. M., Goodman, M., Zhang, F., Zhang, Y., Andreassen, P. R., & Malik, P. (2019). CRISPR-Cas9 fusion to dominant-negative 53BP1 enhances HDR and inhibits NHEJ specifically at Cas9 target sites. *Nature Communications 2019 10:1*, *10*(1), 1–13. https://doi.org/10.1038/s41467-019-10735-7

Jeon, S.-B., Yoon, H. J., Chang, C. Y., Koh, H. S., Jeon, S.-H., & Park, E. J. (2010). Galectin-3 Exerts Cytokine-Like Regulatory Actions through the JAK–STAT Pathway. *The Journal of Immunology*, *185*(11), 7037–7046. https://doi.org/10.4049/JIMMUNOL.1000154

Jiang, R., Diaz-Castro, B., Looger, L. L., & Khakh, B. S. (2016). Dysfunctional Calcium and Glutamate Signaling in Striatal Astrocytes from Huntington's Disease Model Mice. *Journal of Neuroscience*, *36*(12), 3453–3470. https://doi.org/10.1523/JNEUROSCI.3693-15.2016

Jinek, M., Chylinski, K., Fonfara, I., Hauer, M., Doudna, J. A., & Charpentier, E. (2012). A programmable dual-RNA-guided DNA endonuclease in adaptive bacterial immunity. *Science*, *337*(6096), 816–821. https://doi.org/10.1126/SCIENCE.1225829/SUPPL_FILE/JINEK.SM.PDF

Johnson, E. B., Ziegler, G., Penny, W., Rees, G., Tabrizi, S. J., Scahill, R. I., & Gregory, S. (2021). Dynamics of Cortical Degeneration Over a Decade in Huntington's Disease. *Biological Psychiatry*, *89*(8), 807–816. https://doi.org/https://doi.org/10.1016/j.biopsych.2020.11.009

Johri, A., Chandra, A., & Beal, M. F. (2013). PGC-1α, mitochondrial dysfunction, and Huntington's disease. *Free Radical Biology and Medicine*, *62*, 37–46. https://doi.org/10.1016/J.FREERADBIOMED.2013.04.016

Juenemann, K., Schipper-Krom, S., Wiemhoefer, A., Kloss, A., Sanz, A. S., & Reits, E. A. J. (2013). Expanded Polyglutamine-containing N-terminal Huntingtin Fragments Are Entirely Degraded by Mammalian Proteasomes. *Journal of Biological Chemistry*, *288*(38), 27068–27084. https://doi.org/10.1074/JBC.M113.486076

Kaemmerer, W. F., & Grondin, R. C. (2019). The effects of huntingtin-lowering: what do we know so far? *Degenerative Neurological and Neuromuscular Disease*, *9*, 3–17. https://doi.org/10.2147/DNND.S163808

Kan, Y. W., & Dozy, A. M. (1978). Polymorphism of DNA sequence adjacent to human beta-globin structural gene: relationship to sickle mutation. *Proceedings of the National Academy of Sciences of the United States of America*, *75*(11), 5631. https://doi.org/10.1073/PNAS.75.11.5631

Kato-Inui, T., Takahashi, G., Hsu, S., & Miyaoka, Y. (2018). Clustered regularly interspaced short palindromic repeats (CRISPR)/CRISPR-associated protein 9 with improved proof-reading enhances homology-directed repair. *Nucleic Acids Research*, *46*(9), 4677–4688. https://doi.org/10.1093/NAR/GKY264

Kato, S., Kobayashi, K., & Kobayashi, K. (2014). Improved transduction efficiency of a lentiviral vector for neuron-specific retrograde gene transfer by optimizing the junction of fusion envelope glycoprotein. *Journal of Neuroscience Methods*, *227*, 151–158. https://doi.org/10.1016/J.JNEUMETH.2014.02.015

Kato, S., Kobayashi, K., Kuramochi, M., Takasumi, K., Kobayashi, K., Inoue, K. I., Takahara, D., Hitoshi, S., Ikenaka, K., Shimada, T., & Takada, M. (2011). Neuron-specific gene transfer through retrograde transport of lentiviral vector pseudotyped with a novel type of fusion envelope glycoprotein. *Human Gene Therapy*, *22*(12), 1511–1523. https://doi.org/10.1089/HUM.2011.111/ASSET/IMAGES/LARGE/FIGURE6.JPEG

Kay, C., Collins, J. A., Caron, N. S., Agostinho, L. de A., Findlay-Black, H., Casal, L., Sumathipala, D.,

Dissanayake, V. H. W., Cornejo-Olivas, M., Baine, F., Krause, A., Greenberg, J. L., Paiva, C. L. A., Squitieri, F., & Hayden, M. R. (2019). A Comprehensive Haplotype-Targeting Strategy for Allele-Specific HTT Suppression in Huntington Disease. *The American Journal of Human Genetics*, *105*(6), 1112–1125. https://doi.org/10.1016/J.AJHG.2019.10.011

Kay, C., Collins, J. A., Skotte, N. H., Southwell, A. L., Warby, S. C., Caron, N. S., Doty, C. N., Nguyen, B., Griguoli, A., Ross, C. J., Squitieri, F., & Hayden, M. R. (2015). Huntingtin Haplotypes Provide Prioritized Target Panels for Allele-specific Silencing in Huntington Disease Patients of European Ancestry. *Molecular Therapy*, *23*(11), 1759–1771. https://doi.org/10.1038/MT.2015.128

Kaye, J., Reisine, T., & Finkbeiner, S. (2022). Huntington's disease iPSC models—using human patient cells to understand the pathology caused by expanded CAG repeats. *Faculty Reviews*, *11*. https://doi.org/10.12703/R/11-16

Kedaigle, A. J., Fraenkel, E., Atwal, R. S., Wu, M., Gusella, J. F., MacDonald, M. E., Kaye, J. A., Finkbeiner, S., Mattis, V. B., Tom, C. M., Svendsen, C., King, A. R., Chen, Y., Stocksdale, J. T., Lim, R. G., Casale, M., Wang, P. H., Thompson, L. M., Akimov, S. S., … Ross, C. A. (2020). Bioenergetic deficits in Huntington's disease iPSC-derived neural cells and rescue with glycolytic metabolites. *Human Molecular Genetics*, *29*(11), 1757–1771. https://doi.org/10.1093/HMG/DDY430

Keller, C. G., Shin, Y., Monteys, A. M., Renaud, N., Beibel, M., Teider, N., Peters, T., Faller, T., St-Cyr, S., Knehr, J., Roma, G., Reyes, A., Hild, M., Lukashev, D., Theil, D., Dales, N., Cha, J. H., Borowsky, B., Dolmetsch, R., … Sivasankaran, R. (2022). An orally available, brain penetrant, small molecule lowers huntingtin levels by enhancing pseudoexon inclusion. *Nature Communications 2022 13:1*, *13*(1), 1–11. https://doi.org/10.1038/s41467-022-28653-6

Kennedy, M. A., Greco, T. M., Song, B., & Cristea, I. M. (2022). HTT-OMNI: A Web-based Platform for Huntingtin Interaction Exploration and Multi-omics Data Integration. *Molecular & Cellular Proteomics*, *21*(10), 100275. https://doi.org/10.1016/J.MCPRO.2022.100275

Keryer, G., Pineda, J. R., Liot, G., Kim, J., Dietrich, P., Benstaali, C., Smith, K., Cordelières, F. P., Spassky, N., Ferrante, R. J., Dragatsis, I., & Saudou, F. (2011). Ciliogenesis is regulated by a huntingtin-HAP1-PCM1 pathway and is altered in Huntington disease. *The Journal of Clinical Investigation*, *121*(11), 4372–4382. https://doi.org/10.1172/JCI57552

Kieburtz, K. (1996). Unified Huntington's disease rating scale: Reliability and consistency. *Movement Disorders*, *11*(2), 136–142. https://doi.org/10.1002/MDS.870110204

Kim, Chelliah, Y., Kim, S. W., Otwinowski, Z., & Bezprozvanny, I. (2009). Secondary Structure of Huntingtin Amino-Terminal Region. *Structure*, *17*(9), 1205–1212. https://doi.org/10.1016/J.STR.2009.08.002

Kim, M. S., & Kini, A. G. (2017). Engineering and Application of Zinc Finger Proteins and TALEs for Biomedical Research. *Moleucles and Cells*, *40*(8), 533–541. https://doi.org/10.14348/MOLCELLS.2017.0139

Kim, Moody, J. P., Edgerly, C. K., Bordiuk, O. L., Cormier, K., Smith, K., Flint Beal, M., & Ferrante, R. J. (2010). Mitochondrial loss, dysfunction and altered dynamics in Huntington's disease. *Human Molecular Genetics*, *19*(20), 3919–3935. https://doi.org/10.1093/HMG/DDQ306

Kinnunen, K. M., Schwarz, A. J., Turner, E. C., Pustina, D., Gantman, E. C., Gordon, M. F., Joules, R., Mullin, A. P., Scahill, R. I., & Georgiou-Karistianis, N. (2021). Volumetric MRI-Based Biomarkers in Huntington's Disease: An Evidentiary Review. *Frontiers in Neurology*, *12*, 1552. https://doi.org/10.3389/FNEUR.2021.712555/BIBTEX

Kirschneck, C., Batschkus, S., Proff, P., Köstler, J., Spanier, G., & Schröder, A. (2017). Valid gene expression normalization by RT-qPCR in studies on hPDL fibroblasts with focus on orthodontic tooth movement and periodontitis. *Scientific Reports 2017 7:1*, *7*(1), 1–13. https://doi.org/10.1038/s41598-017-15281-0

Kleinstiver, B. P., Pattanayak, V., Prew, M. S., Tsai, S. Q., Nguyen, N. T., Zheng, Z., & Joung, J. K. (2016). High-fidelity CRISPR–Cas9 nucleases with no detectable genome-wide off-target effects. *Nature*, *529*(7587), 490–495. https://doi.org/10.1038/nature16526

Kocak, D. D., Josephs, E. A., Bhandarkar, V., Adkar, S. S., Kwon, J. B., & Gersbach, C. A. (2019). Increasing the specificity of CRISPR systems with engineered RNA secondary structures. *Nature Biotechnology*, *37*(6), 657–666. https://doi.org/10.1038/s41587-019-0095-1

Komatsu, H., Maruyama, M., Yao, S., Shinohara, T., Sakuma, K., Imaichi, S., Chikatsu, T., Kuniyeda, K., Siu, F. K., Peng, L. S., Zhuo, K., Mun, L. S., Han, T. M., Matsumoto, Y., Hashimoto, T., Miyajima, N., Itoh, Y., Ogi, K., Habata, Y., & Mori, M. (2014). Anatomical Transcriptome of G Protein-Coupled

Receptors Leads to the Identification of a Novel Therapeutic Candidate GPR52 for Psychiatric Disorders. *PLOS ONE*, *9*(2), e90134. https://doi.org/10.1371/JOURNAL.PONE.0090134

Kordasiewicz, H. B., Stanek, L. M., Wancewicz, E. V., Mazur, C., McAlonis, M. M., Pytel, K. A., Artates, J. W., Weiss, A., Cheng, S. H., Shihabuddin, L. S., Hung, G., Bennett, C. F., & Cleveland, D. W. (2012). Sustained Therapeutic Reversal of Huntington's Disease by Transient Repression of Huntingtin Synthesis. *Neuron*, *74*(6), 1031–1044. https://doi.org/10.1016/J.NEURON.2012.05.009

Kosior, N., & Leavitt, B. R. (2018). Murine models of Huntington's disease for evaluating therapeutics. *Methods in Molecular Biology*, *1780*, 179–207. https://doi.org/10.1007/978-1-4939-7825-0_10/COVER

Kotterman, M. A., Chalberg, T. W., & Schaffer, D. V. (2015). Viral Vectors for Gene Therapy: Translational and Clinical Outlook. *Https://Doi.Org/10.1146/Annurev-Bioeng-071813-104938*, *17*, 63–89. https://doi.org/10.1146/ANNUREV-BIOENG-071813-104938

Koyuncu, S., Fatima, A., Gutierrez-Garcia, R., & Vilchez, D. (2017). Proteostasis of Huntingtin in Health and Disease. *International Journal of Molecular Sciences 2017, Vol. 18, Page 1568*, *18*(7), 1568. https://doi.org/10.3390/IJMS18071568

Kramer, P. F., Christensen, C. H., Hazelwood, L. A., Dobi, A., Bock, R., Sibley, D. R., Mateo, Y., & Alvarez, V. A. (2011). Dopamine D2 Receptor Overexpression Alters Behavior and Physiology in Drd2-EGFP Mice. *J Neurosci*, *31*(1), 126–132. https://doi.org/https://doi.org/10.1523/jneurosci.4287-10.2011

Kremer, B., Almqvist, E., Theilmann, J., Spence, N., Telenius, H., Goldberg, Y. P., & Hayden, M. R. (1995). Sex-dependent mechanisms for expansions and contractions of the CAG repeat on affected Huntington disease chromosomes. *American Journal of Human Genetics*, *57*(2), 343. /pmc/articles/PMC1801544/?report=abstract

Krooss, S. A., Dai, Z., Schmidt, F., Rovai, A., Fakhiri, J., Dhingra, A., Yuan, Q., Yang, T., Balakrishnan, A., Steinbrück, L., Srivaratharajan, S., Manns, M. P., Schambach, A., Grimm, D., Bohne, J., Sharma, A. D., Büning, H., & Ott, M. (2020). Ex Vivo/In vivo Gene Editing in Hepatocytes Using "All-in-One" CRISPR-Adeno-Associated Virus Vectors with a Self-Linearizing Repair Template. *IScience*, *23*(1), 100764. https://doi.org/https://doi.org/10.1016/j.isci.2019.100764

Kurihara, T., Kouyama-Suzuki, E., Satoga, M., Li, X., Badawi, M., Thiha, Baig, D. N., Yanagawa, T., Uemura, T., Mori, T., & Tabuchi, K. (2020). DNA repair protein RAD51 enhances the CRISPR/Cas9-mediated knock-in efficiency in brain neurons. *Biochemical and Biophysical Research Communications*, *524*(3), 621–628. https://doi.org/10.1016/J.BBRC.2020.01.132

Labbadia, J., & Morimoto, R. I. (2013). Huntington's disease: underlying molecular mechanisms and emerging concepts. *Trends in Biochemical Sciences*, *38*(8), 378–385. https://doi.org/10.1016/J.TIBS.2013.05.003

Lajoie, P., & Snapp, E. L. (2010). Formation and Toxicity of Soluble Polyglutamine Oligomers in Living Cells. *PLOS ONE*, *5*(12), e15245. https://doi.org/10.1371/JOURNAL.PONE.0015245

Landles, C., Milton, R. E., Jean, A., McLarnon, S., McAteer, S. J., Taxy, B. A., Osborne, G. F., Zhang, C., Duan, W., Howland, D., & Bates, G. P. (2021). Development of novel bioassays to detect soluble and aggregated Huntingtin proteins on three technology platforms. *Brain Communications*, *3*(1). https://doi.org/10.1093/BRAINCOMMS/FCAA231

Landles, C., Sathasivam, K., Weiss, A., Woodman, B., Moffitt, H., Finkbeiner, S., Sun, B., Gafni, J., Ellerby, L. M., Trottier, Y., Richards, W. G., Osmand, A., Paganetti, P., & Bates, G. P. (2010). Proteolysis of Mutant Huntingtin Produces an Exon 1 Fragment That Accumulates as an Aggregated Protein in Neuronal Nuclei in Huntington Disease. *Journal of Biological Chemistry*, *285*(12), 8808–8823. https://doi.org/10.1074/JBC.M109.075028

Lang, J. F., Toulmin, S. A., Brida, K. L., Eisenlohr, L. C., & Davidson, B. L. (2019). Standard screening methods underreport AAV-mediated transduction and gene editing. *Nature Communications 2019 10:1*, *10*(1), 1–10. https://doi.org/10.1038/s41467-019-11321-7

Langbehn, K. E., Cochran, A. M., van der Plas, E., Conrad, A. L., Epping, E., Martin, E., Espe-Pfeifer, P., & Nopoulos, P. (2020). Behavioral Deficits in Juvenile Onset Huntington's Disease. *Brain Sciences 2020, Vol. 10, Page 543*, *10*(8), 543. https://doi.org/10.3390/BRAINSCI10080543

Lee, J. M., Correia, K., Loupe, J., Kim, K. H., Barker, D., Hong, E. P., Chao, M. J., Long, J. D., Lucente, D., Vonsattel, J. P. G., Pinto, R. M., Abu Elneel, K., Ramos, E. M., Mysore, J. S., Gillis, T., Wheeler, V. C., MacDonald, M. E., Gusella, J. F., McAllister, B., … Myers, R. H. (2019). CAG Repeat Not Polyglutamine Length Determines Timing of Huntington's Disease Onset. *Cell*, *178*(4), 887-900.e14.

https://doi.org/10.1016/J.CELL.2019.06.036
Lee, J. M., Gillis, T., Mysore, J. S., Ramos, E. M., Myers, R. H., Hayden, M. R., Morrison, P. J., Nance, M., Ross, C. A., Margolis, R. L., Squitieri, F., Griguoli, A., Di Donato, S., Gomez-Tortosa, E., Ayuso, C., Suchowersky, O., Trent, R. J., McCusker, E., Novelletto, A., … Gusella, J. F. (2012). Common SNP-Based Haplotype Analysis of the 4p16.3 Huntington Disease Gene Region. *The American Journal of Human Genetics*, *90*(3), 434–444. https://doi.org/10.1016/J.AJHG.2012.01.005
Lee, J. M., Kim, K. H., Shin, A., Chao, M. J., Abu Elneel, K., Gillis, T., Mysore, J. S., Kaye, J. A., Zahed, H., Kratter, I. H., Daub, A. C., Finkbeiner, S., Li, H., Roach, J. C., Goodman, N., Hood, L., Myers, R. H., MacDonald, M. E., & Gusella, J. F. (2015). Sequence-Level Analysis of the Major European Huntington Disease Haplotype. *The American Journal of Human Genetics*, *97*(3), 435–444. https://doi.org/10.1016/J.AJHG.2015.07.017
Lee, & McMurray, C. T. (2014). Trinucleotide expansion in disease: why is there a length threshold? *Current Opinion in Genetics & Development*, *26*, 131–140. https://doi.org/10.1016/J.GDE.2014.07.003
Lee, Park, E. H., Couture, G., Harvey, I., Garneau, P., & Pelletier, J. (2002). An upstream open reading frame impedes translation of the huntingtin gene. *Nucleic Acids Research*, *30*(23), 5110–5119. https://doi.org/10.1093/NAR/GKF664
Lee, Reyes, R. C., Gottipati, M. K., Lewis, K., Lesort, M., Parpura, V., & Gray, M. (2013). Enhanced Ca2 +-dependent glutamate release from astrocytes of the BACHD Huntington's disease mouse model. *Neurobiology of Disease*, *58*, 192–199. https://doi.org/10.1016/J.NBD.2013.06.002
Li, Lee, C. M., Hurley, A. E., Jarrett, K. E., De Giorgi, M., Lu, W., Balderrama, K. S., Doerfler, A. M., Deshmukh, H., Ray, A., Bao, G., & Lagor, W. R. (2018). A Self-Deleting AAV-CRISPR System for In Vivo Genome Editing. *Molecular Therapy. Methods & Clinical Development*, *12*, 111–122. https://doi.org/https://doi.org/10.1016/j.omtm.2018.11.009
Li, Su, J., Liu, Y., Jin, X., Zhong, X., Mo, L., Wang, Q., Deng, H., & Yang, Y. (2021). In vivo PCSK9 gene editing using an all-in-one self-cleavage AAV-CRISPR system. *Molecular Therapy - Methods and Clinical Development*, *20*, 652–659. https://doi.org/https://doi.org/10.1016/j.omtm.2021.02.005
Li, Wang, C., Wang, Z., Zhu, C., Li, J., Sha, T., Ma, L., Gao, C., Yang, Y., Sun, Y., Wang, J., Sun, X., Lu, C., Difiglia, M., Mei, Y., Ding, C., Luo, S., Dang, Y., Ding, Y., … Lu, B. (2019). Allele-selective lowering of mutant HTT protein by HTT–LC3 linker compounds. *Nature 2019 575:7781*, *575*(7781), 203–209. https://doi.org/10.1038/s41586-019-1722-1
Li, Zhang, L., Li, Z., Xu, C., Du, X., & Wu, S. (2020). Cas12a mediates efficient and precise endogenous gene tagging via MITI: microhomology-dependent targeted integrations. *Cellular and Molecular Life Sciences*, *77*(19), 3875–3884. https://doi.org/10.1007/S00018-019-03396-8/FIGURES/5
Liddelow, S. A., Guttenplan, K. A., Clarke, L. E., Bennett, F. C., Bohlen, C. J., Schirmer, L., Bennett, M. L., Münch, A. E., Chung, W. S., Peterson, T. C., Wilton, D. K., Frouin, A., Napier, B. A., Panicker, N., Kumar, M., Buckwalter, M. S., Rowitch, D. H., Dawson, V. L., Dawson, T. M., … Barres, B. A. (2017). Neurotoxic reactive astrocytes are induced by activated microglia. *Nature 2017 541:7638*, *541*(7638), 481–487. https://doi.org/10.1038/nature21029
Lieberman, A. P., Shakkottai, V. G., & Albin, R. L. (2019). Polyglutamine Repeats in Neurodegenerative Diseases. *Https://Doi.Org/10.1146/Annurev-Pathmechdis-012418-012857*, *14*, 1–27. https://doi.org/10.1146/ANNUREV-PATHMECHDIS-012418-012857
Liebmann, T., Renier, N., Bettayeb, K., Greengard, P., Tessier-Lavigne, M., & Flajolet, M. (2016). Three-Dimensional Study of Alzheimer's Disease Hallmarks Using the iDISCO Clearing Method. *Cell Reports*, *16*(4), 1138–1152. https://doi.org/https://doi.org/10.1016/j.celrep.2016.06.060
Liévens, J. C., Woodman, B., Mahal, A., Spasic-Boscovic, O., Samuel, D., Kerkerian-Le Goff, L., & Bates, G. P. (2001). Impaired Glutamate Uptake in the R6 Huntington's Disease Transgenic Mice. *Neurobiology of Disease*, *8*(5), 807–821. https://doi.org/10.1006/NBDI.2001.0430
Lim, R. G., Salazar, L. L., Wilton, D. K., King, A. R., Stocksdale, J. T., Sharifabad, D., Lau, A. L., Stevens, B., Reidling, J. C., Winokur, S. T., Casale, M. S., Thompson, L. M., Pardo, M., Díaz-Barriga, A. G. G., Straccia, M., Sanders, P., Alberch, J., Canals, J. M., Kaye, J. A., … Svendsen, C. N. (2017). Developmental alterations in Huntington's disease neural cells and pharmacological rescue in cells and mice. *Nature Neuroscience 2017 20:5*, *20*(5), 648–660. https://doi.org/10.1038/nn.4532
Lin, Chang, W.-C., Chen, H.-M., Lai, H.-L., Chen, C.-Y., Tao, M.-H., & Chern, Y. (2013). Regulation of Feedback between Protein Kinase A and the Proteasome System Worsens Huntington's Disease. *Molecular and Cellular Biology*, *33*(5), 1073–1084. https://doi.org/10.1128/MCB.01434-

12/SUPPL_FILE/ZMB999109881SO1.PDF
Lin, Nasir, J., Kalchman, M. A., McDonald, H., Zeisler, J., Goldberg, Y. P., & Hayden, M. R. (1995). Structural analysis of the 5′ region of mouse and human huntington disease genes reveals conservation of putative promoter region and di- and trinucleotide polymorphisms. *Genomics*, *25*(3), 707–715. https://doi.org/10.1016/0888-7543(95)80014-D
Lin, R., Zhou, Y., Yan, T., Wang, R., Li, H., Wu, Z., Zhang, X., Zhou, X., Zhao, F., Zhang, L., Li, Y., & Luo, M. (2022). Directed evolution of adeno-associated virus for efficient gene delivery to microglia. *Nature Methods*, *19*(8), 976–985. https://doi.org/https://doi.org/10.1038/s41592-022-01547-7
Lin, Rommens, J. M., Graham, R. K., Kalchman, M., Macdonald, H., Nasir, J., Delaney, A., Goldberg, Y. P., & Hayden, M. R. (1993). Differential 3′ polyadenylation of the Huntington disease gene results in two mRNA species with variable tissue expression. *Human Molecular Genetics*, *2*(10), 1541–1545. https://doi.org/10.1093/HMG/2.10.1541
Lin, Zhong, X., Li, L., Ying, M., Yang, T., Zhang, Z., He, X., & Xu, F. (2020). AAV9-Retro mediates efficient transduction with axon terminal absorption and blood–brain barrier transportation. *Molecular Brain*, *13*(1), 1–12. https://doi.org/10.1186/S13041-020-00679-1/FIGURES/6
Liu, Long, J. D., Zhang, Y., Raymond, L. A., Marder, K., Rosser, A., McCusker, E. A., Mills, J. A., & Paulsen, J. S. (2015). Motor onset and diagnosis in Huntington disease using the diagnostic confidence level. *Journal of Neurology*, *262*(12), 2691–2698. https://doi.org/10.1007/s00415-015-7900-7
Liu, H., Zhang, C., Xu, J., Jin, J., Cheng, L., Miao, X., Wu, Q., Wei, Z., Liu, P., Lu, H., Van Zijl, P. C. M., Ross, C. A., Hua, J., & Duan, W. (2021a). Huntingtin silencing delays onset and slows progression of Huntington's disease: a biomarker study. *Brain*, *144*(10), 3101–3113. https://doi.org/10.1093/BRAIN/AWAB190
Liu, Zhu, M., Zhang, Y., & Diao, Y. (2021b). Crossing the blood-brain barrier with AAV vectors. *Metabolic Brain Disease*, *36*(1), 45–52. https://doi.org/https://doi.org/10.1007/s11011-020-00630-2
Long, J., Luo, X., Fang, D., Song, H., Fang, W., Shan, H., Liu, P., Lu, B., Yin, X. M., Hong, L., & Li, M. (2022). Discovery of an autophagy inducer J3 to lower mutant huntingtin and alleviate Huntington's disease-related phenotype. *Cell and Bioscience*, *12*(1), 1–16. https://doi.org/10.1186/S13578-022-00906-3/FIGURES/7
Lontay, B., Kiss, A., Virág, L., & Tar, K. (2020). How Do Post-Translational Modifications Influence the Pathomechanistic Landscape of Huntington's Disease? A Comprehensive Review. *International Journal of Molecular Sciences 2020, Vol. 21, Page 4282*, *21*(12), 4282. https://doi.org/10.3390/IJMS21124282
Lopes, M. M., Paysan, J., Rino, J., Lopes, S. M., Pereira de Almeida, L., Cortes, L., & Nobre, R. J. (2022). A new protocol for whole-brain biodistribution analysis of AAVs by tissue clearing, light-sheet microscopy and semi-automated spatial quantification. *Gene Therapy*. https://doi.org/https://doi.org/10.1038/s41434-022-00372-z
Löw, K., Aebischer, P., & Schneider, B. L. (2013). Direct and retrograde transduction of nigral neurons with AAV6, 8, and 9 and intraneuronal persistence of viral particles. *Human Gene Therapy*, *24*(6), 613–629. https://doi.org/https://doi.org/10.1089/hum.2012.174
Maat-Schieman, M. L. C., Dorsman, J. C., Smoor, M. A., Siesling, S., Van Duinen, S. G., Verschuuren, J. J. G. M., Den Dunnen, J. T., Van Ommen, G. J. B., & Roos, R. A. C. (1999). Distribution of Inclusions in Neuronal Nuclei and Dystrophic Neurites in Huntington Disease Brain. *Journal of Neuropathology & Experimental Neurology*, *58*(2), 129–137. https://doi.org/10.1097/00005072-199902000-00003
MacDonald, M. E., Ambrose, C. M., Duyao, M. P., Myers, R. H., Lin, C., Srinidhi, L., Barnes, G., Taylor, S. A., James, M., Groot, N., MacFarlane, H., Jenkins, B., Anderson, M. A., Wexler, N. S., Gusella, J. F., Bates, G. P., Baxendale, S., Hummerich, H., Kirby, S., … Harper, P. S. (1993). A novel gene containing a trinucleotide repeat that is expanded and unstable on Huntington's disease chromosomes. *Cell*, *72*(6), 971–983. https://doi.org/10.1016/0092-8674(93)90585-E
MacDonald, M. E., & Gusella, J. F. (1996). Huntington's disease: translating a CAG repeat into a pathogenic mechanism. *Current Opinion in Neurobiology*, *6*(5), 638–643. https://doi.org/10.1016/S0959-4388(96)80097-3
MacDonald, M. E., Lin, C., Srinidhi, L., Bates, G., Altherr, M., Whaley, W. L., Lehrach, H., Wasmuth, J., & Gusella, J. F. (1991). Complex patterns of linkage disequilibrium in the Huntington disease region. *American Journal of Human Genetics*, *49*(4), 723. /pmc/articles/PMC1683155/?report=abstract
Maeder, M. L., Stefanidakis, M., Wilson, C. J., Baral, R., Barrera, L. A., Bounoutas, G. S., Bumcrot, D.,

Chao, H., Ciulla, D. M., DaSilva, J. A., Dass, A., Dhanapal, V., Fennell, T. J., Friedland, A. E., Giannoukos, G., Gloskowski, S. W., Glucksmann, A., Gotta, G. M., Jayaram, H., … Jiang, H. (2019). Development of a gene-editing approach to restore vision loss in Leber congenital amaurosis type 10. *Nature Medicine 2019 25:2*, *25*(2), 229–233. https://doi.org/10.1038/s41591-018-0327-9

Makarova, K. S., Wolf, Y. I., Iranzo, J., Shmakov, S. A., Alkhnbashi, O. S., Brouns, S. J. J., Charpentier, E., Cheng, D., Haft, D. H., Horvath, P., Moineau, S., Mojica, F. J. M., Scott, D., Shah, S. A., Siksnys, V., Terns, M. P., Venclovas, Č., White, M. F., Yakunin, A. F., … Koonin, E. V. (2020). Evolutionary classification of CRISPR–Cas systems: a burst of class 2 and derived variants. *Nature Reviews Microbiology*, *18*(2), 67–83. https://doi.org/10.1038/s41579-019-0299-x

Mali, P., Yang, L., Esvelt, K. M., Aach, J., Guell, M., DiCarlo, J. E., Norville, J. E., & Church, G. M. (2013). RNA-guided human genome engineering via Cas9. *Science*, *339*(6121), 823–826. https://doi.org/10.1126/SCIENCE.1232033/SUPPL_FILE/MALI.SM.PDF

Mangiarini, L., Sathasivam, K., Seller, M., Cozens, B., Harper, A., Hetherington, C., Lawton, M., Trottier, Y., Lehrach, H., Davies, S. W., & Bates, G. P. (1996). Exon 1 of the HD Gene with an Expanded CAG Repeat Is Sufficient to Cause a Progressive Neurological Phenotype in Transgenic Mice. *Cell*, *87*(3), 493–506. https://doi.org/10.1016/S0092-8674(00)81369-0

Marques Sousa, C., & Humbert, S. (2013). Huntingtin: Here, There, Everywhere! *Journal of Huntington's Disease*, *2*(4), 395–403. https://doi.org/10.3233/JHD-130082

Marshall, F. J. (2006). Tetrabenazine as antichorea therapy in Huntington disease. *Neurology*, *66*(3), 366–372. https://doi.org/10.1212/01.WNL.0000198586.85250.13

Martin, D. D. O., Ladha, S., Ehrnhoefer, D. E., & Hayden, M. R. (2015). Autophagy in Huntington disease and huntingtin in autophagy. *Trends in Neurosciences*, *38*(1), 26–35. https://doi.org/10.1016/J.TINS.2014.09.003

Martinez-Vicente, M., Talloczy, Z., Wong, E., Tang, G., Koga, H., Kaushik, S., De Vries, R., Arias, E., Harris, S., Sulzer, D., & Cuervo, A. M. (2010). Cargo recognition failure is responsible for inefficient autophagy in Huntington's disease. *Nature Neuroscience 2010 13:5*, *13*(5), 567–576. https://doi.org/10.1038/nn.2528

Matamales, M., Bertran-Gonzalez, J., Salomon, L., Degos, B., Deniau, J. M., Valjent, E., Hervé, D., & Girault, J. A. (2009). Striatal Medium-Sized Spiny Neurons: Identification by Nuclear Staining and Study of Neuronal Subpopulations in BAC Transgenic Mice. *PLOS ONE*, *4*(3), e4770. https://doi.org/https://doi.org/10.1371/journal.pone.0004770

Maturana, C. J., Verpeut, J. L., Kooshkbaghi, M., & Engel, E. A. (2021). Novel tool to quantify with single-cell resolution the number of incoming AAV genomes co-expressed in the mouse nervous system. *Gene Therapy 2021*, 1–6. https://doi.org/10.1038/s41434-021-00272-8

McAllister, B., Gusella, J. F., Landwehrmeyer, G. B., Lee, J. M., MacDonald, M. E., Orth, M., Rosser, A. E., Williams, N. M., Holmans, P., Jones, L., & Massey, T. H. (2021). Timing and Impact of Psychiatric, Cognitive, and Motor Abnormalities in Huntington Disease. *Neurology*, *96*(19), e2395–e2406. https://doi.org/10.1212/WNL.0000000000011893

McBride, J. L., Boudreau, R. L., Harper, S. Q., Staber, P. D., Monteys, A. M., Martins, I., Gilmore, B. L., Burstein, H., Peluso, R. W., Polisky, B., Carter, B. J., & Davidson, B. L. (2008). Artificial miRNAs mitigate shRNA-mediated toxicity in the brain: Implications for the therapeutic development of RNAi. *Proceedings of the National Academy of Sciences of the United States of America*, *105*(15), 5868–5873. https://doi.org/10.1073/PNAS.0801775105/SUPPL_FILE/0801775105SI.PDF

McBride, J. L., Pitzer, M. R., Boudreau, R. L., Dufour, B., Hobbs, T., Ojeda, S. R., & Davidson, B. L. (2011). Preclinical safety of RNAi-mediated HTT suppression in the rhesus macaque as a potential therapy for Huntington's disease. *Molecular Therapy*, *19*(12), 2152–2162. https://doi.org/10.1038/MT.2011.219/ATTACHMENT/9965D1EC-F757-430B-87C0-69B140B95BAA/MMC8.MP4

McColgan, P., Joubert, J., Tabrizi, S. J., & Rees, G. (2020). The human motor cortex microcircuit: insights for neurodegenerative disease. *Nature Reviews Neuroscience 2020 21:8*, *21*(8), 401–415. https://doi.org/10.1038/s41583-020-0315-1

McColgan, P., Seunarine, K. K., Razi, A., Cole, J. H., Gregory, S., Durr, A., Roos, R. A. C., Stout, J. C., Landwehrmeyer, B., Scahill, R. I., Clark, C. A., Rees, G., & Tabrizi, S. J. (2015). Selective vulnerability of Rich Club brain regions is an organizational principle of structural connectivity loss in Huntington's disease. *Brain*, *138*(11), 3327–3344. https://doi.org/10.1093/BRAIN/AWV259

McKinstry, S. U., Karadeniz, Y. B., Worthington, A. K., Hayrapetyan, V. Y., Ilcim Ozlu, M., Serafin-Molina, K., Christopher Risher, W., Ustunkaya, T., Dragatsis, I., Zeitlin, S., Yin, H. H., & Eroglu, C. (2014). Huntingtin Is Required for Normal Excitatory Synapse Development in Cortical and Striatal Circuits. *Journal of Neuroscience*, *34*(28), 9455–9472. https://doi.org/10.1523/JNEUROSCI.4699-13.2014

McNeil, S. M., Novelletto, A., Srinidhi, J., Barnes, G., Kornbluth, I., Altherr, M. R., Wasmuth, J. J., Gusella, J. F., MacDonald, M. E., & Myers, R. H. (1997). Reduced Penetrance of the Huntington's Disease Mutation. *Human Molecular Genetics*, *6*(5), 775–779. https://doi.org/10.1093/HMG/6.5.775

Medina, A., Mahjoub, Y., Shaver, L., & Pringsheim, T. (2022). Prevalence and Incidence of Huntington's Disease: An Updated Systematic Review and Meta-Analysis. *Movement Disorders*. https://doi.org/10.1002/MDS.29228

Menalled, L., Zanjani, H., MacKenzie, L., Koppel, A., Carpenter, E., Zeitlin, S., & Chesselet, M. F. (2000). Decrease in Striatal Enkephalin mRNA in Mouse Models of Huntington's Disease. *Experimental Neurology*, *162*(2), 328–342. https://doi.org/10.1006/EXNR.1999.7327

Mendell, J. R., Al-Zaidy, S., Shell, R., Arnold, W. D., Rodino-Klapac, L. R., Prior, T. W., Lowes, L., Alfano, L., Berry, K., Church, K., Kissel, J. T., Nagendran, S., L'Italien, J., Sproule, D. M., Wells, C., Cardenas, J. A., Heitzer, M. D., Kaspar, A., Corcoran, S., … Kaspar, B. K. (2017). Single-Dose Gene-Replacement Therapy for Spinal Muscular Atrophy. *N Engl J Med*, *377*(18), 1713–1722. https://doi.org/https://doi.org/10.1056/nejmoa1706198

Merienne, N., Meunier, C., Schneider, A., Seguin, J., Nair, S. S., Rocher, A. B., Le Gras, S., Keime, C., Faull, R., Pellerin, L., Chatton, J. Y., Neri, C., Merienne, K., & Déglon, N. (2019). Cell-Type-Specific Gene Expression Profiling in Adult Mouse Brain Reveals Normal and Disease-State Signatures. *Cell Reports*, *26*(9), 2477-2493.e9. https://doi.org/10.1016/J.CELREP.2019.02.003

Merienne, N., Vachey, G., de Longprez, L., Meunier, C., Zimmer, V., Perriard, G., Canales, M., Mathias, A., Herrgott, L., Beltraminelli, T., Maulet, A., Dequesne, T., Pythoud, C., Rey, M., Pellerin, L., Brouillet, E., Perrier, A. L., du Pasquier, R., & Déglon, N. (2017). The Self-Inactivating KamiCas9 System for the Editing of CNS Disease Genes. *Cell Reports*, *20*(12), 2980–2991. https://doi.org/https://doi.org/10.1016/j.celrep.2017.08.075

Mestre, T. A., Forjaz, M. J., Mahlknecht, P., Cardoso, F., Ferreira, J. J., Reilmann, R., Sampaio, C., Goetz, C. G., Cubo, E., Martinez-Martin, P., & Stebbins, G. T. (2018). Rating Scales for Motor Symptoms and Signs in Huntington's Disease: Critique and Recommendations. *Movement Disorders Clinical Practice*, *5*(2), 111–117. https://doi.org/10.1002/MDC3.12571

Michalik, A., & Van Broeckhoven, C. (2004). Proteasome degrades soluble expanded polyglutamine completely and efficiently. *Neurobiology of Disease*, *16*(1), 202–211. https://doi.org/10.1016/J.NBD.2003.12.020

Milone, M. C., & O'Doherty, U. (2018). Clinical use of lentiviral vectors. *Leukemia 2018 32:7*, *32*(7), 1529–1541. https://doi.org/10.1038/s41375-018-0106-0

Miniarikova, J., Zimmer, V., Martier, R., Brouwers, C. C., Pythoud, C., Richetin, K., Rey, M., Lubelski, J., Evers, M. M., Van Deventer, S. J., Petry, H., Déglon, N., & Konstantinova, P. (2017). AAV5-miHTT gene therapy demonstrates suppression of mutant huntingtin aggregation and neuronal dysfunction in a rat model of Huntington's disease. *Gene Therapy*, *24*(10), 630–639. https://doi.org/10.1038/gt.2017.71

Miyoshi, H., Blömer, U., Takahashi, M., Gage, F. H., & Verma, I. M. (1998). Development of a Self-Inactivating Lentivirus Vector. *Journal of Virology*, *72*(10), 8150–8157. https://doi.org/10.1128/JVI.72.10.8150-8157.1998/ASSET/32AC1DD1-FB6F-4B31-8359-913B456E37AA/ASSETS/GRAPHIC/JV1080670005.JPEG

Mondo, E., Moser, R., Gao, G., Mueller, C., Sena-Esteves, M., Sapp, E., Pfister, E., O'Connell, D., Takle, K., Erger, K. E., Liu, W., Conlon, T. J., Di Figlia, M., Gounis, M. J., & Aronin, N. (2018). Selective Neuronal Uptake and Distribution of AAVrh8, AAV9, and AAVrh10 in Sheep After Intra-Striatal Administration. *Journal of Huntington's Disease*, *7*(4), 309–319. https://doi.org/10.3233/JHD-180302

Monteys, A. M., Ebanks, S. A., Keiser, M. S., & Davidson, B. L. (2017). CRISPR/Cas9 Editing of the Mutant Huntingtin Allele In Vitro and In Vivo. *Mol Ther*, *25*(1), 12–23. https://doi.org/https://doi.org/10.1016/j.ymthe.2016.11.010

Morelli, K. H., Wu, Q., Gosztyla, M. L., Liu, H., Yao, M., Zhang, C., Chen, J., Marina, R. J., Lee, K., Jones, K. L., Huang, M. Y., Li, A., Smith-Geater, C., Thompson, L. M., Duan, W., & Yeo, G. W. (2022). An RNA-targeting CRISPR–Cas13d system alleviates disease-related phenotypes in Huntington's

disease models. *Nature Neuroscience 2022*, 1–12. https://doi.org/10.1038/s41593-022-01207-1

Morigaki, R., & Goto, S. (2017). Striatal Vulnerability in Huntington's Disease: Neuroprotection Versus Neurotoxicity. *Brain Sciences*, *7*(6), 02–25. https://doi.org/10.3390/BRAINSCI7060063

Moss, D. J. H., Tabrizi, S. J., Mead, S., Lo, K., Pardiñas, A. F., Holmans, P., Jones, L., Langbehn, D., Coleman, A., Santos, R. D., Decolongon, J., Sturrock, A., Bardinet, E., Ret, C. J., Justo, D., Lehericy, S., Marelli, C., Nigaud, K., Valabrègue, R., … Tan, L. (2017). Identification of genetic variants associated with Huntington's disease progression: a genome-wide association study. *The Lancet Neurology*, *16*(9), 701–711. https://doi.org/10.1016/S1474-4422(17)30161-8

Muñoz-Castañeda, R., Zingg, B., Matho, K. S., Chen, X., Wang, Q., Foster, N. N., Li, A., Narasimhan, A., Hirokawa, K. E., Huo, B., Bannerjee, S., Korobkova, L., Park, C. S., Park, Y. G., Bienkowski, M. S., Chon, U., Wheeler, D. W., Li, X., Wang, Y., … Dong, H. W. (2021). Cellular anatomy of the mouse primary motor cortex. *Nature*, *598*(7879), 159–166. https://doi.org/https://doi.org/10.1038/s41586-021-03970-w

Myers, R. H., Leavitt, J., Farrer, L. A., Jagadeesh, J., McFarlane, H., Mastromauro, C. A., Mark, R. J., & Gusella, J. F. (1989). Homozygote for Huntington disease. *American Journal of Human Genetics*, *45*(4), 615. /pmc/articles/PMC1683503/?report=abstract

Nalavade, R., Griesche, N., Ryan, D. P., Hildebrand, S., & Krauß, S. (2013). Mechanisms of RNA-induced toxicity in CAG repeat disorders. *Cell Death & Disease 2013 4:8*, *4*(8), e752–e752. https://doi.org/10.1038/cddis.2013.276

Nasir, J., Floresco, S. B., O'Kusky, J. R., Diewert, V. M., Richman, J. M., Zeisler, J., Borowski, A., Marth, J. D., Phillips, A. G., & Hayden, M. R. (1995). Targeted disruption of the Huntington's disease gene results in embryonic lethality and behavioral and morphological changes in heterozygotes. *Cell*, *81*(5), 811–823. https://doi.org/10.1016/0092-8674(95)90542-1

Nekrasov, E. D., Vigont, V. A., Klyushnikov, S. A., Lebedeva, O. S., Vassina, E. M., Bogomazova, A. N., Chestkov, I. V., Semashko, T. A., Kiseleva, E., Suldina, L. A., Bobrovsky, P. A., Zimina, O. A., Ryazantseva, M. A., Skopin, A. Y., Illarioshkin, S. N., Kaznacheyeva, E. V., Lagarkova, M. A., & Kiselev, S. L. (2016). Manifestation of Huntington's disease pathology in human induced pluripotent stem cell-derived neurons. *Molecular Neurodegeneration*, *11*(1), 1–15. https://doi.org/10.1186/S13024-016-0092-5/FIGURES/5

Nelson, C. E., Wu, Y., Gemberling, M. P., Oliver, M. L., Waller, M. A., Bohning, J. D., Robinson-Hamm, J. N., Bulaklak, K., Castellanos Rivera, R. M., Collier, J. H., Asokan, A., & Gersbach, C. A. (2019). Long-term evaluation of AAV-CRISPR genome editing for Duchenne muscular dystrophy. *Nature Medicine 2019 25:3*, *25*(3), 427–432. https://doi.org/10.1038/s41591-019-0344-3

Neueder, A., Landles, C., Ghosh, R., Howland, D., Myers, R. H., Faull, R. L. M., Tabrizi, S. J., & Bates, G. P. (2017). The pathogenic exon 1 HTT protein is produced by incomplete splicing in Huntington's disease patients. *Scientific Reports*, *7*(1), 1–10. https://doi.org/10.1038/s41598-017-01510-z

Nicoleau, C., Varela, C., Bonnefond, C., Maury, Y., Bugi, A., Aubry, L., Viegas, P., Bourgois-Rocha, F., Peschanski, M., & Perrier, A. L. (2013). Embryonic stem cells neural differentiation qualifies the role of Wnt/β-Catenin signals in human telencephalic specification and regionalization. *Stem Cells*, *31*(9), 1763–1774. https://doi.org/10.1002/STEM.1462

Nishiyama, J., Mikuni, T., & Yasuda, R. (2017). Virus-Mediated Genome Editing via Homology-Directed Repair in Mitotic and Postmitotic Cells in Mammalian Brain. *Neuron*, *96*(4), 755–768. https://doi.org/https://doi.org/10.1016/j.neuron.2017.10.004

Novak, M. J. U., Seunarine, K. K., Gibbard, C. R., Mccolgan, P., Draganski, B., Friston, K., Clark, C. A., & Tabrizi, S. J. (2015). Basal ganglia-cortical structural connectivity in Huntington's disease. *Human Brain Mapping*, *36*(5), 1728–1740. https://doi.org/10.1002/HBM.22733

Octeau, J. C., Chai, H., Jiang, R., Bonanno, S. L., Martin, K. C., & Khakh, B. S. (2018). An Optical Neuron-Astrocyte Proximity Assay at Synaptic Distance Scales. *Neuron*, *98*(1), 49-66.e9. https://doi.org/10.1016/J.NEURON.2018.03.003

Oikemus, S. R., Pfister, E. L., Sapp, E., Chase, K. O., Kennington, L. A., Hudgens, E., Miller, R., Zhu, L. J., Chaudhary, A., Mick, E. O., Sena-Esteves, M., Wolfe, S. A., Difiglia, M., Aronin, N., & Brodsky, M. H. (2022). Allele-Specific Knockdown of Mutant Huntingtin Protein via Editing at Coding Region Single Nucleotide Polymorphism Heterozygosities. *Human Gene Therapy*, *33*(1–2), 25–36. https://doi.org/https://doi.org/10.1089/hum.2020.323

Okamoto, S. I., Pouladi, M. A., Talantova, M., Yao, D., Xia, P., Ehrnhoefer, D. E., Zaidi, R., Clemente, A.,

Kaul, M., Graham, R. K., Zhang, D., Vincent Chen, H. S., Tong, G., Hayden, M. R., & Lipton, S. A. (2009). Balance between synaptic versus extrasynaptic NMDA receptor activity influences inclusions and neurotoxicity of mutant huntingtin. *Nature Medicine 2009 15:12*, *15*(12), 1407–1413. https://doi.org/10.1038/nm.2056

Okun, M. S., & Thommi, N. (2004). Americo Negrette (1924 to 2003). Diagnosing Huntington disease in Venezuela. *Neurology*, *63*(2), 340–343. https://doi.org/10.1212/01.WNL.0000129827.16522.78

Ordway, J. M., Tallaksen-Greene, S., Gutekunst, C. A., Bernstein, E. M., Cearley, J. A., Wiener, H. W., Dure IV, L. S., Lindsey, R., Hersch, S. M., Jope, R. S., Albin, R. L., & Detloff, P. J. (1997). Ectopically Expressed CAG Repeats Cause Intranuclear Inclusions and a Progressive Late Onset Neurological Phenotype in the Mouse. *Cell*, *91*(6), 753–763. https://doi.org/10.1016/S0092-8674(00)80464-X

Orr, A. L., Li, S., Wang, C. E., Li, H., Wang, J., Rong, J., Xu, X., Mastroberardino, P. G., Greenamyre, J. T., & Li, X. J. (2008). N-Terminal Mutant Huntingtin Associates with Mitochondria and Impairs Mitochondrial Trafficking. *Journal of Neuroscience*, *28*(11), 2783–2792. https://doi.org/10.1523/JNEUROSCI.0106-08.2008

Ortega, Z., & Lucas, J. J. (2014). Ubiquitin-proteasome system involvement in huntington's disease. *Frontiers in Molecular Neuroscience*, *7*(SEP), 77. https://doi.org/10.3389/FNMOL.2014.00077/BIBTEX

Panov, A. V., Gutekunst, C. A., Leavitt, B. R., Hayden, M. R., Burke, J. R., Strittmatter, W. J., & Greenamyre, J. T. (2002). Early mitochondrial calcium defects in Huntington's disease are a direct effect of polyglutamines. *Nature Neuroscience 2002 5:8*, *5*(8), 731–736. https://doi.org/10.1038/nn884

Papadia, S., & Hardingham, G. E. (2007). The dichotomy of NMDA receptor signalling. *The Neuroscientist : A Review Journal Bringing Neurobiology, Neurology and Psychiatry*, *13*(6), 572. https://doi.org/10.1177/1073858407013006040

Parent, A., & Hazrati, L. N. (1995). Functional anatomy of the basal ganglia. I. The cortico-basal ganglia-thalamo-cortical loop. *Brain Research Reviews*, *20*(1), 91–127. https://doi.org/10.1016/0165-0173(94)00007-C

Paulsen, J. S., Long, J. D., Johnson, H. J., Aylward, E. H., Ross, C. A., Williams, J. K., Nance, M. A., Erwin, C. J., Westervelt, H. J., Harrington, D. L., Bockholt, H. J., Zhang, Y., McCusker, E. A., Chiu, E. M., Panegyres, P. K., Cross, S., Ryan, P., Epping, E. A., Preston, J., … Dubinsky, R. (2014). Clinical and biomarker changes in premanifest Huntington disease show trial feasibility: A decade of the PREDICT-HD study. *Frontiers in Aging Neuroscience*, *6*(APR), 78. https://doi.org/10.3389/FNAGI.2014.00078/ABSTRACT

Pecho-Vrieseling, E., Rieker, C., Fuchs, S., Bleckmann, D., Esposito, M. S., Botta, P., Goldstein, C., Bernhard, M., Galimberti, I., Müller, M., Lüthi, A., Arber, S., Bouwmeester, T., Van Der Putten, H., & Di Giorgio, F. P. (2014). Transneuronal propagation of mutant huntingtin contributes to non–cell autonomous pathology in neurons. *Nature Neuroscience 2014 17:8*, *17*(8), 1064–1072. https://doi.org/10.1038/nn.3761

Penney, J. B., Vonsattel, J. P., MacDonald, M. E., Gusella, J. F., & Myers, R. H. (1997). CAG repeat number governs the development rate of pathology in Huntington's disease. *Annals of Neurology*, *41*(5), 689–692. https://doi.org/10.1002/ANA.410410521

Perens, J., & Hecksher-Sørensen, J. (2022). Digital Brain Maps and Virtual Neuroscience: An Emerging Role for Light-Sheet Fluorescence Microscopy in Drug Development. *Frontiers in Neuroscience*, *16*, 510. https://doi.org/https://doi.org/10.3389/fnins.2022.866884

Pfister, E. L., Dinardo, N., Mondo, E., Borel, F., Conroy, F., Fraser, C., Gernoux, G., Han, X., Hu, D., Johnson, E., Kennington, L., Liu, P., Reid, S. J., Sapp, E., Vodicka, P., Kuchel, T., Morton, A. J., Howland, D., Moser, R., … Aronin, N. (2018). Artificial miRNAs Reduce Human Mutant Huntingtin Throughout the Striatum in a Transgenic Sheep Model of Huntington's Disease. *Https://Home.Liebertpub.Com/Hum*, *29*(6), 663–673. https://doi.org/10.1089/HUM.2017.199

Pfister, E. L., Kennington, L., Straubhaar, J., Wagh, S., Liu, W., DiFiglia, M., Landwehrmeyer, B., Vonsattel, J. P., Zamore, P. D., & Aronin, N. (2009). Five siRNAs Targeting Three SNPs May Provide Therapy for Three-Quarters of Huntington's Disease Patients. *Current Biology*, *19*(9), 774–778. https://doi.org/10.1016/j.cub.2009.03.030

Piao, X., Meng, D., Zhang, X., Song, Q., Lv, H., & Jia, Y. (2022). Dual-gRNA approach with limited off-target effect corrects C9ORF72 repeat expansion in vivo. *Scientific Reports 2022 12:1*, *12*(1), 1–15. https://doi.org/10.1038/s41598-022-07746-8

Pido-Lopez, J., Andre, R., Benjamin, A. C., Ali, N., Farag, S., Tabrizi, S. J., & Bates, G. P. (2018). In vivo neutralization of the protagonist role of macrophages during the chronic inflammatory stage of Huntington's disease. *Scientific Reports 2018 8:1*, *8*(1), 1–14. https://doi.org/10.1038/s41598-018-29792-x

Pinto, R. M., Arning, L., Giordano, J. V., Razghandi, P., Andrew, M. A., Gillis, T., Correia, K., Mysore, J. S., Grote Urtubey, D. M., Parwez, C. R., von Hein, S. M., Brent Clark, H., Nguyen, H. P., Förster, E., Beller, A., Jayadaev, S., Dirk Keene, C., Bird, T. D., Lucente, D., … Wheeler, V. C. (2020). Patterns of CAG repeat instability in the central nervous system and periphery in Huntington's disease and in spinocerebellar ataxia type 1. *Human Molecular Genetics*, *29*(15), 2551–2567. https://doi.org/10.1093/HMG/DDAA139

Pla, P., Orvoen, S., Benstaali, C., Dodier, S., Gardier, A. M., David, D. J., Humbert, S., & Saudou, F. (2013). Huntingtin Acts Non Cell-Autonomously on Hippocampal Neurogenesis and Controls Anxiety-Related Behaviors in Adult Mouse. *PLOS ONE*, *8*(9), e73902. https://doi.org/10.1371/JOURNAL.PONE.0073902

Porro, A., Mohiuddin, M., Zurfluh, C., Spegg, V., Dai, J., Iehl, F., Ropars, V., Collotta, G., Fishwick, K. M., Mozaffari, N. L., Guérois, R., Jiricny, J., Altmeyer, M., Charbonnier, J. B., Pearson, C. E., & Sartori, A. A. (2021). FAN1-MLH1 interaction affects repair of DNA interstrand cross-links and slipped-CAG/CTG repeats. *Science Advances*, *7*(31). https://doi.org/10.1126/SCIADV.ABF7906/SUPPL_FILE/SCIADV.ABF7906_SM.PDF

Pouladi, M. A., Stanek, L. M., Xie, Y., Franciosi, S., Southwell, A. L., Deng, Y., Butland, S., Zhang, W., Cheng, S. H., Shihabuddin, L. S., & Hayden, M. R. (2012). Marked differences in neurochemistry and aggregates despite similar behavioural and neuropathological features of Huntington disease in the full-length BACHD and YAC128 mice. *Human Molecular Genetics*, *21*(10), 2219–2232. https://doi.org/10.1093/HMG/DDS037

Pouladi, M. A., Xie, Y., Skotte, N. H., Ehrnhoefer, D. E., Graham, R. K., Kim, J. E., Bissada, N., Yang, X. W., Paganetti, P., Friedlander, R. M., Leavitt, B. R., & Hayden, M. R. (2010). Full-length huntingtin levels modulate body weight by influencing insulin-like growth factor 1 expression. *Human Molecular Genetics*, *19*(8), 1528–1538. https://doi.org/10.1093/HMG/DDQ026

Powell, J. E., Lim, C. K. W., Krishnan, R., McCallister, T. X., Saporito-Magriña, C., Zeballos, M. A., McPheron, G. D., & Gaj, T. (2022). Targeted gene silencing in the nervous system with CRISPR-Cas13. *Science Advances*, *8*(3), 2485. https://doi.org/10.1126/SCIADV.ABK2485

Pringsheim, T., Wiltshire, K., Day, L., Dykeman, J., Steeves, T., & Jette, N. (2012). The incidence and prevalence of Huntington's disease: A systematic review and meta-analysis. *Movement Disorders*, *27*(9), 1083–1091. https://doi.org/10.1002/MDS.25075

Quinn, L., Kegelmeyer, D., Kloos, A., Rao, A. K., Busse, M., & Fritz, N. E. (2020). Clinical recommendations to guide physical therapy practice for Huntington disease. *Neurology*, *94*(5), 217–228. https://doi.org/10.1212/WNL.0000000000008887

Ramdas, P., Sahu, A. K., Mishra, T., Bhardwaj, V., & Chande, A. (2020). From Entry to Egress: Strategic Exploitation of the Cellular Processes by HIV-1. *Frontiers in Microbiology*, *11*, 3021. https://doi.org/10.3389/FMICB.2020.559792/BIBTEX

Ramezani, A., & Hawley, R. G. (2002). Overview of the HIV-1 Lentiviral Vector System. *Current Protocols in Molecular Biology*, *60*(1), 16.21.1-16.21.15. https://doi.org/10.1002/0471142727.MB1621S60

Ramírez-Jarquín, U. N., Sharma, M., Shahani, N., Li, Y., Boregowda, S., & Subramaniam, S. (2022). Rhes protein transits from neuron to neuron and facilitates mutant huntingtin spreading in the brain. *Science Advances*, *8*(12), 3877. https://doi.org/10.1126/SCIADV.ABM3877/SUPPL_FILE/SCIADV.ABM3877_SM.PDF

Rauskolb, S., Zagrebelsky, M., Dreznjak, A., Deogracias, R., Matsumoto, T., Wiese, S., Erne, B., Sendtner, M., Schaeren-Wiemers, N., Korte, M., & Barde, Y. A. (2010). Global Deprivation of Brain-Derived Neurotrophic Factor in the CNS Reveals an Area-Specific Requirement for Dendritic Growth. *Journal of Neuroscience*, *30*(5), 1739–1749. https://doi.org/10.1523/JNEUROSCI.5100-09.2010

Ravikumar, B., Vacher, C., Berger, Z., Davies, J. E., Luo, S., Oroz, L. G., Scaravilli, F., Easton, D. F., Duden, R., O'Kane, C. J., & Rubinsztein, D. C. (2004). Inhibition of mTOR induces autophagy and reduces toxicity of polyglutamine expansions in fly and mouse models of Huntington disease. *Nature Genetics 2004 36:6*, *36*(6), 585–595. https://doi.org/10.1038/ng1362

Regan, M. R., Huang, Y. H., Yu, S. K., Dykes-Hoberg, M. I., Jin, L., Watkins, A. M., Bergles, D. E., &

Rothstein, J. D. (2007). Variations in Promoter Activity Reveal a Differential Expression and Physiology of Glutamate Transporters by Glia in the Developing and Mature CNS. *J Neurosci*, *27*(25), 6607–6619. https://doi.org/https://doi.org/10.1523/jneurosci.0790-07.2007

Reiner, A., Del Mar, N., Meade, C. A., Yang, H., Dragatsis, I., Zeitlin, S., & Goldowitz, D. (2001). Neurons Lacking Huntingtin Differentially Colonize Brain and Survive in Chimeric Mice. *Journal of Neuroscience*, *21*(19), 7608–7619. https://doi.org/10.1523/JNEUROSCI.21-19-07608.2001

Renier, N., Adams, E. L., Kirst, C., Wu, Z., Azevedo, R., Kohl, J., Autry, A. E., Kadiri, L., Umadevi Venkataraju, K., Zhou, Y., Wang, V. X., Tang, C. Y., Olsen, O., Dulac, C., Osten, P., & Tessier-Lavigne, M. (2016). Mapping of Brain Activity by Automated Volume Analysis of Immediate Early Genes. *Cell*, *165*(7), 1789–1802. https://doi.org/https://doi.org/10.1016/j.cell.2016.05.007

Riguet, N., Mahul-Mellier, A. L., Maharjan, N., Burtscher, J., Croisier, M., Knott, G., Hastings, J., Patin, A., Reiterer, V., Farhan, H., Nasarov, S., & Lashuel, H. A. (2021). Nuclear and cytoplasmic huntingtin inclusions exhibit distinct biochemical composition, interactome and ultrastructural properties. *Nature Communications 2021 12:1*, *12*(1), 1–27. https://doi.org/10.1038/s41467-021-26684-z

Rodrigues, F. B., Byrne, L. M., Tortelli, R., Johnson, E. B., Wijeratne, P. A., Arridge, M., de Vita, E., Ghazaleh, N., Houghton, R., Furby, H., Alexander, D. C., Tabrizi, S. J., Schobel, S., Scahill, R. I., Heslegrave, A., Zetterberg, H., & Wild, E. J. (2020). Mutant huntingtin and neurofilament light have distinct longitudinal dynamics in Huntington's disease. *Science Translational Medicine*, *12*(574), 2888. https://doi.org/10.1126/SCITRANSLMED.ABC2888/SUPPL_FILE/ABC2888_SM.PDF

Rodriguez-Lebron, E., Denovan-Wright, E. M., Nash, K., Lewin, A. S., & Mandel, R. J. (2005). Intrastriatal rAAV-mediated delivery of anti-huntingtin shRNAs induces partial reversal of disease progression in R6/1 Huntington's disease transgenic mice. *Molecular Therapy*, *12*(4), 618–633. https://doi.org/10.1016/J.YMTHE.2005.05.006

Romo, L., Ashar-Patel, A., Pfister, E., & Aronin, N. (2017). Alterations in mRNA 3′ UTR Isoform Abundance Accompany Gene Expression Changes in Human Huntington's Disease Brains. *Cell Reports*, *20*(13), 3057–3070. https://doi.org/10.1016/J.CELREP.2017.09.009

Rook, M. E., & Southwell, A. L. (2022). Antisense Oligonucleotide Therapy: From Design to the Huntington Disease Clinic. *BioDrugs 2022 36:2*, *36*(2), 105–119. https://doi.org/10.1007/S40259-022-00519-9

Rosas, H. D., Salat, D. H., Lee, S. Y., Zaleta, A. K., Pappu, V., Fischl, B., Greve, D., Hevelone, N., & Hersch, S. M. (2008). Cerebral cortex and the clinical expression of Huntington's disease: complexity and heterogeneity. *Brain*, *131*(4), 1057–1068. https://doi.org/10.1093/BRAIN/AWN025

Ross, C. A., Aylward, E. H., Wild, E. J., Langbehn, D. R., Long, J. D., Warner, J. H., Scahill, R. I., Leavitt, B. R., Stout, J. C., Paulsen, J. S., Reilmann, R., Unschuld, P. G., Wexler, A., Margolis, R. L., & Tabrizi, S. J. (2014). Huntington disease: natural history, biomarkers and prospects for therapeutics. *Nature Reviews Neurology*, *10*(4), 204–216. https://doi.org/10.1038/nrneurol.2014.24

Ross, C. A., Reilmann, R., Cardoso, F., McCusker, E. A., Testa, C. M., Stout, J. C., Leavitt, B. R., Pei, Z., Landwehrmeyer, B., Martinez, A., Levey, J., Srajer, T., Bang, J., & Tabrizi, S. J. (2019). Movement Disorder Society Task Force Viewpoint: Huntington's Disease Diagnostic Categories. *Movement Disorders Clinical Practice*, *6*(7), 541–546. https://doi.org/10.1002/MDC3.12808

Ross, C. A., & Shoulson, I. (2009). Huntington disease: pathogenesis, biomarkers, and approaches to experimental therapeutics. *Parkinsonism & Related Disorders*, *15*. https://doi.org/10.1016/S1353-8020(09)70800-4

Rudich, P., Watkins, S., & Lamitina, T. (2020). PolyQ-independent toxicity associated with novel translational products from CAG repeat expansions. *PLOS ONE*, *15*(4), e0227464. https://doi.org/10.1371/JOURNAL.PONE.0227464

Rui, Y. N., Xu, Z., Patel, B., Chen, Z., Chen, D., Tito, A., David, G., Sun, Y., Stimming, E. F., Bellen, H. J., Cuervo, A. M., & Zhang, S. (2015). Huntingtin functions as a scaffold for selective macroautophagy. *Nature Cell Biology 2014 17:3*, *17*(3), 262–275. https://doi.org/10.1038/ncb3101

Ruzo, A., Ismailoglu, I., Popowski, M., Haremaki, T., Croft, G. F., Deglincerti, A., & Brivanlou, A. H. (2015). Discovery of Novel Isoforms of Huntingtin Reveals a New Hominid-Specific Exon. *PLOS ONE*, *10*(5), e0127687. https://doi.org/10.1371/JOURNAL.PONE.0127687

Sakuma, T., Barry, M. A., & Ikeda, Y. (2012). Lentiviral vectors: basic to translational. *Biochemical Journal*, *443*(3), 603–618. https://doi.org/10.1042/BJ20120146

Salinas, C. B. G., Lu, T. T. H., Gabery, S., Marstal, K., Alanentalo, T., Mercer, A. J., Cornea, A., Conradsen, K., Hecksher-Sørensen, J., Dahl, A. B., Knudsen, L. B., & Secher, A. (2018). Integrated Brain Atlas

for Unbiased Mapping of Nervous System Effects Following Liraglutide Treatment. *Scientific Reports*, *8*(1), 1–12. https://doi.org/https://doi.org/10.1038/s41598-018-28496-6

Sapp, E., Ge, P., Aizawa, H., Bird, E., Penney, J., Young, A. B., Vonsattel, J. P., & Difiglia, M. (1995). Evidence for a preferential loss of enkephalin immunoreactivity in the external globus pallidus in low grade Huntington's disease using high resolution image analysis. *Neuroscience*, *64*(2), 397–404. https://doi.org/10.1016/0306-4522(94)00427-7

Sathasivam, K., Neueder, A., Gipson, T. A., Landles, C., Benjamin, A. C., Bondulich, M. K., Smith, D. L., Faull, R. L. M., Roos, R. A. C., Howland, D., Detloff, P. J., Housman, D. E., & Bates, G. P. (2013). Aberrant splicing of HTT generates the pathogenic exon 1 protein in Huntington disease. *Proceedings of the National Academy of Sciences of the United States of America*, *110*(6), 2366–2370. https://doi.org/10.1073/PNAS.1221891110/SUPPL_FILE/PNAS.201221891SI.PDF

Saudou, F., & Humbert, S. (2016). The Biology of Huntingtin. *Neuron*, *89*(5), 910–926. https://doi.org/10.1016/J.NEURON.2016.02.003

Scahill, R. I., Zeun, P., Osborne-Crowley, K., Johnson, E. B., Gregory, S., Parker, C., Lowe, J., Nair, A., O'Callaghan, C., Langley, C., Papoutsi, M., McColgan, P., Estevez-Fraga, C., Fayer, K., Wellington, H., Rodrigues, F. B., Byrne, L. M., Heselgrave, A., Hyare, H., … Tabrizi, S. J. (2020). Biological and clinical characteristics of gene carriers far from predicted onset in the Huntington's disease Young Adult Study (HD-YAS): a cross-sectional analysis. *The Lancet Neurology*, *19*(6), 502–512. https://doi.org/10.1016/S1474-4422(20)30143-5

Schilling, G., Becher, M. W., Sharp, A. H., Jinnah, H. A., Duan, K., Kotzuk, J. A., Slunt, H. H., Ratovitski, T., Cooper, J. K., Jenkins, N. A., Copeland, N. G., Price, D. L., Ross, C. A., & Borchelt, D. R. (1999). Intranuclear Inclusions and Neuritic Aggregates in Transgenic Mice Expressing a Mutant N-Terminal Fragment of Huntingtin. *Human Molecular Genetics*, *8*(3), 397–407. https://doi.org/10.1093/HMG/8.3.397

Schipper-Krom, S., Juenemann, K., Jansen, A. H., Wiemhoefer, A., Van Den Nieuwendijk, R., Smith, D. L., Hink, M. A., Bates, G. P., Overkleeft, H., Ovaa, H., & Reits, E. (2014). Dynamic recruitment of active proteasomes into polyglutamine initiated inclusion bodies. *FEBS Letters*, *588*(1), 151–159. https://doi.org/10.1016/J.FEBSLET.2013.11.023

Schmidt, U., Weigert, M., Broaddus, C., & Myers, G. (2018). Cell detection with star-convex polygons. In *Medical Image Computing and Computer Assisted Intervention – MICCAI* (Vol. 11071, pp. 265–273). Springer, Cham. https://doi.org/https://doi.org/10.1007/978-3-030-00934-2_30

Schoch, K. M., & Miller, T. M. (2017). Antisense Oligonucleotides: Translation from Mouse Models to Human Neurodegenerative Diseases. *Neuron*, *94*(6), 1056–1070. https://doi.org/10.1016/J.NEURON.2017.04.010

Scholler, J., Pagès, S., & Batti, L. (2022). MOTA: map objects to atlas. *Zenodo*. https://doi.org/https://doi.org/10.5281/zenodo.6961917

Semaka, A., Kay, C., Doty, C., Collins, J. A., Bijlsma, E. K., Richards, F., Goldberg, Y. P., & Hayden, M. R. (2013). CAG size-specific risk estimates for intermediate allele repeat instability in Huntington disease. *Journal of Medical Genetics*, *50*(10), 696–703. https://doi.org/10.1136/JMEDGENET-2013-101796

Seong, I. S., Ivanova, E., Lee, J. M., Choo, Y. S., Fossale, E., Anderson, M. A., Gusella, J. F., Laramie, J. M., Myers, R. H., Lesort, M., & MacDonald, M. E. (2005). HD CAG repeat implicates a dominant property of huntingtin in mitochondrial energy metabolism. *Human Molecular Genetics*, *14*(19), 2871–2880. https://doi.org/10.1093/HMG/DDI319

Shenoy, S. A., Zheng, S., Liu, W., Dai, Y., Liu, Y., Hou, Z., Mori, S., Tang, Y., Cheng, J., Duan, W., & Li, C. (2022). A novel and accurate full-length HTT mouse model for Huntington's disease. *ELife*, *11*. https://doi.org/10.7554/ELIFE.70217

Shin, J. W., Kim, K. H., Chao, M. J., Atwal, R. S., Gillis, T., MacDonald, M. E., Gusella, J. F., & Lee, J. M. (2016). Permanent inactivation of Huntington's disease mutation by personalized allele-specific CRISPR/Cas9. *Human Molecular Genetics*, *25*(20), 4566–4576. https://doi.org/10.1093/HMG/DDW286

Shin, J. W., Hong, E. P., Park, S. S., Choi, D. E., Zeng, S., Chen, R. Z., & Lee, J. M. (2022a). PAM-altering SNP-based allele-specific CRISPR-Cas9 therapeutic strategies for Huntington's disease. *Molecular Therapy - Methods & Clinical Development*, *26*, 547–561. https://doi.org/10.1016/J.OMTM.2022.08.005

Shin, J. W., Shin, A., Park, S. S., & Lee, J. M. (2022b). Haplotype-specific insertion-deletion variations for allele-specific targeting in Huntington's disease. *Molecular Therapy - Methods & Clinical Development*, *25*, 84–95. https://doi.org/https://doi.org/10.1016/j.omtm.2022.03.001

Shin, J. W., Hong, E. P., Park, S. S., Choi, D. E., Seong, I. S., Whittaker, M. N., Kleinstiver, B. P., Chen, R. Z., & Lee, J. M. (2022c). Allele-specific silencing of the gain-of-function mutation in Huntington's disease using CRISPR/Cas9. *JCI Insight*, *7*(19). https://doi.org/10.1172/JCI.INSIGHT.141042

Shirasaki, D. I., Greiner, E. R., Al-Ramahi, I., Gray, M., Boontheung, P., Geschwind, D. H., Botas, J., Coppola, G., Horvath, S., Loo, J. A., & Yang, X. W. (2012). Network Organization of the Huntingtin Proteomic Interactome in Mammalian Brain. *Neuron*, *75*(1), 41–57. https://doi.org/10.1016/J.NEURON.2012.05.024

Siew, J. J., Chen, H. M., Chen, H. Y., Chen, H. L., Chen, C. M., Soong, B. W., Wu, Y. R., Chang, C. P., Chan, Y. C., Lin, C. H., Liu, F. T., & Chern, Y. (2019). Galectin-3 is required for the microglia-mediated brain inflammation in a model of Huntington's disease. *Nature Communications 2019 10:1*, *10*(1), 1–18. https://doi.org/10.1038/s41467-019-11441-0

Simpson, B. P., Yrigollen, C. M., Izda, A., & Davidson, B. L. (2023). Targeted long-read sequencing captures CRISPR editing and AAV integration outcomes in brain. *Molecular Therapy*, *0*(0). https://doi.org/10.1016/j.ymthe.2023.01.004

Sipione, S., Rigamonti, D., Valenza, M., Zuccato, C., Conti, L., Pritchard, J., Kooperberg, C., Olson, J. M., & Cattaneo, E. (2002). Early transcriptional profiles in huntingtin-inducible striatal cells by microarray analyses. *Human Molecular Genetics*, *11*(17), 1953–1965. https://doi.org/10.1093/HMG/11.17.1953

Slow, E. J., van Raamsdonk, J., Rogers, D., Coleman, S. H., Graham, R. K., Deng, Y., Oh, R., Bissada, N., Hossain, S. M., Yang, Y. Z., Li, X. J., Simpson, E. M., Gutekunst, C. A., Leavitt, B. R., & Hayden, M. R. (2003). Selective striatal neuronal loss in a YAC128 mouse model of Huntington disease. *Human Molecular Genetics*, *12*(13), 1555–1567. https://doi.org/10.1093/HMG/DDG169

Smith, E. J., Farshim, P. P., Flomen, R., Jones, S. T., McAteer, S. J., Deverman, B. E., Gradinaru, V., & Bates, G. P. (2021). Use of high-content imaging to quantify transduction of AAV-PHP viruses in the brain following systemic delivery. *Brain Communications*, *3*(2), 105. https://doi.org/https://doi.org/10.1093/braincomms/fcab105

Snell, R. G., Lazarou, L. P., Youngman, S., Quarrell, O. W. J., Wasmuth, J. J., Shaw, D. J., & Harper, P. S. (1989). Linkage disequilibrium in Huntington's disease: an improved localisation for the gene. *Journal of Medical Genetics*, *26*(11), 673–675. https://doi.org/10.1136/JMG.26.11.673

Snell, R. G., Macmillan, J. C., Cheadle, J. P., Fenton, I., Lazarou, L. P., Davies, P., Macdonald, M. E., Gusella, J. F., Harper, P. S., & Shaw, D. J. (1993). Relationship between trinucleotide repeat expansion and phenotypic variation in Huntington's disease. *Nature Genetics 1993 4:4*, *4*(4), 393–397. https://doi.org/10.1038/ng0893-393

Song, C., Zhang, Y., Parsons, C. G., & Liu, Y. F. (2003). Expression of Polyglutamine-expanded Huntingtin Induces Tyrosine Phosphorylation of N-Methyl-D-aspartate Receptors. *Journal of Biological Chemistry*, *278*(35), 33364–33369. https://doi.org/10.1074/JBC.M304240200

Song, Chen, J., Petrilli, A., Liot, G., Klinglmayr, E., Zhou, Y., Poquiz, P., Tjong, J., Pouladi, M. A., Hayden, M. R., Masliah, E., Ellisman, M., Rouiller, I., Schwarzenbacher, R., Bossy, B., Perkins, G., & Bossy-Wetzel, E. (2011). Mutant huntingtin binds the mitochondrial fission GTPase dynamin-related protein-1 and increases its enzymatic activity. *Nature Medicine 2011 17:3*, *17*(3), 377–382. https://doi.org/10.1038/nm.2313

Sotrel, A., Paskevich, P. A., Kiely, D. K., Bird, E. D., Williams, R. S., & Myers, R. H. (1991). Morphometric analysis of the prefrontal cortex in Huntington's disease. *Neurology*, *41*(7), 1117–1117. https://doi.org/10.1212/WNL.41.7.1117

Southwell, A. L., Kordasiewicz, H. B., Langbehn, D., Skotte, N. H., Parsons, M. P., Villanueva, E. B., Caron, N. S., Ostergaard, M. E., Anderson, L. M., Xie, Y., Cengio, L. D., Findlay-Black, H., Doty, C. N., Fitsimmons, B., Swayze, E. E., Seth, P. P., Raymond, L. A., Bennett, C. F., & Hayden, M. R. (2018). Huntingtin suppression restores cognitive function in a mouse model of Huntington's disease. *Science Translational Medicine*, *10*(461), 3959. https://doi.org/10.1126/SCITRANSLMED.AAR3959/SUPPL_FILE/AAR3959_TABLE_S6.XLSX

Southwell, A. L., Skotte, N. H., Kordasiewicz, H. B., Østergaard, M. E., Watt, A. T., Carroll, J. B., Doty, C. N., Villanueva, E. B., Petoukhov, E., Vaid, K., Xie, Y., Freier, S. M., Swayze, E. E., Seth, P. P., Bennett, C. F., & Hayden, M. R. (2014). In Vivo Evaluation of Candidate Allele-specific Mutant Huntingtin Gene

Silencing Antisense Oligonucleotides. *Molecular Therapy*, *22*(12), 2093–2106. https://doi.org/10.1038/MT.2014.153

Southwell, A. L., Skotte, N. H., Villanueva, E. B., Østergaard, M. E., Gu, X., Kordasiewicz, H. B., Kay, C., Cheung, D., Xie, Y., Waltl, S., Cengio, L. D., Findlay-Black, H., Doty, C. N., Petoukhov, E., Iworima, D., Slama, R., Ooi, J., Pouladi, M. A., Yang, X. W., … Hayden, M. R. (2017). A novel humanized mouse model of Huntington disease for preclinical development of therapeutics targeting mutant huntingtin alleles. *Human Molecular Genetics*, *26*(6), 1115–1132. https://doi.org/10.1093/HMG/DDX021

Southwell, A. L., Smith, S. E. P., Davis, T. R., Caron, N. S., Villanueva, E. B., Xie, Y., Collins, J. A., Li Ye, M., Sturrock, A., Leavitt, B. R., Schrum, A. G., & Hayden, M. R. (2015). Ultrasensitive measurement of huntingtin protein in cerebrospinal fluid demonstrates increase with Huntington disease stage and decrease following brain huntingtin suppression. *Scientific Reports 2015 5:1*, *5*(1), 1–11. https://doi.org/10.1038/srep12166

Southwell, A. L., Warby, S. C., Carroll, J. B., Doty, C. N., Skotte, N. H., Zhang, W., Villanueva, E. B., Kovalik, V., Xie, Y., Pouladi, M. A., Collins, J. A., Yang, X. W., Franciosi, S., & Hayden, M. R. (2013). A fully humanized transgenic mouse model of Huntington disease. *Human Molecular Genetics*, *22*(1), 18–34. https://doi.org/https://doi.org/10.1093/hmg/dds397

Steffan, J. S., Kazantsev, A., Spasic-Boskovic, O., Greenwald, M., Zhu, Y. Z., Gohler, H., Wanker, E. E., Bates, G. P., Housman, D. E., & Thompson, L. M. (2000). The Huntington's disease protein interacts with p53 and CREB-binding protein and represses transcription. *Proceedings of the National Academy of Sciences of the United States of America*, *97*(12), 6763–6768. https://doi.org/10.1073/PNAS.100110097/ASSET/835A51E6-43FB-4DE4-8B77-11F877BA26AF/ASSETS/GRAPHIC/PQ1001100003.JPEG

Stoker, T. B., Mason, S. L., Greenland, J. C., Holden, S. T., Santini, H., & Barker, R. A. (2022). Huntington's disease: diagnosis and management. *Practical Neurology*, *22*(1), 32–41. https://doi.org/10.1136/PRACTNEUROL-2021-003074

Strand, A. D., Baquet, Z. C., Aragaki, A. K., Holmans, P., Yang, L., Cleren, C., Beal, M. F., Jones, L., Kooperberg, C., Olson, J. M., & Jones, K. R. (2007). Expression Profiling of Huntington's Disease Models Suggests That Brain-Derived Neurotrophic Factor Depletion Plays a Major Role in Striatal Degeneration. *Journal of Neuroscience*, *27*(43), 11758–11768. https://doi.org/10.1523/JNEUROSCI.2461-07.2007

Sun, Y., Savanenin, A., Reddy, P. H., & Liu, Y. F. (2001). Polyglutamine-expanded Huntingtin Promotes Sensitization of N-Methyl-d-aspartate Receptors via Post-synaptic Density 95. *Journal of Biological Chemistry*, *276*(27), 24713–24718. https://doi.org/10.1074/JBC.M103501200

Suzuki, K., Tsunekawa, Y., Hernandez-Benitez, R., Wu, J., Zhu, J., Kim, E. J., Hatanaka, F., Yamamoto, M., Araoka, T., Li, Z., Kurita, M., Hishida, T., Li, M., Aizawa, E., Guo, S., Chen, S., Goebl, A., Soligalla, R. D., Qu, J., … Belmonte, J. C. I. (2016). In vivo genome editing via CRISPR/Cas9 mediated homology-independent targeted integration. *Nature 2016 540:7631*, *540*(7631), 144–149. https://doi.org/10.1038/nature20565

Suzuki, K., Yamamoto, M., Hernandez-Benitez, R., Li, Z., Wei, C., Soligalla, R. D., Aizawa, E., Hatanaka, F., Kurita, M., Reddy, P., Ocampo, A., Hishida, T., Sakurai, M., Nemeth, A. N., Nuñez Delicado, E., Campistol, J. M., Magistretti, P., Guillen, P., Rodriguez Esteban, C., … Izpisua Belmonte, J. C. (2019). Precise in vivo genome editing via single homology arm donor mediated intron-targeting gene integration for genetic disease correction. *Cell Research 2019 29:10*, *29*(10), 804–819. https://doi.org/10.1038/s41422-019-0213-0

Swami, M., Hendricks, A. E., Gillis, T., Massood, T., Mysore, J., Myers, R. H., & Wheeler, V. C. (2009). Somatic expansion of the Huntington's disease CAG repeat in the brain is associated with an earlier age of disease onset. *Human Molecular Genetics*, *18*(16), 3039–3047. https://doi.org/10.1093/HMG/DDP242

Tabrizi, S. J., Schobel, S., Gantman, E. C., Mansbach, A., Borowsky, B., Konstantinova, P., Mestre, T. A., Panagoulias, J., Ross, C. A., Zauderer, M., Mullin, A. P., Romero, K., Sivakumaran, S., Turner, E. C., Long, J. D., & Sampaio, C. (2022a). A biological classification of Huntington's disease: the Integrated Staging System. *The Lancet Neurology*, *21*(7), 632–644. https://doi.org/10.1016/S1474-4422(22)00120-X

Tabrizi, S. J., Estevez-Fraga, C., van Roon-Mom, W. M. C., Flower, M. D., Scahill, R. I., Wild, E. J., Muñoz-

Sanjuan, I., Sampaio, C., Rosser, A. E., & Leavitt, B. R. (2022b). Potential disease-modifying therapies for Huntington's disease: lessons learned and future opportunities. *The Lancet Neurology*, *21*(7), 645–658. https://doi.org/10.1016/S1474-4422(22)00121-1

Tabrizi, S. J., Flower, M. D., Ross, C. A., & Wild, E. J. (2020). Huntington disease: new insights into molecular pathogenesis and therapeutic opportunities. *Nature Reviews Neurology*, *16*(10), 529–546. https://doi.org/https://doi.org/10.1038/s41582-020-0389-4

Tabrizi, S. J., Leavitt, B. R., Landwehrmeyer, G. B., Wild, E. J., Saft, C., Barker, R. A., Blair, N. F., Craufurd, D., Priller, J., Rickards, H., Rosser, A., Kordasiewicz, H. B., Czech, C., Swayze, E. E., Norris, D. A., Baumann, T., Gerlach, I., Schobel, S. A., Paz, E., … Lane, R. M. (2019). Targeting Huntingtin Expression in Patients with Huntington's Disease. *New England Journal of Medicine*, *380*(24), 2307–2316. https://doi.org/10.1056/NEJMOA1900907/SUPPL_FILE/NEJMOA1900907_DATA-SHARING.PDF

Tabrizi, S. J., Reilmann, R., Roos, R. A. C., Durr, A., Leavitt, B., Owen, G., Jones, R., Johnson, H., Craufurd, D., Hicks, S. L., Kennard, C., Landwehrmeyer, B., Stout, J. C., Borowsky, B., Scahill, R. I., Frost, C., & Langbehn, D. R. (2012). Potential endpoints for clinical trials in premanifest and early Huntington's disease in the TRACK-HD study: analysis of 24 month observational data. *The Lancet Neurology*, *11*(1), 42–53. https://doi.org/10.1016/S1474-4422(11)70263-0

Tabrizi, S. J., Scahill, R. I., Durr, A., Roos, R. A. C., Leavitt, B. R., Jones, R., Landwehrmeyer, G. B., Fox, N. C., Johnson, H., Hicks, S. L., Kennard, C., Craufurd, D., Frost, C., Langbehn, D. R., Reilmann, R., & Stout, J. C. (2011). Biological and clinical changes in premanifest and early stage Huntington's disease in the TRACK-HD study: the 12-month longitudinal analysis. *The Lancet Neurology*, *10*(1), 31–42. https://doi.org/10.1016/S1474-4422(10)70276-3

Tabrizi, S. J., Scahill, R. I., Owen, G., Durr, A., Leavitt, B. R., Roos, R. A., Borowsky, B., Landwehrmeyer, B., Frost, C., Johnson, H., Craufurd, D., Reilmann, R., Stout, J. C., & Langbehn, D. R. (2013). Predictors of phenotypic progression and disease onset in premanifest and early-stage Huntington's disease in the TRACK-HD study: Analysis of 36-month observational data. *The Lancet Neurology*, *12*(7), 637–649. https://doi.org/10.1016/S1474-4422(13)70088-7

Tai, C. H., Lee, N. C., Chien, Y. H., Byrne, B. J., Muramatsu, S. I., Tseng, S. H., & Hwu, W. L. (2022). Long-term efficacy and safety of eladocagene exuparvovec in patients with AADC deficiency. *Mol Ther*, *30*(2), 509–518. https://doi.org/https://doi.org/10.1016/j.ymthe.2021.11.005

Takahashi, K., Tanabe, K., Ohnuki, M., Narita, M., Ichisaka, T., Tomoda, K., & Yamanaka, S. (2007). Induction of Pluripotent Stem Cells from Adult Human Fibroblasts by Defined Factors. *Cell*, *131*(5), 861–872. https://doi.org/10.1016/J.CELL.2007.11.019

Tanaka, K., Shouguchi-Miyata, J., Miyamoto, N., & Ikeda, J. E. (2004). Novel Nuclear Shuttle Proteins, HDBP1 and HDBP2, Bind to Neuronal Cell-specific cis-Regulatory Element in the Promoter for the Human Huntington's Disease Gene. *Journal of Biological Chemistry*, *279*(8), 7275–7286. https://doi.org/10.1074/JBC.M310726200

Taran, A. S., Shuvalova, L. D., Lagarkova, M. A., & Alieva, I. B. (2020). Huntington's Disease—An Outlook on the Interplay of the HTT Protein, Microtubules and Actin Cytoskeletal Components. *Cells 2020, Vol. 9, Page 1514*, *9*(6), 1514. https://doi.org/10.3390/CELLS9061514

Taylor, J. P., Tanaka, F., Robitschek, J., Sandoval, C. M., Taye, A., Markovic-Plese, S., & Fischbeck, K. H. (2003). Aggresomes protect cells by enhancing the degradation of toxic polyglutamine-containing protein. *Human Molecular Genetics*, *12*(7), 749–757. https://doi.org/10.1093/HMG/DDG074

Tervo, D. G. R., Hwang, B. Y., Viswanathan, S., Gaj, T., Lavzin, M., Ritola, K. D., Lindo, S., Michael, S., Kuleshova, E., Ojala, D., Huang, C. C., Gerfen, C. R., Schiller, J., Dudman, J. T., Hantman, A. W., Looger, L. L., Schaffer, D. V., & Karpova, A. Y. (2016). A Designer AAV Variant Permits Efficient Retrograde Access to Projection Neurons. *Neuron*, *92*(2), 372–382. https://doi.org/https://doi.org/10.1016/j.neuron.2016.09.021

Thompson, J. A., Cruickshank, T. M., Penailillo, L. E., Lee, J. W., Newton, R. U., Barker, R. A., & Ziman, M. R. (2013). The effects of multidisciplinary rehabilitation in patients with early-to-middle-stage Huntington's disease: a pilot study. *European Journal of Neurology*, *20*(9), 1325–1329. https://doi.org/10.1111/ENE.12053

Thomson, S. B., & Leavitt, B. R. (2018). Transcriptional Regulation of the Huntingtin Gene. *Journal of Huntington's Disease*, *7*(4), 289–296. https://doi.org/10.3233/JHD-180331

Tong, Ao, Y., Faas, G. C., Nwaobi, S. E., Xu, J., Haustein, M. D., Anderson, M. A., Mody, I., Olsen, M. L.,

Sofroniew, M. V., & Khakh, B. S. (2014). Astrocyte Kir4.1 ion channel deficits contribute to neuronal dysfunction in Huntington's disease model mice. *Nature Neuroscience 2014 17:5*, *17*(5), 694–703. https://doi.org/10.1038/nn.3691

Tong, Y., Ha, T. J., Liu, L., Nishimoto, A., Reiner, A., & Goldowitz, D. (2011). Spatial and Temporal Requirements for huntingtin (Htt) in Neuronal Migration and Survival during Brain Development. *Journal of Neuroscience*, *31*(41), 14794–14799. https://doi.org/10.1523/JNEUROSCI.2774-11.2011

Trovato, B., Magrì, B., Castorina, A., Maugeri, G., D'agata, V., & Musumeci, G. (2022). Effects of Exercise on Skeletal Muscle Pathophysiology in Huntington’s Disease. *Journal of Functional Morphology and Kinesiology 2022, Vol. 7, Page 40*, *7*(2), 40. https://doi.org/10.3390/JFMK7020040

Vale, T. C., & Cardoso, F. (2015). Chorea: A Journey through History. *Tremor and Other Hyperkinetic Movements*, *5*(0), 5. https://doi.org/10.5334/TOHM.275/METRICS/

Valles, A., Evers, M. M., Stam, A., Gonzalez, M. S., Brouwers, C., Tornero, C. V., Broekmans, S. A., Paerels, L., Klima, J., Bohuslavova, B., Pintauro, R., Fodale, V., Bresciani, A., Liscak, R., Urgosik, D., Starek, Z., Crha, M., Blits, B., Petry, H., … Konstantinova, P. (2021). Widespread and sustained target engagement in Huntington s disease minipigs upon intrastriatal microRNA-based gene therapy. *Science Translational Medicine*, *13*(588). https://doi.org/10.1126/SCITRANSLMED.ABB8920/SUPPL_FILE/ABB8920_SM.PDF

van der Burg, J. M., Björkqvist, M., & Brundin, P. (2009). Beyond the brain: widespread pathology in Huntington's disease. *The Lancet Neurology*, *8*(8), 765–774. https://doi.org/10.1016/S1474-4422(09)70178-4

Van Raamsdonk, J. M., Pearson, J., Murphy, Z., Hayden, M. R., & Leavitt, B. R. (2006). Wild-type huntingtin ameliorates striatal neuronal atrophy but does not prevent other abnormalities in the YAC128 mouse model of Huntington disease. *BMC Neuroscience*, *7*(1), 1–9. https://doi.org/10.1186/1471-2202-7-80/TABLES/2

Vanamee, É. S., Santagata, S., & Aggarwal, A. K. (2001). FokI requires two specific DNA sites for cleavage. *Journal of Molecular Biology*, *309*(1), 69–78. https://doi.org/10.1006/JMBI.2001.4635

Verkuijl, S. A., & Rots, M. G. (2019). The influence of eukaryotic chromatin state on CRISPR–Cas9 editing efficiencies. *Current Opinion in Biotechnology*, *55*, 68–73. https://doi.org/10.1016/J.COPBIO.2018.07.005

Waelter, S., Scherzinger, E., Hasenbank, R., Nordhoff, E., Lurz, R., Goehler, H., Gauss, C., Sathasivam, K., Bates, G. P., Lehrach, H., & Wanker, E. E. (2001a). The huntingtin interacting protein HIP1 is a clathrin and α-adaptin-binding protein involved in receptor-mediated endocytosis. *Human Molecular Genetics*, *10*(17), 1807–1817. https://doi.org/10.1093/HMG/10.17.1807

Waelter, S., Boeddrich, A., Lurz, R., Scherzinger, E., Lueder, G., Lehrach, H., & Wanker, E. E. (2001b). Accumulation of mutant huntingtin fragments in aggresome-like inclusion bodies as a result of insufficient protein degradation. *Molecular Biology of the Cell*, *12*(5), 1393–1407. https://doi.org/10.1091/MBC.12.5.1393/ASSET/IMAGES/LARGE/MK0511501009.JPEG

Waldvogel, H. J., Kim, E. H., Tippett, L. J., Vonsattel, J. P. G., & Faull, R. L. M. (2014). The neuropathology of Huntington's disease. *Current Topics in Behavioral Neurosciences*, *22*, 33–80. https://doi.org/10.1007/7854_2014_354/COVER

Walton, R. T., Christie, K. A., Whittaker, M. N., & Kleinstiver, B. P. (2020). Unconstrained genome targeting with near-PAMless engineered CRISPR-Cas9 variants. *Science*, *368*(6488), 290–296. https://doi.org/10.1126/SCIENCE.ABA8853/SUPPL_FILE/ABA8853_WALTON_SM.PDF

Wang, D., Tai, P. W. L., & Gao, G. (2019). Adeno-associated virus vector as a platform for gene therapy delivery. *Nature Reviews Drug Discovery*, *18*(5), 358–378. https://doi.org/10.1038/s41573-019-0012-9

Wang, Ding, S. L., Li, Y., Royall, J., Feng, D., Lesnar, P., Graddis, N., Naeemi, M., Facer, B., Ho, A., Dolbeare, T., Blanchard, B., Dee, N., Wakeman, W., Hirokawa, K. E., Szafer, A., Sunkin, S. M., Oh, S. W., Bernard, A., … Ng, L. (2020). The Allen Mouse Brain Common Coordinate Framework: A 3D Reference Atlas. *Cell*, *181*(4), 936–953. https://doi.org/https://doi.org/10.1016/j.cell.2020.04.007

Wang, Liu, W., Wada, E., Murata, M., Wada, K., & Kanazawa, I. (2005). Clinico-pathological rescue of a model mouse of Huntington's disease by siRNA. *Neuroscience Research*, *53*(3), 241–249. https://doi.org/10.1016/J.NEURES.2005.06.021

Wang, Liu, X., Gaertig, M. A., Li, S., & Li, X. J. (2016). Ablation of huntingtin in adult neurons is nondeleterious but its depletion in young mice causes acute pancreatitis. *Proceedings of the National*

Academy of Sciences of the United States of America, *113*(12), 3359–3364. https://doi.org/10.1073/PNAS.1524575113/-/DCSUPPLEMENTAL

Wang, Zhang, Y. F., Guo, S., Zhao, Q., Zeng, Y., Xie, Z., Xie, X., Lu, B., & Hu, Y. (2021). GPR52 Antagonist Reduces Huntingtin Levels and Ameliorates Huntington's Disease-Related Phenotypes. *Journal of Medicinal Chemistry*, *64*(2), 941–957. https://doi.org/10.1021/ACS.JMEDCHEM.0C01133/SUPPL_FILE/JM0C01133_SI_002.CSV

Warby, S. C., Montpetit, A., Hayden, A. R., Carroll, J. B., Butland, S. L., Visscher, H., Collins, J. A., Semaka, A., Hudson, T. J., & Hayden, M. R. (2009). CAG Expansion in the Huntington Disease Gene Is Associated with a Specific and Targetable Predisposing Haplogroup. *The American Journal of Human Genetics*, *84*(3), 351–366. https://doi.org/10.1016/J.AJHG.2009.02.003

Warby, S. C., Visscher, H., Collins, J. A., Doty, C. N., Carter, C., Butland, S. L., Hayden, A. R., Kanazawa, I., Ross, C. J., & Hayden, M. R. (2011). HTT haplotypes contribute to differences in Huntington disease prevalence between Europe and East Asia. *European Journal of Human Genetics*, *19*(5), 561–566. https://doi.org/10.1038/ejhg.2010.229

Warner, J. H., Long, J. D., Mills, J. A., Langbehn, D. R., Ware, J., Mohan, A., & Sampaio, C. (2022). Standardizing the CAP Score in Huntington's Disease by Predicting Age-at-Onset. *Journal of Huntington's Disease*, *11*(2), 153–171. https://doi.org/10.3233/JHD-210475

Waters, C. (1842). *Description of chorea* (Dunglison). Lea & Blanchard.

Weiss, A. R., Liguore, W. A., Domire, J. S., Button, D., & McBride, J. L. (2020). Intra-striatal AAV2.retro administration leads to extensive retrograde transport in the rhesus macaque brain: implications for disease modeling and therapeutic development. *Scientific Reports*, *10*(1), 1–14. https://doi.org/https://doi.org/10.1038/s41598-020-63559-7

Wexler, N. S., Young, A. B., Tanzi, R. E., Travers, H., Starosta-Rubinstein, S., Penney, J. B., Snodgrass, S. R., Shoulson, I., Gomez, F., Arroyo, M. A. R., Penchaszadeh, G. K., Moreno, H., Gibbons, K., Faryniarz, A., Hobbs, W., Anderson, M. A., Bonilla, E., Conneally, P. M., & Gusella, J. F. (1987). Homozygotes for Huntington's disease. *Nature*, *326*(6109), 194–197. https://doi.org/10.1038/326194a0

Wilton, D. K., & Stevens, B. (2020). The contribution of glial cells to Huntington's disease pathogenesis. *Neurobiology of Disease*, *143*, 104963. https://doi.org/10.1016/J.NBD.2020.104963

Wood, T. E., Barry, J., Yang, Z., Cepeda, C., Levine, M. S., & Gray, M. (2019). Mutant huntingtin reduction in astrocytes slows disease progression in the BACHD conditional Huntington's disease mouse model. *Human Molecular Genetics*, *28*(3), 487–500. https://doi.org/10.1093/HMG/DDY363

Wright, A. V., Nuñez, J. K., & Doudna, J. A. (2016). Biology and Applications of CRISPR Systems: Harnessing Nature's Toolbox for Genome Engineering. *Cell*, *164*(1–2), 29–44. https://doi.org/10.1016/J.CELL.2015.12.035

Wu, J., Corbett, A. H., & Berland, K. M. (2009). The Intracellular Mobility of Nuclear Import Receptors and NLS Cargoes. *Biophysical Journal*, *96*(9), 3840–3849. https://doi.org/10.1016/J.BPJ.2009.01.050

Xu, H., An, J. J., & Xu, B. (2017). Distinct cellular toxicity of two mutant huntingtin mRNA variants due to translation regulation. *PLOS ONE*, *12*(5), e0177610. https://doi.org/10.1371/JOURNAL.PONE.0177610

Yablonska, S., Ganesan, V., Ferrando, L. M., Kim, J. H., Pyzel, A., Baranova, O. V., Khattar, N. K., Larkin, T. M., Baranov, S. V., Chen, N., Strohlein, C. E., Stevens, D. A., Wang, X., Chang, Y. F., Schurdak, M. E., Carlisle, D. L., Minden, J. S., & Friedlander, R. M. (2019). Mutant huntingtin disrupts mitochondrial proteostasis by interacting with TIM23. *Proceedings of the National Academy of Sciences of the United States of America*, *116*(33), 16593–16602. https://doi.org/10.1073/PNAS.1904101116/SUPPL_FILE/PNAS.1904101116.SAPP.PDF

Yan, S., Zheng, X., Lin, Y., Li, C., Liu, Z., Li, J., Tu, Z., Zhao, Y., Huang, C., Chen, Y., Li, J., Song, X., Han, B., Wang, W., Liang, W., Lai, L., Li, X.-J., & Li, S. (2023). Cas9-mediated replacement of expanded CAG repeats in a pig model of Huntington's disease. *Nature Biomedical Engineering 2023*, 1–18. https://doi.org/10.1038/s41551-023-01007-3

Yang, Cheng, P. H., Banta, H., Piotrowska-Nitsche, K., Yang, J. J., Cheng, E. C. H., Snyder, B., Larkin, K., Liu, J., Orkin, J., Fang, Z. H., Smith, Y., Bachevalier, J., Zola, S. M., Li, S. H., Li, X. J., & Chan, A. W. S. (2008). Towards a transgenic model of Huntington's disease in a non-human primate. *Nature 2008 453:7197*, *453*(7197), 921–924. https://doi.org/10.1038/nature06975

Yang, S., Chang, R., Yang, H., Zhao, T., Hong, Y., Kong, H. E., Sun, X., Qin, Z., Jin, P., Li, S., & Li, X. J.

(2017). CRISPR/Cas9-mediated gene editing ameliorates neurotoxicity in mouse model of Huntington's disease. *The Journal of Clinical Investigation*, *127*(7), 2719–2724. https://doi.org/https://doi.org/10.1172/jci92087

Yang, Yang, S., Jing, L., Huang, L., Chen, L., Zhao, X., Yang, W., Pan, Y., Yin, P., Qin, Z. S., Li, S., & Li, X. J. (2020a). Truncation of mutant huntingtin in knock-in mice demonstrates exon1 huntingtin is a key pathogenic form. *Nature Communications 2020 11:1*, *11*(1), 1–15. https://doi.org/10.1038/s41467-020-16318-1

Yang, Yang, H., Huang, L., Chen, L., Qin, Z., Li, S., & Li, X. J. (2020b). Lack of RAN-mediated toxicity in Huntington's disease knock-in mice. *Proceedings of the National Academy of Sciences of the United States of America*, *117*(8), 4411–4417. https://doi.org/10.1073/PNAS.1919197117/-/DCSUPPLEMENTAL

Yao, Cui, X., Al-Ramahi, I., Sun, X., Li, B., Hou, J., Difiglia, M., Palacino, J., Wu, Z. Y., Ma, L., Botas, J., & Lu, B. (2015). A striatal-enriched intronic GPCR modulates huntingtin levels and toxicity. *ELife*, *2015*(4). https://doi.org/10.7554/ELIFE.05449

Yao, X., Wang, X., Liu, J., Hu, X., Shi, L., Shen, X., Ying, W., Sun, X., Wang, X., Huang, P., & Yang, H. (2017a). CRISPR/Cas9 – Mediated Precise Targeted Integration In Vivo Using a Double Cut Donor with Short Homology Arms. *EBioMedicine*, *20*, 19–26. https://doi.org/10.1016/J.EBIOM.2017.05.015/ATTACHMENT/97AA1855-7027-42B8-9A03-6A3211BB23B7/MMC1.DOCX

Yao, X., Wang, X., Hu, X., Liu, Z., Liu, J., Zhou, H., Shen, X., Wei, Y., Huang, Z., Ying, W., Wang, Y., Nie, Y. H., Zhang, C. C., Li, S., Cheng, L., Wang, Q., Wu, Y., Huang, P., Sun, Q., … Yang, H. (2017b). Homology-mediated end joining-based targeted integration using CRISPR/Cas9. *Cell Research*, *27*(6), 801–814. https://doi.org/10.1038/cr.2017.76

Yeh, C. D., Richardson, C. D., & Corn, J. E. (2019). Advances in genome editing through control of DNA repair pathways. *Nature Cell Biology*, *21*(12), 1468–1478. https://doi.org/10.1038/s41556-019-0425-z

Yu, J., Vodyanik, M. A., Smuga-Otto, K., Antosiewicz-Bourget, J., Frane, J. L., Tian, S., Nie, J., Jonsdottir, G. A., Ruotti, V., Stewart, R., Slukvin, I. I., & Thomson, J. A. (2007). Induced pluripotent stem cell lines derived from human somatic cells. *Science*, *318*(5858), 1917–1920. https://doi.org/10.1126/SCIENCE.1151526/SUPPL_FILE/YU.SOM.REVISION.1.PDF

Yu, Taylor, A. M. W., Nagai, J., Golshani, P., Evans, C. J., Coppola, G., & Khakh, B. S. (2018). Reducing Astrocyte Calcium Signaling In Vivo Alters Striatal Microcircuits and Causes Repetitive Behavior. *Neuron*, *99*(6), 1170-1187.e9. https://doi.org/10.1016/J.NEURON.2018.08.015

Zeitler, B., Froelich, S., Marlen, K., Shivak, D. A., Yu, Q., Li, D., Pearl, J. R., Miller, J. C., Zhang, L., Paschon, D. E., Hinkley, S. J., Ankoudinova, I., Lam, S., Guschin, D., Kopan, L., Cherone, J. M., Nguyen, H. O. B., Qiao, G., Ataei, Y., … Zhang, H. S. (2019). Allele-selective transcriptional repression of mutant HTT for the treatment of Huntington's disease. *Nature Medicine*, *25*(7), 1131–1142. https://doi.org/10.1038/s41591-019-0478-3

Zeitlin, S., Liu, J. P., Chapman, D. L., Papaioannou, V. E., & Efstratiadis, A. (1995). Increased apoptosis and early embryonic lethality in mice nullizygous for the Huntington's disease gene homologue. *Nature Genetics 1995 11:2*, *11*(2), 155–163. https://doi.org/10.1038/ng1095-155

Zhang, An, M. C., Montoro, D., & Ellerby, L. M. (2010). Characterization of Human Huntington's Disease Cell Model from Induced Pluripotent Stem Cells. *PLoS Currents*, *2*(OCT), 1–11. https://doi.org/10.1371/CURRENTS.RRN1193

Zhang, L., Rube, H. T., Vakulskas, C. A., Behlke, M. A., Bussemaker, H. J., & Pufall, M. A. (2020). Systematic in vitro profiling of off-target affinity, cleavage and efficiency for CRISPR enzymes. *Nucleic Acids Research*, *48*(9), 5037–5053. https://doi.org/10.1093/NAR/GKAA231

Zhang, Long, J. D., Mills, J. A., Warner, J. H., Lu, W., & Paulsen, J. S. (2011). Indexing disease progression at study entry with individuals at-risk for Huntington disease. *American Journal of Medical Genetics Part B: Neuropsychiatric Genetics*, *156*(7), 751–763. https://doi.org/10.1002/AJMG.B.31232

Zhang, Yao, X., Yin, X., Ding, Z., Huang, T., Huo, Y., Ji, R., Peng, H., & Guo, Z. V. (2021). Multi-Scale Light-Sheet Fluorescence Microscopy for Fast Whole Brain Imaging. *Frontiers in Neuroanatomy*, *15*, 63. https://doi.org/https://doi.org/10.3389/fnana.2021.732464

Zhao, P., Zhang, Z., Lv, X., Zhao, X., Suehiro, Y., Jiang, Y., Wang, X., Mitani, S., Gong, H., & Xue, D. (2016). One-step homozygosity in precise gene editing by an improved CRISPR/Cas9 system. *Cell*

Research 2016 26:5, *26*(5), 633–636. https://doi.org/10.1038/cr.2016.46

Zhu, L. J., Holmes, B. R., Aronin, N., & Brodsky, M. H. (2014). CRISPRseek: A Bioconductor Package to Identify Target-Specific Guide RNAs for CRISPR-Cas9 Genome-Editing Systems. *PLOS ONE*, *9*(9), e108424. https://doi.org/10.1371/JOURNAL.PONE.0108424

Zhu, Schieferecke, A. J., Lopez, P. A., & Schaffer, D. V. (2021). Adeno-Associated Virus Vector for Central Nervous System Gene Therapy. *Trends in Molecular Medicine*, *27*(6), 524–537. https://doi.org/10.1016/J.MOLMED.2021.03.010

Zuccato, C., & Cattaneo, E. (2015). Huntington's disease. *Handbook of Experimental Pharmacology*, *220*, 357–409. https://doi.org/10.1007/978-3-642-45106-5_14/COVER

Zuccato, C., Valenza, M., & Cattaneo, E. (2010). Molecular mechanisms and potential therapeutical targets in Huntington's disease. *Physiological Reviews*, *90*(3), 905–981. https://doi.org/10.1152/PHYSREV.00041.2009/ASSET/IMAGES/LARGE/Z9J0031025490010.JPEG

Zufferey, R., Dull, T., Mandel, R. J., Bukovsky, A., Quiroz, D., Naldini, L., & Trono, D. (1998). Self-Inactivating Lentivirus Vector for Safe and Efficient In Vivo Gene Delivery. *Journal of Virology*, *72*(12), 9873–9880. https://doi.org/10.1128/JVI.72.12.9873-9880.1998/ASSET/34005AA5-87A5-4E0D-8A14-AF1960E1277B/ASSETS/GRAPHIC/JV1280899005.JPEG

7. Annex

REVIEW

Genome Editing for CNS Disorders

frontiers in Neuroscience

REVIEW
published: 22 October 2020
doi: 10.3389/fnins.2020.579062

Genome Editing for CNS Disorders

Fábio Duarte[1,2] *and Nicole Déglon*[1,2]*

[1] Laboratory of Neurotherapies and NeuroModulation, Department of Clinical Neurosciences, Lausanne University Hospital and Lausanne University, Lausanne, Switzerland, [2] Laboratory of Neurotherapies and NeuroModulation, Neuroscience Research Center, Lausanne University Hospital and Lausanne University, Lausanne, Switzerland

Central nervous system (CNS) disorders have a social and economic burden on modern societies, and the development of effective therapies is urgently required. Gene editing may prevent or cure a disease by inducing genetic changes at endogenous loci. Genome editing includes not only the insertion, deletion or replacement of nucleotides, but also the modulation of gene expression and epigenetic editing. Emerging technologies based on ZFs, TALEs, and CRISPR/Cas systems have extended the boundaries of genome manipulation and promoted genome editing approaches to the level of promising strategies for counteracting genetic diseases. The parallel development of efficient delivery systems has also increased our access to the CNS. In this review, we describe the various tools available for genome editing and summarize *in vivo* preclinical studies of CNS genome editing, whilst considering current limitations and alternative approaches to overcome some bottlenecks.

Keywords: CNS, genome editing, ZFs, TALEs, CRISPR/Cas

OPEN ACCESS

Edited by:
Michael F. Miles,
Virginia Commonwealth University, United States

Reviewed by:
Jun Zhang,
Texas Tech University Health Sciences Center, United States
Santhosh Girirajan,
Pennsylvania State University (PSU), United States

***Correspondence:**
Nicole Déglon
nicole.deglon@chuv.ch

Specialty section:
This article was submitted to Neurogenomics, a section of the journal Frontiers in Neuroscience

Received: *01 July 2020*
Accepted: *08 September 2020*
Published: *22 October 2020*

Citation:
Duarte F and Déglon N (2020) Genome Editing for CNS Disorders. Front. Neurosci. 14:579062. doi: 10.3389/fnins.2020.579062

INTRODUCTION

Neurological disorders are the principal cause of disability and the second leading cause of death worldwide (Feigin et al., 2019). Central nervous system (CNS) diseases include diverse infections (meningitis and encephalitis), vascular disorders (stroke and other hemorrhages), structural (brain or spinal injury), functional (epilepsy and migraines) and neurodegenerative (Alzheimer's and Parkinson's disease) conditions. With steady increases in the size and age of the world population, the prevalence of these diseases is likely to increase, and they have thus become a priority area of research. The age-standardized frequencies of neurological diseases have declined, but the number of people affected worldwide has continued to increase. The continual aging of the population is, thus, outstripping our ability to counteract these disorders (Feigin et al., 2019).

The development of therapeutic strategies for CNS disorders is challenging, given the considerable diversity of cells involved, the extreme complexity of the neural circuits and associated functions, poor tissue regeneration and our incomplete understanding of the underlying pathological processes. Pharmacological efficacy depends on our ability to take all of these factors into account. For some disorders, such as traumatic and neurodegenerative conditions, the timing of treatment may also be important, with therapeutic success decreasing as neurodegeneration progresses. Moreover, the blood–brain barrier (BBB) limits the diffusion of most molecules delivered by conventional methods. Consequently, the doses of drugs delivered systemically often have to be increased to ensure that therapeutic concentrations are reached in the CNS, which may lead to toxicity.

As a result of these challenges, approval rates are much lower for CNS-targeting drugs than for drugs targeting other parts of the body (Kesselheim et al., 2015; Gribkoff and Kaczmarek, 2017). This has led to a revision of CNS drug development guidelines and to the implementation of innovative and efficient therapeutic models. One particular treatment strategy, gene therapy, has progressed remarkably over the last 15 years. It involves the introduction of recombinant nucleic acids into the patient's cells, to fight or prevent a disease (Klug et al., 2012). Two different therapeutic approaches can be used: *ex vivo* and *in vivo*. *Ex vivo* gene therapy entails: (1) the collection of cells from the patient, (2) the culture and modification of these cells *in vitro* and (3) the transplantation of the modified cells back into the recipient. The *in vivo* approach involves modification of cells directly in the individual. One of the major advantages of gene therapy is that it can be used to modify most biological pathways through the targeting of the underlying genes. It can halt or reverse disease progression by targeting the underlying pathogenic processes, whereas conventional medicine often focuses on symptom relief. In addition, stable transgene expression or permanent genome modification may make it possible to treat disorders in a single administration.

The most straightforward application of gene therapy is the treatment of monogenic disorders. A classical approach to the treatment of diseases caused by loss-of-function (LOF) mutations is based on the replacement of the defective gene with the wild-type (WT) cDNA. The treatment of familial lipoprotein lipase deficiency (LPLD) with Glybera (a rAAV1 encoding the lipoprotein lipase variant LPLS447X; Ylä-Herttuala, 2012), a rare form of inherited blindness with Luxturna (a rAAV2 encoding a normal copy of the retinal pigment epithelium-specific 65 kDa protein; Russell et al., 2017), and spinal muscular atrophy (SMA) with Zolgensma (a rAAV9 encoding the survival motor neuron 1 protein; Hoy, 2019) provide examples of approved products. The treatment of autosomal dominant disorders caused by gain-of-function (GOF) mutations generally involves decreasing the levels of mutant mRNA by RNA interference (RNAi) or with antisense oligonucleotides (ASO). An example is provided by mipomersen, an ASO targeting the apolipoprotein B mRNA, which can be used to treat homozygous familial hypercholesterolemia (Hair et al., 2013). Gene therapy products have been also developed to combat genes in which the pathological mutation alters transcript splicing. Examples include eteplirsen for Duchenne muscular dystrophy (DMD) (Syed, 2016) and nusinersen (Spinraza®) for SMA (Hoy, 2017). These products deliver nucleic acids targeting the mutant primary transcripts, and modify the splicing of these transcripts into non-pathogenic isoforms. Finally, gene-based therapeutic approaches have also been successfully used for the treatment of polygenic diseases, such as cancer and infectious diseases (Shahryari et al., 2019). In such cases, the strategies developed target one of the identified pathogenic genes (LOF or GOF) or deliver transgenes encoding factors with protective functions.

Gene replacement approaches have been successfully applied to some disorders, but (1) the size of the transgene may be limited by the delivery system, (2) this approach is usually restricted to the expression of a single gene isoform and (3) the lack of a transgene chromatin signature often results in non-physiological levels of expression (Khabou et al., 2018). Conversely, gene silencing with RNAi/ASO (1) does not completely knockout the pathological gene, and a total knockout may be essential for highly damaging genes, (2) its therapeutic efficacy depend on the turnover of the targeted transcript and (3) may require continuous drug administration to maintain the therapeutic benefit (Sledz and Williams, 2005).

Genome editing has emerged as a complementary gene therapy strategy. It operates at native DNA loci, and can be used for the complete inactivation of a toxic gene, gene repair or regulation of an endogenous gene (Doudna, 2020). Genome editing tools have been available for 30 years, but their limited efficacy, complex production and the lack of efficient delivery vehicles have delayed their clinical application. Over the last decade, more sophisticated and precise editing tools have rendered genome engineering not only promising for gene-based therapeutic approaches, but also useful as a technique for basic biology, genetic diagnosis and drug discovery purposes (Doudna, 2020; Li et al., 2020; Sandoval et al., 2020; Wertz et al., 2020). Indeed, therapeutic genome editing is no longer a concept for the distant future, and several *ex vivo* and *in vivo* therapeutic approaches are currently undergoing clinical testing for the treatment of various diseases (Schacker and Seimetz, 2019; Li et al., 2020). In this review, we describe the various genome editing tools available and summarize some of the preclinical studies of *in vivo* CNS genome editing published to date, while discussing current limitations and alternative approaches to overcome some of the bottlenecks.

DNA-BINDING PLATFORMS

Editing platforms have two key features essential for the specific and efficient modification of target sequences within the genome: (1) a DNA-binding domain recognizing a unique target sequence and (2) an effector element for inducing precise genetic/epigenetic modifications. The genome editing tools currently available are based on three major DNA-binding platforms: zinc fingers (ZFs), transcription-activator like effectors (TALEs), and clustered regularly interspaced short palindromic repeats (CRISPR/Cas).

Zinc fingers are eukaryotic DNA-binding domains consisting of two anti-parallel β-sheets and one α-helix, the residue composition of which specifies binding to particular triplets (Miller et al., 1985; Pavletich and Pabo, 1991). Merging six ZFs, is sufficient to create larger DNA-recognition domains targeting unique sequences (18 base pairs) in eukaryotic genomes (Urnov et al., 2010). The construction of extensive libraries of ZFs has made it possible to engineer zinc finger proteins (ZFPs) targeting almost any sequence desired.

Transcription-activator like effectors were first discovered in *Xanthomonas*, a plant-pathogenic bacterium (Bonas et al., 1989; Boch and Bonas, 2010). These proteins bind the DNA via a central region containing an array of 33- to 35-amino acid motifs. The amino-acid sequences of arrays are similar except for two positions, conferring nucleotide-binding specificity. Unlike ZFs,

in which each domain recognizes a specific trinucleotide, each TALE array recognizes a single nucleotide.

CRISPR/Cas are the most recently developed tools for genome engineering. They are based on an RNA-guided nuclease, the DNA-binding properties of which are easily modulated by a short RNA sequence (Fineran and Charpentier, 2012; Wiedenheft et al., 2012). They are involved in bacterial adaptable immunity and can be grouped into two main classes according to the complexity of the nuclease effector (Makarova et al., 2015, 2020). Class 1 systems (types I, III, and IV) involve a large complex of several effector proteins, whereas class 2 systems (types II, V, and VI) use a single Cas protein to mediate the recognition and cleavage of foreign nucleic acids. Class 2 systems are the most widely used for genome editing, because of their simple structure. Type II and type V CRISPR/Cas ribonucleoprotein complexes recognize specific DNA sequences through RNA-DNA base pairing. Cas binding and interference are determined by the spacer sequence (∼20 bp) of the single guide RNA (sgRNA), and the protospacer adjacent motif (PAM) on the target DNA. The spacer is complementary to the target sequence and the PAM is a short DNA motif immediately adjacent to the target region. Cas9 (type II) and Cas12a (type V) have been extensively explored for genome editing (Jinek et al., 2012; Cong et al., 2013; Mali et al., 2013; Zetsche et al., 2015). Cas9 requires a 3′ PAM to the target sequence, whereas Cas12a recognizes a 5′ PAM on the non-targeted strand. Cas9 induces PAM-proximal blunt double-strand breaks (DSBs) and Cas12a creates PAM-distal staggered DSBs. PAM requirements make it impossible for a single CRISPR/Cas system to target all genomic sequences, but the use of different Cas9 and Cas12a orthologs with different PAM specifications has greatly expanded targeting capabilities (Cebrian-Serrano and Davies, 2017). In addition, Cas9 proteins have been engineered to accept different and less restrictive PAMs, although sometimes compromising the specificity (Hu et al., 2018; Walton et al., 2020). By contrast, other groups have restricted Cas9 binding parameters to increase specificity, which however reduce the editing efficiency (Kleinstiver et al., 2016; Kocak et al., 2019). The major advantage of CRISPR/Cas-based tools over ZFs and TALEs for genome editing is the ease of engineering of the DNA-binding domain to recognize unique sequences. The DNA-binding specificity of ZFs and TALEs is dependent on protein-DNA interactions and the targeting of particular sequences therefore requires protein design. The genome-targeting specificity of CRISPR/Cas is provided by the sgRNAs, which are simpler and less expensive to design.

FUSING DNA-BINDING DOMAINS TO EFFECTOR DOMAINS: GENOME EDITING APPROACHES

Genome editing can be grouped into four approaches, depending on the effector domains used (**Table 1**). The DNA sequence can be permanently altered by gene editing or base editing, whereas a transient or stable modification of DNA function/expression can be achieved with gene regulation or epigenetic editing.

Gene Editing

The effector domain of gene editing platforms is a nuclease that induces DSBs at the target DNA sequence (Doudna, 2020; Li et al., 2020). Cas proteins possess intrinsic nuclease activity, whereas ZF nucleases (ZFNs) and TALE nucleases (TALENs) have been engineered by fusing the catalytic domain of the *Fok*I nuclease to ZFs and TALEs, respectively (**Figure 1A**). *Fok*I is a bipartite endonuclease that must dimerize to cleave the target sequence (Vanamee et al., 2001). ZFNs and TALENs therefore have two fused *Fok*I domains binding opposite strands of adjacent sequences in reverse orientations, to promote *Fok*I dimerization and genome restriction (**Figure 1A**). Spatial orientation and module spacing requirements decrease the probability of off-target cutting events. Site-specific DNA cleavage activates cellular DNA repair pathways, which then delete, insert or replace nucleotide sequences (Yeh et al., 2019). The two main DNA repair pathways for DSBs are the non-homologous end-joining (NHEJ) and homology-directed repair (HDR) pathways. NHEJ is error-prone, often introducing small insertions or deletions (indels), whereas HDR uses homologous sequences as a template, to ensure the correct repair of damaged DNA (**Figure 1B**). The NHEJ pathway is frequently used to inactivate toxic genes (**Figure 1B**). The introduction of indels at the 5′ end of the target gene results in frameshift mutations, generating premature stop codons. Other applications include the disruption of aberrant splicing sites or the deletion of large fragments of DNA through the creation of two DSBs in the same chromosome (**Figure 1B**). By contrast, the accuracy of the HDR pathway allows precise nucleotide insertions, deletions or substitutions at the target site (**Figure 1B**). This is achieved by using double- or single-stranded DNA templates containing the intended modification, flanked by homologous sequences. HDR can, thus, be used to correct both GOF and LOF mutations, for gene repair. HDR can also be exploited as an alternative approach to classical gene replacement, to improve control over the copy number of the gene of interest and to prevent insertional mutagenesis due to the random integration of viral vectors. HDR-mediated gene replacement involves the site-specific insertion of full transgenes (cDNA) at "safe harbor" locations, defined as sites within the genome at which the addition of sequences does not interfere with the neighboring genes and results in safe robust transgene expression (**Figure 1B**).

HDR-mediated gene editing is a promising approach for therapeutic applications, but it is generally less efficient than NHEJ and mostly restricted to the G2 and S phases of the cell cycle (Yeh et al., 2019). This imposes additional challenges for the application of HDR-based editing to post-mitotic cells and, therefore, to CNS disorders. Nishiyama and colleagues reported a high efficiency of HDR in the mouse brain (Nishiyama et al., 2017), but most groups have struggled to achieve such success with this approach. Several groups have proposed NHEJ-like strategies to overcome this limitation through precise gene editing in non-replicative cells by microhomology-mediated end-joining (MMEJ) (Yao et al., 2017b), homology-independent targeted integration (HITI) (Suzuki et al., 2016), and microhomology-dependent targeted integration (MITI) (Li et al., 2019). Other groups have explored HDR-like mechanisms, such

TABLE 1 | Comparison of the different genome editing approaches.

Editing approaches	Advantages	Disadvantages
Gene editing	Efficient Permanent All possible modifications: insertion, deletion and substitution	Off-target cleavage Chromosomal instability Target sequence restriction (PAM for CRISPR; 5'-T for TALENs) NHEJ is heterogeneous HDR is inefficient (especially in post-mitotic cells)
Base editing	Permanent No need to induce DSBs Few or no indels	Off-target at both DNA and RNA level Bystander base editing Target sequence restriction (PAM) Efficiency is low Only substitutions are possible
Transcriptional regulation	Physiological expression level Low off-target effects Cell reprogramming	Efficacy depends on the level of gene expression Large genomic areas can be affected Most modifications are not permanent
Epigenetic editing	Long-term modification Cell reprogramming	Lack of information on epigenetic marks for some targeted genes May affect large genomic regions Simultaneous modification of several epigenetic marks may be necessary

as homology-mediated end joining (HMEJ) (Yao et al., 2017a) and single homology arm donor-mediated intron-targeting integration (SATI) (Suzuki et al., 2019). These techniques have yielded significantly higher rates of gene insertion in post-mitotic cells, although the mechanisms involved are not fully understood. Other groups have suggested approaches in which HDR repair is promoted by fusing the Cas9 nuclease to factors involved in the regulation of NHEJ/HDR pathways. For instance, p53-binding protein 1 (53BP1), which plays a major role in balancing NHEJ/HDR ratio, promotes DSB repair via the NHEJ pathway by preventing the DNA end resection required for HDR (Bunting et al., 2010). Cas9 fused to a dominant-negative 53BP1 enhances HDR and inhibits NHEJ in a target-specific manner, without modifying cellular DNA repair mechanisms overall (Jayavaradhan et al., 2019). Efforts have also been made to improve HDR by fusing Cas9 to RecA (RAD51 in eukaryotes), which plays a key role in homologous recombination (Cai et al., 2019; Kurihara et al., 2020), or by altering the conformational checkpoints for Cas9 binding to DNA (Kato-Inui et al., 2018).

No product for therapeutic gene editing has yet been approved, but the first clinical trials based on this technology have demonstrated the safety of this approach (Schacker and Seimetz, 2019). However, as gene editing permanently modifies the DNA, several biosafety concerns have been raised concerning the induction of off-target DSBs and increases in genomic instability (Mills et al., 2003). Unlike DSBs, DNA single-strand breaks (SSBs) are common events under physiological conditions, and are less harmful than DSBs (Caldecott, 2008). Nickases were developed by mutating one of the catalytic sites of Cas9 (nCas9), such that only one strand of the DNA is cut (Doudna, 2020) (**Figure 1A**). Paired nickases targeting nearby sequences on opposing strands can create specific DSBs, while decreasing the chances of producing off-target DSBs (Dabrowska et al., 2018; Ge and Hunter, 2019). The use of SSBs and ssDNA repair templates to insert specific sequences has been explored as an alternative to DSB-mediated HDR (Rees et al., 2019). Nickase variants have improved the HDR:indel ratio, but, overall, this approach remains less efficient than DSB-mediated recombination.

BASE EDITING

DNA base editing can be used to modify single nucleotides without the need to introduce DSBs, reducing the risk of creating off-target indels (Rees and Liu, 2018; Molla and Yang, 2019). Base editing could potentially be used to correct pathogenic point mutations, the most common type of human genetic disorders (Landrum et al., 2016). DNA base editors have been generated by fusing catalysis-deficient Cas9 (dCas9) or nCas9 to deaminase enzymes, which convert specific nucleotides (Komor et al., 2016; Nishida et al., 2016; Gaudelli et al., 2017) (**Figure 2A**). These tools make use of the sgRNA/Cas-mediated R-loop structure to target the transient ssDNA with cytosine or adenosine deaminases. Cytosine base editors (CBEs) convert cytosine into uracil (C→U), which has similar base-pairing properties to thymine (T). The U is then converted to T via DNA repair mechanisms based on base excision repair (BER) or mismatch repair (MMR), resulting in the conversion of C·G into T·A base pairs. The first generation of CBEs (BE1) was developed by fusing dCas9 to the apolipoprotein B mRNA-editing enzyme, catalytic polypeptide 1 (APOBEC1) (Komor et al., 2016). This tool converted cytosine nucleotides in the test tube, but not in eukaryotic cells. The authors rapidly realized that the poor cytosine conversion in cells might be due to intrinsic U:G mismatch repair mechanisms. Uracil is one of the most common non-canonical bases in DNA and its removal by DNA repair mechanisms is important, to prevent mutagenesis. Uracil removal is initiated by uracil DNA glycolase (UDG), which excises the uracil and triggers the conversion of U:G into C:G base pairs by BER. Consequently, the second generation of CBEs (BE2) were fused to a uracil DNA glycosylase inhibitor (UGI), to prevent uracil base excision repair, considerably improving cytosine editing. Attempts were then made, in the third generation of CBEs (BE3) to favor the incorporation of the modified nucleotide through the use of nCas9 rather than dCas9, to induce a "nick" in the unedited strand, thereby favoring the correction of the non-edited nucleotides by the DNA mismatch repair machinery. This resulted in higher cytosine conversion efficiencies, but also

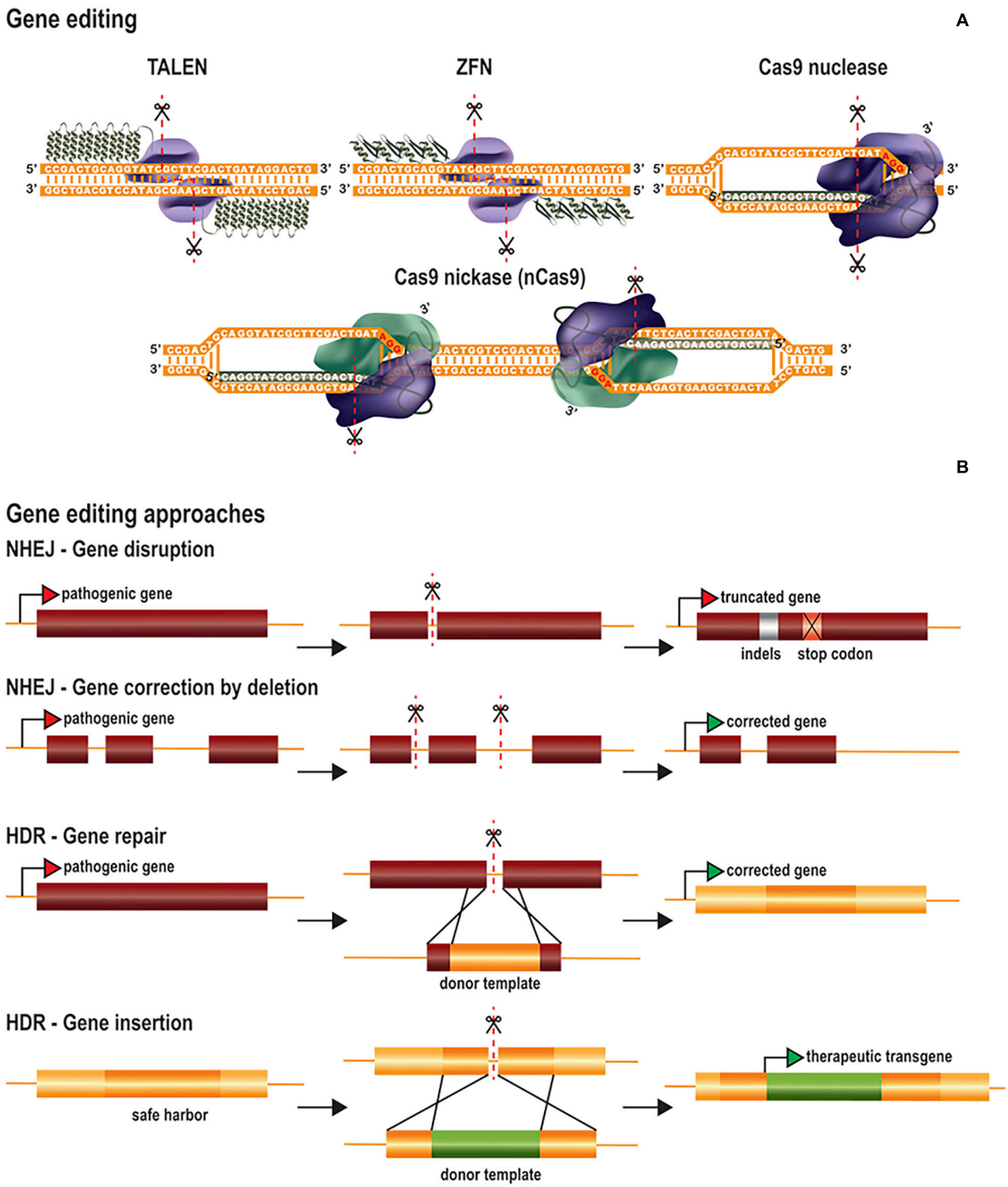

FIGURE 1 | Gene editing tools and therapeutic approaches. **(A)** Gene editing tools are based on TALEs, ZFs and CRISPR/Cas platforms. Site-specific TALENs and ZFNs consist of two modules of TALEs and ZFs fused to the *Fok*I nuclease. Both modules recognize adjacent sequences in opposite strands to promote the dimerization of *Fok*I and sequence cleavage in a staggered fashion. In contrast, CRISPR/Cas systems hold intrinsic nuclease activity. Cas nucleases or Cas nickases are explored to produce either DSBs or SSBs in the targeted sequence, respectively. Alternatively, paired nickases targeting adjacent sequences in opposite strands generate staggered DSBs. **(B)** Gene editing therapeutic approaches rely on the intrinsic DNA repair mechanisms NHEJ and HDR after generation of DSBs. Gene disruption by NHEJ involves the introduction of indels after generation of DSBs at the coding region of a pathogenic gene, resulting in the formation of a premature stop codon. Gene correction by NHEJ implicates the targeting of the non-coding region of a pathogenic gene. It includes the removal of deleterious exons by the simultaneous cleavage in both upstream and downstream intronic regions and/or disruption of splicing regulation sites. Both gene repair and gene insertion by HDR involve the use of donor templates containing intended sequences flanked by homology arms. In the first case, the template is targeted to the pathogenic gene and contains the corrected sequence allowing gene restoration. In contrast, gene insertion by HDR targets safe harbor locations in the genome to introduce therapeutic transgene expression cassettes.

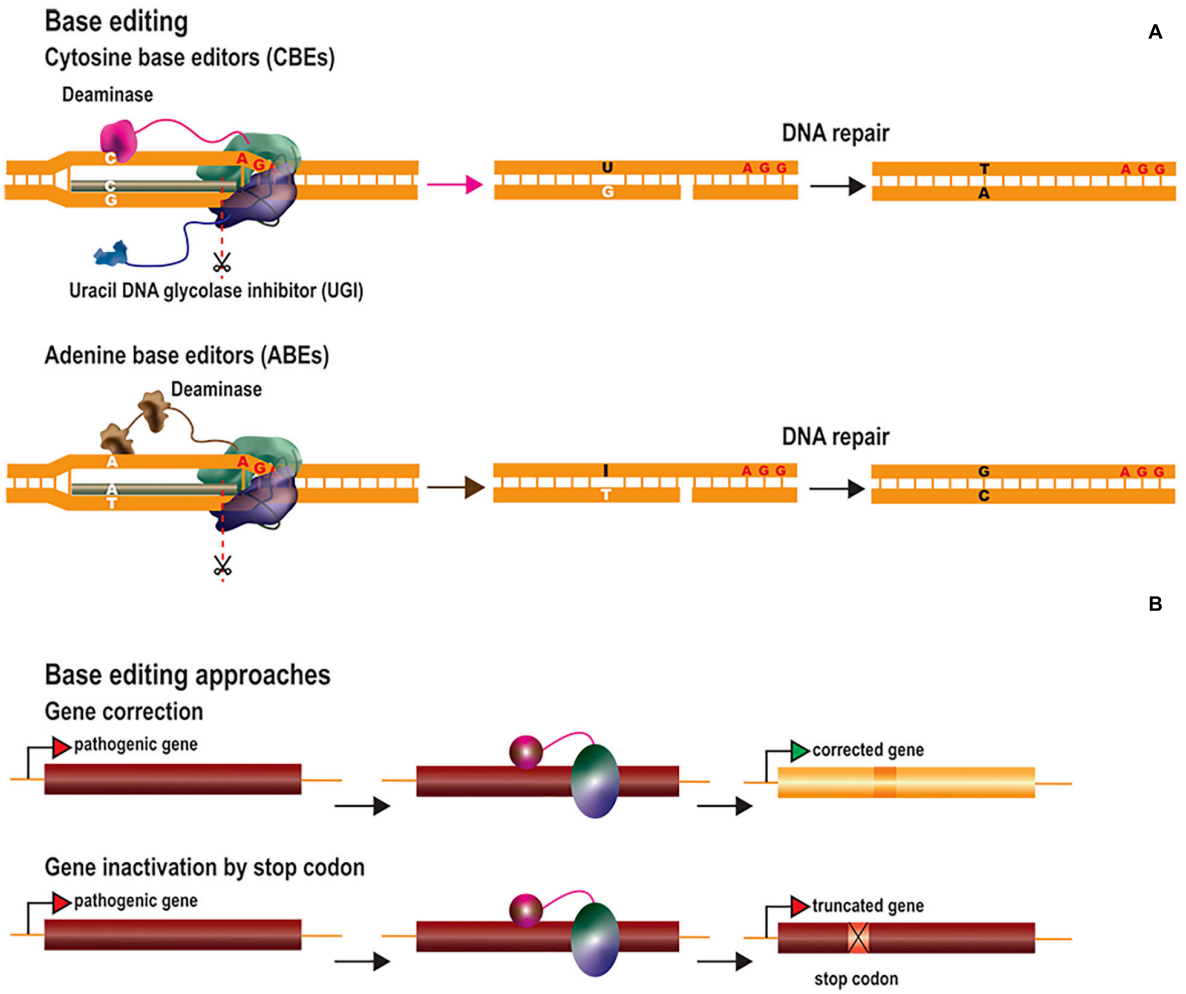

FIGURE 2 | Base editing tools and therapeutic approaches. **(A)** Base editors consist of Cas nickases fused to cytosine (CBEs) or adenine ssDNA deaminases (ABEs). CBEs are fused to either AID or APOBEC1 (pink), which convert C into U, whereas ABEs are fused to an evolved TadA (TadA*) followed by a wild-type TadA fusion (brown), which convert A into I. The consequent G:U and T:I mismatches are then corrected by the cellular DNA repair mechanisms. To favor the correction of the non-edited nucleotides by the DNA mismatch repair machinery, the nickase introduces a "nick" in the unedited strand. The correction of the non-edited strand results in a final conversion of C:G into T:A base pairs and A:T into G:C base pairs by CBEs and ABEs, respectively. CBEs are usually fused to the UGI to prevent the rapid removal of uracil by BER (blue). **(B)** Base editing therapeutic approaches include the repair of pathogenic genes by correcting point mutations or the inactivation of toxic genes by generating a premature stop codon.

increased the frequency of indel events. Indel formation in this context probably results from the creation of two adjacent DNA nicks on opposite strands (by nCas9 on the unedited strand and by BER enzymes on the edited strand), leading to the generation and NHEJ-mediated processing of transient DSBs. For this reason, a fourth generation of CBEs was generated by fusing nCas9 to two UGIs (BE4) and/or to the bacteriophage Mu-derived Gam (BE4-GAM), which binds to DSBs and protects them from degradation (Komor et al., 2017). The BE4 editors underwent further improvement, based on the modification of nuclear localization signals, codon optimization and deaminase reconstruction (BE4max) (Koblan et al., 2018). In parallel, CBEs were generated with an ortholog of activation-induced cytidine deaminase A (AID) from sea lamprey (PmCDA1) rather than APOBEC1 (Nishida et al., 2016). CDA1-nCas9-UGI had editing rates similar to those of APOBEC1-nCas9-UGI, but achieved through periodic decreases in incubation temperature to 25°C, the optimal temperature for PmCDA1. An extended toolbox of DNA CBEs is now available. These editors differ in terms of their Cas proteins (Cas9 or Cas12a), nuclease activity (dCas or nCas), cytosine deaminase (APOBEC1 or CDA1), number of UGIs, nuclear localization signals and the linker sizes between domains (Rees and Liu, 2018; Molla and Yang, 2019).

Adenine base editors (ABEs) transform adenine into ionosine (A→I), which is then converted to guanine (G), resulting in the conversion of A·T into G·C base pairs (**Figure 2A**). ABEs were generated based on the tRNA adenine deaminase (TadA) of *Escherichia coli* (Gaudelli et al., 2017). After several rounds of development, it was established that the fusion of nCas9 to an evolved TadA (TadA*) followed by a wild-type TadA

resulted in the most efficient ABE (ABE 7.10). The DNA repair mechanisms for removing ionosine from the DNA are less efficient than those for removing uracil, and these tools were, therefore, able to induce high levels of adenine conversion without the need for ionosine repair inhibitors. Consequently, indel events were much less frequent (barely detectable) than in untreated samples. As for BE4max, the efficiency of ABE7.10 was also increased by the development of ABEmax (Koblan et al., 2018). The TadA*-TadA effector domain was fused to several Cas9 variants, recognizing different PAMs, to increase the breadth of targeting possible for ABEs (Rees and Liu, 2018; Molla and Yang, 2019).

Base editing is dependent on DNA mismatch repair rather than homologous recombination. It therefore constitutes an alternative approach to HDR-mediated gene editing for correcting point mutations in post-mitotic cells. CBEs and ABEs have been used to correct both LOF and GOF pathogenic point mutations implicated in various diseases (Komor et al., 2016; Gaudelli et al., 2017; Liang et al., 2017; Koblan et al., 2018; Zeng et al., 2018) (**Figure 2B**). *In vivo* base editing applications have been described for hypercholesterolemia (Chadwick et al., 2017; Rossidis et al., 2018), hearing loss (Yeh et al., 2018, 2020), hereditary tyrosinemia type 1 (Rossidis et al., 2018), phenylketonuria (Villiger et al., 2018), DMD (Ryu et al., 2018) and amyotrophic lateral sclerosis (ALS) (Lim et al., 2020). Another therapeutic strategy involves the generation of a premature stop codon for gene inactivation, as an alternative to NHEJ-mediated gene editing (Billon et al., 2017; Kuscu et al., 2017) (**Figure 2B**).

Base editing is a promising therapeutic strategy, but it is subject to limitations in terms of the purity of the edited products, bystander base editing and distal off-target activity. Product purity is defined as the ratio of intended to unintended editing events at the targeted site. Uracil is more prone to repair by base excision repair mechanisms, so product purity is lower for CBEs than for ABEs. This translates into a higher rate of C to non-T nucleotide conversion and indel events than of A to non-G conversions and indels generated by ABEs. Bystander base editing also lowers product purity by modifying base pairs adjacent to the targeted nucleotide. Bystander editing of adjacent Cs or As can be counteracted by employing base editors with narrow editing windows, although some such editors are less efficient. For distal off-target editing, CBEs have been shown to generate more off-target mutations than ABEs (Lee H.K. et al., 2018; Zuo et al., 2019). Base editors have been shown to induce unintended modifications in both DNA and RNA. Indeed, a recent report demonstrated substantial levels of off-target editing in RNA, for both CBEs and ABEs (Zhou et al., 2019). Distal off-target editing may result from non-specific Cas protein binding to DNA and RNA or random contacts between the deaminase domains and RNA or ssDNA during DNA replication and transcription (Rees and Liu, 2018; Molla and Yang, 2019). Cas-dependent off-target editing has been reduced by the use of high-fidelity Cas variants, and other types of off-target editing can be limited by altering the intrinsic DNA and RNA affinity of deaminase domains.

Genome Regulation

Genome regulation offers additional therapeutic options through the modulation of gene expression at native loci. Gene expression is regulated by multiple factors, including both *cis* and *trans* elements, ultimately leading to the recruitment of RNA polymerases to promoter regions. Genome expression is also regulated by epigenetic marks, which determine chromatin accessibility state and comprise multiple elements, including the three-dimensional architecture of the DNA and histone or DNA modifications (Holtzman and Gersbach, 2018). An extensive list of possible histone modifications, including acetylation, methylation and phosphorylation, has been described, and all these processes can be altered to modulate gene expression (Holtzman and Gersbach, 2018). Epigenetic modifications, particularly for histone tails and DNA methylation status, have provided insight into the role of such changes in gene regulation and their contribution to disease. For instance, cytosine methylation (5C-methylcytosine) at CpG dinucleotides is usually enriched in silenced promoters (Weber et al., 2007; Kundaje et al., 2015) and has been implicated in genomic imprinting (Laan et al., 1999), whereas H3K9 acetylation is associated with active promoters (Ernst et al., 2011). For the alteration or restoration of gene expression profiles, ZFs, TALEs, and dCas proteins have been fused to scaffold transcriptional modulators or epigenetic modifiers (**Figure 3A**). Genome regulation strategies can be used to upregulate or repress gene expression by two different approaches: (1) transcriptional modulation through the recruitment of transcription factors and chromatin remodelers and (2) epigenome editing through the direct modification of epigenetic marks.

Transcriptional activation has been achieved through the tethering of ZFs, TALEs, and dCas9 to several copies of herpes simplex virus protein 16 (VP16), the transactivating domain of the NF-kB p65 subunit (p65), heat shock factor 1 (HSF1) and Epstein–Barr virus R transactivator (RTA) (**Figure 3B**). The targeting of multiple copies of transactivating domains to promoter regions was rapidly shown to have a synergistic activation effect. This led to the development of dCas-based second-generation activators, which can target multiple transactivating domains to a single locus. Chavez and coworkers evaluated the potency of several dCas9 activators in different cell lines and showed that the synergistic activator mediator (SAM) (Konermann et al., 2015), SUperNova Tagging (SunTag) (Tanenbaum et al., 2014) and the tripartite VP64-p65-RTA (VPR) (Chavez et al., 2015) systems were the most efficient at inducing gene activation (Chavez et al., 2016). These systems have been adapted to activate genes *in vivo* (Chew et al., 2016; Liao et al., 2017; Moreno et al., 2018; Zhou et al., 2018; Breinig et al., 2019; Savell et al., 2019; Zhan et al., 2019). Gene expression profiles can also be altered to reprogram cells to differentiate into particular cell types. Liao and coworkers reprogrammed hepatic cells into pancreatic-like beta cells, by activating the Pdx1 (Liao et al., 2017). They also improved DMD symptoms by activating the Utrn gene. Savell and coworkers demonstrated robust Fosb activation in several regions of the brain *in vivo* (Savell et al., 2019). Similarly, Zhou et al. demonstrated the

in vivo genetic reprogramming of neurons in mouse brain by simultaneously activating the expression of Ascl1, Neurog2, and Neurod1 (Zhou et al., 2018). Breinig and coworkers recently altered the sgRNA length of a Cas12a-VPR variant to induce either gene activation or knockout *in vivo* (Breinig et al., 2019). This work has added an additional degree of complexity to these systems, allowing not only the targeting of multiple genes, but also a larger range of modifications. Artificial transcriptional repressors have also been generated by fusing the Kruppel-associated box protein (KRAB) domain to the DNA-binding platforms (Bailus et al., 2016; Zeitler et al., 2019) (**Figure 3B**). KRAB is a scaffold protein involved in recruiting KAP1/TIF1β corepressor complexes, which in turn recruit DNA methylases or histone modifier factors (Kim et al., 1996; Ying et al., 2015). The effects of KRAB on gene repression can be permanent or reversible, depending on developmental stage (Ying et al., 2015).

Unlike the recruitment of activating or repressing complexes/factors, epigenetic editing can modify epigenetic marks by targeting specific enzymes. Epigenetic activation has been achieved through site-specific DNA methylation by the DNA demethylase 10–11 translocation methylcytosine dioxygenase 1 (TET1) (Maeder et al., 2013; Choudhury et al., 2016a; Liu et al., 2016; Xu et al., 2016) or with enzymes promoting activating histone signatures, such as the histone acetylase core subunit p300 (Hilton et al., 2015) and histone methyltransferases (Cano-Rodriguez et al., 2016) (**Figures 3C,D**). For instance, Liu and coworkers described the *in vivo* demethylation of a methylation-sensitive Snrpn-GFP cassette in transgenic mice (Liu et al., 2016). Heterozygous mice carrying a paternal copy of the transgene do not express GFP, due to the methylated status of this copy of the gene. The authors reported the targeted active demethylation of the transgenic cassette and a 70% activation of GFP expression after lentiviral injections of dCas9-Tet1 into the brain. Rather than active DNA demethylation, Hilton et al. demonstrated that the fusion of p300 to the three DNA-binding platforms activated the expression of multiple endogenous genes (*ilrn1, oct4,* and *myod1*) through histone acetylation (Hilton et al., 2015). Finally, epigenetic repression has been achieved through direct DNA methylation (Bernstein et al., 2015), histone deacetylation (Kwon et al., 2017), and histone demethylation (Kearns et al., 2015) (**Figures 3C,D**).

GENOME EDITING FOR CNS DISORDERS

Alzheimer's Disease

Alzheimer's disease (AD) is the main cause of dementia, affecting millions of people worldwide (Winblad et al., 2016; Dos Santos Picanco et al., 2018). One of the hallmarks of AD is the presence of scattered extracellular senile plaques, due to the accumulation of amyloid-β (Aβ) in the brain. Aβ is a secondary metabolite generated by the processing of amyloid precursor protein (APP) by β-secretase 1 (BACE1). Alternatively, APP may be processed via a non-amyloidogenic pathway involving α-secretases, leading to the generation of neuroprotective products (Richter et al., 2018). In a study of the treatment of a familial form of AD caused by the Swedish mutation of APP (APPsw), CRISPR-mediated NHEJ was used to inactivate the mutant APP (György et al., 2018). This can be achieved by designing sgRNAs targeting single nucleotide polymorphisms (SNPs) in the target sequence of the sgRNA (mismatch-based selectivity) or in the PAM (PAM-based selectivity). György and coworkers detected 1.3% indels in the APPsw allele after the hippocampal injection of a mismatch-based selective CRISPR/Cas9 system split into two AAV9 vectors (because of the limited capacity of AAV vectors of ∼4.8 kb) in Tg2576 mice (György et al., 2018). By contrast, Sun and coworkers used a non-allele selective CRISPR-mediated NHEJ strategy to push APP processing toward the non-amyloidogenic pathway (Sun et al., 2019). Based on evidence suggesting that deletion of the C-terminus of APP can mitigate Aβ generation (Koo and Squazzo, 1994) and reduce APP interactions with the BACE-1 enzyme (Das et al., 2016), the authors used CRISPR to generate C-terminally truncated APP, thereby circumventing the amyloidogenic processing of APP (Sun et al., 2019). In this study, APP truncation in WT and heterozygous APP-London human iPSC-derived neurons increased the production of the neuroprotective sAPPα and reduced the secretion of Aβ40/42 and the sAPPβ fragment. For *in vivo* studies in adult mice, the CRISPR-APP system was split into two AAV9 vectors and delivered to the dentate gyrus of WT mouse brains. The injection of CRISPR-APP led to a halving of full-length APP levels relative to both controls not receiving injections and controls receiving control vector injections. No additional *in vivo* tests were performed to evaluate treatment efficacy in the context of AD (György et al., 2018; Sun et al., 2019), but these therapeutic strategies targeting the C-terminal part of APP are of interest because the aim was to attenuate pathological properties (Aβ generation) while potentially maintaining other physiological functions of APP. Another approach, developed by Park and coworkers, uses CRISPR-Cas9-loaded nanocomplexes targeting BACE1 in the 5XFAD and APP transgenic mouse models to reduce the generation of Aβ and improve AD symptoms (Park et al., 2019). Four weeks after CRISPR injection into the CA3 hippocampal region of 5XFAD mice, 45% of target sequences contained indels, and a 34% decrease in Bace1 expression was observed, revealing this method to be more efficient than the use of chemical BACE1 inhibitors. They also observed a decrease in Aβ plaque accumulation by a factor of more than two, together with a significant rescue of associative learning (fear conditioning test) and spatial working memory (Morris water maze) in the treated 5XFAD mice. These molecular and behavioral improvements were maintained for up to 12 weeks. Off-target evaluation by whole-genome sequencing (WGS), whole-exome sequencing (WES), Digenome-sequencing (Digenome-seq) and deep sequencing identified a few off-target mutations and small-scale chromosomal rearrangements.

Bustos and coworkers investigated the potential of epigenome editing for AD by targeting the dlg4 gene, encoding the PSD95 protein (Bustos et al., 2017). PSD95 is a scaffolding protein present at the excitatory post-synaptic density, and is involved in the regulation and organization of post-synaptic synapses (Elias and Nicoll, 2007). Abnormal PSD95 expression has been

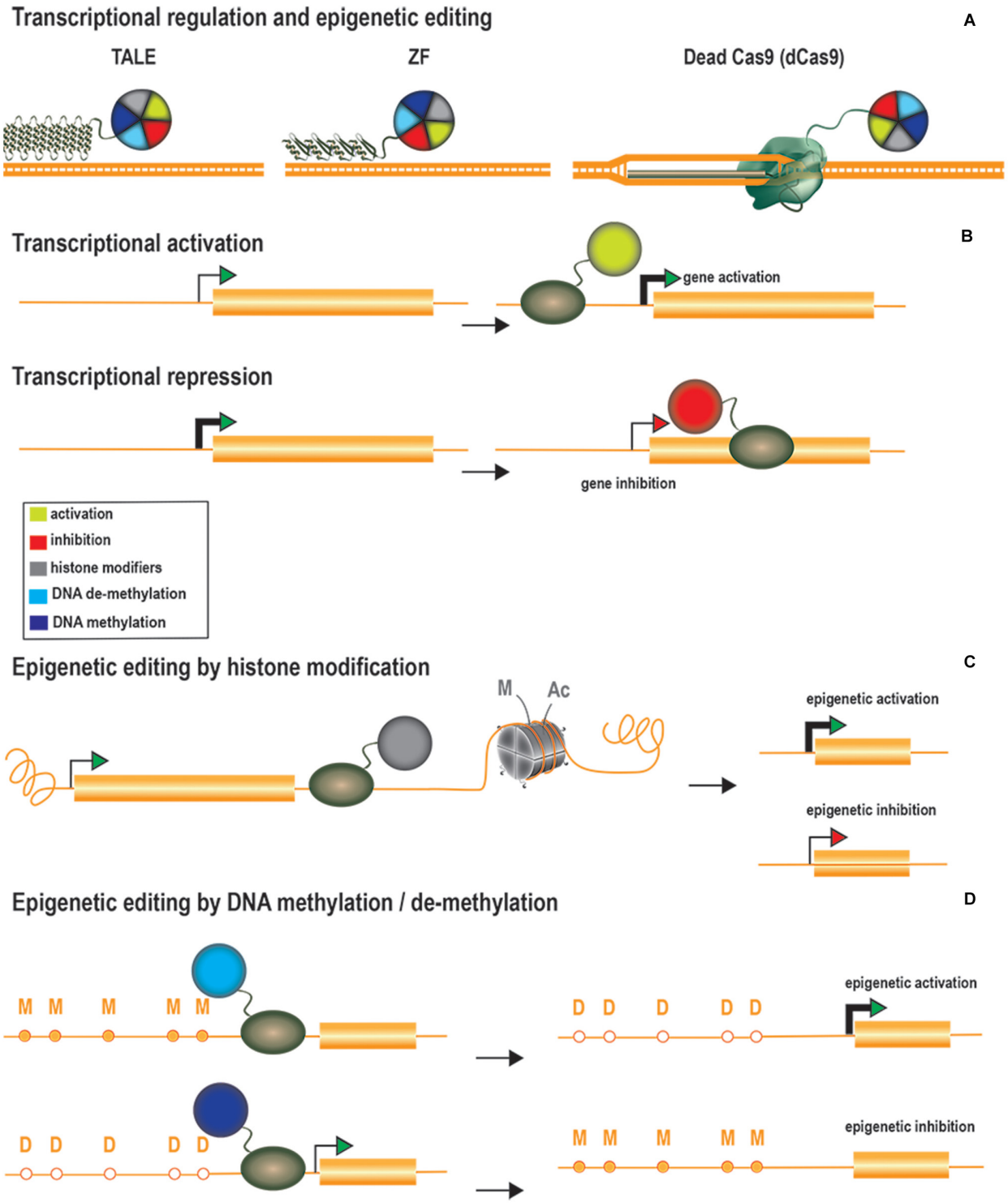

FIGURE 3 | Transcriptional regulators, epigenetic modifiers, and therapeutic approaches. **(A)** Gene expression regulation tools are generated by fusing TALEs, ZFs or dCas proteins to scaffold transcriptional modulators or to epigenetic modifiers **(B)** Therapeutic approaches by transcriptional regulation. Transcriptional activation or repression is explored to upregulate therapeutic genes or to downregulate deleterious genes, respectively. Transcriptional activators are targeted at the promoter region whereas transcriptional repressors are usually targeted downstream to the transcription starting site to further block the RNA polymerase activity. **(C)** Therapeutic approaches through histone modification. Histone (de)acetylases and (de)methylases are the most common employed enzymes to modify histone marks and the epigenetic activation or inhibition effect of such modifications is frequently context-specific. **(D)** Therapeutic approaches by editing the DNA methylation state. Epigenetic editors based on DNA demethylases are used to activate gene expression whereas the ones based on DNA methylases result in gene expression inhibition.

described not only in AD, but also in other neurological disorders, such as Huntington's disease (HD) and schizophrenia. The authors developed and validated *in vitro* several ZF-based epigenome modifiers targeting the proximal promoter region of dlg4/PSD95 for the activation or repression of PSD95 expression (Bustos et al., 2017). They demonstrated that alterations in expression were specifically associated with histone modifications rather than other changes, such as CpG methylation in DNA. The fusion of zinc fingers to the histone methyltransferase G9a (PSD95-6ZF-G9a) induced gene repression associated with an increase in the di- and tri-methylation of H3K9, whereas PSD95-6ZF-VP64 gene activation was coupled to H3 activation, probably through the recruitment of histone acetylases by the VP64 domain. PSD95-6ZF-VP64 was also shown to have neuroprotective effects. AβPPswe/PS-1 mice receiving AAV-PSD95-6ZF-VP64 injections into the hippocampus had higher levels of PSD95 expression and displayed a rescue of memory and spatial learning performances to normal aged-matched levels.

Parkinson's Disease

Parkinson's disease (PD) is the second most common neurodegenerative disorder, affecting 2–3% of people under the age of 65 years (Poewe et al., 2017). PD patients display motor movement dysfunction, but also cognitive impairment, depression and dementia. At the cellular and molecular levels, PD is characterized by a striatal dopamine deficiency due to progressive neuronal loss in the substantia nigra, and by the formation of intracellular aggregates containing α-synuclein. Dopamine loss and basal ganglia circuitry disruption are well-defined features in PD, but this disease is extremely complex and driven by diverse molecular and neurophysiological mechanisms.

Several gene-based therapies for PD have been proposed, including the targeting of α-synuclein, cellular oxidation and the autophagy-lysosomal pathway (Poewe et al., 2017). Genome editing for PD has mostly been used for disease modeling *in vitro* (Safari et al., 2019). For instance, Kantor and coworkers induced the hypermethylation of CpG islands in SNCA intron 1 in iPS-derived dopaminergic progenitor neurons, through lentiviral transduction with a dCas9-DNMT3A system (Kantor et al., 2018). They observed a ∼ 25% decrease in α-synuclein protein levels and the rescue of mitochondrial-associated superoxide production and cell viability. They observed no overall change in the methylation status of the treated cells, identifying the dCas9-DNMT3A-mediated targeting of SNCA as a promising approach for PD treatment. Another potential therapeutic target is glial cell line-derived neurotrophic factor (GDNF), which has been shown to have neuroprotective effects and to improve Parkinsonian symptoms (Kordower et al., 2000; Tenenbaum and Humbert-Claude, 2017). Laganiere and colleagues used a ZF-p65 fusion to upregulate the expression of endogenous GDNF in a 6-OHDA rat model of Parkinson's disease (Laganiere et al., 2010). They observed an increase in the number of TH-positive fibers in both the medial forebrain bundle and the substantia nigra after 7 weeks of AAV2-rGDNF-ZFP infusion (Laganiere et al., 2010). The rGDNF-ZFP-treated group performed better in the corridor test, the cylinder test and the drug-induced rotational test than the GFP-treated control. This study yielded promising results, but a clinical trial based on the direct infusion of GDNF into the putamen resulted in no significant improvement of Parkinson's disease symptoms (Lang et al., 2006; Whone et al., 2019), raising questions about therapeutic efficacy of GDNF.

Huntington's Disease

Huntington's disease (HD) is a neurodegenerative disorder caused by an inherited dominant CAG trinucleotide expansion mutation on the HTT gene. *In vivo* genome editing strategies for HD have explored NHEJ-mediated gene inactivation (Merienne et al., 2017; Monteys et al., 2017; Yang et al., 2017) and the transcriptional repression of HTT (Zeitler et al., 2019). Yang et al. used two separate AAVs expressing SpCas9 and two sgRNAs targeting the flanking regions of the CAG repeat in a non–allele-specific manner in the HD140Q-KI mouse model (Yang et al., 2017). The injection of neuron-specific AAV-Cas9-HTT resulted in the efficient transduction of medium spiny neurons, significantly decreasing the accumulation of both mutant (mHTT) and WT HTT in the striatum of 9-month-old homozygous and heterozygous HD140Q-KI mice. The treated heterozygous mice performed better in the rotarod, beam and grip strength tests. Although no deleterious effects of depleting both mutant HTT copies from homozygous HD140Q-KI mice were detected (Yang et al., 2017), it still remains a matter of debate whether disruption of the normal physiological functions of WT HTT lead to harmful effects at adult stages (Liu and Zeitlin, 2017). With this in mind, Monteys and coworkers designed a PAM-based strategy targeting a SNP for specific inactivation of the mutant *HTT* allele (Monteys et al., 2017). They demonstrated the allele selectivity of the chosen sgRNAs *in vitro* in fibroblasts from human HD patients and showed efficient HTT exon-1-targeted deletion following the injection of allele-selective AAV1 CRISPR-HTT into BACHD transgenic mice. This treatment halved the levels of human mHTT mRNA in the striatum. However, it should be noted that heterozygous BACHD transgenic mice have about five tandem copies of the human mHTT gene and two copies of the endogenous mouse WT gene (Gray et al., 2008). In these studies, the spCas9 was constitutively expressed. The stable and permanent expression of nucleases eventually leads to higher levels of on-targeting editing, but it also increases the occurrence of off-target events and immunogenic responses. We have tried to overcome this problem by developing the self-inactivating KamiCas9 system, for transient Cas9 expression (Merienne et al., 2017). This system is based on a lentiviral vector with a larger cloning capacity than AAV. It is composed of the Cas9 nuclease, a sgRNA targeting HTT and a second sgRNA targeting the translation start site of the Cas9 nuclease. High on-target efficiency and inactivation of the Cas9 nuclease over time are ensured by the use of a strong PolIII promoter (H1) to drive the sgHTT and a weak PolIII promoter (7sk) to drive the sgCas9. We demonstrated high levels of exogenous hHTT-82Q (20–35%) and Cas9 (∼40%) editing following the injection of LV-KamiCas9 and hHTT-82Q into mouse striatum. Western blot analysis of striatal samples from mice receiving LV-KamiCas9 injections revealed an almost-complete absence of the Cas9 protein after 2 months.

Garriga-Canut et al. (2012) attempted to design a CAG copy number-dependent ZF-based transcription repressor exclusively targeting the mHTT allele. This first tool established the proof-of-principle for HTT repression *in vivo*, decreasing mHTT mRNA levels by about 30% in the brains of R2/6 mice receiving AAV1-ZF-Kox1 injections. Despite the achievement of selective repression *in vivo*, the mutant allele in R6/2 mice contains 115–160 repeats, a number not consistent with the degree of CAG expansion in most HD patients. Zeitler and coworkers recently generated a second-generation ZF-KRAB that preferentially recognizes pathogenic CAG repeats, and demonstrated highly significant mHTT suppression with wild-type allele preservation in patient derived-iPSCs (Zeitler et al., 2019). They observed beneficial behavioral effects in R6/2 mice for 7 weeks after the intrastriatal injection of AAV-ZF-KRAB, and demonstrated the absence of inflammation or adverse effects of long-term expression in mouse brain.

Amyotrophic Lateral Sclerosis

Amyotrophic lateral sclerosis is a neurodegenerative disease caused by the progressive neurodegeneration of both upper and lower motor neurons (Rowland and Shneider, 2001). Muscle atrophy begins in adult patients with ALS and progresses to total paralysis and, eventually, death. Approximately 2% of ALS cases result from a dominant mutation of the SOD1 gene. Gaj et al. (2017) mitigated ALS symptoms and improved the survival of a mouse model of ALS, G93A-SOD1 mice, containing 25 copies of the human mutant SOD1, by disrupting the human SOD1 gene with the *Staphylococcus aureus* Cas9 (SaCas9). The CRISPR system was packaged into a single AAV9 variant (double-tyrosine mutant) shown to enhance gene transfer to the CNS (Petrs-Silva et al., 2009; Dalkara et al., 2012). The authors demonstrated efficient neuronal transduction of the ventral horn of the spinal cord, with up to 74% of motor neurons expressing the nuclease, after systemic injections in neonatal transgenic mice (Gaj et al., 2017). Western blot analysis revealed a 2.5- to 3-fold decrease in mutant SOD1 protein levels, but sequencing data showed that only a small fraction of the total human SOD1 transgenes had been edited (0.2–0.4%). This discrepancy may reflect the large numbers of glial cells in the gray matter of the spinal cord, which were not efficiently transduced, or differences in SOD1 expression in transduced and non-transduced regions of the spinal cord. Regardless of this divergence, the onset of disease in animals treated with SaCas9-SOD1 was delayed by 33 days, and survival was 28–30 days longer than in the control. In age-matched mice, the editing of SOD1 improved rotarod performance, prevented weight loss and reduced muscular atrophy. The treatment was unable to slow the progression of the disease after its onset, but end-stage tissue analysis in SaCas9-SOD1-treated mice revealed the presence of ∼50% more motor neurons. SOD1 inclusion bodies were observed in astrocytes, suggesting that glial cell targeting might be required to slow the progression of the disease, since these cells have been shown to play a role in disease progression (Boillée et al., 2006; Yamanaka et al., 2008).

Angelman Syndrome

Angelman syndrome is a neurological disorder caused by a genetic UBE3A deficiency resulting in intellectual disability, ataxia and seizures (Laan et al., 1999). The paternal Ube3a allele is specifically silenced by a brain-specific antisense transcript (Ube3a-ATS). LOF mutations in the maternal allele therefore lead to UBE3A deficiency. Bailus and coworkers developed a ZF-KRAB repressor targeting the transcription start site of Ube3a-ATS (Snurf/Snrpn promoter), to overcome the paternal imprinting of the Ube3a gene (Bailus et al., 2016). The systemic injection of TAT-S1-linked UBE3a-6ZF-KRAB repressor partially rescued Ube3a expression levels in the hippocampus and cerebellum of a mouse model of Angelman syndrome. However, this therapeutic approach may require multiple treatments, because the repressor function of the KRAB domain has been shown to be transient (Gilbert et al., 2014; Ying et al., 2015).

MECP2 Duplication Syndrome

MECP2 encodes a nuclear protein involved in the transcriptional and post-transcriptional regulation of many genes (Cheng and Qiu, 2014). Duplication or triplication of Xq28 leads to MECP2 GOF mutations mostly affecting boys (Ramocki et al., 2009). This syndrome is characterized by intellectual disability, poor speech development, motor dysfunction and anxiety. Yu and coworkers reported that the normalization of MeCP2 levels in the medial prefrontal cortex of adult MECP2 transgenic mice through CRISPR/Cas9-mediated NHEJ can reverse the social recognition deficit (Yu et al., 2020). The CRISPR system was packaged into two AAV particles (SpCas9 + sgRNA), which were stereotaxically injected into the mouse brain. Immunostaining and western blotting 6 weeks after treatment showed that MeCP2 protein levels had almost halved. Despite improvements in social recognition behavior, the treatment had no effect on locomotor activity, or heightened anxiety-like behaviors, suggesting that different brain areas or neural circuits may contribute to the diverse aspects of the syndrome.

Fragile X Syndrome

Fragile X syndrome (FXS) is the most common single-gene form of autism spectrum disorders (ASDs), for which there is currently no effective treatment (Kaplan and McCracken, 2012). It is caused by a trinucleotide CGG repeat expansion in the 5′ UTR of the fragile X mental retardation 1 (FMR1) gene, encoding the fragile X mental retardation protein (FMRP) (Dölen and Bear, 2008; Persico and Napolioni, 2013). This mutation inactivates the gene, due to hypermethylation of the expanded repeats and heterochromatin formation. Excessive mGluR5 signaling has been observed not only in FXS, but also in other ASDs (Silverman et al., 2012). Lee and coworkers explored the CRISPR-mediated disruption of metabotropic glutamate receptor 5 (mGluR5) as a mean of counteracting FXS by delivering RNPs SpCas9 or Cas12a targeting the mGluR5 to the striatum of Fmr1-knockout mice (a mouse model of FXS) (Lee B. et al., 2018). The editing tool was delivered with CRISPR-gold technology, which combines gold nanoparticles conjugated with oligonucleotides and the endosomal disruptive polymer

PAsp(DET), for the transfer of RNPs into cells by endocytosis (Lee et al., 2017). The indel frequency was 14.6%, and a 40–50% decrease in mGluR5 mRNA and protein levels was observed. In addition, behavioral analysis revealed that mGluR5-CRISPR-Gold rescued the excessive digging and exaggerated repetitive jumping behaviors of treated mice.

Traumatic CNS Injury

Traumatic CNS injuries and stroke are very common causes of disability, and the treatments currently available are very limited. CNS trauma involves an initial mechanical injury, which is followed by a cascade of molecular and cellular phenomena, ultimately leading to neuronal death by apoptosis. Genome editing therapy strategies have focused on VEGF, which is a neuroprotective factor that favors endothelial cell proliferation and blood vessel formation (Shweiki et al., 1992). These studies used engineered ZFs targeting the proximal promoter of VEGF fused to the transactivating domain of the NF-kB p65 subunit. Michael Fehlings's laboratory has demonstrated an increase in the number of blood vessels and angiogenesis, a decrease in neurodegeneration and an improvement of behavioral outcomes in a rat model of SCI following the intraspinal microinjection of AdV-ZFP-VEGF and AAV2-ZFP-VEGF activators (Liu et al., 2010). The timing of treatment for traumatic damage is an important parameter for clinical application. Beneficial effects have been shown following the administration of AdV-ZFP-VEGF 24 h after injury (Figley et al., 2014). In addition, Siddiq et al. (2012) used the unilateral fluid percussion injury model in rats to demonstrate the neuroprotective and angiogenic effects of ZFP-VEGF delivery to the cortex or hippocampus by intracerebral injection. Treatment did not improve performance in the Morris water maze or balance beam latency experiments relative to control, but the treated group performed significantly better than controls in the rotarod test.

GM2-Gangliosidoses

GM2-gangliosidoses are autosomal recessive disorders caused by the deficiency of a lysosomal enzyme, β-hexosaminidase, resulting in the accumulation of GM2 gangliosides. Biallelic LOF mutations of the Hex α-subunit (HEXA) or Hex β-subunit (HEXB) genes lead to Tay-Sachs disease and Sandhoff disease, respectively. Ou and coworkers recently used a cross-correction strategy based on liver-targeted HDR-mediated CRISPR editing to restore the function of β-hexosaminidase in the brain, in a Sandhoff mouse model (Ou et al., 2020). They injected a dual AAV system consisting of AAV8-SaCas9 and AAV8-HEXM-sgRNA targeting the albumin safe harbor locus into neonatal Sandhoff mice, to introduce, via HDR, the coding sequence of a modified human Hex μ subunit (HEXM) able to process GM2 gangliosides (Karumuthil-Melethil et al., 2016). Four months after the systemic delivery of this sequence, levels of MUGS and MUG activity in the brain were significantly higher than those in untreated Sandhoff mice. Mice receiving the AAV8-HEXM-sgRNA alone displayed no such increase in MUGS and MUG activities, indicating an absence of HEXM expression from the episomal donor template vector. In addition, treated mice performed better in the rotarod test and one in three mice had lower levels of neuronal lysosomal accumulation, indicating that hepatocyte editing can lead to neurological improvements. Indeed, the HEXM variant has been reported to improve gangliosidosis in both the Sandhoff and Tay-Sachs models (Karumuthil-Melethil et al., 2016; Osmon et al., 2016), suggesting that this strategy may provide protection against both disorders.

Hearing Loss Disorders (DFNA36 and DFNB7/11)

About 20% of the 100 or so alleles associated with deafness result from GOF mutations (Müller and Barr-Gillespie, 2015). DFNA36 is a progressive hearing loss disease caused by dominant mutations of the *tmc1* gene, leading to the neurodegeneration of sensory hair cells. This disease is of particular interest due to the existence of an orthologous mouse mutation, Beethoven (Bth), which also causes hearing loss in mice (Zhao et al., 2014). Two recent reports described the use *in vivo* of allele-specific CRISPR-mediated NHEJ as a therapeutic strategy for DFNA36 (Gao et al., 2018; György et al., 2019). Gao and coworkers used SpCas9 together with a sgRNA matching the mutant allele, but not the WT allele, to knockout the mutant allele (Gao et al., 2018). They delivered RNP complexes bound to cationic lipids and, even though the targeting of the mutant allele was highly selective (96% of mutant/WT), the frequency of indels was low (1.8%). Nevertheless, the treatment was sufficiently effective to promote hair cell survival, particularly for inner hair cells (IHCs), and to improve cochlear function significantly between the frequencies of 8 and 23 kHz (Gao et al., 2018). However, at 8 weeks, an analysis of cochlear function in treated Tmc1Bth/ + mice revealed less evident improvements relative to the control, suggesting that higher levels of mutant gene inactivation might be required to stop neurodegeneration, or that the small proportion of WT alleles inactivated might neutralize the benefits of mutant knockout over time. This strategy resulted in allele-specific editing, but PAM-based strategies are generally more selective, as demonstrated by György and coworkers (György et al., 2019). They used the SaCas9-KKH variant to edit the mutant allele in a PAM selective manner (György et al., 2019). The SaCas9-KKH/sgRNA treatment via AAV-Anc80L65 was more selective that the treatment used in the previous study, with no detectable indels in the WT allele and a frequency of 2.2% indels for the mutant allele. At the age of 6 months, SaCas9-KKH/sgRNA-treated mice had significantly higher survival rates for both inner hairy cells and outer hair cells (OHCs), with normal hair bundle morphology in all cochlea, except for the OHCs in the basal region, which were absent. The authors also demonstrated the stable maintenance of low thresholds of auditory brainstem responses for up to 40 weeks. Finally, GUIDESeq analysis detected no genome-wide off-target events in Tmc1WT/WT fibroblasts, further highlighting the potential interest of AAV-SaCas9-KKH-sgTmc as a therapeutic strategy for DFNA36 hearing loss.

DNFA36 results from GOF mutations of the *tmc1* gene, whereas LOF mutations in both *tmc1* alleles result in the autosomal recessive congenital DFNB7/B11 hearing loss disorder. Gene disruption approaches are not suitable for the treatment of DFNB7/B11. Yeh and coworkers explored

TABLE 2 | Preclinical studies of genome editing for CNS pathologies.

Editing approach	Disease	Gene	Model	Editing tool	Delivery	Selectivity	Target efficiency (indels/expression)	Behavioral improvements	Publication
NHEJ	MECP2 duplication syndrome	Mecp2	MECP2-TG mouse	SpCas9	AAV-split system	Non-selective	50% reduction MECP2 protein	Improvements in social recognition	Yu et al., 2020
	Fragile X syndrome	mGluR5	Fmr1 knockout mouse	SpCas9	CRISPR-Gold RNP complexes	Non-selective	14.6% indels 40–50% reduction mGluR5 mRNA and protein	Rescued the excessive digging and repetitive jumping	Lee B. et al., 2018
	Alzheimer's disease	Bace1	5XFAD and APP-KI mouse	SpCas9	Amphiphilic RNP complexes	Non-selective	45% indels 34% reduction Bace1 mRNA	Behavioral improvements	Park et al., 2019
		APP	WT mouse	SpCas9	AAV9-split system	Non-selective	50% reduction full-lenght APP protein	No data	Sun et al., 2019
		APP-SW	Tg2576 mouse	SpCas9	AAV9-split system	Mismatch-based	1.3% indels (APPsw alleles)	No data	György et al., 2018
	DFNA36 (hearing loss)	Tmc1	Beethoven mouse (Bth/wt)	SpCas9	Cationic lipid-mediated RNP complexes	Mismatch-based	1.8% indels (mutant alleles)	Protection of the acoustic behavioral reflexes	Gao et al., 2018
		Tmc1	Beethoven mouse (Bth/wt)	SaCas9-KKH	AAV-Anc80L65	PAM-based	2.2% indels (mutant alleles)	Stable maintenance of auditory brainstem responses	György et al., 2019
	ALS	SOD1	G93A-SOD1 mouse	SaCas9	AAV9	Non-selective	0.2–0.4% indels 65% reduction SOD1 protein	Improved survival, motor deficits and muscular strenght	Gaj et al., 2017
	Huntington's disease	HTT	HD140Q-KI mouse	SpCas9	AAV-split system	Non-selective	10–80% reduction HTT protein	Improved motor deficits	Yang et al., 2017
		HTT	BacHD mouse	SpCas9	AAV1-split system	PAM-based	50% reduction mHTT mRNA	No data	Monteys et al., 2017
		HTT	LV-hHTT-82Q mouse	SpCas9 (self-inactivating)	LV-split system	Non-selective	30% HTT indels (exogenous)	No data	Merienne et al., 2017
	LCA10	CEP290	CEP290 IVS26-KI mouse and monkeys	SaCas9	AAV5	Non-selective	21.4% and 27.9% indels	No data	Maeder et al., 2019
HDR	Sandhoff and Tay–Sachs diseases	ALB	Sandhoff mouse	SaCas9 + dsTemplate-HEXM	AAV8	Non-selective	144- and 17-fold increase MUGS and MUG activities (indirect)	Improved motor deficits (totarod test)	Ou et al., 2020
	Retinitis pigmentosa	Pde6b	Rodless (rd1) mouse	SpCas9 + RecA-MS2 + sgRNA-MS2 loops + ssTemplate	Plasmid electroporation	Non-selective	2% gene correction	Partial rescue of the pupillary light reflexes	Cai et al., 2019
Base editing	DFNB7/B11 (hearing loss)	Tmc1	Tmc1 (Y182C/Y182C) mouse	SpCas9-based AID-BE4max	AAV-Anc80L65-split system	Non-selective	2.3% gene correction	Improved auditory brainstem responses	Yeh et al., 2020

(Continued)

TABLE 2 | Continued

Editing approach	Disease	Gene	Model	Editing tool	Delivery	Selectivity	Target efficiency (indels/expression)	Behavioral improvements	Publication
Transcriptional activation	Parkinson's disease	GDNF	6-OHDA rat	GDNF-6ZF-p65	AAV2	Non-selective	60% increase GDNF mRNA	Rescued motor deficits	Laganiere et al., 2010
	Alzheimer's disease	Dlg4	AβPPswe/PS-1 mouse	PSD95-6ZF-VP64	AAV-PHP.B	Non-selective	31% increase Bace1 mRNA	Rescued memory deficits	Bustos et al., 2017
	Spinal cord injury	VEGF-A	Aneurysm clip compression rat	VEGF-3ZF-p65	Ad and AAV2	Non-selective	33% increase VEGF mRNA 55% increase VEGF protein	Improved motor deficits	Liu et al., 2010;
	Traumatic brain injury	VEGF-A	Unilateral FPI rat	VEGF-3ZF-p65	Ad and AAV2	Non-selective	25–50% increase VEGF protein	Improved motor deficits (rotarod test)	Siddiq et al., 2012
Transcriptional repression	Huntington's disease	HTT	R6/2 mouse	mHTT-6ZF-KRAB	AAV1	CAG selective (120 repeats)	30% reduction mHTT mRNA	Improved motor deficits and clasping behavior	Garriga-Canut et al., 2012
		HTT	R6/2 and HdhQ50 mouse	mHTT-6ZF-KRAB	AAV1	CAG selective (50 repeats)	55–67% reduction mHTT mRNA	Improved clasping behavior	Zeitler et al., 2019
	Angelman syndrome	Snurf/Snrpn	Maternally Ube3a-deficient mouse	UBE3a-6ZF-KRAB	HIV TAT cell-penetrating peptide	Non-selective	20% increase UBE3A mRNA (indirect)	No data	Bailus et al., 2016

the use of a base editing strategy to correct the *tmc1* alleles in *Tmc1*$^{Y182C/Y182C}$ mice (Yeh et al., 2020). They reported 2.3% base editing in a bulk organ of Corti at P14 after the injection of a dual AAV system encoding AID-BE into the inner ear at P1. Tmc1 is expressed only in hair cells. The authors therefore analyzed base editing at the RNA level, to improve the quantification of editing in these cells. They observed ∼ 50% editing in the cDNA, but these results must be interpreted with caution because they may not reflect the editing at the DNA level. The treatment of mice resulted in the preservation of hair bundle morphology and a restoration of the mechanotransduction current in the sensory hair cells. There were 46% more hair cells in the treated mice 4 weeks after injection, with a progressive decrease in cell numbers thereafter, until 6 weeks. The decrease in cell survival was followed by a decline in hearing function, suggesting that more efficient base editing is required to prevent the degeneration of hair cells over time.

Retinitis Pigmentosa

Retinitis pigmentosa (RP) is an inherited disorder and the most common cause of progressive vision loss (Kalloniatis and Fletcher, 2004). It is defined by an initial progressive loss of rod photoreceptors, followed by cone photoreceptor degeneration. One form of RP results from a biallelic LOF mutation in the PDE6B gene, introducing a premature stop codon. Cai et al. used HDR-mediated CRISPR editing to correct the mutation (Cai et al., 2019). In this study, the authors developed an improved CRISPR system for HDR (Cas9/RecA) consisting of a sgRNA with MS2 aptamers for the recruitment of MS2-RecA fusion proteins to the target site to promote recombination between the cleavage site and a ssDNA donor template. The potential of this tool to repair the PDE6B gene was evaluated by electroporating the retinas of WT and rd1 mice with four plasmids (SpCas9 + sgRNA-MS2apt + MS2-RecA + ssTemplate) at P0. A 2% restoration of PDE6B WT protein levels was observed in Cas9/RecA-treated mice, whereas no wild-type PDE6B protein was detected in Cas9-treated mice (SpCas9 + sgRNA-MS2apt + ssTemplate), indicating that Cas9/RecA enhances HDR efficiency. Cas/RecA treatment at P0 rescued both rod and cone photoreceptors, but the degree of rescue was 1.8- and 1.6-fold lower, respectively, when mice were treated at P3, suggesting that the loss of photoreceptor proliferation had a negative effect on HDR-mediated correction. In addition, an analysis of visual function and pupillary light reflexes revealed that Cas9/RecA partially rescued the pupillary light reflexes of rd1 mice, demonstrating beneficial effects of treatment.

Leber Congenital Amaurosis Type 10

Leber congenital amaurosis type 10 (LCA10) is an autosomal recessive condition causing early blindness in infancy (Stone, 2007; Stone et al., 2017). It is defined by LOF mutations of both *CEP290* alleles. The IVS26 point mutation creating a new splice donor site is the most frequent defect. It alters transcript splicing and generates a premature stop codon in the processed mRNA. Maeder and coworkers recently reported an exhaustive drug dosing study of the use of AAV5-SaCas9-mediated NHEJ to correct the IVS26-driven aberrant CEP290 splicing in

retina photoreceptor cells (EDIT-101) (Maeder et al., 2019). The proposed strategy induced a cleavage on either side of the mutation, with a pair of sgRNAs used to delete or invert the fragment containing the IVS26 mutation. The authors evaluated the kinetics and dose response of the editing system in the retina of CEP290 IVS26-KI mice and cynomolgus monkeys, in which maximum editing rates of 21.4 and 27.9%, respectively, were obtained. They also demonstrated ocular tolerability in all animals, except those without immunosuppression regimens, which displayed mild inflammation. This report resulted in the first approved preclinical study of CNS genome editing for clinical trial continuation in humans (NCT03872479). The *cep290* cDNA is ∼7.5 kb long, a size well-beyond the capacity of the AAV vectors used for gene replacement. This approach demonstrates the therapeutic potential of gene repair for counteracting CNS disorders without the need to provide exogenous WT transgenes.

FUTURE PERSPECTIVES IN GENOME EDITING FOR CNS DISORDERS

The field of genome editing is rapidly evolving and there is now a broad genome editing toolbox that can be used for therapeutic purposes. The efficacy of genome-editing therapies for CNS disorders will depend on the choice of the most appropriate tool to tackle the genetic defect and the type and magnitude of editing required for therapeutic benefit. In addition, the types of cells and CNS areas to be edited should be taken into account. Local genome editing may be sufficient for some disorders, but others may require the editing of large areas. For instance, eye disorders are more accessible due to their peripheral localization and the relatively small area targeted, whereas the neuronal damage in AD covers large brain regions (Dos Santos Picanco et al., 2018). It is, therefore, crucial to select the most suitable delivery vehicle according to the editing tool used and the target area. The delivery of genome editing tools is probably one of the major limiting steps when targeting the CNS. Viral-mediated delivery by lentiviral (LV) and AAV vectors is the approach most frequently used to date, due to their high efficiency to transfer genetic material into cells (Spencer et al., 2020). LV have a large loading capacity but integrate into the host genome, potentially leading to insertional mutagenesis, whereas AAVs mostly persist as an extrachromosomal episome but have a limited cloning capacity. The generation of non-integrative lentiviral vectors (Shaw et al., 2017) and the use of dual AAV delivery systems (Yang et al., 2017; György et al., 2018; Sun et al., 2019) are two alternatives for overcoming these problems. Viral tropism has also been used to target specific cell types and to increase the area of transduction by either viral neuronal retrograde transport or through the use of serotypes with wide diffusion properties (Lykken et al., 2018). Local intraparenchymal injections are the most common delivery method for circumventing the BBB, but some AAV serotypes have been shown to cross the BBB after systemic delivery (Choudhury et al., 2016b; Chan et al., 2017; Hudry et al., 2018). Non-viral vehicles are generally less efficient than viral vectors, but the development of non-viral delivery methods for the CNS is an intense field of research and may open up new possibilities for treatment in the near future (Wang and Huang, 2019).

The immunogenicity induced by genome editing tools is another topic of concern due to potential inflammatory responses (Shim et al., 2017). For instance, the injection of non-host-matched, but not host-matched ZFNs, into the mouse brain resulted in microglial activation and mild neuronal death (Agustín-Pavón et al., 2016). Similarly, CRISPR/Cas9 was shown to induce the both cellular and humoral immune responses in mouse models (Mehta and Merkel, 2020). Immunogenicity can be minimized by transient expression. Transient expression strategies have been mainly developed for CRISPR/Cas-based tools either through the delivery of RNPs or ON/OFF expression systems. These include self-inactivation systems (Merienne et al., 2017; Li et al., 2018) and the use of drug inducible promoters, such as the doxycycline (dox)-induced Tet or the Tamoxifen-dependent Cre promoters (Zhang et al., 2019). However, the optimization of self-inactivation kinetics and the requirement of additional molecules to regulate promoters will delay the translation of these strategies to the clinic. Additionally, these strategies will be only suitable if the transient expression of the tool is sufficient to achieve therapeutic benefit.

Transient systems have also been developed to decrease off-target modifications. We showed that off-target events were reduced with the KamiCas9 compared to the constitutively expressed Cas9 (Merienne et al., 2017). Other groups have engineered Cas9 binding properties to increase specificity and attenuate off-target editing (Cebrian-Serrano and Davies, 2017; Hu et al., 2018; Kocak et al., 2019). Similarly, base editors and transcriptional/epigenetic editors also present off-target effects. For instance, base editors induce off-targets at both DNA and RNA levels (Zhou et al., 2019) whereas the KRAB domain has been shown to affect long chromosomal regions (Groner et al., 2010). There is thus the need for the development of highly specific editing systems to minimize safety concerns and ease their clinical application.

Finally, on-target events should also be properly characterized. Gene editing generates chimeric outcomes by introducing heterogeneous indels. For instance, the CRISPR/Cas9 targeting of the HTT translation starting site followed by NHEJ may generate truncated proteins with polyserine or polyalanine expansions, which have been shown to play a role in the disease (Berger et al., 2006). Furthermore, when attempting HDR-based strategies, NHEJ and HDR are competing pathways, and DSBs may be repaired by both mechanisms in the presence of a repair template (Weisheit et al., 2020). Likewise, bystander editing during base editing may give rise to unintended edited products which might even intensify the pathological processes. In addition, genome editing events may also be neutralized by intrinsic compensatory mechanisms, reducing the therapeutic effects (Smits et al., 2019).

In this review, we have focused on examples of *in vivo* therapies for CNS disorders (**Table 2**), but extensive efforts have been conducted to improve genome editing strategies. Two examples are the recently proposed prime editing approach (Anzalone et al., 2019) and the usage of transposases for genome engineering, which may become alternative options

for the treatment of CNS disorders in the near future (Anzalone et al., 2020; Doudna, 2020). In summary, it is acknowledged that multiple aspects require further improvement to establish CNS genome-editing therapies but the field is advancing at an astonishing pace, bringing us closer every day to possible clinical applications.

AUTHOR CONTRIBUTIONS

Both authors listed have made a substantial, direct and intellectual contribution to the work, and approved it for publication.

FUNDING

This work was partially supported by the Swiss National Science Foundation (FN 310030_184761/1) and a research agreement from the CHDI Foundation (A-14069).

ACKNOWLEDGMENTS

We wish to thank Maria Rey for the production of the figures as well as Sara Regio, Margareta Rybarikova, and Gabriel Vachey for their valuable comments on the manuscript.

REFERENCES

Agustín-Pavón, C., Mielcarek, M., Garriga-Canut, M., and Isalan, M. (2016). Deimmunization for gene therapy: host matching of synthetic zinc finger constructs enables long-term mutant Huntingtin repression in mice. *Mol. Neurodegener.* 11:64. doi: 10.1186/s13024-016-0128-x

Anzalone, A. V., Koblan, L. W., and Liu, D. R. (2020). Genome editing with CRISPR–Cas nucleases, base editors, transposases and prime editors. *Nat. Biotechnol.* 38, 824–844. doi: 10.1038/s41587-020-0561-9

Anzalone, A. V., Randolph, P. B., Davis, J. R., Sousa, A. A., Koblan, L. W., Levy, J. M., et al. (2019). Search-and-replace genome editing without double-strand breaks or donor DNA. *Nature* 576, 149–157. doi: 10.1038/s41586-019-1711-4

Bailus, B. J., Pyles, B., McAlister, M. M., O'Geen, H., Lockwood, S. H., Adams, A. N., et al. (2016). Protein delivery of an artificial transcription factor restores widespread ube3a expression in an angelman syndrome mouse brain. *Mol. Ther.* 24, 548–555. doi: 10.1038/mt.2015.236

Berger, Z., Davies, J. E., Luo, S., Pasco, M. Y., Majoul, I., O'Kane, C. J., et al. (2006). Deleterious and protective properties of an aggregate-prone protein with a polyalanine expansion. *Hum. Mol. Genet.* 15, 453–465. doi: 10.1093/hmg/ddi460

Bernstein, D. L., Lay, J. E. L., Ruano, E. G., and Kaestner, K. H. (2015). TALE-mediated epigenetic suppression of *CDKN2A* increases replication in human fibroblasts. *J. Clin. Invest.* 125, 1998–2006. doi: 10.1172/JCI77321

Billon, P., Bryant, E. E., Joseph, S. A., Nambiar, T. S., Hayward, S. B., Rothstein, R., et al. (2017). CRISPR-mediated base editing enables efficient disruption of eukaryotic genes through induction of STOP Codons. *Mol. Cell* 67, 1068–1079.e4. doi: 10.1016/j.molcel.2017.08.008

Boch, J., and Bonas, U. (2010). Xanthomonas AvrBs3 family-type III effectors: discovery and function. *Annu. Rev. Phytopathol.* 48, 419–436.

Boillée, S., Yamanaka, K., Lobsiger, C. S., Copeland, N. G., Jenkins, N. A., Kassiotis, G., et al. (2006). Onset and progression in inherited ALS determined by motor neurons and microglia. *Science* 312, 1389–1392. doi: 10.1126/science.1123511

Bonas, U., Stall, R. E., and Staskawicz, B. (1989). Genetic and structural characterization of the avirulence gene avrBs3 from *Xanthomonas campestris* pv. *vesicatoria*. *Mol. Gen. Genet.* 218, 127–136. doi: 10.1007/BF00330575

Breinig, M., Schweitzer, A. Y., Herianto, A. M., Revia, S., Schaefer, L., Wendler, L., et al. (2019). Multiplexed orthogonal genome editing and transcriptional activation by Cas12a. *Nat. Methods* 16, 51–54. doi: 10.1038/s41592-018-0262-1

Bunting, S. F., Callén, E., Wong, N., Chen, H.-T., Polato, F., Gunn, A., et al. (2010). 53BP1 inhibits homologous recombination in brca1-deficient cells by blocking resection of DNA breaks. *Cell* 141, 243–254. doi: 10.1016/j.cell.2010.03.012

Bustos, F. J., Ampuero, E., Jury, N., Aguilar, R., Falahi, F., Toledo, J., et al. (2017). Epigenetic editing of the Dlg4/PSD95 gene improves cognition in aged and Alzheimer's disease mice. *Brain* 140, 3252–3268. doi: 10.1093/brain/awx272

Cai, Y., Cheng, T., Yao, Y., Li, X., Ma, Y., Li, L., et al. (2019). *In vivo* genome editing rescues photoreceptor degeneration via a Cas9/RecA-mediated homology-directed repair pathway. *Sci. Adv.* 5:eaav3335. doi: 10.1126/sciadv.aav3335

Caldecott, K. W. (2008). Single-strand break repair and genetic disease. *Nat. Rev. Genet.* 9, 619–631. doi: 10.1038/nrg2380

Cano-Rodriguez, D., Gjaltema, R. A. F., Jilderda, L. J., Jellema, P., Dokter-Fokkens, J., Ruiters, M. H. J., et al. (2016). Writing of H3K4Me3 overcomes epigenetic silencing in a sustained but context-dependent manner. *Nat. Commun.* 7:12284. doi: 10.1038/ncomms12284

Cebrian-Serrano, A., and Davies, B. (2017). CRISPR-Cas orthologues and variants: optimizing the repertoire, specificity and delivery of genome engineering tools. *Mamm. Genome* 28, 247–261. doi: 10.1007/s00335-017-9697-4

Chadwick, A. C., Xiao, W., and Musunuru, K. (2017). *In vivo* base editing of PCSK9 (Proprotein Convertase Subtilisin/Kexin Type 9) as a Therapeutic Alternative to Genome Editing. *Arterioscler. Thromb. Vasc. Biol.* 37, 1741–1747. doi: 10.1161/ATVBAHA.117.309881

Chan, K. Y., Jang, M. J., Yoo, B. B., Greenbaum, A., Ravi, N., Wu, W.-L., et al. (2017). Engineered AAVs for efficient noninvasive gene delivery to the central and peripheral nervous systems. *Nat. Neurosci.* 20, 1172–1179. doi: 10.1038/nn.4593

Chavez, A., Scheiman, J., Vora, S., Pruitt, B. W., Tuttle, M., Iyer, E. P. R., et al. (2015). Highly efficient Cas9-mediated transcriptional programming. *Nat. Methods* 12, 326–328. doi: 10.1038/nmeth.3312

Chavez, A., Tuttle, M., Pruitt, B. W., Ewen-Campen, B., Chari, R., Ter-Ovanesyan, D., et al. (2016). Comparison of Cas9 activators in multiple species. *Nat. Methods* 13, 563–567. doi: 10.1038/nmeth.3871

Cheng, T.-L., and Qiu, Z. (2014). MeCP2: multifaceted roles in gene regulation and neural development. *Neurosci. Bull.* 30, 601–609. doi: 10.1007/s12264-014-1452-6

Chew, W. L., Tabebordbar, M., Cheng, J. K. W., Mali, P., Wu, E. Y., Ng, A. H. M., et al. (2016). A multifunctional AAV–CRISPR–Cas9 and its host response. *Nat. Methods* 13, 868–874. doi: 10.1038/nmeth.3993

Choudhury, S. R., Cui, Y., Lubecka, K., Stefanska, B., and Irudayaraj, J. (2016a). CRISPR-dCas9 mediated TET1 targeting for selective DNA demethylation at BRCA1 promoter. *Oncotarget* 7, 46545–46556. doi: 10.18632/oncotarget.10234

Choudhury, S. R., Harris, A. F., Cabral, D. J., Keeler, A. M., Sapp, E., Ferreira, J. S., et al. (2016b). Widespread central nervous system gene transfer and silencing after systemic delivery of novel AAV-AS vector. *Mol. Ther.* 24, 726–735. doi: 10.1038/mt.2015.231

Cong, L., Ran, F. A., Cox, D., Lin, S., Barretto, R., Habib, N., et al. (2013). Multiplex genome engineering using CRISPR/Cas systems. *Science* 339, 819–823. doi: 10.1126/science.1231143

Dabrowska, M., Juzwa, W., Krzyzosiak, W. J., and Olejniczak, M. (2018). Precise excision of the CAG tract from the huntingtin gene by Cas9 Nickases. *Front. Neurosci.* 12:74. doi: 10.3389/fnins.2018.00075

Dalkara, D., Byrne, L. C., Lee, T., Hoffmann, N. V., Schaffer, D. V., and Flannery, J. G. (2012). Enhanced gene delivery to the neonatal retina through systemic administration of tyrosine-mutated AAV9. *Gene Ther.* 19, 176–181. doi: 10.1038/gt.2011.163

Das, U., Wang, L., Ganguly, A., Saikia, J. M., Wagner, S. L., Koo, E. H., et al. (2016). Visualizing APP and BACE-1 approximation in neurons yields insight into the amyloidogenic pathway. *Nat. Neurosci.* 19, 55–64. doi: 10.1038/nn.4188

Dölen, G., and Bear, M. F. (2008). Role for metabotropic glutamate receptor 5 (mGluR5) in the pathogenesis of fragile X syndrome. *J. Physiol.* 586, 1503–1508. doi: 10.1113/jphysiol.2008.150722

Dos Santos Picanco, L. C., Ozela, P. F., de Fatima de Brito Brito, M., Pinheiro, A. A., Padilha, E. C., Braga, F. S., et al. (2018). Alzheimer's disease: a review from the pathophysiology to diagnosis, new perspectives for pharmacological treatment. *Curr. Med. Chem.* 25, 3141–3159. doi: 10.2174/0929867323666161213101126

Doudna, J. A. (2020). The promise and challenge of therapeutic genome editing. *Nature* 578, 229–236. doi: 10.1038/s41586-020-1978-5

Elias, G. M., and Nicoll, R. A. (2007). Synaptic trafficking of glutamate receptors by MAGUK scaffolding proteins. *Trends Cell Biol.* 17, 343–352. doi: 10.1016/j.tcb.2007.07.005

Ernst, J., Kheradpour, P., Mikkelsen, T. S., Shoresh, N., Ward, L. D., Epstein, C. B., et al. (2011). Mapping and analysis of chromatin state dynamics in nine human cell types. *Nature* 473, 43–49. doi: 10.1038/nature09906

Feigin, V. L., Nichols, E., Alam, T., Bannick, M. S., Beghi, E., Blake, N., et al. (2019). Global, regional, and national burden of neurological disorders, 1990–2016: a systematic analysis for the Global Burden of Disease Study 2016. *Lancet Neurol.* 18, 459–480. doi: 10.1016/S1474-4422(18)30499-X

Figley, S. A., Liu, Y., Karadimas, S. K., Satkunendrarajah, K., Fettes, P., Spratt, S. K., et al. (2014). Delayed administration of a bio-engineered zinc-finger VEGF-A gene therapy is neuroprotective and attenuates allodynia following traumatic spinal cord injury. *PLoS One* 9:e96137. doi: 10.1371/journal.pone.0096137

Fineran, P. C., and Charpentier, E. (2012). Memory of viral infections by CRISPR-Cas adaptive immune systems: acquisition of new information. *Virology* 434, 202–209. doi: 10.1016/j.virol.2012.10.003

Gaj, T., Ojala, D. S., Ekman, F. K., Byrne, L. C., Limsirichai, P., and Schaffer, D. V. (2017). *In vivo Genome Editing Improves Motor Function and Extends Survival in A Mouse Model of ALS | Science Advances*. Available online at: https://advances.sciencemag.org/content/3/12/eaar3952 (accessed May 8, 2020).

Gao, X., Tao, Y., Lamas, V., Huang, M., Yeh, W.-H., Pan, B., et al. (2018). Treatment of autosomal dominant hearing loss by *in vivo* delivery of genome editing agents. *Nature* 553, 217–221. doi: 10.1038/nature25164

Garriga-Canut, M., Agustín-Pavón, C., Herrmann, F., Sánchez, A., Dierssen, M., Fillat, C., et al. (2012). Synthetic zinc finger repressors reduce mutant huntingtin expression in the brain of R6/2 mice. *Proc. Natl. Acad. Sci. U.S.A.* 109, E3136–E3145. doi: 10.1073/pnas.1206506109

Gaudelli, N. M., Komor, A. C., Rees, H. A., Packer, M. S., Badran, A. H., Bryson, D. I., et al. (2017). Programmable base editing of A·T to G·C in genomic DNA without DNA cleavage. *Nature* 551, 464–471. doi: 10.1038/nature24644

Ge, X. A., and Hunter, C. P. (2019). Efficient homologous recombination in mice using long single stranded DNA and CRISPR Cas9 Nickase. *G3* 9, 281–286. doi: 10.1534/g3.118.200758

Gilbert, L. A., Horlbeck, M. A., Adamson, B., Villalta, J. E., Chen, Y., Whitehead, E. H., et al. (2014). Genome-Scale CRISPR-mediated control of gene repression and activation. *Cell* 159, 647–661. doi: 10.1016/j.cell.2014.09.029

Gray, M., Shirasaki, D. I., Cepeda, C., Andre, V. M., Wilburn, B., Lu, X.-H., et al. (2008). Full-Length Human mutant huntingtin with a stable polyglutamine repeat can elicit progressive and selective neuropathogenesis in BACHD Mice. *J. Neurosci.* 28, 6182–6195. doi: 10.1523/JNEUROSCI.0857-08.2008

Gribkoff, V. K., and Kaczmarek, L. K. (2017). The need for new approaches in CNS drug discovery: Why drugs have failed, and what can be done to improve outcomes. *Neuropharmacology* 120, 11–19. doi: 10.1016/j.neuropharm.2016.03.021

Groner, A. C., Meylan, S., Ciuffi, A., Zangger, N., Ambrosini, G., Dénervaud, N., et al. (2010). KRAB–Zinc finger proteins and KAP1 can mediate long-range transcriptional repression through heterochromatin spreading. *PLoS Genet.* 6:e1000869. doi: 10.1371/journal.pgen.1000869

György, B., Lööv, C., Zaborowski, M. P., Takeda, S., Kleinstiver, B. P., Commins, C., et al. (2018). CRISPR/Cas9 mediated disruption of the Swedish APP allele as a therapeutic approach for early-onset Alzheimer's disease. *Mol. Ther. Nucleic Acids* 11, 429–440. doi: 10.1016/j.omtn.2018.03.007

György, B., Nist-Lund, C., Pan, B., Asai, Y., Karavitaki, K. D., Kleinstiver, B. P., et al. (2019). Allele-specific gene editing prevents deafness in a model of dominant progressive hearing loss. *Nat. Med.* 25, 1123–1130. doi: 10.1038/s41591-019-0500-9

Hair, P., Cameron, F., and McKeage, K. (2013). Mipomersen sodium: first global approval. *Drugs* 73, 487–493. doi: 10.1007/s40265-013-0042-2

Hilton, I. B., D'Ippolito, A. M., Vockley, C. M., Thakore, P. I., Crawford, G. E., Reddy, T. E., et al. (2015). Epigenome editing by a CRISPR-Cas9-based acetyltransferase activates genes from promoters and enhancers. *Nat. Biotechnol.* 33, 510–517. doi: 10.1038/nbt.3199

Holtzman, L., and Gersbach, C. A. (2018). Editing the epigenome: reshaping the genomic landscape. *Annu. Rev. Genomics Hum. Genet.* 19, 43–71. doi: 10.1146/annurev-genom-083117-021632

Hoy, S. M. (2017). Nusinersen: first global approval. *Drugs* 77, 473–479. doi: 10.1007/s40265-017-0711-7

Hoy, S. M. (2019). Onasemnogene abeparvovec: first global approval. *Drugs* 79, 1255–1262. doi: 10.1007/s40265-019-01162-5

Hu, J. H., Miller, S. M., Geurts, M. H., Tang, W., Chen, L., Sun, N., et al. (2018). Evolved Cas9 variants with broad PAM compatibility and high DNA specificity. *Nature* 556, 57–63. doi: 10.1038/nature26155

Hudry, E., Andres-Mateos, E., Lerner, E. P., Volak, A., Cohen, O., Hyman, B. T., et al. (2018). Efficient Gene Transfer to the Central Nervous System by Single-Stranded Anc80L65. *Mol. Ther. Methods Clin. Dev.* 10, 197–209. doi: 10.1016/j.omtm.2018.07.006

Jayavaradhan, R., Pillis, D. M., Goodman, M., Zhang, F., Zhang, Y., Andreassen, P. R., et al. (2019). CRISPR-Cas9 fusion to dominant-negative 53BP1 enhances HDR and inhibits NHEJ specifically at Cas9 target sites. *Nat. Commun.* 10:2866. doi: 10.1038/s41467-019-10735-7

Jinek, M., Chylinski, K., Fonfara, I., Hauer, M., Doudna, J. A., and Charpentier, E. (2012). A Programmable Dual-RNA–Guided DNA endonuclease in adaptive bacterial immunity. *Science* 337, 816–821. doi: 10.1126/science.1225829

Kalloniatis, M., and Fletcher, E. L. (2004). Retinitis pigmentosa: understanding the clinical presentation, mechanisms and treatment options. *Clin. Exp. Optom.* 87, 65–80. doi: 10.1111/j.1444-0938.2004.tb03152.x

Kantor, B., Tagliafierro, L., Gu, J., Zamora, M. E., Ilich, E., Grenier, C., et al. (2018). Downregulation of SNCA expression by targeted editing of DNA methylation: a potential strategy for precision therapy in PD. *Mol. Ther.* 26, 2638–2649. doi: 10.1016/j.ymthe.2018.08.019

Kaplan, G., and McCracken, J. T. (2012). Psychopharmacology of Autism Spectrum Disorders. *Pediatr. Clin. North Am.* 59, 175–187. doi: 10.1016/j.pcl.2011.10.005

Karumuthil-Melethil, S., Nagabhushan Kalburgi, S., Thompson, P., Tropak, M., Kaytor, M. D., Keimel, J. G., et al. (2016). Novel Vector Design and Hexosaminidase Variant Enabling Self-Complementary Adeno-Associated Virus for the Treatment of Tay-Sachs Disease. *Hum. Gene Ther.* 27, 509–521. doi: 10.1089/hum.2016.013

Kato-Inui, T., Takahashi, G., Hsu, S., and Miyaoka, Y. (2018). Clustered regularly interspaced short palindromic repeats (CRISPR)/CRISPR-associated protein 9 with improved proof-reading enhances homology-directed repair. *Nucleic Acids Res.* 46, 4677–4688. doi: 10.1093/nar/gky264

Kearns, N. A., Pham, H., Tabak, B., Genga, R. M., Silverstein, N. J., Garber, M., et al. (2015). Functional annotation of native enhancers with a Cas9–histone demethylase fusion. *Nat. Methods* 12, 401–403. doi: 10.1038/nmeth.3325

Kesselheim, A. S., Hwang, T. J., and Franklin, J. M. (2015). Two decades of new drug development for central nervous system disorders. *Nat. Rev. Drug Discov.* 14, 815–816. doi: 10.1038/nrd4793

Khabou, H., Cordeau, C., Pacot, L., Fisson, S., and Dalkara, D. (2018). Dosage thresholds and influence of transgene cassette in adeno-associated virus–related toxicity. *Hum. Gene Ther.* 29, 1235–1241. doi: 10.1089/hum.2018.144

Kim, S.-S., Chen, Y.-M., O'Leary, E., Witzgall, R., Vidal, M., and Bonventre, J. V. (1996). A novel member of the RING finger family. KRIP-1, associates with the KRAB-A transcriptional repressor domain of zinc finger proteins. *Proc. Natl. Acad. Sci. U.S.A.* 93, 15299–15304.

Kleinstiver, B. P., Pattanayak, V., Prew, M. S., Tsai, S. Q., Nguyen, N. T., Zheng, Z., et al. (2016). High-fidelity CRISPR–Cas9 nucleases with no detectable genome-wide off-target effects. *Nature* 529, 490–495. doi: 10.1038/nature16526

Klug, B., Celis, P., Carr, M., and Reinhardt, J. (2012). "Chapter Seventeen - Regulatory Structures for Gene Therapy Medicinal Products in the European Union," in *Methods in Enzymology Gene Transfer Vectors for Clinical Application*, ed. T. Friedmann (Cambridge, MA: Academic Press), 337–354. doi: 10.1016/B978-0-12-386509-0.00017-X

Koblan, L. W., Doman, J. L., Wilson, C., Levy, J. M., Tay, T., Newby, G. A., et al. (2018). Improving cytidine and adenine base editors by expression optimization and ancestral reconstruction. *Nat. Biotechnol.* 36, 843–846. doi: 10.1038/nbt.4172

Kocak, D. D., Josephs, E. A., Bhandarkar, V., Adkar, S. S., Kwon, J. B., and Gersbach, C. A. (2019). Increasing the specificity of CRISPR systems with engineered RNA secondary structures. *Nat. Biotechnol.* 37, 657–666. doi: 10.1038/s41587-019-0095-1

Komor, A. C., Kim, Y. B., Packer, M. S., Zuris, J. A., and Liu, D. R. (2016). Programmable editing of a target base in genomic DNA without double-stranded DNA cleavage. *Nature* 533, 420–424. doi: 10.1038/nature17946

Komor, A. C., Zhao, K. T., Packer, M. S., Gaudelli, N. M., Waterbury, A. L., Koblan, L. W., et al. (2017). Improved base excision repair inhibition and bacteriophage Mu Gam protein yields C:G-to-T:A base editors with higher efficiency and product purity. *Sci. Adv.* 3:eaao4774. doi: 10.1126/sciadv.aao4774

Konermann, S., Brigham, M. D., Trevino, A. E., Joung, J., Abudayyeh, O. O., Barcena, C., et al. (2015). Genome-scale transcriptional activation by an engineered CRISPR-Cas9 complex. *Nature* 517, 583–588. doi: 10.1038/nature14136

Koo, E. H., and Squazzo, S. L. (1994). Evidence that production and release of amyloid beta-protein involves the endocytic pathway. *J. Biol. Chem.* 269, 17386–17389.

Kordower, J. H., Emborg, M. E., Bloch, J., Ma, S. Y., Chu, Y., Leventhal, L., et al. (2000). Neurodegeneration prevented by lentiviral vector delivery of GDNF in primate models of Parkinson's disease. *Science* 290, 767–773. doi: 10.1126/science.290.5492.767

Kundaje, A., Meuleman, W., Ernst, J., Bilenky, M., Yen, A., Heravi-Moussavi, A., et al. (2015). Integrative analysis of 111 reference human epigenomes. *Nature* 518, 317–330. doi: 10.1038/nature14248

Kurihara, T., Kouyama-Suzuki, E., Satoga, M., Li, X., Badawi, M., Thiha, et al. (2020). DNA repair protein RAD51 enhances the CRISPR/Cas9-mediated knock-in efficiency in brain neurons. *Biochem. Biophys. Res. Commun.* 524, 621–628. doi: 10.1016/j.bbrc.2020.01.132

Kuscu, C., Parlak, M., Tufan, T., Yang, J., Szlachta, K., Wei, X., et al. (2017). CRISPR-STOP: gene silencing through base-editing-induced nonsense mutations. *Nat. Methods* 14, 710–712. doi: 10.1038/nmeth.4327

Kwon, D. Y., Zhao, Y.-T., Lamonica, J. M., and Zhou, Z. (2017). Locus-specific histone deacetylation using a synthetic CRISPR-Cas9-based HDAC. *Nat. Commun.* 8:15315. doi: 10.1038/ncomms15315

Laan, L. A., Haeringen, A. V., and Brouwer, O. F. (1999). Angelman syndrome: a review of clinical and genetic aspects. *Clin. Neurol. Neurosurg.* 101, 161–170. doi: 10.1016/S0303-8467(99)00030-X

Laganiere, J., Kells, A. P., Lai, J. T., Guschin, D., Paschon, D. E., Meng, X., et al. (2010). An engineered zinc finger protein activator of the endogenous Glial Cell line-derived neurotrophic factor gene provides functional neuroprotection in a rat model of Parkinson's disease. *J. Neurosci.* 30, 16469–16474. doi: 10.1523/JNEUROSCI.2440-10.2010

Landrum, M. J., Lee, J. M., Benson, M., Brown, G., Chao, C., Chitipiralla, S., et al. (2016). ClinVar: public archive of interpretations of clinically relevant variants. *Nucleic Acids Res.* 44, D862–D868. doi: 10.1093/nar/gkv1222

Lang, A. E., Gill, S., Patel, N. K., Lozano, A., Nutt, J. G., Penn, R., et al. (2006). Randomized controlled trial of intraputamenal glial cell line–derived neurotrophic factor infusion in Parkinson disease. *Ann. Neurol.* 59, 459–466. doi: 10.1002/ana.20737

Lee, B., Lee, K., Panda, S., Gonzales-Rojas, R., Chong, A., Bugay, V., et al. (2018). Nanoparticle delivery of CRISPR into the brain rescues a mouse model of fragile X syndrome from exaggerated repetitive behaviours. *Nat. Biomed. Eng.* 2, 497–507. doi: 10.1038/s41551-018-0252-8

Lee, H. K., Willi, M., Miller, S. M., Kim, S., Liu, C., Liu, D. R., et al. (2018). Targeting fidelity of adenine and cytosine base editors in mouse embryos. *Nat. Commun.* 9:4804. doi: 10.1038/s41467-018-07322-7

Lee, K., Conboy, M., Park, H. M., Jiang, F., Kim, H. J., Dewitt, M. A., et al. (2017). Nanoparticle delivery of Cas9 ribonucleoprotein and donor DNA *in vivo* induces homology-directed DNA repair. *Nat. Biomed. Eng.* 1, 889–901. doi: 10.1038/s41551-017-0137-2

Li, A., Lee, C. M., Hurley, A. E., Jarrett, K. E., De Giorgi, M., Lu, W., et al. (2018). A self-deleting AAV-CRISPR system for *in vivo* genome editing. *Mol. Ther. Methods Clin. Dev.* 12, 111–122. doi: 10.1016/j.omtm.2018.11.009

Li, H., Yang, Y., Hong, W., Huang, M., Wu, M., and Zhao, X. (2020). Applications of genome editing technology in the targeted therapy of human diseases: mechanisms, advances and prospects. *Signal Transduct. Target. Ther.* 5, 1–23. doi: 10.1038/s41392-019-0089-y

Li, P., Zhang, L., Li, Z., Xu, C., Du, X., and Wu, S. (2019). Cas12a mediates efficient and precise endogenous gene tagging via MITI: microhomology-dependent targeted integrations. *Cell. Mol. Life Sci.* 77, 3875–3884. doi: 10.1007/s00018-019-03396-8

Liang, P., Ding, C., Sun, H., Xie, X., Xu, Y., Zhang, X., et al. (2017). Correction of β-thalassemia mutant by base editor in human embryos. *Protein Cell* 8, 811–822. doi: 10.1007/s13238-017-0475-6

Liao, H.-K., Hatanaka, F., Araoka, T., Reddy, P., Wu, M.-Z., Sui, Y., et al. (2017). *In vivo* target gene activation via CRISPR/Cas9-mediated trans-epigenetic modulation. *Cell* 171, 1495–1507.e15. doi: 10.1016/j.cell.2017.10.025

Lim, C. K. W., Gapinske, M., Brooks, A. K., Woods, W. S., Powell, J. E., Zeballos, C. M. A., et al. (2020). Treatment of a mouse model of ALS by *in vivo* base editing. *Mol. Ther.* 28, 1177–1189. doi: 10.1016/j.ymthe.2020.01.005

Liu, J.-P., and Zeitlin, S. O. (2017). Is Huntingtin dispensable in the adult brain? *J. Huntingt. Dis.* 6, 1–17. doi: 10.3233/JHD-170235

Liu, X. S., Wu, H., Ji, X., Stelzer, Y., Wu, X., Czauderna, S., et al. (2016). Editing DNA methylation in the mammalian genome. *Cell* 167, 233–247.e17. doi: 10.1016/j.cell.2016.08.056

Liu, Y., Figley, S., Spratt, S. K., Lee, G., Ando, D., Surosky, R., et al. (2010). An engineered transcription factor which activates VEGF-A enhances recovery after spinal cord injury. *Neurobiol. Dis.* 37, 384–393. doi: 10.1016/j.nbd.2009.10.018

Lykken, E. A., Shyng, C., Edwards, R. J., Rozenberg, A., and Gray, S. J. (2018). Recent progress and considerations for AAV gene therapies targeting the central nervous system. *J. Neurodev. Disord.* 10:16. doi: 10.1186/s11689-018-9234-0

Maeder, M. L., Angstman, J. F., Richardson, M. E., Linder, S. J., Cascio, V. M., Tsai, S. Q., et al. (2013). Targeted DNA demethylation and activation of endogenous genes using programmable TALE-TET1 fusion proteins. *Nat. Biotechnol.* 31, 1137–1142. doi: 10.1038/nbt.2726

Maeder, M. L., Stefanidakis, M., Wilson, C. J., Baral, R., Barrera, L. A., Bounoutas, G. S., et al. (2019). Development of a gene-editing approach to restore vision loss in Leber congenital amaurosis type 10. *Nat. Med.* 25, 229–233. doi: 10.1038/s41591-018-0327-9

Makarova, K. S., Wolf, Y. I., Alkhnbashi, O. S., Costa, F., Shah, S. A., Saunders, S. J., et al. (2015). An updated evolutionary classification of CRISPR–Cas systems. *Nat. Rev. Microbiol.* 13, 722–736. doi: 10.1038/nrmicro3569

Makarova, K. S., Wolf, Y. I., Iranzo, J., Shmakov, S. A., Alkhnbashi, O. S., Brouns, S. J. J., et al. (2020). Evolutionary classification of CRISPR–Cas systems: a burst of class 2 and derived variants. *Nat. Rev. Microbiol.* 18, 67–83. doi: 10.1038/s41579-019-0299-x

Mali, P., Yang, L., Esvelt, K. M., Aach, J., Guell, M., DiCarlo, J. E., et al. (2013). RNA-guided human genome engineering via Cas9. *Science* 339, 823–826. doi: 10.1126/science.1232033

Mehta, A., and Merkel, O. M. (2020). Immunogenicity of Cas9 protein. *J. Pharm. Sci.* 109, 62–67. doi: 10.1016/j.xphs.2019.10.003

Merienne, N., Vachey, G., de Longprez, L., Meunier, C., Zimmer, V., Perriard, G., et al. (2017). The self-inactivating KamiCas9 system for the editing of CNS disease genes. *Cell Rep.* 20, 2980–2991. doi: 10.1016/j.celrep.2017.08.075

Miller, J., McLachlan, A. D., and Klug, A. (1985). Repetitive zinc-binding domains in the protein transcription factor IIIA from Xenopus oocytes. *EMBO J.* 4, 1609–1614. doi: 10.1002/j.1460-2075.1985.tb03825.x

Mills, K. D., Ferguson, D. O., and Alt, F. W. (2003). The role of DNA breaks in genomic instability and tumorigenesis. *Immunol. Rev.* 194, 77–95. doi: 10.1034/j.1600-065X.2003.00060.x

Molla, K. A., and Yang, Y. (2019). CRISPR/Cas-mediated base editing: technical considerations and practical applications. *Trends Biotechnol.* 37, 1121–1142. doi: 10.1016/j.tibtech.2019.03.008

Monteys, A. M., Ebanks, S. A., Keiser, M. S., and Davidson, B. L. (2017). CRISPR/Cas9 editing of the mutant huntingtin allele *in vitro* and *in vivo*. *Mol. Ther.* 25, 12–23. doi: 10.1016/j.ymthe.2016.11.010

Moreno, A. M., Fu, X., Zhu, J., Katrekar, D., Shih, Y.-R. V., Marlett, J., et al. (2018). *In situ* gene therapy via AAV-CRISPR-Cas9-mediated targeted gene regulation. *Mol. Ther.* 26, 1818–1827. doi: 10.1016/j.ymthe.2018.04.017

Müller, U., and Barr-Gillespie, P. G. (2015). New treatment options for hearing loss. *Nat. Rev. Drug Discov.* 14, 346–365. doi: 10.1038/nrd4533

Nishida, K., Arazoe, T., Yachie, N., Banno, S., Kakimoto, M., Tabata, M., et al. (2016). Targeted nucleotide editing using hybrid prokaryotic and vertebrate adaptive immune systems. *Science* 353:aaf8729. doi: 10.1126/science.aaf8729

Nishiyama, J., Mikuni, T., and Yasuda, R. (2017). Virus-mediated genome editing via homology-directed repair in mitotic and postmitotic cells in mammalian brain. *Neuron* 96, 755–768.e5. doi: 10.1016/j.neuron.2017.10.004

Osmon, K. J. L., Woodley, E., Thompson, P., Ong, K., Karumuthil-Melethil, S., Keimel, J. G., et al. (2016). Systemic gene transfer of a hexosaminidase variant using an scAAV9.47 vector corrects GM2 Gangliosidosis in Sandhoff Mice. *Hum. Gene Ther.* 27, 497–508. doi: 10.1089/hum.2016.015

Ou, L., Przybilla, M. J., Tābāran, A.-F., Overn, P., O'Sullivan, M. G., Jiang, X., et al. (2020). A novel gene editing system to treat both Tay–Sachs and Sandhoff diseases. *Gene Ther.* 27, 226–236. doi: 10.1038/s41434-019-01205

Park, H., Oh, J., Shim, G., Cho, B., Chang, Y., Kim, S., et al. (2019). *In vivo* neuronal gene editing via CRISPR–Cas9 amphiphilic nanocomplexes alleviates deficits in mouse models of Alzheimer's disease. *Nat. Neurosci.* 22, 524–528. doi: 10.1038/s41593-019-0352-0

Pavletich, N. P., and Pabo, C. O. (1991). Zinc finger-DNA recognition: crystal structure of a Zif268-DNA complex at 2.1 A. *Science* 252, 809–817. doi: 10.1126/science.2028256

Persico, A. M., and Napolioni, V. (2013). Autism genetics. *Behav. Brain Res.* 251, 95–112. doi: 10.1016/j.bbr.2013.06.012

Petrs-Silva, H., Dinculescu, A., Li, Q., Min, S.-H., Chiodo, V., Pang, J.-J., et al. (2009). High-efficiency transduction of the mouse retina by Tyrosine-mutant AAV serotype vectors. *Mol. Ther.* 17, 463–471. doi: 10.1038/mt.2008.269

Poewe, W., Seppi, K., Tanner, C. M., Halliday, G. M., Brundin, P., Volkmann, J., et al. (2017). Parkinson disease. *Nat. Rev. Dis. Primer* 3, 1–21. doi: 10.1038/nrdp.2017.13

Ramocki, M. B., Peters, S. U., Tavyev, Y. J., Zhang, F., Carvalho, C. M. B., Schaaf, C. P., et al. (2009). Autism and other neuropsychiatric symptoms are prevalent in individuals with MeCP2 duplication syndrome. *Ann. Neurol.* 66, 771–782. doi: 10.1002/ana.21715

Rees, H. A., and Liu, D. R. (2018). Base editing: precision chemistry on the genome and transcriptome of living cells. *Nat. Rev. Genet.* 19, 770–788. doi: 10.1038/s41576-018-0059-1

Rees, H. A., Yeh, W.-H., and Liu, D. R. (2019). Development of hRad51–Cas9 nickase fusions that mediate HDR without double-stranded breaks. *Nat. Commun.* 10:2212. doi: 10.1038/s41467-019-09983-4

Richter, M. C., Ludewig, S., Winschel, A., Abel, T., Bold, C., Salzburger, L. R., et al. (2018). Distinct *in vivo* roles of secreted APP ectodomain variants APPsα and APPsβ in regulation of spine density, synaptic plasticity, and cognition. *EMBO J.* 37:e98335. doi: 10.15252/embj.201798335

Rossidis, A. C., Stratigis, J. D., Chadwick, A. C., Hartman, H. A., Ahn, N. J., Li, H., et al. (2018). In utero CRISPR-mediated therapeutic editing of metabolic genes. *Nat. Med.* 24, 1513–1518. doi: 10.1038/s41591-018-0184-6

Rowland, L. P., and Shneider, N. A. (2001). Amyotrophic lateral sclerosis. *N. Engl. J. Med.* 344, 1688–1700. doi: 10.1056/NEJM200105313442207

Russell, S., Bennett, J., Wellman, J. A., Chung, D. C., Yu, Z.-F., Tillman, A., et al. (2017). Efficacy and safety of voretigene neparvovec (AAV2-hRPE65v2) in patients with RPE65-mediated inherited retinal dystrophy: a randomised, controlled, open-label, phase 3 trial. *Lancet* 390, 849–860. doi: 10.1016/S0140-6736(17)31868-8

Ryu, S.-M., Koo, T., Kim, K., Lim, K., Baek, G., Kim, S.-T., et al. (2018). Adenine base editing in mouse embryos and an adult mouse model of Duchenne muscular dystrophy. *Nat. Biotechnol.* 36, 536–539. doi: 10.1038/nbt.4148

Safari, F., Hatam, G., Behbahani, A. B., Rezaei, V., Barekati-Mowahed, M., Petramfar, P., et al. (2019). CRISPR system: a high-throughput toolbox for research and treatment of Parkinson's disease. *Cell. Mol. Neurobiol.* 40, 477–493. doi: 10.1007/s10571-019-00761-w

Sandoval, A., Elahi, H., and Ploski, J. E. (2020). Genetically engineering the nervous system with CRISPR-Cas. *eNeuro* 7:ENEURO.0419-19.2020. doi: 10.1523/ENEURO.0419-19.2020

Savell, K. E., Bach, S. V., Zipperly, M. E., Revanna, J. S., Goska, N. A., Tuscher, J. J., et al. (2019). A neuron-optimized CRISPR/dCas9 activation system for robust and specific gene regulation. *eNeuro* 6:ENEURO.0495-18.2019. doi: 10.1523/ENEURO.0495-18.2019

Schacker, M., and Seimetz, D. (2019). From fiction to science: clinical potentials and regulatory considerations of gene editing. *Clin. Transl. Med.* 8:27. doi: 10.1186/s40169-019-0244-7

Shahryari, A., Saghaeian Jazi, M., Mohammadi, S., Razavi Nikoo, H., Nazari, Z., Hosseini, E. S., et al. (2019). Development and clinical translation of approved gene therapy products for genetic disorders. *Front. Genet.* 10:868. doi: 10.3389/fgene.2019.00868

Shaw, A. M., Joseph, G. L., Jasti, A. C., Sastry-Dent, L., Witting, S., and Cornetta, K. (2017). Differences in vector-genome processing and illegitimate integration of non-integrating lentiviral vectors. *Gene Ther.* 24, 12–20. doi: 10.1038/gt.2016.69

Shim, G., Kim, D., Park, G. T., Jin, H., Suh, S.-K., and Oh, Y.-K. (2017). Therapeutic gene editing: delivery and regulatory perspectives. *Acta Pharmacol. Sin.* 38, 738–753. doi: 10.1038/aps.2017.2

Shweiki, D., Itin, A., Soffer, D., and Keshet, E. (1992). Vascular endothelial growth factor induced by hypoxia may mediate hypoxia-initiated angiogenesis. *Nature* 359, 843–845. doi: 10.1038/359843a0

Siddiq, I., Park, E., Liu, E., Spratt, S. K., Surosky, R., Lee, G., et al. (2012). Treatment of traumatic brain injury using zinc-finger protein gene therapy targeting VEGF-A. *J. Neurotrauma* 29, 2647–2659. doi: 10.1089/neu.2012.2444

Silverman, J. L., Smith, D. G., Rizzo, S. J. S., Karras, M. N., Turner, S. M., Tolu, S. S., et al. (2012). Negative allosteric modulation of the mGluR5 receptor reduces repetitive behaviors and rescues social deficits in mouse models of autism. *Sci. Transl. Med.* 4:131ra51. doi: 10.1126/scitranslmed.3003501

Sledz, C. A., and Williams, B. R. G. (2005). RNA interference in biology and disease. *Blood* 106, 787–794. doi: 10.1182/blood-2004-12-4643

Smits, A. H., Ziebell, F., Joberty, G., Zinn, N., Mueller, W. F., Clauder-Münster, S., et al. (2019). Biological plasticity rescues target activity in CRISPR knock outs. *Nat. Methods* 16, 1087–1093. doi: 10.1038/s41592-019-0614-5

Spencer, A. P., Torrado, M., Custódio, B., Silva-Reis, S. C., Santos, S. D., Leiro, V., et al. (2020). Breaking barriers: bioinspired strategies for targeted neuronal delivery to the central nervous system. *Pharmaceutics* 12:192. doi: 10.3390/pharmaceutics12020192

Stone, E. M. (2007). Leber Congenital Amaurosis–a model for efficient genetic testing of heterogeneous disorders: LXIV edward jackson memorial lecture. *Am. J. Ophthalmol.* 144, 791–811.e6. doi: 10.1016/j.ajo.2007.08.022

Stone, E. M., Andorf, J. L., Whitmore, S. S., DeLuca, A. P., Giacalone, J. C., Streb, L. M., et al. (2017). Clinically focused molecular investigation of 1000 consecutive families with inherited retinal Disease. *Ophthalmology* 124, 1314–1331. doi: 10.1016/j.ophtha.2017.04.008

Sun, J., Carlson-Stevermer, J., Das, U., Shen, M., Delenclos, M., Snead, A. M., et al. (2019). CRISPR/Cas9 editing of APP C-terminus attenuates β-cleavage and promotes α-cleavage. *Nat. Commun.* 10:53. doi: 10.1038/s41467-018-07971-8

Suzuki, K., Tsunekawa, Y., Hernandez-Benitez, R., Wu, J., Zhu, J., Kim, E. J., et al. (2016). *In vivo* genome editing via CRISPR/Cas9 mediated homology-independent targeted integration. *Nature* 540, 144–149. doi: 10.1038/nature20565

Suzuki, K., Yamamoto, M., Hernandez-Benitez, R., Li, Z., Wei, C., Soligalla, R. D., et al. (2019). Precise *in vivo* genome editing via single homology arm donor mediated intron-targeting gene integration for genetic disease correction. *Cell Res.* 29, 804–819. doi: 10.1038/s41422-019-0213-0

Syed, Y. Y. (2016). Eteplirsen: first global approval. *Drugs* 76, 1699–1704. doi: 10.1007/s40265-016-0657-1

Tanenbaum, M. E., Gilbert, L. A., Qi, L. S., Weissman, J. S., and Vale, R. D. (2014). A protein-tagging system for signal amplification in gene expression and fluorescence imaging. *Cell* 159, 635–646. doi: 10.1016/j.cell.2014.09.039

Tenenbaum, L., and Humbert-Claude, M. (2017). Glial cell line-derived neurotrophic factor gene delivery in Parkinson's disease: a delicate balance between neuroprotection, trophic effects, and unwanted compensatory mechanisms. *Front. Neuroanat.* 11:29. doi: 10.3389/fnana.2017.00029

Urnov, F. D., Rebar, E. J., Holmes, M. C., Zhang, H. S., and Gregory, P. D. (2010). Genome editing with engineered zinc finger nucleases. *Nat. Rev. Genet.* 11, 636–646. doi: 10.1038/nrg2842

Vanamee, ÉS., Santagata, S., and Aggarwal, A. K. (2001). FokI requires two specific DNA sites for cleavage. *J. Mol. Biol.* 309, 69–78. doi: 10.1006/jmbi.2001.4635

Villiger, L., Grisch-Chan, H. M., Lindsay, H., Ringnalda, F., Pogliano, C. B., Allegri, G., et al. (2018). Treatment of a metabolic liver disease by *in vivo* genome

base editing in adult mice. *Nat. Med.* 24, 1519–1525. doi: 10.1038/s41591-018-0209-1

Walton, R. T., Christie, K. A., Whittaker, M. N., and Kleinstiver, B. P. (2020). Unconstrained genome targeting with near-PAMless engineered CRISPR-Cas9 variants. *Science* 368, 290–296. doi: 10.1126/science.aba8853

Wang, S., and Huang, R. (2019). Non-viral nucleic acid delivery to the central nervous system and brain tumors. *J. Gene Med.* 21:e3091. doi: 10.1002/jgm.3091

Weber, M., Hellmann, I., Stadler, M. B., Ramos, L., Pääbo, S., Rebhan, M., et al. (2007). Distribution, silencing potential and evolutionary impact of promoter DNA methylation in the human genome. *Nat. Genet.* 39, 457–466. doi: 10.1038/ng1990

Weisheit, I., Kroeger, J. A., Malik, R., Klimmt, J., Crusius, D., Dannert, A., et al. (2020). Detection of deleterious on-target effects after HDR-mediated CRISPR editing. *Cell Rep.* 31:107689. doi: 10.1016/j.celrep.2020.107689

Wertz, M. H., Mitchem, M. R., Pineda, S. S., Hachigian, L. J., Lee, H., Lau, V., et al. (2020). Genome-wide *in vivo* CNS screening identifies genes that modify CNS Neuronal survival and mHTT toxicity. *Neuron* 106, 76–89.e8. doi: 10.1016/j.neuron.2020.01.004

Whone, A. L., Boca, M., Luz, M., Woolley, M., Mooney, L., Dharia, S., et al. (2019). Extended treatment with Glial cell line-derived neurotrophic factor in Parkinson's disease. *J. Parkinsons Dis.* 9, 301–313. doi: 10.3233/JPD-191576

Wiedenheft, B., Sternberg, S. H., and Doudna, J. A. (2012). RNA-guided genetic silencing systems in bacteria and archaea. *Nature* 482, 331–338. doi: 10.1038/nature10886

Winblad, B., Amouyel, P., Andrieu, S., Ballard, C., Brayne, C., Brodaty, H., et al. (2016). Defeating Alzheimer's disease and other dementias: a priority for European science and society. *Lancet Neurol.* 15, 455–532. doi: 10.1016/S1474-4422(16)00062-4

Xu, X., Tao, Y., Gao, X., Zhang, L., Li, X., Zou, W., et al. (2016). A CRISPR-based approach for targeted DNA demethylation. *Cell Discov.* 2:16009. doi: 10.1038/celldisc.2016.9

Yamanaka, K., Chun, S. J., Boillee, S., Fujimori-Tonou, N., Yamashita, H., Gutmann, D. H., et al. (2008). Astrocytes as determinants of disease progression in inherited amyotrophic lateral sclerosis. *Nat. Neurosci.* 11, 251–253. doi: 10.1038/nn2047

Yang, S., Chang, R., Yang, H., Zhao, T., Hong, Y., Kong, H. E., et al. (2017). CRISPR/Cas9-mediated gene editing ameliorates neurotoxicity in mouse model of Huntington's disease. *J. Clin. Invest.* 127, 2719–2724. doi: 10.1172/JCI92087

Yao, X., Wang, X., Hu, X., Liu, Z., Liu, J., Zhou, H., et al. (2017a). Homology-mediated end joining-based targeted integration using CRISPR/Cas9. *Cell Res.* 27, 801–814. doi: 10.1038/cr.2017.76

Yao, X., Wang, X., Liu, J., Hu, X., Shi, L., Shen, X., et al. (2017b). CRISPR/Cas9 – mediated precise targeted integration *in vivo* using a double cut donor with short homology arms. *EBioMedicine* 20, 19–26. doi: 10.1016/j.ebiom.2017.05.015

Yeh, C. D., Richardson, C. D., and Corn, J. E. (2019). Advances in genome editing through control of DNA repair pathways. *Nat. Cell Biol.* 21, 1468–1478. doi: 10.1038/s41556-019-0425-z

Yeh, W.-H., Chiang, H., Rees, H. A., Edge, A. S. B., and Liu, D. R. (2018). *In vivo* base editing of post-mitotic sensory cells. *Nat. Commun.* 9:2184. doi: 10.1038/s41467-018-04580-3

Yeh, W.-H., Shubina-Oleinik, O., Levy, J. M., Pan, B., Newby, G. A., Wornow, M., et al. (2020). *In vivo* base editing restores sensory transduction and transiently improves auditory function in a mouse model of recessive deafness. *Sci. Transl. Med.* 12:eaay9101. doi: 10.1126/scitranslmed.aay9101

Ying, Y., Yang, X., Zhao, K., Mao, J., Kuang, Y., Wang, Z., et al. (2015). The Krüppel-associated box repressor domain induces reversible and irreversible regulation of endogenous mouse genes by mediating different chromatin states. *Nucleic Acids Res.* 43, 1549–1561. doi: 10.1093/nar/gkv016

Ylä-Herttuala, S. (2012). Endgame: Glybera finally recommended for approval as the first gene therapy drug in the European Union. *Mol. Ther.* 20, 1831–1832. doi: 10.1038/mt.2012.194

Yu, B., Yuan, B., Dai, J.-K., Cheng, T., Xia, S.-N., He, L.-J., et al. (2020). Reversal of social recognition deficit in Adult Mice with MECP2 duplication via normalization of MeCP2 in the medial prefrontal cortex. *Neurosci. Bull.* 36, 570–584. doi: 10.1007/s12264-020-00467-w

Zeitler, B., Froelich, S., Marlen, K., Shivak, D. A., Yu, Q., Li, D., et al. (2019). Allele-selective transcriptional repression of mutant HTT for the treatment of Huntington's disease. *Nat. Med.* 25, 1131–1142. doi: 10.1038/s41591-019-0478-3

Zeng, Y., Li, J., Li, G., Huang, S., Yu, W., Zhang, Y., et al. (2018). Correction of the Marfan syndrome pathogenic FBN1 mutation by base editing in human cells and heterozygous embryos. *Mol. Ther.* 26, 2631–2637. doi: 10.1016/j.ymthe.2018.08.007

Zetsche, B., Gootenberg, J. S., Abudayyeh, O. O., Slaymaker, I. M., Makarova, K. S., Essletzbichler, P., et al. (2015). Cpf1 is a single RNA-guided endonuclease of a class 2 CRISPR-Cas system. *Cell* 163, 759–771. doi: 10.1016/j.cell.2015.09.038

Zhan, H., Zhou, Q., Gao, Q., Li, J., Huang, W., and Liu, Y. (2019). Multiplexed promoterless gene expression with CRISPReader. *Genome Biol.* 20:113. doi: 10.1186/s13059-019-1712-5

Zhang, J., Chen, L., Zhang, J., and Wang, Y. (2019). Drug inducible CRISPR/Cas systems. *Comput. Struct. Biotechnol. J.* 17, 1171–1177. doi: 10.1016/j.csbj.2019.07.015

Zhao, Y., Wang, D., Zong, L., Zhao, F., Guan, L., Zhang, P., et al. (2014). A Novel DFNA36 Mutation in TMC1 Orthologous to the Beethoven (Bth) mouse associated with autosomal dominant hearing loss in a Chinese family. *PLoS One* 9:e97064. doi: 10.1371/journal.pone.0097064

Zhou, C., Sun, Y., Yan, R., Liu, Y., Zuo, E., Gu, C., et al. (2019). Off-target RNA mutation induced by DNA base editing and its elimination by mutagenesis. *Nature* 571, 275–278. doi: 10.1038/s41586-019-1314-0

Zhou, H., Liu, J., Zhou, C., Gao, N., Rao, Z., Li, H., et al. (2018). *In vivo* simultaneous transcriptional activation of multiple genes in the brain using CRISPR–dCas9-activator transgenic mice. *Nat. Neurosci.* 21, 440–446. doi: 10.1038/s41593-017-0060-6

Zuo, E., Sun, Y., Wei, W., Yuan, T., Ying, W., Sun, H., et al. (2019). Cytosine base editor generates substantial off-target single-nucleotide variants in mouse embryos. *Science* 364, 289–292. doi: 10.1126/science.aav9973

Conflict of Interest: The authors declare that the research was conducted in the absence of any commercial or financial relationships that could be construed as a potential conflict of interest.